Patterns, mechanisms, and legacies of abrupt climate change: examining the Younger Dryas in eastern North America

By

David Fastovich

A dissertation submitted in partial fulfillment of

the requirements for the degree of

Doctor of Philosophy

(Geography)

at the

UNIVERSITY OF WISCONSIN-MADISON

2022

Date of final oral examination: 04/29/2022

The dissertation is approved by the following members of the Final Oral Committee:

John W. Williams (Chair), Professor, Geography

Joseph A. Mason, Professor, Geography

Shaun A. Marcott, Associate Professor, Geoscience

Monica G. Turner, Professor, Integrative Biology

Benjamin Zuckerberg, Associate Professor, Forest and Wildlife Ecology

Acknowledgements

This dissertation was only possible because of the help and support of many wonderful people, and I will forever be grateful. My master's and doctoral advisor, Jack Williams, has been a constant source of scientific and professional support and guidance. This dissertation would not have been possible without his insight and patience in the face of countless questions during our weekly meetings. Jack's intellectual curiosity and flexibility allowed me to pursue research that I was passionate about and challenged me to grow as a scientific researcher.

I'm thankful to my dissertation committee members for their time and expertise. Joe Mason and Shaun Marcott instilled a deep appreciation of glacial geology, paleoclimatology, and geomorphology that underpin much of the work presented here. Monica Turner and Benjamin Zuckerberg expanded my scientific inquiry and taught me the skills and background I needed to explore the biological legacies of past climate changes. I am a more well-rounded researcher because of the input and knowledge of every committee member, and I will carry forward these perspectives in all future research.

Every chapter of this dissertation included data shared by individuals and entire scientific communities. Jim Russell opened his lab to me during the summers and taught me the fundamentals of organic geochemistry, brGDGT analysis, and aided me in climatological interpretation. I am indebted to everyone that has contributed to the Neotoma Paleoecology Database, providing me with the fossil-pollen counts needed for Chapter 2. Ruza Ivanovic, Eric Galbraith, Feng He, and Masa Kageyama shared climate model output for Chapters 3 and 4 and answered many short and long questions as I became acquainted with climate model output. The International Union for Conservation of Nature and BirdLife International freely provided species range maps needed for Chapter 4.

I made many friends along the way towards completing this dissertation and the laughs we shared were a source of happiness when graduate school became difficult. I owe many thanks to Scott Farley, Kevin Burke, Yue Wang, Allie Jensen, Claire Rubbelke, Matthias Trachsel, Simon Goring, Allison Stegner, Adrian George, Angie Perrotti, Robert Sarkisian, Jacob Nesemeier, and Ben Watson from the William's Lab for keeping graduate school fun. I will always cherish my time in the Williams' Lab.

My two families, the Fastovich's and the Gandy's, have been a source of emotional support throughout this dissertation, giving me the confidence and strength I needed during the most challenging times. I wanted to thank my mother and father, Taisiya and Vladimir Fastovich, for leaving their home, friends, and family when I was a five-month-old infant, 27 years ago, and moving to the United States and providing me with a life that would not have been possible in Belarus. Finally, I wanted to thank my wife, Lydia, though thanks alone are not enough. Lydia has selflessly supported me through the highs and lows of graduate school and has always been an advocate and cheerleader for me, even when I felt undeserving.

Abstract

Increasing global temperatures from anthropogenic greenhouse gas emissions are driving widespread climatological and ecological changes globally. Abrupt global changes that share rates of climate change similar to those experienced today (Overpeck et al. 2003; Williams and Burke 2019) are recorded throughout the geologic record and offer important insights that can help predict future anthropogenic change. The Deglacial period (19,000 to 11,000 years before present) after the Last Glacial Maximum has been a key interval for understanding ecological and climatological responses to increasing greenhouse gas concentrations and a warming climate (COHMAP Project Members 1988; Nolan et al. 2018; Mottl et al. 2021). Imposed on this gradual warming are abrupt climate oscillations that onset within decades to centuries, last for millennia, and are commonly attributed to changes in the Atlantic meridional overturning circulation forced by the input of freshwater into the North Atlantic Ocean. The most recent of these millennial-scale climate events is the Younger Dryas (ca. 12,900 to 11,700 years before present) and caused spatially complex climate changes globally. In this dissertation, we first aim to determine the spatial patterns of climate change and the atmospheric mechanisms responsible for driving abrupt climate change regionally in eastern North America through the use of organic temperature biomarkers (brGDGTs) and climate models. Second, we seek to disentangle the contributions of glacial and millennial-scale climate variability upon modern patterns of species richness in eastern North America.

Chapter 2 seeks to determine the spatial fingerprint of Younger Dryas temperature changes in eastern North America. We develop a spatially dense multiproxy network of temperature reconstructions relying upon statistical transfer functions applied to fossil-pollen abundances and an independent proxy, based on organic biomarkers (brGDGTs). This analysis

indicates that temperature changes during the Younger Dryas followed a dipole pattern in eastern North America. Temperatures lowered abruptly in maritime Canada and the northeastern United States nearly synchronously with temperature records from Greenland (Severinghaus et al. 1998). Cooling is also reconstructed in the Great Lakes region but delayed by ~400 years. Sites south of 35°N exhibited an antiphased response and lack YD cooling, with Florida sites indicating a thermal maximum. Warming in Florida during the Younger Dryas suggests that the 'bipolar-seesaw' conceptualization is an oversimplification of the spatial patterns of global climate changes. Focus must be placed on constraining regional climate changes to refine the mechanisms of abrupt climate change. Chapter 3 aims to better understand the atmospheric mechanisms for these antiphased temperature changes in eastern North America. We accomplish this by combining our multiproxy temperature network with a synthesis of hydroclimate reconstructions to compare against four climate models with meltwater hosing experiments that resemble the onset of the Younger Dryas. Precipitation changes followed a tripole pattern with wetting in the northeastern United States and Florida and drying from the Great Lakes region to the Carolinas, in contrast to the temperature dipole resolved in Chapter 2. Analysis of the climate models highlights the dual role of ice sheets and meltwater-induced weakening of the Atlantic meridional overturning circulation as the key drivers of the reconstructed warming and wetting in the southeastern United States. Reduced northward oceanic heat transport in the Atlantic Ocean increased the latitudinal temperature gradient and strengthened the jet stream, leading to upper-level divergence over eastern North America and the transport of warmer and moister air into the southeastern United States. For Chapter 4, we use our multiproxy temperature and precipitation reconstruction from prior chapters, alongside 11 climate simulations of millennial-scale climate events forced by meltwater pulses, to assess whether legacies of these climate

changes can be detected in the contemporary diversity of amphibians, birds, mammals, reptiles, and trees in eastern North America. Generalized additive models that use both contemporary and paleoclimatic predictors suggest that past millennial scale climate oscillations have left an imprint on contemporary amphibian and arboreal biodiversity, though the exact role of past climate changes remains uncertain. Generalized additive models that use the multiproxy network of Younger Dryas climate reconstructions and a subset of the climate models analyzed suggest that greater millennial scale climate variability is predictive of greater contemporary biodiversity. However, generalized additive models that use four of the climate models suggest that millennial-scale climate stability is predictive of greater contemporary richness in eastern North America. Disagreement in the sign, magnitude, and spatial fingerprint of climate changes among the 11 climate simulations and the multiproxy climate reconstructions precludes further refining the role of millennial-scale climate oscillations at this time. This uncertainty highlights that caution should be used when attempting to model contemporary biodiversity based on individual paleoclimatic simulations. Higher resolution climate simulations forced with accurate boundary conditions are necessary to constrain the relationship between past millennial-scale climate changes and contemporary biodiversity.

Table of Contents

Table of Figures

Chapter 1 Introduction: Younger Dryas ecological and climatological history of eastern North America

The Earth is experiencing rapid and unprecedented climate change as greenhouse gas concentrations continue to increase from anthropogenic sources. Such global scale changes are not unique in the geologic record and the deglaciation from the Last Glacial Maximum (21,000 thousand years ago) to pre-Industrial (1850 AD) period is a natural experiment to understand how the atmosphere, oceans, flora, and fauna respond to climate warming. During the most recent deglaciation expansive Northern Hemispheric ice sheets faded and atmospheric carbon dioxide concentrations increased from ~185 to ~265 parts per million (Clark et al. 2012; WAIS Divide Project Members 2015). Abrupt climate changes are punctuated throughout the most recent deglaciation with rates of change similar to projected rates of change at regional scales under various emission scenarios (Overpeck et al. 2003; Williams and Burke 2019). Three of these abrupt climate events occurred during the most recent deglaciation, lasting one to several thousand years and include Heinrich stadial 1, the Bølling-Allerød, and the Younger Dryas, with varying global- to hemispheric-scale climate changes. Temperatures abruptly decreased throughout the Northern Hemisphere with the onset of Heinrich stadial 1, abruptly increased during the Bølling-Allerød, and abruptly decreased again during the Younger Dryas (Clark et al. 2012). These climate events onset within decades changing local temperatures by as much as ~9 °C, locally, as reconstructed from the Greenland ice cores (Buizert et al. 2014). Just as the most recent deglaciation can serve to understand projected climate changes, millennial scale climate oscillations are not unique to the most recent deglaciation and have occurred throughout the last 250,000 years, marking a key mode of climate variability (Dansgaard et al. 1982, 1993; North Greenland Ice Core Project Members 2004). Disentangling the regional patterns and mechanisms

of abrupt changes during the most recent deglaciation is relevant to understanding fundamental features of millennial scale climate events beyond the most recent deglaciation.

Changes in deep ocean circulation beginning in the North Atlantic Ocean is a favored hypothesis to explaining the onset and termination of millennial scale climate events (Clark et al. 2002; Liu et al. 2009; McManus et al. 2004; Stouffer et al. 2006). Deep ocean currents redistribute heat globally (Ganachaud and Wunsch 2000) and are sensitive to changes in surface water density in the North Atlantic Ocean. During the most recent deglaciation, melting ice sheets released meltwater in discrete intervals into the North Atlantic Ocean, altering the Atlantic limb of deep ocean circulation (Boyle and Keigwin 1987; Broecker et al. 1989; Carlson et al. 2007; Keigwin et al. 1991; McManus et al. 2004), called the Atlantic meridional overturning circulation (AMOC), thereby causing climate events like Heinrich stadial 1 and the Younger Dryas. As northward heat transport by the AMOC weakened, sea surface temperatures decreased in the North Atlantic first, causing a cascade of feedbacks that resulted in hemispheric scale climate cooling (Broecker 1998).

Eastern North America is particularly well suited to examine the climatological and ecological impacts of millennial scale climate events. Eastern North America is adjacent to the North Atlantic and sensitive to changes in the AMOC. Additionally, the glacial history of eastern North America produced thousands of kettle lakes throughout, that are ideal environments for capturing ecological and climatological signals in sediments. Within these lacustrine sediments, a key proxy of ecological and climatological change is fossil-pollen. Arboreal and floral species migrated in response to deglacial warming and abrupt climate changes individualistically and these migrations are recorded in pollen microfossils preserved in lacustrine sediments (Solomon and Webb 1985; Webb 1986; Webb et al. 2003). Analysis of contemporary pollen rain into lake

surfaces identifies temperature and precipitation as important determinants of pollen deposited in contemporary lake surfaces (Bartlein et al. 1986). That is, in warmer environments pollen from warm adapted taxa would be strongly represented in lake surface samples.

The Younger Dryas is the most recent of the millennial scale climate events and is well represented throughout lacustrine archives in eastern North America. Past assemblages of arboreal and non-arboreal taxa reconstructed from fossil-pollen demonstrate rapid and synchronous responses to Younger Dryas cooling in New England in decades to centuries (Williams et al. 2002). These changes included the establishment of cold adapted boreal, needleleaf taxa like *Pinus*, *Abies*, and *Picea*, in favor of mesic taxa assemblages of *Quercus*, *Ostrya*/*Carpinus*, *Fraxinus*, *Ulmus*, and *Acer* that were common during the Bølling-Allerød. These changes were likely in response to decreased temperatures in New England and the adjacent North Atlantic (Shuman et al. 2002), however precipitation changes also determined ecological reorganization. Records from New England suggest that hydrologic changes were local with some sites demonstrating an increase in precipitation during the Younger Dryas (Shuman et al. 2001) while other sites indicate drier conditions (Newby et al. 2000, 2009).

Younger Dryas induced floral reshuffling is present outside of New England in the Great Lakes region the southeastern United States. Ecological turnover in the Great Lakes region mirrors changes in New England. No-analog communities of mesic, broadleaf taxa and boreal, needleleaf taxa were replaced nearly entirely by boreal fossil-pollen assemblages. Ecological change was not uniform throughout the region. Sites such as Bonnett Lake (Fastovich et al. 2020b), Triangle Lake Bog (Jensen et al. 2021), Ladd Lake (Shane and Anderson 1993), and Smoot Lake Bog (Shane and Anderson 1993) all demonstrate a rapid reestablishment of *Pinus* populations and minimal increases in *Picea*. Adjacent sites in Ohio exhibit an opposing response,

where *Picea* and *Pinus* pollen proportions both increase during the Younger Dryas (Gill et al. 2009; Jensen et al. 2021; Shane and Anderson 1993; Watson et al. 2018). The role of fire has been suggested in controlling these local ecological changes but does not completely resolve these discrepancies (Jensen et al. 2021). Although the causes of these locally unique ecological histories in the Great Lakes region is unresolved, the establishment of boreal taxa during the Younger Dryas throughout the region suggests decreased temperatures, shared with sites in New England. Although ecological changes between these two region are shared, the timing of these changes disagree. Crystal Lake, IL is a well dated record (35 radiocarbon dates, Gonzales and Grimm 2009) that suggests the Younger Dryas onset may have been delayed in the Great Lakes region with authors proposing that proglacial lakes may have altered the onset of Younger Dryas cooling. Subregional effects of proglacial lakes have been simulated to impact local climate within climate models (Hostetler et al. 2000) suggesting that a lagged Younger Dryas onset may be present in additional sites throughout the Great Lakes region, yet the spatial coherence of this recorded delay is unknown.

The southeastern United States represents a unique ecological history in response to the Younger Dryas cooling in the North Atlantic. Sites in Virginia, Missouri, and South Carolina all lack a signature of the Younger Dryas. Two recently developed fossil-pollen records at White Pond, SC and Cupola Pond, MO demonstrate that during the Younger Dryas, high abundances of *Quercus*, *Ostrya*/*Carpinus*, and *Fraxinus* were supported despite cooling conditions elsewhere in eastern North America (Jones et al. 2017; Krause et al. 2018). Prior interpretations of these fossil-pollen records have suggested that Younger Dryas cooling was nonexistent in this portion of eastern North America (Watts 1980a). brGDGT records at White Pond, SC support this interpretation but only offer a local perspective of climate change in the southeastern United

States (Krause et al. 2018). Paradoxically, sites further south and more distant from the North Atlantic Ocean demonstrate a strong response to the Younger Dryas. The most well dated of these Florida sites is Lake Tulane, FL and demonstrates a consistent increase in mesic populations of *Pinus* during the Younger Dryas and other Heinrich stadials (Grimm et al. 1993, 2006). These communities of *Pinus* replace oak savannahs leading authors to hypothesize that the Younger Dryas was an abrupt warming in Florida with an increase in precipitation which has been supported by climate models of intermediate complexity (Donders et al. 2011).

Chapter 2 Spatial fingerprint of Younger Dryas cooling and warming in eastern North America

2.1 Abstract

The Younger Dryas (YD, 12.9-11.7 ka) is the most recent, near-global interval of abrupt climate change with rates similar to modern global warming. Understanding the causes and biodiversity effects of YD climate changes requires determining the spatial fingerprints of past temperature changes. Here we build pollen- and branched glycerol dialkyl glycerol tetraether-based temperature reconstructions in eastern North America (ENA) to better understand deglacial temperature evolution. YD cooling was pronounced in the northeastern United States (US) and muted in the north-central US. Florida sites warmed during the YD, while other southeastern sites maintained a relatively stable climate. This fingerprint is consistent with an intensified subtropical high during the YD and demonstrates that interhemispheric responses were more complex spatially in ENA than predicted by the bipolar seesaw model. Reduced-amplitude or antiphased millennial-scale temperature variability in the southeastern US may support regional hotspots of biodiversity and endemism.

2.2 Introduction

The most recent deglaciation, 19.0 to 8.2 ka BP, contained several large hemispheric- to global-scale abrupt temperature changes with rates that are regionally comparable to projected

21st-century climate change (Williams and Burke 2019). Such millennial-scale climate variability profoundly affected vegetation and megafauna in Europe (Cooper et al. 2015; Huntley et al. 2013; Rey et al. 2017). In particular, the Younger Dryas (YD), dated to 12.9 to 11.7 ka (Rasmussen et al. 2006), is recorded in many Northern Hemispheric records (Clark et al. 2012) as a return to cold conditions. This cooling is attributed to a weakening of the Atlantic Meridional Overturning Circulation (AMOC) (Keigwin et al. 1991), causing a southward shift of the Intertropical Convergence Zone and weakened Northern Hemisphere monsoons (Kageyama et al. 2013; Talbot et al. 2007). The canonical bipolar seesaw hypothesis predicts that the YD and other stadials were caused by AMOC slowdown and reduced interhemispheric heat transport (Stocker 1998). Prior global-scale data syntheses (Shakun and Carlson 2010) and freshwater hosing experiments with climate models of varying complexity (Kageyama et al. 2013; Stocker et al. 1992) have shown hemispheric-scale fingerprints (Northern Hemisphere cooling, Southern Hemisphere warming) consistent with the bipolar seesaw. Earth System Models (ESMs) predict more complex intrahemispheric fingerprints of temperature variations (Kageyama et al. 2013; Liu et al. 2009; Okumura et al. 2009), but these simulations remain poorly constrained by proxy data. This data gap limits our understanding of the mechanisms of heat redistribution following rapid changes in the AMOC (Pedro et al. 2018) and how biodiversity hotspots persisted during abrupt millennial-scale climate variations (Brown et al. 2020).

Eastern North America (east of 92° W) (ENA) has a dense network of paleoclimatic proxy records (Bartlein et al. 2011; Kaufman et al. 2020a) and is a classic region for data-model comparisons (COHMAP Project Members 1988). Earlier proxy-data syntheses of YD temperature variations in ENA are hampered by inaccuracies in conventional bulk-sediment radiocarbon dates (Grimm et al. 2009; Shuman et al. 2002) and prior global proxy syntheses for

the YD emphasized marine records with few or no terrestrial ENA paleoclimatic records (Clark et al. 2012; Shakun and Carlson 2010). A comparison of hosing experiments indicates that ENA is an area of high divergence among ESMs, with some predicting that ENA follows Northern Hemisphere cooling trends and others indicating no change or even regional warming (Kageyama et al. 2013). These differences among models for ENA result from uncertainty about the atmospheric and oceanic teleconnections by which the AMOC signal propagates from the North Atlantic.

Within ENA, the southeastern US (between 30°N and 39°N) (SEUS) is climatically and biologically distinct. For example, a 'warming hole' during the 20th and 21st century in the SEUS may be linked to decadal variability in the North Atlantic (Kumar et al. 2013) or the Pacific (Meehl et al. 2012). Climatic variations associated with the North Atlantic Oscillation (NAO) cause antiphased warm and dry/cool and wet climate anomalies in the SEUS and northeastern US (Hurrell et al. 2003) – a climatic dipole that might affect past climate changes. The SEUS is a biodiversity hotspot, with high richness and endemism in amphibians, birds, reptiles, and plants (Jenkins et al. 2015). Climate stability during glacial-interglacial variations is one proposed mechanism for contemporary biodiversity and endemism (Brown et al. 2020; Sandel et al. 2011), but millennial-climate variability in the SEUS is largely unexplored.

Here, we present new reconstructions and syntheses of the deglacial temperature evolution in ENA, drawing upon a network of well-dated lacustrine multiproxy records and nearby marine records. We reconstruct mean annual temperatures from fossil pollen and branched glycerol dialkyl glycerol tetraethers (brGDGT) from sites spanning a 21.5° latitudinal gradient. We combine recently published brGDGT and pollen records from Bonnett Lake, OH (Fastovich et al. 2020b), Silver Lake, OH (Watson et al. 2018), and White Pond, SC (Krause et

al. 2018) with two new brGDGT records from Sheelar Lake, FL, Cupola Pond, MO, 42 well-dated pollen records from the Neotoma Paleoecology Database (Williams et al. 2018), and three nearby marine records of sea surface temperatures (SSTs) and storminess (Carlson et al. 2008; Toomey et al. 2017; Ziegler et al. 2008)(Figure S1.1). We discuss the implications of the reported patterns for understanding mechanisms of deglacial climate evolution and contemporary patterns of biodiversity.

2.3 Methods

2.3.1 Site selection and age-depth modeling

Fossil pollen records and geochronological controls were obtained from the Neotoma Paleoecology Database (Goring et al. 2015; Williams et al. 2018). We performed an initial search for all sites east of 92°W, including several sites recently contributed by the authors of this study (Fastovich et al. 2020b; Krause et al. 2018; Watson et al. 2018). As a second-pass filter, we used all fossil pollen records according to the following chronological and sampling criteria: (i) two or more chronological controls in the record, (ii) one or more chronological controls from 15.5 ka to 10.9 ka, and (iii) at least four pollen samples from 13.8 ka to 11.1 ka. When setting these criteria, we sought to balance a tradeoff between minimizing temporal uncertainty and maximizing spatial coverage. We used 42 records for the late-glacial spatial fingerprint analyses, of which 27 extended to 15.5 ka and so were included in the principal components analysis (Table S1., Figure S1.1). New age-depth relationships were built using *Bacon* (Blaauw and Christen 2011) and *bulk-baconizing* (Wang et al. 2019).

2.3.2 Mean annual temperature reconstructions

brGDGTs are a class of lipids found in bacterial membranes; the relative abundances of brGDGTs is sensitive to environmental factors such as temperature and pH (Weijers et al. 2007).

We analyzed existing sediments from Cupola Pond, MO (Jones et al. 2017) and a new core from Sheelar Lake, FL (Table S1.2, Figure S2.2) for brGDGTs. Previous publications on sediment cores from White Pond and Silver Lake used a then-current chromatographic method, in which 5- and 6- methyl isomers co-elute (Weijers et al. 2007). At the three sites analyzed more recently (Bonnett Lake, Cupola Pond, Sheelar Lake), an updated approach was used that separates 5- and 6-methyl brGDGT isomers (Hopmans et al. 2016) and allows for more precise temperature calibrations (De Jonge et al. 2014) . At Silver Lake, we compared the two analytical approaches by reanalyzing a subset of the original samples using the updated method and found similar temperature reconstructions (Figure S1.3)(Fastovich et al. 2020b). We reconstructed mean annual temperature using the MAT MBT´$_{5Me}$ calibration function for sites where 5- and 6-methyl isomers were separated (De Jonge et al. 2014), and the Peterse et al., (2012) calibration at White Pond (Krause et al. 2018) and Silver Lake (Watson et al. 2018), which are based on the calibration of brGDGTs in soil samples to temperature. These calibrations were selected because they more accurately reconstruct modern mean annual temperature than calibrations built from east African lake sediment samples (e.g. Russell et al., (2018))(Figure S1.4) and the MBT´$_{5Me}$ and MBT´ index quantify brGDGT methylation, which is hypothesized to control membrane fluidity (Sinninghe Damsté et al. 2018). Microbial community composition also affects the abundances of brGDGT molecules (De Jonge et al. 2019).

Errors were calculated using an ensemble of bootstrapped calibration parameters (Loomis et al. 2012) trained on calibration data from Peterse et al., (2012) and De Jonge et al., (2014) to estimate the 95% confidence interval for temperature estimates. The effect of temporal uncertainty was incorporated by creating randomly sampled pairs of bootstrapped temperature estimates with a draw from the posterior age distribution for each brGDGT sample. These pairs

were then interpolated onto an even 100-year interval, generating an ensemble of linearly interpolated temperature estimates for each site.

Pollen-inferred mean annual temperature reconstructions were averaged across three transfer functions: modern analog technique (Overpeck et al. 1985), weighted averaging (Ter Braak 1987; Ter Braak and Prentice 1988), and weighted-average partial least squares (Ter Braak et al. 1993; Ter Braak and Juggins 1993). The transfer functions were trained on modern pollen abundances from the North American Modern Pollen Database (NAMPD) (Whitmore et al. 2005). Pollen abundances in the modern calibration dataset and the fossil pollen were aggregated into 64 taxa (Williams and Shuman 2008). Following Williams and Shuman (2008), taxonomic ambiguity in the NAMPD was addressed by geographically splitting *Picea* into eastern and western types, *Pinus* into northeastern and southeastern types, and Myricaceae into northern and southern types, to reduce the possibility of false matches, using species maps from Thompson (1999a,b). A more detailed procedure was followed for the fossil pollen taxa. All sites in Florida were assumed to consist of southeastern *Pinus* (many species)*,* while all sites above 40 °N were assumed to consist of northeastern *Pinus (P. banksiana, P. resinosa, P. strobus),* for the entirety of the records (Jackson et al. 1997, 2000). Sites between Florida and 40 °N demonstrate a clear temporal separation between the decline of northeastern *Pinus* and the establishment of southeastern *Pinus* (e.g. White Pond, SC (Krause et al. 2018)). Pollen size analyses of *Pinus* at White Pond supports this delineation between northeastern and southeastern *Pinus* (Watts 1980a). At these sites, the earlier period of high *Pinus* abundances was assumed to represent northeastern species and the second period of high abundances was assumed to be southeastern (Table S1.3). *Picea* was assumed to be eastern and all fossil and modern instances of Myricaceae were split into northern and southern populations at 35 °N (Williams 2006). After generating

temperature estimates, fossil-pollen temperatures were interpolated onto an even 100-year interval, regionally averaged to produce regional time series, and spatially averaged into 2-degree bins.

2.3.3 Spatial analysis of temperature reconstructions

Principal components analysis (PCA) of the temperature time series was performed to determine common modes of variation in the temperature reconstructions (Mix et al. 1986a,b; Shakun and Carlson 2010). We also included prior SST reconstructions from Blake Outer Ridge (Carlson et al. 2008) and MD02-2575 (Ziegler et al. 2008) in the PCA. The effect of temporal uncertainty on the PCA was included by creating an ensemble of interpolated temperature estimates for each site, based on randomly selected posterior age estimates. PCA was performed 10,000 times on matrices composed of a randomly sampled temperature ensemble member from each site. The SST records had only point age estimates, with no uncertainties, so these records were incorporated unchanged in all PCA replicates. Although age was not varied in the SST records, sensitivity experiments indicated this had little impact on the uncertainty estimates of the PC time series values (<0.01). All random sampling was performed assuming a uniform distribution, thus equally weighing ensemble members of age and temperature estimates. The 95% high-density interval of the principal components was retained, producing the median and confidence interval in Figure 2.2. We assessed the significance of the PCs in all ensemble members using broken-stick significance testing (Jackson 1993) and the North et al., (1982) uniqueness test (Figure S1.5). PC1 and PC2 explained 58% (95% CI: 44%, 78%) and 16% (95% CI:11%, 23%) of the variance, respectively. PC1 was significant in all ensemble members using the broken-stick test and unique in all of the ensemble members using the North et al., (1982)

"rule of thumb" (Figure S1.5). PC2 was significant in almost all ensemble members (broken-stick test) and unique in 27% of the ensemble members (Figure S1.5).

2.4 Results

2.4.1 Younger Dryas temperatures

Deglacial temperature evolution in ENA exhibits a coherent spatial fingerprint with at least three distinct modes (Figure 2.1, Figure 2.2). The northeast cooled during YD onset (1.0 ℃), with similar timing to Greenland (Rasmussen et al. 2006), and is signaled by the rapid resurgence of boreal plant taxa (Figure 2.1a, Figure 2.1m) and chironomid indicators (Levesque et al. 1997). Pollen and brGDGT temperature estimates in the north-central US also indicate YD cooling, but with a possibly lagged onset of ~400 years (0.9 - 2.0 ℃, Figure 2.1b-d). This apparent lag may be due to regional climatic processes, such as local ice-sheet effects on atmospheric circulation (see Gonzales and Grimm 2009), that overprint AMOC-induced cooling. Overall, sites closer to the North Atlantic cooled more (Figure 2.1m), indicating the sensitivity of northeastern sites to reduced AMOC or greater regional sea ice extent, which would have produced albedo feedbacks and increased cooling (Gildor and Tziperman 2001; North 1984). Additionally, our analysis compares YD temperatures to early-Holocene temperatures, and regions adjacent to the Laurentide Ice Sheet likely experienced a greater deglacial to Holocene warming (Tierney et al. 2020).

In contrast, in the SEUS, temperatures were stable or rising during the YD and, in Florida, were warmer than during the early Holocene (Figure 2.1e-h, Figure 2.1m). All pollen-based paleoclimatic reconstructions indicate SEUS warming during the YD, which is supported by the replacement of boreal conifers (*Picea*, *Pinus*) with temperate conifers (*Tsuga*) at 38.2°N (Kneller and Peteet 1993) and temperate hardwoods (*Quercus*, *Carya*, *Ostrya/Carpinus*,

Corylus) at 36.8°N (Jones et al. 2017). Two of the three southern brGDGT records agree with the pollen-based temperature reconstructions, with Cupola and White Ponds showing no YD cooling, but Sheelar Lake indicates a cooling ($< 3°C$). Despite this disagreement, pollen- and brGDGT-inferred temperatures produce a coherent spatial pattern that discriminates the SEUS and northern sites. PC1, which tracks deglacial warming (Figure 2.2a), shows strong positive loadings for northern sites and strong negative loadings on PC1 for central Florida (Figure 2.2b). PC2, which tracks YD cooling (Figure 2.2a), shows a strong signal in the northeastern US, a variable loading magnitude and sign in the upper Midwest, and a weak signal in the SEUS, where eight of ten records having loadings <0.25 (Figure 2.2c). Small negative loadings in the SEUS indicates that these sites contribute less to PC2 and are negatively correlated with PC2. This suggests that most sites in the SEUS experienced slight warming through the YD, rather than the large cooling inferred from the large positive loadings in the northern regions. As a result, the ENA temperature gradient weakens after 14 ka, with a pause or slight reversal during the YD (Figure S1.6). These analyses suggest that temperature variations were muted in SEUS during the YD, particularly between 30° to 35°N (Figure 2.1m, Figure S1.6). Above 35°N, temperature trends resemble the millennial-scale variations seen in temperature records from the North Atlantic and Greenland (Shakun and Carlson 2010) (Figure 2.1, Figure 2.2, Figure S1.7, Figure S1.8, Figure S1.9).

This temperature fingerprint is consistent with nearby marine records (Figure 2.1i, Figure 2.2) and helps resolve putative outliers in prior global syntheses (Shakun and Carlson 2010). North Atlantic marine records show YD cooling (Bard et al. 2000), similar to the temperature trends for the northeastern and north-central US (Figure 2.1, Figure S1.7, Figure S1.8, Figure S1.9) . SSTs at Blake Outer Ridge (32° 47′ N), in contrast, demonstrate gradual YD warming

(Figure 2.1i) (Carlson et al. 2008). SST estimates from the northeast Gulf of Mexico (Figure 2.1i) (Ziegler et al. 2008) and northern Caribbean (Ruhlemann et al. 1999) also exhibit YD warming and no abrupt onset. Cyclone frequency or intensity in the subtropical Atlantic increased during the YD, consistent with regionally elevated SSTs or lower-amplitude cooling than elsewhere in the Atlantic (Figure 2.1j)(Toomey et al. 2017). Hence, the spatial fingerprint apparent in terrestrial ENA may have also manifested in the adjacent subtropical Atlantic and Gulf of Mexico.

2.5 Discussion

2.5.1 Mechanisms for regionally varying Younger Dryas temperatures

Global climate model (GCM) experiments and the modern climatology of ENA identify several plausible mechanisms for the spatial fingerprint of YD climate change in ENA. One working hypothesis is an enhanced subtropical high that resembles the positive phase of the NAO. The NAO is associated with gradients in mean atmospheric pressure in the North Atlantic and subtropics, and influences temperature and precipitation in ENA through changes in the mean position of the jet stream and westerlies (Walker and Bliss 1932; Wallace and Gutzler 1981) (Figure 2.3). Boreal winters with a large positive index (greater difference in pressure between the Icelandic Low and Azores High) are associated with a stronger and more zonal jet (Bjerknes 1964), shifting storm tracks northward (Rogers 1990). This jet stream configuration produces southerly flow into SEUS and higher temperatures (Deser and Blackmon 1993; Walker and Bliss 1932), and northeasterly flow into the northeastern and north-central US, producing colder winters (Hurrell et al. 2003). NAO-positive years also correlate with increased tropical storm activity (Elsner and Kocher 2000). These patterns are consistent with the observed spatial fingerprint (Figure 2.1, Figure 2.2), with records of tropical storm activity during the YD

(Toomey et al. 2017) (Figure 2.1j), and with pollen-based interpretations of a wet YD in Florida

(Grimm et al. 2006). Several paleoclimatic records in Europe that span the YD demonstrate a

repositioning and strengthening of westerly winds and support our finding for NAO positive

conditions (Baldini et al. 2015; Brauer et al. 2008). Furthermore, GCM experiments with a

freshwater forcing simulate anomalously high pressure near the Azores (Ivanovic et al. 2017;

Renssen et al. 2018). Notably, colder SSTs in the North Atlantic are associated with a more

positive NAO index caused by a deepening of the Icelandic Low (Bjerknes 1964; van Loon and

Rogers 1978), which suggests that AMOC shutdown may have deepened the Icelandic Low,

initiating an NAO-positive climate state. The initiation of NAO-positive conditions can be forced

by SST anomalies in the North Atlantic due to changes to latent heat exchange from the ocean to

atmosphere (Rodwell et al. 1999).

Positive NAO conditions are also associated with higher pressures in the subtropics and

enhanced Hadley cell circulation and trade winds (Wang 2002). An enhanced subtropical high

may have also strengthened surface ocean circulation, drawing heat northward from the

equatorial Atlantic. GCMs and proxies demonstrate a southward shift of the Hadley cell and

strengthened trade winds following AMOC shutdown (McGee et al. 2018a). These in turn may

have enhanced easterly wind stress in the northern tropical Atlantic and the strength of the

subtropical oceanic cell (McCreary and Lu 1994), along with the meridional heat transport

associated with the cell (Klinger and Marotzke 2000). Increased heat transport by the subtropical

cell could further intensify warming associated with southerly atmospheric advection into the

SEUS due to NAO-positive conditions. A strengthening of the northern subtropical cell has been

simulated in the Climate Model 2.1 GCM following hosing (Chang et al. 2008). Experiments

with an Earth-system model of intermediate complexity suggest that warm SSTs in the Gulf of

Mexico are necessary to producing warmer and wetter conditions in Florida following AMOC

shutdown (Donders et al. 2011).

Other climatic influences may have also contributed to a warm SEUS. Paleoclimate

reconstructions in the Gulf of Mexico suggest the presence of an enlarged Atlantic Warm Pool

(Ziegler et al. 2008). Atmospheric circulation changes associated with the melting of the

Laurentide Ice sheet (Gregoire et al. 2015) also may have contributed to SEUS warming during

the YD. Further work with ESMs is needed to better understand and test the potential

contributions of these mechanisms to SEUS warming during the YD and other periods of

enhanced freshwater forcing and AMOC weakening.

2.5.2 Biogeographic implications of a warm Younger Dryas

The SEUS is a biodiversity hotspot for multiple taxonomic groups (Jenkins et al. 2015),

and the muted YD temperature change we document in the SEUS suggest a mechanism for

maintaining regional biological diversity. Various explanations have been offered for the higher

species richness and endemism in ENA than Europe, including different configurations of

climate refugia and mountain barriers to species migration, and differing amplitudes of glacial-

interglacial climate change (Latham and Ricklefs 1993; Lumibao et al. 2017; Sandel et al. 2011).

Other papers have linked the global distribution of biodiversity hotspots to Quaternary climate

stability without disentangling orbital and millennial components (Brown et al. 2020). Our work

suggests that the high climate stability in the SEUS during past abrupt millennial-scale climate

changes may have uniquely positioned the SEUS to be a biodiversity preserve. This contrasts

with western Eurasia, which experienced high-amplitude millennial-scale climate variability,

megafaunal turnover (Cooper et al. 2015), and forest losses during stadials, partially due to its

exposed position downwind of the North Atlantic (Huntley et al. 2013). This hypothesis does not

exclude other hypotheses for the differential biodiversity in the SEUS and Europe (e.g. mountain barriers), but low millennial-scale climatic variability may be a potentially important mechanism for maintaining climatic stability and facilitating biodiversity persistence.

2.5.3 Caveats and uncertainties

Our temperature inferences are subject to various uncertainties, but these can be minimized and do not affect the general conclusions. Temporal uncertainty was reduced by using sites with multiple chronological controls near the period of interest. Moreover, 37 of the 42 sites used in the spatial analysis of temperature change have seven or more chronologic controls with several sites in each region containing ten or more controls (Table S1.). When the effect of temporal uncertainty on early-Holocene and mid-Younger Dryas anomalies is assessed, the SEUS remains climatologically distinct from the other two regions (Figure S1.10).

Ambiguity in *Pinus* pollen can confound pollen-based temperature reconstructions because *Pinus* is a common pollen type and the genus contains thirteen species in ENA distributed from Florida to Canada. We have minimized this bias by splitting *Pinus* pollen into northern and southern types (Williams and Shuman 2008) in the modern calibration dataset and fossil-pollen dataset. Lastly, deglacial vegetation dynamics (and fossil pollen records) were governed by multiple climate variables such as moisture availability, growing degree days, and winter severity. We have focused on mean annual temperature, while acknowledging these other effects. The multivariate transfer functions used here are designed to extract multiple climatic signals from fossil assemblages (Overpeck et al. 1985; Ter Braak 1987; Ter Braak et al. 1993; Ter Braak and Prentice 1988) and the independent temperature reconstructions from brGDGTs agree well with fossil-pollen reconstructions of mean annual temperature (Fastovich et al. 2020b;

Watson et al. 2018) (Figure 2.1). Moreover, PCA as a multivariate method helps deconvolve

multiple climatic signals and other controls on fossil-pollen abundance.

The brGDGT temperature estimates also contain uncertainties, largely sourced from

calibration datasets, but the qualitative temperature trends inferred from brGDGTs are robust,

given the small measurement error, as long as MBT values depend on temperature (Sinninghe

Damsté et al. 2018). Various factors contribute to these uncertainties. Differences in brGDGT

distributions between soils and lake sediments can add uncertainty to temperature estimates, if

sediment provenance and brGDGT sources change over time. The use of soil-based brGDGT in

our study sites is supported by accurate reconstructions of modern mean annual temperature at

all sites (Figure S1.4) and accurate reconstructions of soil pH at Bonnett Lake, Silver Lake, and

White Pond (Fastovich et al. 2020b; Krause et al. 2018; Watson et al. 2018). Seasonality in mid-

latitudinal sites has also recently been identified as a source of error in brGDGT temperature

calibrations (Crampton-Flood et al. 2020). One or several of these various uncertainties may be

relevant at Sheelar Lake, where the brGDGT temperature reconstruction disagrees with the

pollen-based reconstructions and other nearby brGDGT reconstructions. Despite these

uncertainties, the consistency in pattern across multiple independent terrestrial and marine

proxies strongly supports the spatial fingerprint reported here.

2.6 Conclusions

Our multi-proxy fingerprint analysis of YD temperatures in ENA suggests at least three

distinct regional climate histories, consistent with shifts in AMOC and atmospheric heat

transport. Florida and the SEUS warmed during the YD, with nearby marine records indicating

YD warming and intensified storminess (Carlson et al. 2008; Toomey et al. 2017). The

northeastern US resembles Greenland in timing of cooling while cooling in the north-central US

was dampened and with a possible lagged onset. These patterns suggest higher climate stability between 30 and 35ºN and support a more complex model of YD climate change than suggested by the standard bipolar seesaw. AMOC shutdown may have caused local warming in the SEUS through dynamical changes to atmospheric circulation induced by NAO positive conditions or changes in the strength of the subtropical cell. Further analysis using ESMs under hosing conditions is necessary to constrain the relevant mechanisms. Dampened millennial-scale climate variability in the SEUS may have helped enhance regional climate stability thereby preserving regional biodiversity.

2.7 Figures
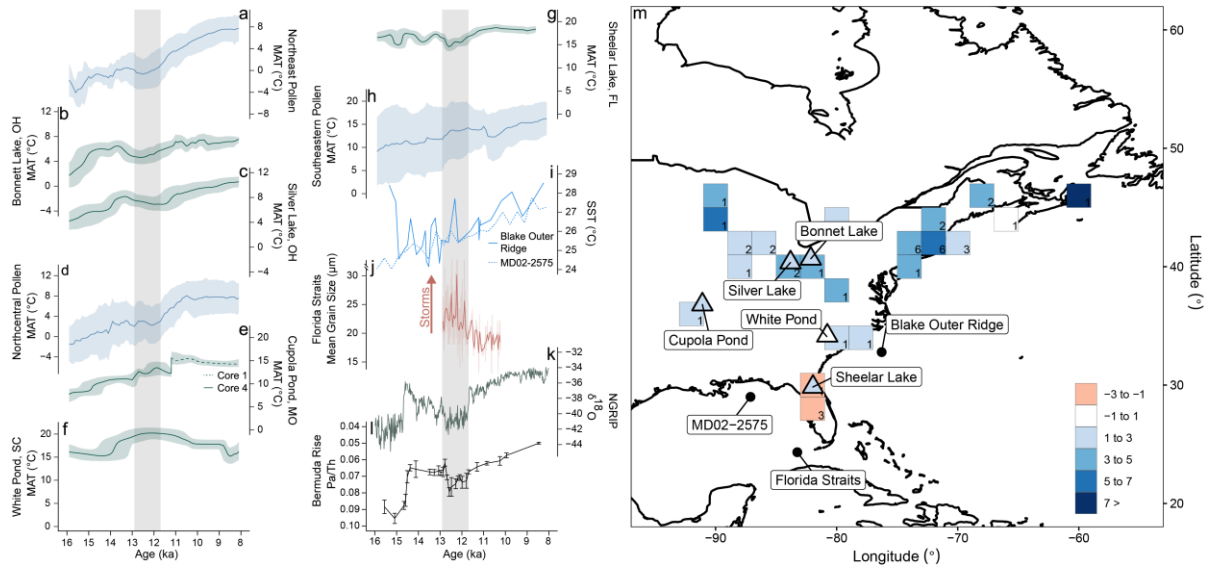
Figure 2.1

A, D, H: Regionally averaged reconstructions of mean annual temperatures for the northeastern (A), north-central (D), and southeastern US (H) based on fossil pollen ensembles. Shading indicates 1-σ intersite standard deviation. B, C, E, F, G: brGDGT-inferred temperatures with the single-site 95% confidence interval. I) Mg/Ca sea surface temperatures (Carlson et al. 2008; Ziegler et al. 2008). J) Mean grain size for core KNR166–2 JPC25 near the Florida Straits as a proxy for hurricane activity (Toomey et al. 2017) with the light green line indicating the raw data and dark green line indicating a 50-year moving mean. K) δ^{18}O oxygen isotopes from NGRIP (Rasmussen et al. 2006). L) AMOC strength, based on Pa/Th ratio (McManus et al. 2004). Gray column indicates the Younger Dryas Interval. M) Temperature differences (°C) from the mid-Younger Dryas (YD, 12.3 ka) to the early Holocene (EH, 11.1 ka) based on brGDGT (triangles) and pollen (grid cells). Anomalies are expressed as EH-YD and color-coded so that blue indicates a cooler YD and red a warmer YD. The number of pollen records is indicated in each grid cell. Other sites from Figure 1 are indicated as black dots.
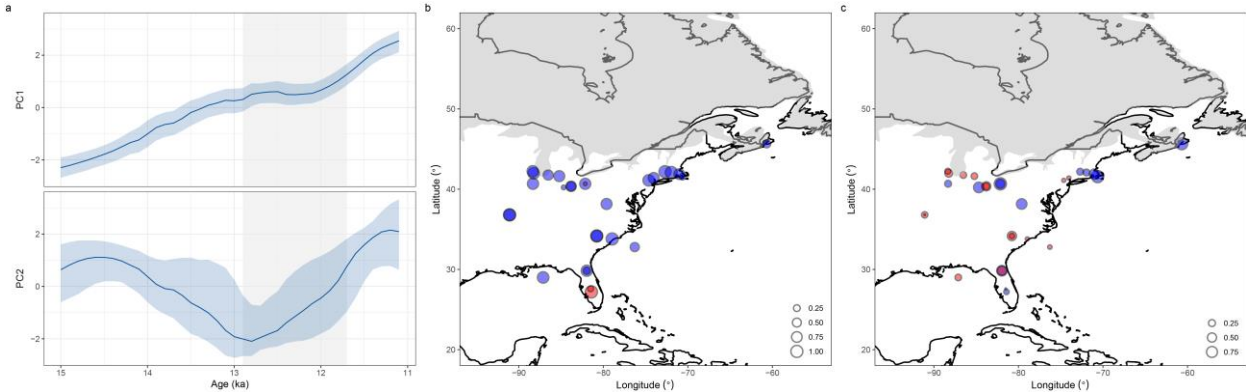
Figure 2.2

A) Time series of PC1 and 2 for all temperature records that extended through the interval of 15 ka to 11 ka. Shading indicates 95% confidence interval. B) PC1 and C) PC2 loadings, with blue indicating positive and red indicating negative loadings. Gray outline represents the extent of the Laurentide Ice Sheet at 12,000 ^{14}C years (Dyke et al. 2003).
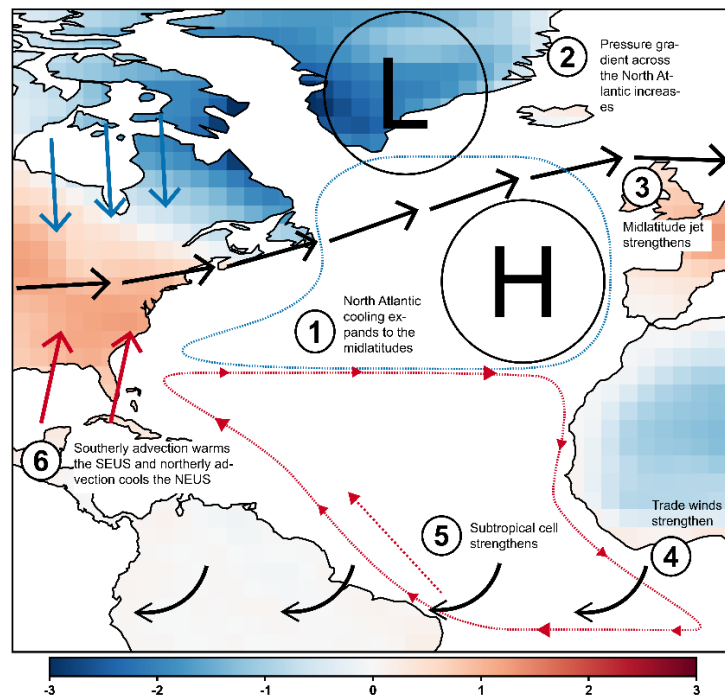
Figure 2.3

Schematic of hypothesized mechanisms for SEUS YD warming and observed temperature fingerprint. Shading corresponds to the slope of a regression of surface temperature on the NAO Index (Hurrell 1995) from the NCEP Reanalysis data product (Kalnay et al. 1996). Positive slope indicates positive correlation of surface temperature to the NAO Index. Solid lines indicate atmospheric processes and dashed lines indicate oceanic processes.

Chapter 3 Spatial fingerprints and mechanisms of precipitation and temperature changes during the Younger Dryas in eastern North America

Note: This chapter is currently in revision as a research article in *Quaternary Science Reviews* with coauthors James M. Russell, Shaun A. Marcott, and John W. Williams.

Citation: Fastovich, D., J. M. Russell, S. A. Marcott, and J. W. Williams, *in revision*: Spatial fingerprints and mechanisms of precipitation and temperature changes during the Younger Dryas in eastern North America. *Quat. Sci. Rev.*

3.1 Abstract

Here we seek to establish the spatial fingerprints of precipitation and temperature changes in eastern North America during the Younger Dryas and explore the role of meltwater forcing in producing this pattern. Our analyses integrate a network of 42 fossil pollen records and 27 other hydroclimate proxy records, three AOGCM experiments with an imposed freshwater forcing, and the TraCE-21ka transient deglacial simulation. A recent synthesis of proxy-based temperature reconstructions suggests that Younger Dryas temperature reversals were limited to sites north of ~35°N, while southern sites experienced either steady warming or a temperature maximum. Proxy records suggest a tripole precipitation pattern during the Younger Dryas and earlier Heinrich events, with the northeastern United States and Florida wetting, while sites from the Great Lakes Region to the Carolinas were dry. Of the AOGCMs analyzed, TraCE-21ka simulates Younger Dryas mean-field temperature and precipitation changes with the most skill but does not simulate warming in the southeastern United States. The likely role of meltwater forcing in producing subregional warming is indicated by the hosing-experiment AOGCMs, which consistently indicate localized warming and tripole precipitation anomalies, but the reconstructed and simulated patterns are poorly aligned, resulting in moderate model skill of mean-field temperature anomalies and negative skill in simulating past fingerprints. The reconstructed tripole helps reconcile prior apparent discrepancies in proxy records about whether

eastern North America was wetter or dryer during the Younger Dryas. Although the hosing-experiment AOGCMs simulate the fingerprints poorly, they show that meltwater forcing can produce subregional warming and wetting in the eastern United States. This is due to enhanced northward heat transport from the Gulf of Mexico induced by a geostrophic adjustment of the midlatitude jet to cooling in the North Atlantic.

3.2 Introduction

Meltwater forcing and the 'bipolar seesaw' hypothesis provides the standard framework for understanding the drivers and patterns of hemispheric-scale climate changes following a reduction in the strength of the Atlantic meridional overturning circulation (AMOC) and subsequent interhemispheric redistribution of heat (Broecker 1998; Stocker 1998). Global proxy-based reconstructions of climate changes following the onset of the Younger Dryas climate event frequently invoke the bipolar seesaw, in which Northern Hemispheric cooling and Southern Hemispheric warming are attributed to a freshwater input into the North Atlantic that weakened the AMOC (e.g. Clark et al. 2012; Pedro et al. 2011; Shakun and Carlson 2010). Atmosphere-ocean general circulation models (AOGCMs) that employ a hosing experimental design with an imposed freshwater forcing into the North Atlantic simulate hemispheric-scale temperature fingerprints that are broadly consistent with the bipolar seesaw hypothesis. However, these simulations also identify regional patterns of temperature change that contrast with the hemispheric patterns and whose mechanisms remain poorly understood (Kageyama et al. 2013, 2010; Liu et al. 2009; Okumura et al. 2009; Tierney et al. 2008). These sub-hemispheric patterns often differ among AOGCMs, due to intermodel differences in the mechanisms of propagation of meltwater forcing in the North Atlantic to other components of the atmosphere-ocean system via altered patterns of atmospheric and oceanic heat transport (Kageyama et al. 2013). Hence,

understanding these mechanisms of propagation of meltwater forcing signals during the Younger

Dryas or other time periods of meltwater forcing at sub-hemispheric scales requires both

intermodel and data-model comparisons at regional to sub-continental scales to assess

simulations in regions of model disagreement.

　　　Eastern North America is a useful region for constraining the effects of meltwater forcing

and other drivers of climate change following the onset of the Younger Dryas, because of

substantive differences among the predicted spatial fingerprints of Earth system model (ESM)

hosing experiments and the dense proxy networks that indicate spatially complex temperature

responses (Fastovich et al. 2020a). Prior hosing experiments demonstrate diverging temperature

responses in eastern North America, with some simulating moderate cooling and others moderate

warming following AMOC weakening (Brown and Galbraith 2016; Ivanovic et al. 2017;

Kageyama et al. 2013). This could be due, in part, to structural differences in the models that

result in competing atmospheric, oceanic, and ice sheet influences on regional climate, as well as

different boundary conditions used in different hosing experiments. Modern climates in eastern

North America are sensitive to changes in the position and configuration of the jet stream

(Wallace and Gutzler 1981) and surface ocean currents (Bjerknes 1964), making this region well

suited for identifying changes in Younger Dryas atmospheric and ocean circulation. Individual

paleoclimatic records suggest that the southeastern United States may have experienced no

cooling during the Younger Dryas or even an antiphased warming (Arnold et al. 2018; Grimm et

al. 2006; Watts 1980a). The most recent synthesis of Younger Dryas temperature changes in

eastern North America reported an apparent temperature dipole, identified through principal

component analysis, following the onset of the Younger Dryas, in which temperatures decreased

in the north-central and northeastern United States (Fastovich et al. 2020a). South of ~35°N,

most sites indicate monotonic warming through the Younger Dryas, with several Florida sites indicating a thermal maximum during the Younger Dryas, perhaps due to a reconfigured midlatitude jet stream (Fastovich et al. 2020a).

There are no recent syntheses of precipitation changes in eastern North America following the onset of the Younger Dryas, and paleoclimatic proxies and models show considerable disagreement. Proxy records in eastern North America suggest both a wetter (Gonzales and Grimm 2009; Menking et al. 2012; Shuman et al. 2001; Voelker et al. 2015) and drier Younger Dryas climate (Newby et al. 2009, 2000), with little clarity on spatial pattern. A shift toward winter precipitation is indicated by the $\delta^{18}O$ of sediment calcite (Ellis et al. 2004; Mandl et al. 2016) in sites in the northeastern United States and is attributed to a shifted polar vortex causing differential water sourcing (Kirby et al. 2002b). Few global-scale hosing experiments have focused on precipitation signals in extratropical regions, with Kageyama et al. (2013) reporting drying in the North Atlantic and a precipitation dipole in the equatorial Atlantic. Intrahemispheric analyses of Younger Dryas precipitation changes identify highly regional changes to precipitation, with wetting in regions of eastern North America and drying in central Europe and Siberia (Renssen et al. 2018). A mesoscale simulation of the Last Glacial Maximum in North America indicates that the seasonal routing of storm tracks across eastern North America was greatly influenced by ice sheet orography and the pressure and temperature gradients adjacent to the Laurentide Ice Sheet (Bromwich et al. 2005, 2004), but a similarly detailed examination of Younger Dryas precipitation changes is lacking. This model and data gap has so far precluded a comprehensive assessment of Younger Dryas hydroclimate patterns and underlying processes.

A better understanding of the seasonal patterns of Younger Dryas climate changes is also important to understanding mechanisms. For instance, moraine and snowline records in Greenland (Denton et al. 2005), plant-indicator temperature assessments in Europe (Bjorck et al. 2002; Isarin and Bohncke 1999), and fossil-beetle assemblages (Atkinson et al. 1987) have been used to infer little change in summer temperatures and pronounced winter cooling during the Younger Dryas. European summer warming has been attributed to atmospheric blocking by the Fennoscandia Ice Sheet from ESM simulations (Schenk et al. 2018) while winter cooling in Greenland may be linked to wintertime sea ice expansion (Atkinson et al. 1987; Buizert et al. 2014). In eastern North America, the seasonal signal of Younger Dryas climate changes is poorly understood. The rapid re-expansion of spruce throughout much of the northcentral United States with Younger Dryas onset (Shane and Anderson 1993) has been interpreted as a response to pronounced winter cooling during the Younger Dryas (Shuman et al. 2002). However, extracting seasonal signals from fossil-pollen abundances is possible in theory but difficult in practice, because of shifting spatiotemporal covariance structures among climate variables that can lead to spurious results if contemporary covariances are assumed to be constant over time (Juggins 2013). Meltwater forcing simulations for the Last Glacial Maximum and Bølling-Allerød, conversely, suggest that meltwater-driven cooling was a summer phenomenon in eastern North America, while temperatures increased in the winter (Ivanovic et al. 2017; Otto-Bliesner and Brady 2010).

Here we seek to 1) better describe the spatial fingerprint of precipitation changes in eastern North America during the Younger Dryas, 2) understand the mechanisms producing the spatial fingerprints of temperature and precipitation change in eastern North America, with particular reference to meltwater forcing, 3) compare proxy climate reconstructions to AOGCM

hosing experiments, and 4) use the AOGCMs for insight into the seasonal signals of Younger Dryas climate changes in eastern North America. To this end, we combine the Younger Dryas mean annual temperature reconstructions from Fastovich et al. (2020a), a new set of spatially explicit reconstructions of total annual precipitation in eastern North America, three previously run AOGCM experiments with an imposed freshwater forcing into the North Atlantic (Brown and Galbraith 2016; He et al. 2013; Ivanovic et al. 2018a), and the TraCE-21ka deglacial transient simulation with orbital, ice sheet, greenhouse gas, and meltwater forcings (He 2011; He et al. 2013; Liu et al. 2009). (Hereafter, HadCM3, CM2Mc, and TraCE-MWF will be referred to as "hosing experiments" because meltwater is the primary forcing changed within these simulations.) The proxy-based precipitation reconstructions are based on a network of 42 well-dated fossil-pollen records and prior reconstructions from the literature. We compare the annual proxy reconstructions to simulated seasonal fingerprints of temperature and precipitation, employing a skill score (Hargreaves et al. 2013) with alternative null hypotheses designed to discriminate model skill in both the magnitude and fingerprint of Younger Dryas climate changes. We find that TraCE-21ka most accurately simulates Younger Dryas climate changes but does not predict the southeastern United States warming indicated by proxy records. Conversely, the AOGCM hosing experiments consistently indicate subregional patterns of warming and wetting in eastern North America, but do not compare well to the spatial fingerprints of simulated Younger Dryas climate changes in eastern North America, likely because of imperfect boundary conditions (Brown and Galbraith 2016; He et al. 2013; Ivanovic et al. 2018a). Comparisons among the three hosing experiments indicate spatial coherence in temperature and precipitation changes following hosing, suggesting a common mechanism. We combine the model and proxy data to further refine hypothesized atmospheric mechanisms for

seasonal warming in southeastern United States in response to enhanced meltwater forcing during the Younger Dryas.

3.3 Paleoclimatic Simulations

3.3.1 Overview

Climate changes during the Younger Dryas and the most recent deglaciation are the result of changes to insolation, atmospheric CO_2 concentration, ice sheet configuration, vegetation feedbacks, meltwater forcing, sea level, and interactions among these forcings. Global- (Shakun and Carlson 2010) and many regional-scale analyses (Fastovich et al. 2020a) of deglacial temperature reconstructions identify atmospheric CO_2 concentration and millennial-scale climate variability as the primary and secondary modes of variability, respectively. Pa/Th records from the North Atlantic suggest at least a slowdown of AMOC during the Younger Dryas (McManus et al. 2004) and perhaps a brief shutdown, given that short shutdowns would not be captured by Pa/Th which has a response time of ~500 years (Marchal et al. 2000; McManus et al. 2004; Yu et al. 1996). These reconstructions of AMOC strength align closely with millennial-scale climate oscillations (McManus et al. 2004), leading to hypotheses that enhanced freshwater inputs into the North Atlantic Ocean caused the Younger Dryas (Broecker et al. 1985; Clark et al. 2002; Li and Born 2019; Rahmstorf 2002). Prior proxy-based reconstructions of the spatial fingerprint of Younger Dryas temperature anomalies suggest a complex pattern, with temperature reversals in northern sites and warming in southern sites (Fastovich et al., 2020). These patterns cannot be readily explained by thermodynamic forcings such as orbital and greenhouse gas forcing, and instead require dynamical changes in ocean and atmospheric heat transport. In light of this, we choose to assess the potential role of freshwater forcing in driving Younger Dryas climate changes in eastern North America in a paleoclimate data-model framework.

The TraCE-21ka experiments (Section 3.3.2) offer a full transient simulation of the last deglaciation, with forcings prescribed for insolation, ice extent and sea level, atmospheric greenhouse gas concentrations, and meltwater pulses (He 2011). Single-forcing experiments are also available, including a meltwater-only forcing (He et al. 2013). Because the prescription of meltwater forcings in AOGCMs remains an area of high uncertainty, as does the modeled response of the climate system to meltwater inputs, we opted to also analyze two additional AOGCM forcing experiments, using the Climate model v2 at Coarse Resolution (CM2Mc, Section 3.3.3) and Hadley Centre Coupled Model 3 (HadCM3, Section 3.3.4) AOGCMs. Note, however, that several of these experiments are initialized with boundary conditions that imperfectly match the Younger Dryas, which will lead to data-model mismatch. Hence, we employ both data-model and model-model analyses to identify areas of agreement and disagreement, and to identify potential mechanisms that produce subregional patterns of warming and wetting in eastern North America during the Younger Dryas.

3.3.2 Community Climate System Model 3: Simulation of the Transient Climate of the Last 21,000 Years Meltwater Forcing Experiment (TraCE-MWF)

The Transient Climate of the Last 21,000 Years Meltwater Forcing Experiments (TraCE-21ka) are full deglacial simulations with the Community Climate System Model, version 3. The primary experiments, which have become pillars of our understanding of deglacial climate evolution, include the transient forcings of greenhouse gas concentration, ice sheet configuration, meltwater fluxes, and orbitally induced seasonality variations during the deglacial period (He 2011; Liu et al. 2009). He et al. (2013) also performed separate "single forcing" experiments where individual forcings evolved through the deglacial simulation while all others were held constant at Last Glacial Maximum values. Here, we use both the meltwater forcing experiment in

which meltwater is first added to the deglacial simulation at 19.0ka (Trace-MWF) and the full

deglacial simulation (TraCE-21ka). To compare to the proxy record, we treat the mid-Younger

Dryas as the 'hosed' climate state (100-year mean centered on 12.3 ka) and the early-Holocene

as the 'unhosed' climate state (100-year mean centered on 11.1 ka) in both TraCE-21ka and

TraCE-MWF. The hosed interval corresponds to a freshwater forcing of 20 m/kyr (~0.229 Sv)

entirely through the St. Lawrence River and the unhosed interval coincides with a total forcing of

7.98 m/kyr (~0.092 Sv) unevenly spread across the St. Lawrence River, Hudson Strait, Barents

Sea, North Sea and Ross Seas (He 2011).

3.3.3 Climate model v2 at Coarse Resolution (CM2Mc)

CM2Mc is a reconfiguration of the Geophysical Fluid Dynamics Laboratory (GFDL)

coupled AOGCM (v2.1) to run on a coarser 3° grid (Galbraith et al. 2011). Brown and Galbraith

(2016) performed hosed simulations where 0.2 Sv of freshwater was applied in the North

Atlantic by overriding the land-to-ocean ice calving flux. The model was run at equilibrium for

1,000 years, then hosing was applied for an additional 1,000 years. Hosing was stopped and the

simulation continued to an equilibrium state for 1,000 years. In addition to hosing, obliquity and

precession parameters were altered to minimize and maximize Northern Hemispheric

seasonality. Obliquity was set to either 22.0 or 24.5° and precession was set to either 90 or 270°,

producing four simulations. Here, we use the average of these four experiments as in McGee et

al. (2018a) and use the last 100 years of the "unhosed" and "hosed" conditions to represent the

mean state of the simulations. The model was initialized at 180 ppm atmospheric CO_2

concentration and Last Glacial Maximum ice sheet configurations from the Paleoclimate Model

Intercomparison Project 3. In all experiments, the AMOC rapidly weakens following the onset of

freshwater hosing (see Figure 2 in Brown and Galbraith, (2016)). Northern Hemispheric annual

average surface temperatures decrease zonally after AMOC weakening, with eastern North America emerging as the only region of simulated anomalous warming in the Northern Hemisphere (Brown and Galbraith 2016). Prior analyses of these simulations have demonstrated accurate simulations of hosed climate states in the global equatorial region and the western United States (McGee et al. 2018a,b).

3.3.4 Hadley Centre Coupled Model 3 (HadCM3)

The HadCM3 simulations used here simulate deglacial climate in response to transient forcing of ice-sheet configuration, meltwater input, and meltwater routing during Heinrich Stadial 1 (Ivanovic et al. 2018a). The transient forcings are driven by the glacial isostatic adjustment model ICE-6G_C VM5a (Peltier et al. 2015) to represent ice sheet forcing of climate from 19.0 to 15.5 ka, with greenhouse gas concentrations set to Last Glacial Maximum conditions, as in TraCE-MWF and CM2Mc. The freshwater forcing applied in this simulation is smaller than the TraCE-MWF or the CM2Mc simulations: rates of freshwater addition averaged ~0.05 Sv, never exceeding 0.09 Sv, and the meltwater is applied throughout regions of likely meltwater routing, rather than entirely into the North Atlantic (Ivanovic et al. 2018a). Despite a smaller addition of meltwater, changes to the AMOC at the beginning and end of the simulation agree well with Pa/Th ratios from a compilation of North Atlantic proxy records (Ivanovic et al., 2018). Here, we use the mean of the first 100 years of the simulation to represent the "unhosed" climate state and the mean of the last 100 years as the "hosed" climate state, as in Ivanovic et al. (2018a).

3.4 Methods

3.4.1 Proxy-based annual precipitation and temperature reconstructions

Our annual precipitation and temperature reconstructions are each based largely on a network of well-dated fossil-pollen records for which climate inferences are derived from transfer functions calibrated to modern pollen abundances and climate. This network of fossil-pollen sites was developed by Fastovich et al. (2020a) with data from the Neotoma Paleoecology Database (Williams et al. 2018) and sought to balance chronological control quality, temporal resolution, and spatial coverage in eastern North America. The mean annual temperature reconstructions are supplemented by estimates based on branched glycerol dialkyl glycerol tetraethers, an organic biomarker sensitive to temperature change (Weijers et al. 2007), while the total annual precipitation reconstructions are supplemented by a literature review of proxy records that infer precipitation change during freshwater-hosing events in the North Atlantic (Table 3.1).

We reconstructed mean annual precipitation and mean annual temperature by averaging three transfer function methods. The modern analog technique (MAT, Overpeck et al. 1985) is a nearest-neighbor approach to paleoclimatic reconstructions in which climate variables are reconstructed by identifying the most similar samples (i.e. modern analogs) in the modern pollen dataset and assigning the associated climate variables to the fossil sample (Chevalier et al. 2020). The accuracy of MAT-based paleoclimatic reconstructions in North America improves when using the average of the nearest three to seven modern analogs and dividing the modern pollen training data into regional groups (Williams and Shuman 2008). Weighted averaging and weighted averaging-partial least squares use the modern-pollen training data to produce a unimodal response for each individual pollen taxon across the climatic gradient for the climate

variable to be reconstructed (i.e. correspondence analysis; Ter Braak and Looman 1986). In weighted averaging, this climate response function can be applied directly to fossil-pollen abundances to reconstruct past climate changes. Weighted-averaging partial least squares improves the fit of the taxa-species gradient by incorporating information from linear combinations of the residuals of the weighted averaging technique (Chevalier et al. 2020; Ter Braak et al. 1993; Ter Braak and Juggins 1993). We trained these transfer functions on modern pollen abundances from the North American Modern Pollen Database (Whitmore et al. 2005) and all fossil-pollen taxa were geographically split as recommended in Williams et al. (2008) (see Fastovich et al. (2020a) for a detailed description of the geographic splitting procedure).

The seasonal patterns of past climate changes is a central question in paleoclimatology (e.g. the Holocene Temperature Conundrum, Liu et al. 2014; Marcott et al. 2013) and many pollen-based paleoclimatic reconstructions have reconstructed summer and/or winter temperatures or bioclimatic correlates such as growing degree days and winter minimum temperatures (e.g. Bartlein et al. 2011; Chevalier et al. 2020). There is a strong autecological basis for pollen-based seasonal temperature reconstructions because winter minima and summer growing season warmth are distinct controls on plant abundances and distributions (Woodward 1987). However, in practice, because transfer functions assume stable covariance structures among variables, reconstructions of secondary or tertiary climatic variables are subject to higher uncertainties and potential biases (Juggins 2013). Seasonal temperature inferences for the late Pleistocene in eastern North America are particularly challenging given the likelihood of past no-analog climates with a higher-than-present temperature seasonality (Williams et al. 2001). These challenges can be partially overcome by ensuring orthogonality among climate variables in the training datasets and by avoiding reconstructions of tertiary variables, which are more sensitive

to biases caused by shifting autocorrelations (Salonen et al. 2019). Recent work with machine learning models demonstrates successful reconstruction of various secondary climate variables with a qualitative agreement between machine learning-based reconstructions and the classic transfer function approaches used here (Salonen et al. 2019). Poor performance with classical transfer function approaches affected the modern analog technique most when no close analogs were available (Salonen et al. 2019). Here, we minimize the potential effects of no-analog climates and shifting covariance structures by limiting our reconstructions to two variables – mean annual temperature and precipitation – that are spatially orthogonal in eastern North America and by not attempting to extract seasonal signals from the fossil pollen data. Furthermore, we use an ensemble of transfer functions to better reduce the sensitivity of any single approach to no-analog conditions (Salonen et al. 2019).

Our temperature proxy network also includes reconstructions based on branched glycerol dialkyl glycerol tetraethers (brGDGT), organic compounds produced by microbes sensitive to environmental changes. We include brGDGT temperature reconstructions for five sites: Bonnett Lake, OH (Fastovich et al. 2020b), Silver Lake, OH (Watson et al. 2018), White Pond, SC (Krause et al. 2018), Sheelar Lake, FL (Fastovich et al. 2020a) and Cupola Pond, MO (Fastovich et al. 2020a). brGDGT analytical methods at White Pond (Krause et al., 2018) and Silver Lake (Watson et al. 2018) used current analytical methods at the time of publication and were calibrated using the Weijers et al. (2007) soil calibration. We used updated analytical methods at Bonnett Lake, Sheelar Lake, and Cupola Pond, calibrated using the De Jonge et al. (2014) calibration. Earlier comparisons of soil and lacustrine calibrations (e.g. Russell et al. (2018)) at these sites demonstrates more accurate reconstructions of modern mean annual temperatures when using soil-based calibrations (Fastovich et al. 2020b), although recent evidence has

identified that brGDGT compounds may be predominantly produced in the warm season (Martinez-Sosa et al. 2021; Raberg et al. 2021).

We support fossil-pollen precipitation reconstructions with various records of precipitation-sensitive proxies (e.g. speleothem isotopic compositions, loess deposits, lake-level reconstruction) from the literature (Table 3.1, Figure S2.1). Aligning with our aim to diagnose the role of freshwater hosing we used any precipitation records that 1) span a North Atlantic freshwater forcing event (i.e. Heinrich events) thought to cause a reduction of the AMOC over the last 100,000 years, 2) include a clear interpretation of precipitation changes within the original publication, 3) fall within the spatial domain of eastern North America, and 4) are chronologically constrained by radiometric dating. Our literature review yielded 27 sites across eastern North America and the Bahamas. Of these 27 records, 21 span the Younger Dryas while six span one to several Heinrich events, of which two are in eastern North America (Brooksville Ridge Cave, Buckeye Creek Cave; Table 3.1) and the other four are in the Bahamas (AB-DC-12, AB-DC-01, AB-DC-03, and AB-DC-09). Brooksville Ridge Cave is near to Lake Tulane, Florida (150 km) and share common climate changes across several Heinrich events (Grimm et al. 2006; van Beynen et al. 2017). Hence, our interpretations of Younger Dryas precipitation changes is likely insensitive to the inclusion of records that only span Heinrich events.

The majority of sites within eastern North America are lake-level reconstructions (e.g. Newby et al. 2009, 2000) and biomarker-based precipitation reconstructions (e.g. Arnold et al. 2018). Speleothem records were most common in the Bahamas and frequently spanned several Heinrich events, but rarely included the Younger Dryas (e.g. Arienzo et al. 2017; Springer et al. 2014; Warken et al. 2019). In all records, we use the interpretation of precipitation changes within the original publication and report the results as qualitative precipitation changes during

hosed climate states relative to an unhosed baseline. These qualitative interpretations cannot be used when calculating climate model skill and are not included during those analyses.

3.4.2 Climate model skill

We quantitatively compare the Younger Dryas mean annual precipitation and mean annual temperature reconstructions to the climate model simulations of seasonal variables using a spatially debiased metric of model skill that assesses the accuracy and precision of simulated precipitation and temperature changes and the spatial patterns of those changes. Our comparison of annual proxy reconstructions to seasonal climate signals is intended to identify possible seasonal signals in the Younger Dryas. For example, close agreement between reconstructed mean annual temperature and simulated winter temperature might indicate that Younger Dryas wintertime temperature changes are most strongly expressed in the proxy network. We use a model skill score defined in Hargreaves et al. (2013):

$$S = 1 - \sqrt{\frac{\Sigma(m_i - o_i)^2 - \Sigma(e_i^2)}{\Sigma(n_i - o_i)^2 - \Sigma(e_i^2)}}$$

where m_i is the simulated results, n_i is the reference results, o_i is the observed (proxy-based) values, and e_i is the 1-standard deviation error of the proxy reconstructions. In this metric, the data-model disagreements (m_i-o) are both assessed relative to the uncertainty in the proxy reconstructions (e_i) and normalized relative to a denominator containing a null model of data-model differences (n_i-o_i). A skill score of 1 indicates perfect AOGCM skill relative to the null model, while a negative value indicates that climate model simulations are less skillful than the null model.

We use two values for the reference results (n_i) that correspond to two null hypotheses. A reference value of zero assesses climate model skill in simulating the sign and magnitude of reconstructed Younger Dryas climate change against a null model of no climate change (Hargreaves et al. 2013; Lora 2018; Lora and Ibarra 2019). For this first test, a model can perform skillfully if it correctly simulates the spatial mean sign and magnitude of Younger Dryas climates, even if the spatial fingerprint is incorrect. The second null hypothesis additionally assesses model skill in simulating the reconstructed spatial fingerprint of climate change during the Younger Dryas by setting the reference results to the mean of the proxy reconstructions (Hargreaves et al. 2013). This test is more stringent and effectively tests whether a model can skillfully simulate the spatial fingerprint of climate change. For this test, negative values indicate a model performed worse than assuming spatially uniform climate change. We performed all model-skill calculations on hosed climate anomalies for the AOGCM simulations and proxy reconstructions. For the proxy data, we interpolated reconstructed temperature and precipitation onto even 100-year intervals at each site and then calculated the difference between mid-Younger Dryas and the early-Holocene (i.e. 12.3 ka – 11.1 ka).

The spatial distribution of the proxy records can influence the resulting skill calculation in two ways. First, the individual proxy sites vary in their distance to climate model grid cells. We address this issue by bilinearly interpolating the simulated climate variables to proxy site location to more accurately compare climate simulations and proxy reconstructions. Second, spatial biases in the distribution of proxy records can skew model skill scores. Within our proxy network, the higher spatial density of sites in the northeastern United States and the Great Lakes regions and the fewer sites in the southeastern United States will tend to favor models that more accurately simulate the climate of the northeastern United States. We address this by spatially

debiasing the proxy network by resampling sites at a grid level 10,000 times, where a single site

is sampled for every grid cell. Resampling resulted in a distribution of model skill scores, from

which we report the median and the 95% confidence interval.

We estimated error in the proxy climate anomalies using a bootstrapping approach in

which initial transfer function reconstruction error was propagated through to the climate

anomalies (Figure S2.2). First, each of the transfer functions were cross-validated and then

bootstrapped to produce an ensemble of possible annual precipitation and mean annual

temperature estimates for each fossil-pollen sample. We used the default bootstrapping

procedure in the *rioja* R-package (Juggins 2015) that subsamples the training data, creating a

new transfer function and associated climate reconstruction (i.e. bagging without replacement).

Second, the ensemble of climate reconstructions from each transfer function was randomly

sampled and then averaged. At each site, this ensemble of MAT/WA/WA-PLS averaged climate

reconstruction time series was randomly sampled and interpolated at 100-year intervals. We then

took the difference between mid-Younger Dryas and the early-Holocene (i.e. 12.3 ka – 11.1 ka)

from this randomly sampled and interpolated time series. This interpolation and differencing was

repeated 100,000 times with all resampling assuming a uniform distribution, producing an

ensemble of hosed climate anomalies at each site. We used the mean and standard deviation of

this ensemble as the observed values (o_i) and error (e_i), respectively, for model skill calculations.

3.5 Results

3.5.1 Spatial fingerprint of Younger Dryas precipitation

The annual precipitation reconstructions demonstrate a tripole of precipitation anomalies

during the Younger Dryas, relative to the early Holocene (Figure 3.1). Increased annual

precipitation is reconstructed in the northeastern United States and Florida while a broad swath

of drying is recorded from the Great Lakes region to the Carolinas (Figure 3.1). In the Great

Lakes region, palynological signals of drying are often associated with rapid increases in *Pinus*

abundance and associated declines in *Picea* and *Abies*, which translates to an inferred abrupt

decrease in precipitation, as in Bonnett Lake, OH (Fastovich et al. 2020b). These reconstructions

appear consistent with the climatic tolerances of black spruce (*Picea mariana*) and balsam fir

(*Abies balsamea*), which occupy wetter climates (Burns and Honkala 1990). Moreover, modern

pollen abundances of these species tend to be higher in wetter climates (Prentice et al. 1991;

Williams 2006). Local declines of no-analog mesic taxa such as ash (*Fraxinus*), hornbeam

(*Carpinus*), and hop hornbean (*Ostrya*) at the onset of the Younger Dryas also likely contributed

to the magnitude of reconstructed drying. However, other sites in the Great Lakes region show

an increase in both *Picea* and *Abies* at the onset of the Younger Dryas, translating to little change

in annual precipitation through the Younger Dryas, as in Crystal Lake, IL (Gonzales and Grimm

2009). Changes in the relative abundances of *Pinus, Picea*, and *Abies* also a key determinant of

precipitation reconstructions in the northeastern United States, where several sites with

reconstructed drying also have high *Pinus* abundances while sites that reconstruct wetting have

high *Picea* and *Abies* abundances (e.g. Blood Pond vs. Deep-Taunton Pond, Shuman et al. 2004).

In Florida, the inference of wetter conditions during the Younger Dryas is based on the presence

of high abundances of southern populations of *Pinus.* At present and during the Holocene, these

southern pine species occupied a region with much higher precipitation than northeastern pine

species, yielding reconstructions of a wet Younger Dryas (Grimm et al. 2006; Thompson et al.

1999a).

3.5.2 Simulated climate patterns and model performance

Hosing experiment simulations (CM2Mc, HadCM3, TraCE-MWF) of precipitation and temperature change following a weakening of the AMOC are spatially coherent and indicate subregional patterns of warming and wetting in eastern North America in response to meltwater forcing, which may signal a common atmospheric control (Figure 3.2, Figure 3.3). The tripole pattern of precipitation changes is most strongly expressed in winter and spring, and is characterized by meltwater-induced wetting throughout eastern North America, adjacent to lower- and higher-latitude drying centered on the Bahamas and maritime Canada, respectively (Figure 3.2). All models simulate the smallest precipitation changes in the summer, with differences among models in sign: precipitation decreases throughout much of eastern North America in TraCE-MWF and HadCM3, while moderate wetting is present in CM2Mc and TraCE-21ka (Figure 3.2). The TraCE-21ka simulation presents the most uniform and weakest response to hosing across the year with drying centered on the Canadian Shield and the Bahamas, and slight wetting in isolated regions throughout eastern North America (Figure 3.2). Although both the proxy data and the hosing experiments suggest a tripole pattern for precipitation anomalies and although there is good intermodel agreement, the simulated tripole is antiphased to the reconstructed tripole (Figure 3.2). Data-model agreement is good in the Bahamas, where numerous speleothem records demonstrate dry conditions over successive Heinrich events (Arienzo et al. 2017; Fensterer et al. 2013; Warken et al. 2019) and all models demonstrate persistent drying throughout the year.

All hosing experiments simulate seasonal warming in eastern North America following a reduction of the AMOC, but with differences among models in the spatial fingerprint and seasonal timing (Figure 3.3). Widespread warming is present in eastern North America during

the spring (MAM) and localized warming in the winter (DJF, Figure 3.3). The TraCE-MWF simulation yields warming throughout the year in eastern North America with the greatest warming consistently centered on the Carolinas, while HadCM3 and CM2Mc simulate a cooling isolated to summer and fall (Figure 3.3). In TraCE-21ka, steep temperature gradients consistently occur along the periphery of the Laurentide Ice Sheet, while the hosing experiments place the greatest changes to temperature gradients near New England and the North Atlantic (Figure 3.3). The hosing experiments demonstrate subregional warming in eastern North America as does the proxy record, but the regions of warming are incorrectly placed relative to the data (Figure 3.3). Hence, as for the precipitation results, both the proxy data and hosing experiments indicate spatially complex climate responses in eastern North America but disagree over the placement of these features. Despite the data-model disagreement, the coherence among the hosing experiment is striking given their somewhat different boundary conditions.

The data-model disagreements in spatial fingerprints result in low climate model skill scores for the hosing experiments and comparatively higher scores in TraCE-21ka. Among all models, TraCE-21ka most skillfully simulates temperature changes with all seasons demonstrating skill greater than the null (Figure 3.4A). Among the hosing experiments, CM2Mc is most skillful at simulating reconstructed Younger Dryas temperature change with all seasons performing better than the baseline of no change (Figure 3.4A). TraCE-MWF simulations are more skillful than the null in winter and spring, while summer and fall do not outperform the null (Figure 3.4A). HadCM3 is the least skillful model with most seasons underperforming the null of no temperature change (Figure 3.4A). Only TraCE-21ka is able to accurately simulate the spatial fingerprint of temperature change, based on setting the reference climate state to the mean of the proxy network (Figure 3.4B, Hargreaves et al., 2013). The strongly negative skill scores for most

seasons and models confirm the visual impression that the simulated temperature fingerprints are antiphased with proxy fingerprints (Figure 3.4B).

The two tests of precipitation skill (Figure 3.5A, B) show similar results because regional-scale average precipitation anomalies from the proxy record are near zero and so the two null reference states produce similar skill scores. The strongly negative skill scores across all hosing experiments and seasons are consistent with the antiphased spatial patterns of precipitation changes between the climate models and fossil-pollen reconstructions (Figure 3.2, Figure 3.5). Poor skill in TraCE-MWF is notable as an analysis of mean annual precipitation across North America using TraCE-21ka, which incorporates all relevant deglacial climate forcings, shows some skill (Figure 3.2, Figure 3.5), e.g. in simulating deglacial drying in the southwestern United States (Lora and Ibarra 2019). Indeed, TraCE-21ka is the only model experiment that outperforms the null with scores similar to those calculated by Lora and Ibarra (2019).

3.5.3 Simulated mechanisms for regional meltwater-induced warming

Although the spatial fingerprints of the proxy reconstructions for the Younger Dryas and simulated temperature anomalies for the hosing experiments disagree in detail (Figure 3.2, Figure 3.3), all hosing-experiment AOGCMs shown here simulate some warming in eastern North America during hosing events (Figure 3.3). Here we explore the hosing experiment AOGCM simulations to better understand the potential atmospheric mechanisms for simulated warming and wetting, while noting that boundary condition mismatches and low skill scores mean that these mechanisms cannot be confidently verified against the data. A common feature in the three hosing experiments is enhanced northward transport over the Gulf of Mexico, facilitating the convergence of heat and moisture in eastern North America (Figure 3.6). This

northward transport is seasonal and tends to be the greatest in fall, spring, and winter, while

slightly weakened in the summer and is likely a result of changes in surface pressures (Figure

3.6). Anomalously high pressure in the subtropical and midlatitude Atlantic is greatest in spring

and fall, coincident with large surface wind anomalies over the Gulf of Mexico (Figure 3.6).

Lower pressures over eastern North America in seasons with warming and wetting are associated

with an anomalous pressure gradient that contributes to the magnitude of surface wind anomalies

(Figure 3.6). Summer demonstrates the relevance of changes to mean sea-level pressures as all

hosing experiments simulate the smallest mean sea-level pressure anomalies, corresponding to

little southern transport and cooling in CM2Mc and HadCM3 (Fig. 6). These patterns also

explain spatial patterns of precipitation changes, where seasons that have the greatest southern

transport simulate the greatest wetting in all models (Figure 3.2, Figure 3.6).

Shifts in the configuration of the midlatitude jet stream are also an important control on

the climate of eastern North America, with interactions between jet stream position and patterns

of regional warming. Large cooling in the North Atlantic and moderate cooling in the

midlatitude Atlantic (Figure 3.3) increases the average regional latitudinal temperature gradient

and thereby alters the geopotential height gradient across the Northern Hemisphere Atlantic

Ocean in all models. This is visible as a lowered 500 mb geopotential over the North Atlantic

with comparatively small changes in the midlatitude Atlantic and eastern North America (Figure

3.7). Temperature is a first-order control on geopotential height, so decreases in the mean

geopotential height over the North Atlantic are greatest in winter and spring when surface

temperature anomalies are the most negative (Figure 3.3, Figure 3.7). The spatially variable

changes in geopotential height lead to enhanced strength of the midlatitude jet stream over the

North Atlantic, due to a geostrophic adjustment to the increased temperature gradient (McGee et

al. 2018b), while largely unchanged over eastern North America (Figure 3.7, Figure S2.3).

Divergence of the upper-level winds (200 mb) indicates that the spatially heterogeneous changes

in the strength of the midlatitude jet stream over the North Atlantic and eastern North America

result in 1) enhanced divergence over eastern North America that is greatest in seasons that

simulate widespread warming and wetting and 2) enhanced convergence over the midlatitude

Atlantic (Fig. 8). Notably, upper-level divergence is mirrored by the mean sea level pressure

changes over eastern North America and the North Atlantic (Figure 3.6, Figure 3.8). Upper-level

convergence drives positive mean sea-level pressure anomalies across the Atlantic and

divergence drives negative mean sea-level pressure anomalies over eastern North America

(Figure 3.6, Figure 3.8), suggesting that the geostrophic adjustment of the midlatitude jet stream

causes the simulated pressure, transport anomalies, and warming and wetting in eastern North

America.

Conversely, little cooling is simulated in the North Atlantic during the summer leading to

an unchanged latitudinal temperature gradient in the North Atlantic, unchanged jet stream, and a

breakdown of anomalous mean sea level pressure changes and southern transport into eastern

North America (Figure 3.2, Figure 3.7). These hypothesized mechanisms suggest that

atmospheric reorganization following the slowdown or shutdown of the AMOC may have

primarily affected winter temperatures in eastern North America and may explain a lack of

Younger Dryas cooling in temperature records from the southeastern United States (Figure 3.1,

Figure 3.6)(Fastovich et al. 2020a). Most of these patterns are missing in TraCE-21ka; rather, the

dominant control on atmospheric dynamics is the changes in the configuration of the Laurentide

Ice Sheet, recognizable in the northerly wind anomalies near the Laurentide (Figure 3.6, Figure

3.7, Figure 3.8; see Section 3.6.3.).

3.6 Discussion

3.6.1 Spatial fingerprints of climate change in eastern North America during the Younger Dryas: reconciling proxy signals and possible seasonal signals

In these analyses, two central features emerge from the paleoclimatic proxy reconstructions: 1) an apparent latitudinal gradient in temperature anomalies, with cooling north of ~35°N and warming south of ~35°N, and 2) an apparent tripole in precipitation anomalies, with wetting in Florida and New England and drying across a broad swath from the upper Midwest to the Carolinas (Figure 3.1). Ten of the 11 temperature reconstructions for sites south of Browns Pond, VA (38.2 °N) all demonstrate warming through the Younger Dryas (Figure S2.4) while all sites north of Browns Pond demonstrate Younger Dryas cooling (Figure 3.1). Principal component analyses suggest a spatial dipole associated with the millennial mode of climate variability, in which- southern sites have small millennial-scale spatial loadings while northern sites have large millennial-scale spatial loadings (Fastovich et al. 2020a). Establishing the tripole in precipitation changes helps resolve prior contradictions in the literature about whether the Younger Dryas was wet or dry in eastern North America. For instance, loess deposits in the Savannah River valley (Swezey et al. 2013), compound-specific hydrogen and carbon isotopic analysis of lipids preserved in lake sediments in North Carolina (Lane et al. 2018), speleothem records (Springer et al. 2014), and paleosols (Dorale et al. 2010) in the central United States all suggest drying during the Younger Dryas. Sites in the northeastern United States (~1000 km) such as Crooked Pond (Shuman et al. 2001), Mohonk Lake (Menking et al. 2012), and Lake Minnewaska (Menking et al. 2012), conversely, all suggest wetter conditions. In addition, several geochemical records from Lake Tulane, Florida (Arnold et al. 2018; Huang et al. 2006) and a $\delta^{18}O$ record from a speleothem in the Brooksville Ridge Cave system in Florida

(BRC03-03, van Beynen et al. 2017) indicate a wetter climate when the AMOC is weakened. Collectively, these records present a heterogeneous pattern of precipitation changes across eastern North America, yet most agree with the pollen-based precipitation reconstructions (Figure 3.2). This interproxy consistency suggests that the reconstructed precipitation tripole is a robust feature of Younger Dryas climatic change in eastern North America. Despite a good agreement between the fossil-pollen precipitation reconstructions and other proxy records, intraregional disagreements among proxies exist. For example, in the northeastern United States, sedimentary data from adjacent sites indicate both high (Shuman et al. 2001) and low lake (Newby et al. 2009, 2000) stands during the Younger Dryas.

The seasonality of simulated temperature changes following hosing is consistent with the fossil-pollen records and modern climatic tolerances of vegetation found throughout eastern North America. The hosing experiments all simulate increased wintertime cooling in the northeastern United States and maritime Canada while the lower latitudes of eastern North America demonstrate wintertime warming (Figure 3.3). This spatial pattern is absent in the summer and cooling of 1 to 2 °C is simulated across all eastern North America (Figure 3.3). These seasonally antiphased temperature changes indicate that temperature seasonality (i.e. difference between winter and summer temperature) increased in the northeastern United States and decreased in the southeastern United States from a meltwater-induced slowdown of the AMOC (Figure 3.3). Enhanced seasonality aligns with model and proxy evidence in Europe that the Younger Dryas cooling was likely isolated to the winter season (Bjorck et al. 2002; Isarin and Bohncke 1999; Schenk et al. 2018), while decreased seasonality may be restricted to the southeastern United States. Temperate tree taxa are sensitive to wintertime low temperatures (Sakai and Weiser 1973), a likely control on the decline of Bølling-Allerød mesic taxa

throughout the Great Lakes region (e.g. Fastovich et al. 2020b; Gill et al. 2012, 2009; Gonzales and Grimm 2009; Watson et al. 2018) following the onset of the Younger Dryas. In the southeastern United States, warmer winters following hosing would enable the persistence of mesic taxa. Although there is a spatial mismatch between the hosing experiments and the fossil-pollen reconstructions, a decline in temperate conifers (Grimm et al. 2006; Kneller and Peteet 1993) and temperate hardwoods (Jones et al. 2017; Krause et al. 2018) is absent in fossil-pollen records throughout the southeastern United States. Therefore, mild winters and summer cooling in the southeastern United States offers a plausible explanation for the reconstructed regional warming in eastern North America during the Younger Dryas (Figure 3.1)(Fastovich et al. 2020a).

Disentangling seasonal precipitation signals from our proxy record remains difficult, although a seasonal signal likely is present within individual proxy records. The precipitation record itself likely carries a summer weighting because the greatest amount of precipitation falls between May and September in eastern North America (Figure S2.5). Moreover, the pollen records may be weighted towards a summer signal, because plant water use and water limitations often are more severe in summer months, as temperatures rise (Gates 1968), although other environmental variables also control plant water use (e.g. atmospheric CO_2 concentration, vapor pressure deficit). Interpretations of $\delta^{18}O$ records of calcite from Seneca Lake, New York (Ellis et al. 2004) and Fayetteville Green Lake, New York (Kirby et al. 2002b) suggest increased wintertime precipitation during the Younger Dryas, but the $\delta^{18}O$ of calcite responds to multiple environmental variables such as temperature, $\delta^{18}O$ of moisture source, and evaporative enrichment (Yu et al. 1997) and need independent verification. Resolving seasonal precipitation

across eastern North America requires further work and proxy records that record seasonal precipitation (e.g. high-resolution speleothems, Batchelor et al. 2022).

3.6.2 Possible mechanisms of spatially-diverse responses to meltwater forcing

The AOGCM hosing experiments simulate localized patterns of increased temperatures and tripoles in precipitation anomalies (Figure 3.2, Figure 3.3), but the reconstructed and simulated fingerprints are not well aligned, resulting in a negative model skill when the proxy reference mean is used as the null model (Figure 3.5). Nonetheless, the AOGCMs help provide possible mechanistic explanations for these spatial fingerprints. North Atlantic hosing and subsequent cooling induce a geostrophic adjustment of the midlatitude jet stream in response to a greater geopotential gradient across the North Atlantic (Figure 3.7)(McGee et al. 2018b). At present, zonal temperature gradients are a primary control on atmospheric circulation and the strength and position of the midlatitude jet over the North Atlantic Ocean (Hall et al. 2015; Wallace and Hobbs 2006). Younger Dryas sea surface temperature reconstructions and foraminiferal assemblages show patterns that agree with the climate simulations analyzed here. MD99-2284 (62 °N) demonstrates a pronounced decrease in sea surface temperatures (Bakke et al. 2009) and an increase in cold-adapted *Neogloboquadrina pachyderma* in core CHN82-2 (43 °N, Keigwin and Lehman 1994) is interpreted as a decrease in ocean temperatures, while Blake Outer Ridge (32 °N, Carlson et al. 2008) exhibits no temperature change. The reconstructed and simulated enhanced latitudinal temperature gradient over the North Atlantic and apparent temperature dipole in eastern North America yields an asymmetric change in the strength of the midlatitude jet with increased upper-level winds over the North Atlantic and unchanged winds over eastern North America (Figure 3.7, Figure S2.3), driving increased upper-level divergence over eastern North America and coupled wetting and warming (Figure 3.2, Figure 3.3, Figure

3.8). A strengthened jet stream has been inferred from varved lake sediments at Lake Meerfelder Maar, where the Younger Dryas was associated with greater varve thickness and stronger winds (Brauer et al. 2008). Early simulations of the Younger Dryas climate also note enhanced westerly winds (Renssen et al. 1996) and recent data-model comparisons in Europe hypothesize that summer Younger Dryas warming in Europe is a result of a positive index of the Arctic Oscillation (Schenk et al. 2018). A positive Arctic Oscillation index is often associated with an enhanced midlatitude jet stream, enhanced westerlies north of ~40 °N (Thompson and Wallace 2000, 1998), and more frequent winter warm extremes in the southeastern United States (Lim and Schubert 2011). In addition, a southward shifted jet stream during the Younger Dryas across Europe and eastern North America has been inferred from tephra in lacustrine deposits (Lane et al. 2013), glacial equilibrium line altitude precipitation reconstructions (Rea et al. 2020), titanium accumulation (Bakke et al. 2009), and $\delta^{18}O_{calcite}$ (Kirby et al. 2002b) as tracers for the mean position of the westerlies. Lastly, $\delta^{18}O_{seawater}$ reconstructions from the north Atlantic demonstrate more saline conditions (Carlson et al. 2008) and may have been caused by enhanced Ekman pumping from stronger surface midlatitude westerlies and tropical easterlies (Chiang et al. 2008). An enhanced and displaced jet due to meltwater forcing may explain the reconstructed temperature fingerprint by driving upper-level divergence, mean sea level pressure changes, and northern transport (Figure 3.6, Figure 3.7, Figure 3.8) thereby producing Younger Dryas warming in Florida and monotonic warming in the southeastern United States. These same conditions may have promoted southward transport off the Laurentide Ice Sheet (Figure 3.6) and may explain cooling north of ~35°N. Seasonally, jet stream strength asymmetry across the North Atlantic and eastern North America and near-surface southern transport are consistently high in

winter across all hosing experiments (Figure S2.3), suggesting that a weakening of the AMOC may have ameliorated wintertime cooling in the southeastern United States (Figure 3.6).

Ice sheet position and the seasonal routing of storm tracks also affect the patterns of temperature and precipitation anomalies in the AOGCM simulations (Figure 3.2, Figure 3.3). Mesoscale simulations of the Last Glacial Maximum climate highlight the regional effects of the Laurentide Ice Sheet on routing storm tracks seasonally (Bromwich et al. 2005, 2004). In these simulations, temperature gradients during the summer were greatest adjacent to the Laurentide Ice Sheet, routing storms over the northeastern United States, while a large glacial anticyclone routed storms over Florida during the winter (Bromwich et al. 2005, 2004). This pattern of precipitation and mean sea level pressure changes are present within the TraCE-21ka simulations for the Younger Dryas, as positive precipitation anomalies in the winter are restricted to Florida and much of the Gulf of Mexico, while positive precipitation anomalies occur in the summer in the northeastern United States (Figure 3.3, Figure 3.6). TraCE-ICE simulates a nearly identical spatial configuration of precipitation anomalies, but with a greater magnitude, which reinforces the importance of the Laurentide Ice Sheet in controlling these precipitation patterns (Figure S2.6). However, meltwater forcing may have contributed to these precipitation changes by increasing the land-ice temperature gradient. Freshwater hosing is necessary to create warming in eastern North America (Figure 3.3, Figure S2.7) that would have further steepened the temperature gradient in eastern North America, likely shifting storm tracks. Additionally, hosing reconfigures the jet stream to drive surface level pressure and wind anomalies necessary for positive precipitation anomalies in eastern North America (Figure 3.2, Figure 3.6, Figure S2.3). TraCE-21ka is the only model analyzed that includes ice sheet configurations and other boundary conditions specifically for the Younger Dryas (He 2011) and has the highest skill in

simulating the proxy-inferred precipitation anomalies, suggesting that combined effects of AMOC-induced jet stream changes (Figure 3.7), mean sea-level pressure changes (Figure 3.6), northward transport (Figure 3.6), and ice sheet configuration are necessary to create the reconstructed precipitation tripole.

The simulated pressure gradients, surface transport anomalies, and corresponding precipitation and temperature anomalies from the AOGCM hosing experiments are similar to modern synoptic climate events that produce mild eastern North American winters. During the positive phases of the North Atlantic Oscillation, El Niño events, and negative phases of the Atlantic multidecadal oscillation, winters in the southeastern United States tend to be milder and wetter and are associated with lowered surface pressures (Enfield et al. 2001; Hurrell 1995; Mo 2010; Visbeck et al. 2001). These milder winters are also associated with increased winter storm frequency in eastern North America (Durkee et al. 2008; Yin 1994), which has been attributed to enhanced southern advection over the Gulf of Mexico (Henderson and Vega 1996). These regional changes in winter climate can result from changes in midlatitude jet stream configuration and strength (e.g. Hurrell et al. 2003; Mo 2010). Moreover, recent analyses attribute increases in precipitation during the 21st century to enhanced northward flow and moisture flux from the Gulf of Mexico caused by enhanced anticyclonic flow on the western edge of the Northern Hemisphere Atlantic subtropical high (Bishop et al. 2019a,b). A similar pattern is seen in the mean sea level pressure and wind anomalies of the subtropical high in several of the hosed AOGCMs (Figure 3.6). Intensified and southward-displaced subtropical high pressures over the mid-Atlantic have been linked to increased precipitation in the southeastern United States between 1948–2007 (Li et al. 2012), which is also seen in the hosed AOGCMs analyzed here (Figure 3.6). Enhanced Hadley circulation is a common feature of

hosing experiments (Broccoli et al. 2006; Clement and Peterson 2008; Kageyama et al. 2010; see Fig. 4 in McGee et al. 2018a) and may cause the simulated higher subtropical pressures, possibly explaining persistent drying in the Bahamas and southern Florida when the AMOC is weakened (Figure 3.2, Figure 3.3)(Arienzo et al. 2017; Springer et al. 2014; Warken et al. 2019).

3.6.3 Effects of individual boundary conditions on Younger Dryas spatial fingerprints

Differences in the reconstructed spatial patterns of climate changes and predictive skill between TraCE-21ka and TraCE-MWF indicate that multiple forcings produce Younger Dryas climate changes in eastern North America, but that meltwater forcing may be the most likely cause of the subregional patterns of warming and wetting. Although TraCE-21ka produces more skillful simulations than TraCE-MWF (Figure 3.4, Figure 3.5), TraCE-MWF simulates Younger Dryas warming in eastern North America (Figure 3.3) identifying a weakening of the AMOC as a key contributor of southeastern United States warming. Indeed, of the single-forcing TraCE experiments, only TraCE-MWF produces widespread warming in eastern North America while all others produce cooling of varying magnitude (Figure S2.7). However, TraCE-MWF inaccurately simulates the position and extent of Younger Dryas warming, suggesting that other boundary conditions are relevant to the spatial configuration of Younger Dryas warming and cooling in eastern North America. Hence, the higher skill of TraCE-21ka indicates that all forcings are essential to accurately simulating Younger Dryas climates, while freshwater input into the North Atlantic appears to be necessary for Younger Dryas warming in the southeastern United States.

Analysis of the TraCE-21ka single-forcing experiments indicates that the shifting position of the Laurentide Ice Sheet is a primary control on the Younger Dryas climate changes in eastern North America. The temperature anomalies in TraCE-ICE exhibit a similar spatial

configuration to TraCE-21ka, but with a smaller magnitude (Figure S2.7). Hence, the changing

glacial extent in TraCE-21ka appears to determine the spatial configuration of Younger Dryas

cooling in eastern North America, while changes in the AMOC amplify cooling in the northern

region and counteract it in the southeast (Figure S2.7). This interpretation coheres with other

models where ice sheet feedbacks amplify temperature changes driven by orbital and greenhouse

gas forcings at high latitudes (Masson-Delmotte et al. 2006; Singarayer and Valdes 2010). In

addition, changes in near-surface winds illustrate the influence of the Laurentide Ice Sheet on

atmospheric circulation in TraCE-21ka. A net transport of air from the Laurentide Ice Sheet

southward into eastern North America is consistent with a larger glacial anticyclone at 12.3 ka

than 11.1 ka (Figure 3.6), an expected result given that this interval spans a large reduction in ice

extent and volume in the Laurentide Ice Sheet (He 2011; Peltier 2004). Hence, changes in ice-

sheet configuration overprint temperature, pressure, and near-surface wind changes caused by a

weakened AMOC in TraCE-21ka.

Ice sheet boundary conditions may also explain why TraCE-21ka is the most skillful

model analyzed. Northern sites closer to the Laurentide Ice Sheet are overrepresented in our

proxy record and may bias model skill towards models with accurate ice sheet boundary

conditions despite our spatial debiasing procedure. CM2Mc and TraCE-MWF use Last Glacial

Maximum configurations of the Laurentide and Cordilleran Ice Sheets and HadCM3 uses

transient ice sheet configurations that span the interval from 19.0 ka to 15.5 ka (Brown and

Galbraith 2016; He et al. 2013; Ivanovic et al. 2018a). These configurations place the Laurentide

Ice Sheet farther south than the reconstructed extent during the Younger Dryas by as much as

~6° in eastern North America and include the Cordilleran Ice Sheet, which began decaying at

~14.5 ka (Dalton et al. 2020; Gregoire et al. 2012). The hosing experiments reinforce the

importance of ice sheet boundary conditions, as all share similar boundary conditions and demonstrate remarkably similar changes to atmospheric circulation, temperature, and precipitation in eastern North America (Figure 3.2, Figure 3.3, Figure 3.6).

Greenhouse gas, ice sheet, and orbital forcings in TraCE-21ka also modulate the strength of the AMOC recovery and thereby weaken the Younger Dryas temperature anomalies relative to the hosing-only experiment. The AMOC weakens by a similar magnitude in TraCE-21ka and TraCE-MWF during the Younger Dryas, but AMOC recovery differs between the two experiments (Figure S2.8). In TraCE-MWF, the AMOC recovers to a strength of ~11 Sv after Younger Dryas termination (11.1 ka), while TraCE-21ka only simulates an AMOC recovery to ~8 Sv (Figure S2.8). A stronger AMOC leads to greater heat transport into the North Atlantic and larger-magnitude Younger Dryas-early-Holocene temperature anomalies in TraCE-MWF (Figure 3.3, Figure S2.8). Hence, greenhouse gas, ice sheet, and orbital forcings appear to influence the sensitivity of the AMOC to freshwater forcing cessation.

3.6.4 Possible causes of data-model mismatch and recommended solutions

Although the climate simulations agree with each other in the trends and patterns of climate change across most seasons following hosing, data-model mismatch and low model skill scores indicate that some structural aspects of the AOGCM or experimental setups are causing misalignments between simulations and reconstructions. Possible explanations include 1) boundary conditions (e.g. ice sheet configuration), 2) model grid cell size, and 3) uncertainties with the proxy-based reconstructions

Firstly, a mismatch between boundary conditions and hosing experimental design is likely a primary source of uncertainty. Our analyses focused on the influences of freshwater forcing on the eastern North America climate, yet our proxy reconstructions integrate all

deglacial climate forcings. In particular, the Laurentide Ice Sheet exerted a large control on the eastern North American climate during the Last Glacial Maximum through albedo and orography (Bromwich et al. 2005, 2004). Of the AOGCMs analyzed here, only TraCE-21ka had ice-sheet extent and orography set for the Younger Dryas. Analysis of the TraCE-21ka simulations associates an abrupt change in the atmospheric configuration and climate of the western United States with a reduction in ice-sheet extent and volume at 14 ka (Lora et al. 2016), highlighting the sensitivity of these climate models to ice sheet boundary conditions. Indeed, TraCE-21ka, the model with the most accurate Younger Dryas ice sheet configuration, produces the most skillful simulations of Younger Dryas climate changes in eastern North America (Figure 3.4, Figure 3.5).

Second, the coarse resolution of the analyzed AOGCMs hampers the ability to simulate the fine-scale spatial patterns of temperature and precipitation change in the proxy record. The average atmospheric model resolution of the AOGCMs used here is ~3° while the distance between warm and cold sites is as small as 2° (Figure 3.1). For instance, Browns Pond (Kneller and Peteet 1993) is the northernmost site analyzed here that lacks Younger Dryas cooling and is only separated from sites in the Great Lakes Region and the northeastern United States by ~400 km, indicating that the temperature gradient underlying the Younger Dryas temperature fingerprint in eastern North America may be too steep to be captured at the typical AOGCM resolution (see section 3.3).

Third, uncertainties within the proxy data may also be a contributor to the data-model mismatch. Precipitation was likely a second-order control on vegetation during the most recent deglaciation and so is more subject to biases resulting from weaknesses in the assumption of stable covariance structures (Juggins 2013). For instance, precipitation seasonality is ecologically

relevant but likely changed during the Younger Dryas in eastern North America (Kirby et al. 2002a,b; Mandl et al. 2016). That is, winter precipitation may have increased or summer precipitation may have decreased, violating the assumption that the covariance between the modern pollen training dataset and annual precipitation in space was likely stable through time. Despite uncertainties in the fossil-pollen precipitation reconstructions our reconstruction demonstrate coherence with independent proxy records from various locations in eastern North America (Figure 3.1A).

Given the above, a key priority to better assess these hypothesized mechanisms of Younger Dryas climate change is for higher-resolution climate simulations with more accurate representations of ice sheet position and other boundary conditions, accompanied by quantitative measures of climate change from sites across eastern North America. Updates to the Polar Mesoscale Model 5 used in Bromwich et al. (2004) and Bromwich et al. (2005) (now Polar-Weather Research and Forecasting Model) improve performance and physical parameterization, enabling more accurate simulations (Gilliam and Pleim 2010). Performing such mesoscale simulations using Younger Dryas boundary conditions would produce results at sufficient resolution to assess the atmospheric hypotheses outlined here and elsewhere (Gonzales et al. 2009; Kageyama et al. 2013; Rea et al. 2020; Shuman et al. 2002). Quantitative estimates of Younger Dryas precipitation sources using proxies such as leaf wax isotopes (e.g. Feakins et al. 2014; Schartman et al. 2020; Shuman et al. 2006) could serve to assess hypotheses in storm track routing (Bromwich et al. 2005, 2004) as the isotopic composition of rainwater within eastern North America varies depending on storm track configuration (Burnett and Mullins 2002; Ellis et al. 2004; Kirby et al. 2002a,b; Sjostrom and Welker 2009).

3.7 Conclusion

Here we compare a new synthesis of proxy-based reconstructions of Younger Dryas mean annual precipitation in eastern North America, an existing network of temperature reconstructions (Fastovich et al. 2020a), three previously run AOGCM hosing experiments, and a transient deglacial AOGCM to assess possible mechanisms for regional Younger Dryas climate change. Younger Dryas precipitation anomalies follow a tripole pattern, with wetting in the northeastern United States, drying from the Great Lakes to the Carolinas, and wetting in Florida. This tripole pattern helps resolve prior apparent contradictions in interpretations about whether eastern North America was wet or dry during the Younger Dryas and contrasts with the latitudinal pattern previously reconstructed for Younger Dryas temperature anomalies (Figure 3.1)(Fastovich et al. 2020a). The hosing experiments also appear to simulate areas of regional warming and precipitation tripole, with wetting throughout eastern North America and drying in the Bahamas and maritime Canada, but simulated precipitation patterns are antiphased to the proxy records, yielding low skill scores. TraCE-21ka simulates the Younger Dryas climate more accurately than the three hosing-only AOGCM experiments, yet only the meltwater hosing experiments appear able to produce the proxy-reconstructed Younger Dryas warming in the southeastern United States. Although the reconstructed and simulated fingerprints poorly align, the AOGCM experiments consistently indicate that regional warming in eastern North America during hosing episodes such as the Younger Dryas can be attributed to a geostrophic adjustment of the midlatitude jet stream, driving lower pressure over eastern North America, and transport of heat and moisture from southern sources. Data-model discrepancies are likely attributable to boundary conditions, climate model resolution, and error in the precipitation reconstructions. Both higher resolution or mesoscale climate simulations with Younger Dryas boundary

conditions and independent, quantitative precipitation reconstructions are necessary next steps

for understanding the patterns and drivers of Younger Dryas climate change at sub-hemispheric

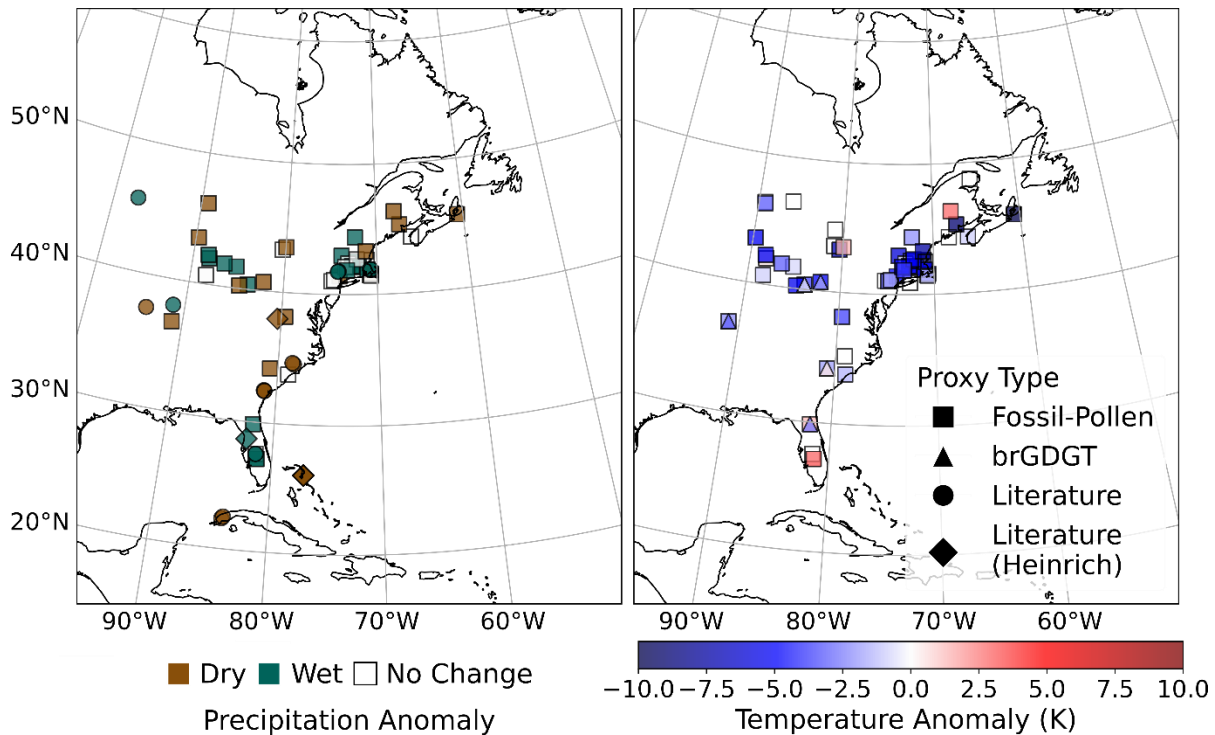scales.

3.8 Figures

Figure 3.1

Mean annual climate anomalies of mid-Younger Dryas – early Holocene (12.3 ka – 11.1 ka) for

A) precipitation reconstructions (based on fossil pollen and literature and B) temperature

reconstructions (based on fossil-pollen and brGDGT). For literature-based inferences, see Table

3.1. For consistency, the direction of the anomaly calculation follows that of the hosed-unhosed

AOGCM experiments. Precipitation anomalies are shown categorically to make the quantitative

fossil-pollen reconstructions comparable to the categorical precipitation changes from the

literature. Fossil-pollen sites were designated as 'No Change' if the precipitation anomaly was

less than the 1σ standard deviation of the precipitation reconstruction time series among all

bootstrap samples. Maps use the Albers Equal Area conic projection (origin: 40°N, 73°W,
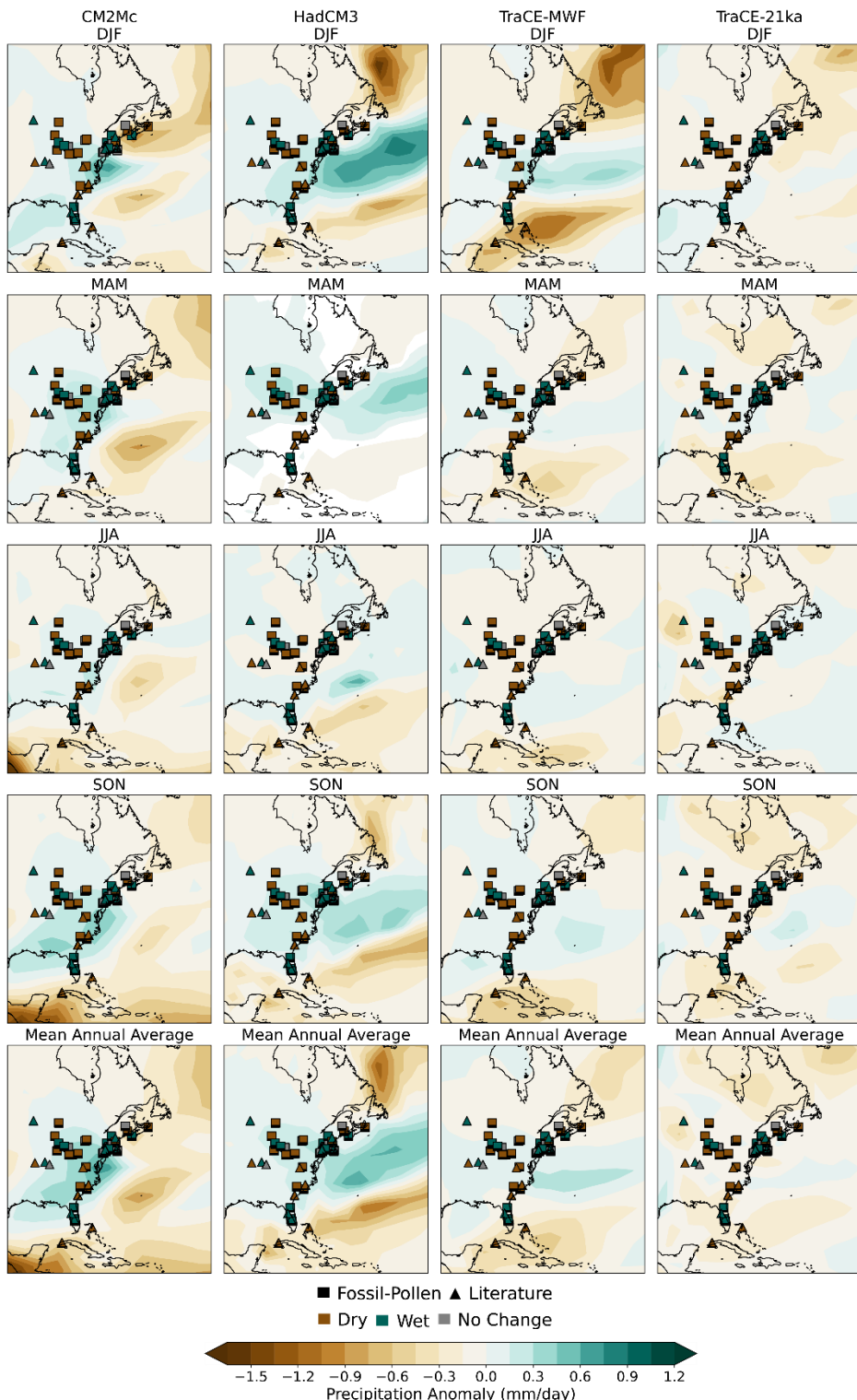
standard parallels: 20°N, 50°N).

Figure 3.2

Spatial fingerprints of mean seasonal precipitation response to freshwater hosing (hosed -

unhosed) and mean annual anomalies of fossil-pollen and precipitation reconstructions (12.3 ka –

11.1 ka). The calculation and display of precipitation anomalies follows Fig. 1, as does the map
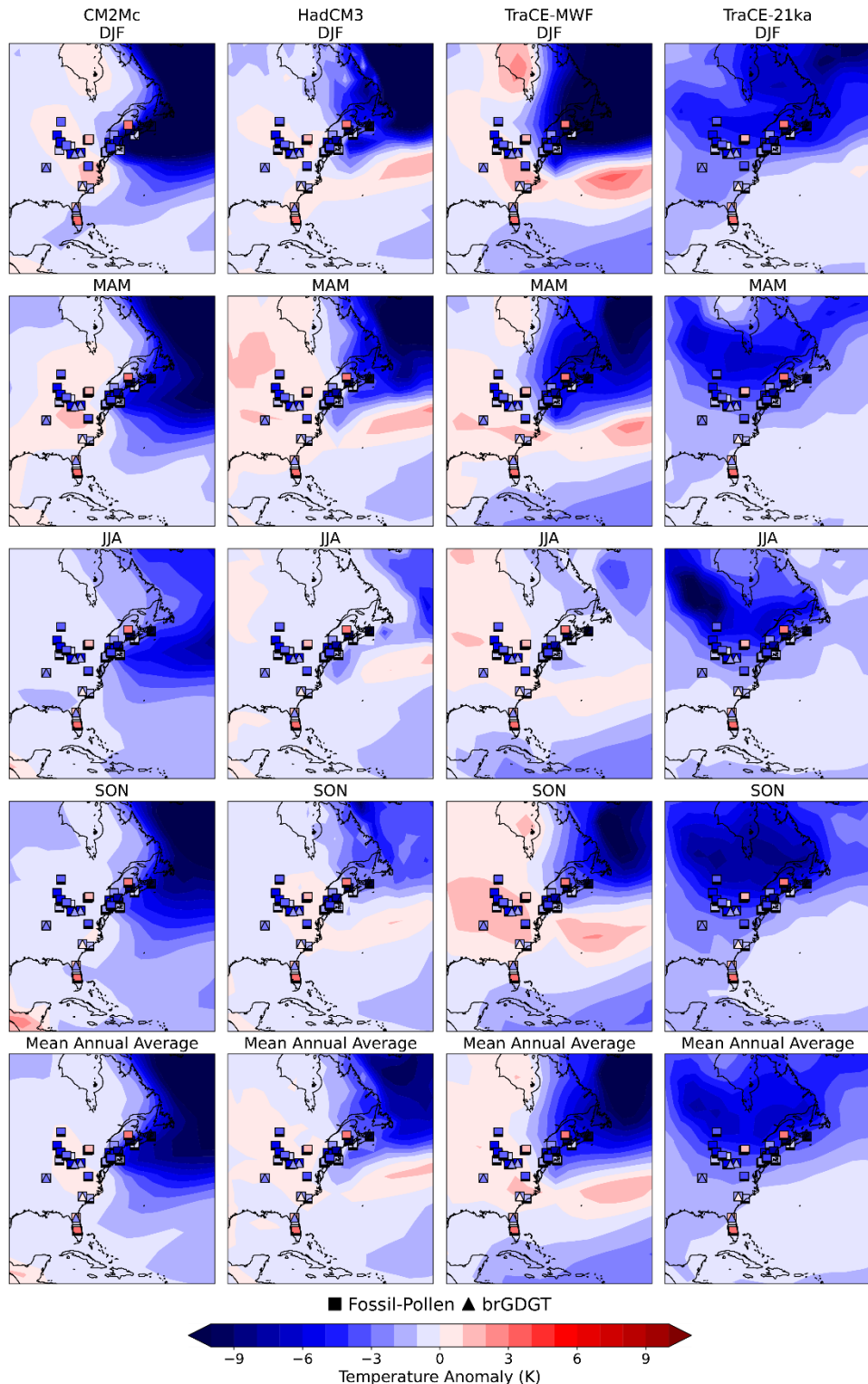
projection.

Figure 3.3

Spatial fingerprints of mean seasonal surface air temperature response to freshwater hosing

(background colors; hosed - unhosed) and mean annual anomalies of fossil-pollen and brGDGT

temperature reconstructions (dots; 12.3 ka – 11.1 ka). Map projection and fossil-pollen

precipitation anomaly categories follow Figure 1.
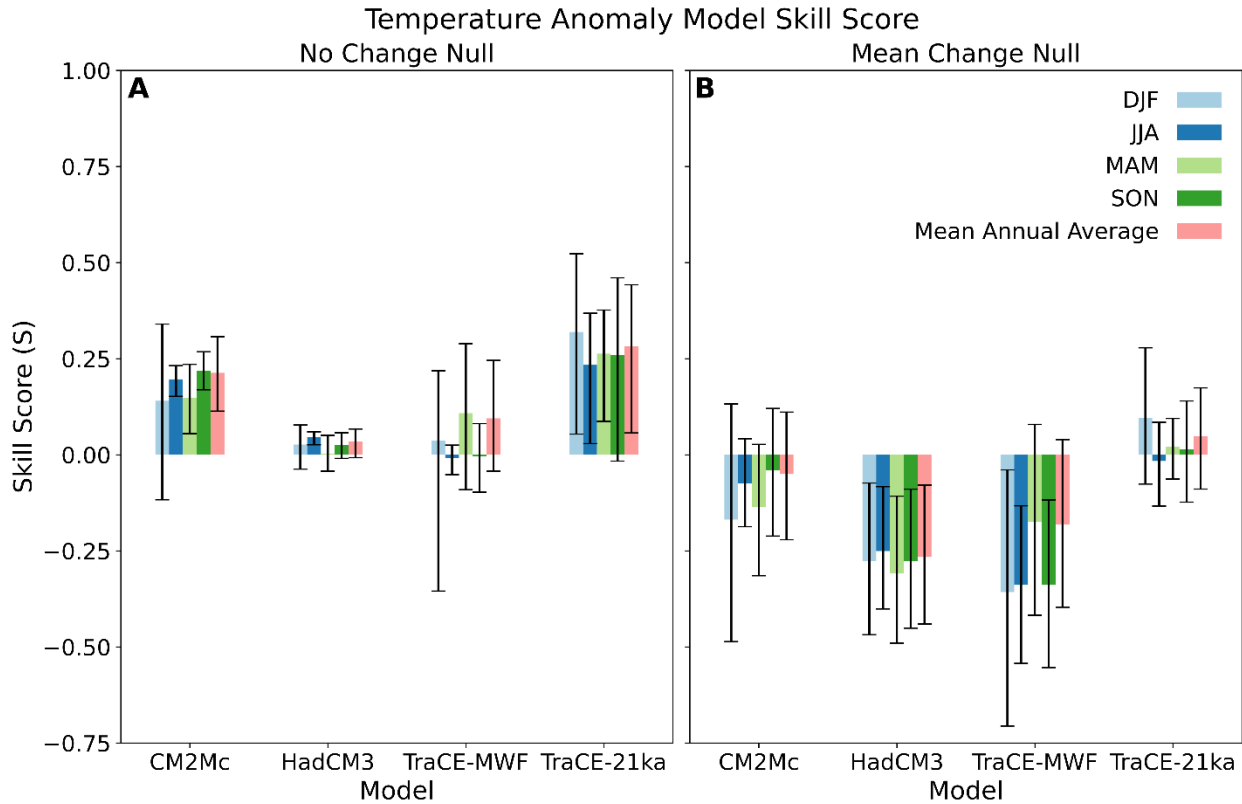
Figure 3.4

Spatially debiased assessments of AOGCM skill in simulating proxy-based temperature

anomalies in comparison to A) a baseline of no change and B) a baseline change corresponding

to the mean change of the proxy records. The no-change baseline assesses climate model skill in

simulating the sign and magnitude of Younger Dryas temperature change while the proxy-mean

baseline assesses climate model skill in simulating the spatial fingerprint of Younger Dryas

temperature change (Hargreaves et al. 2013).
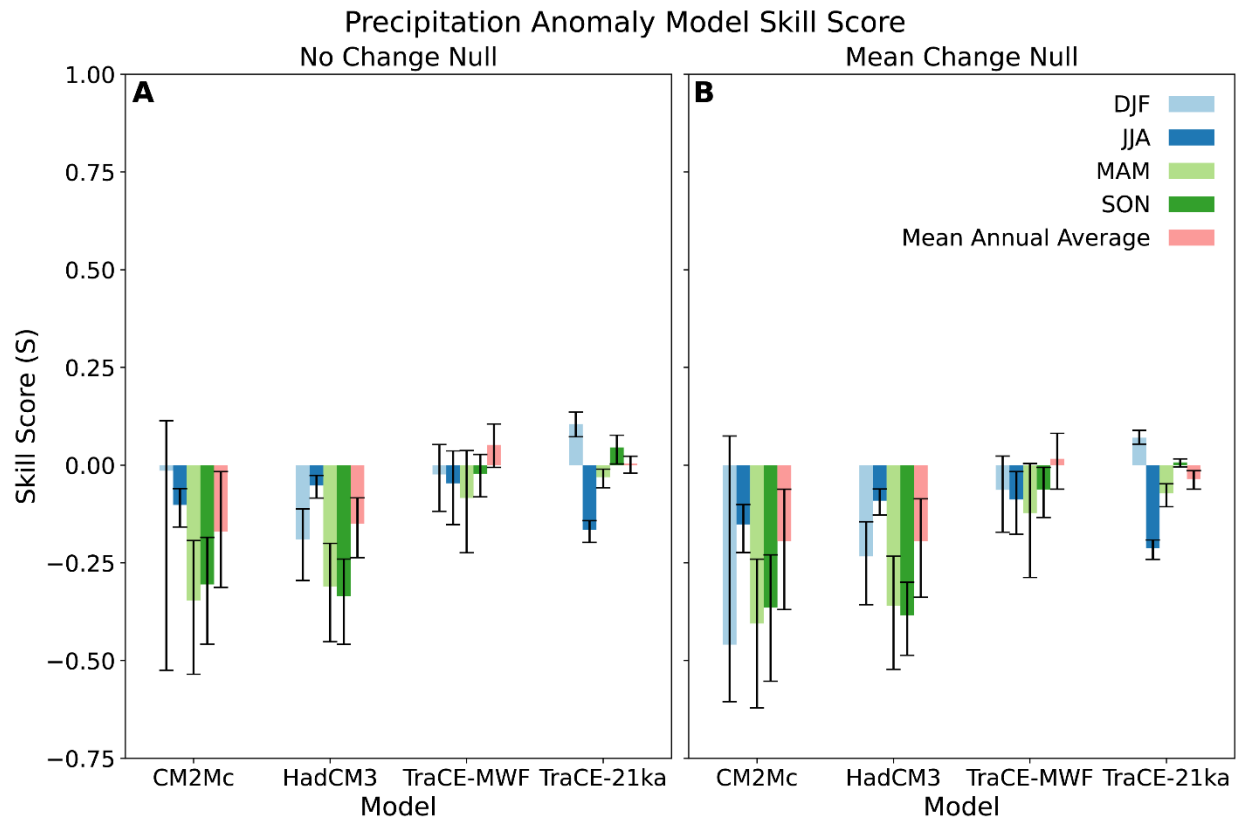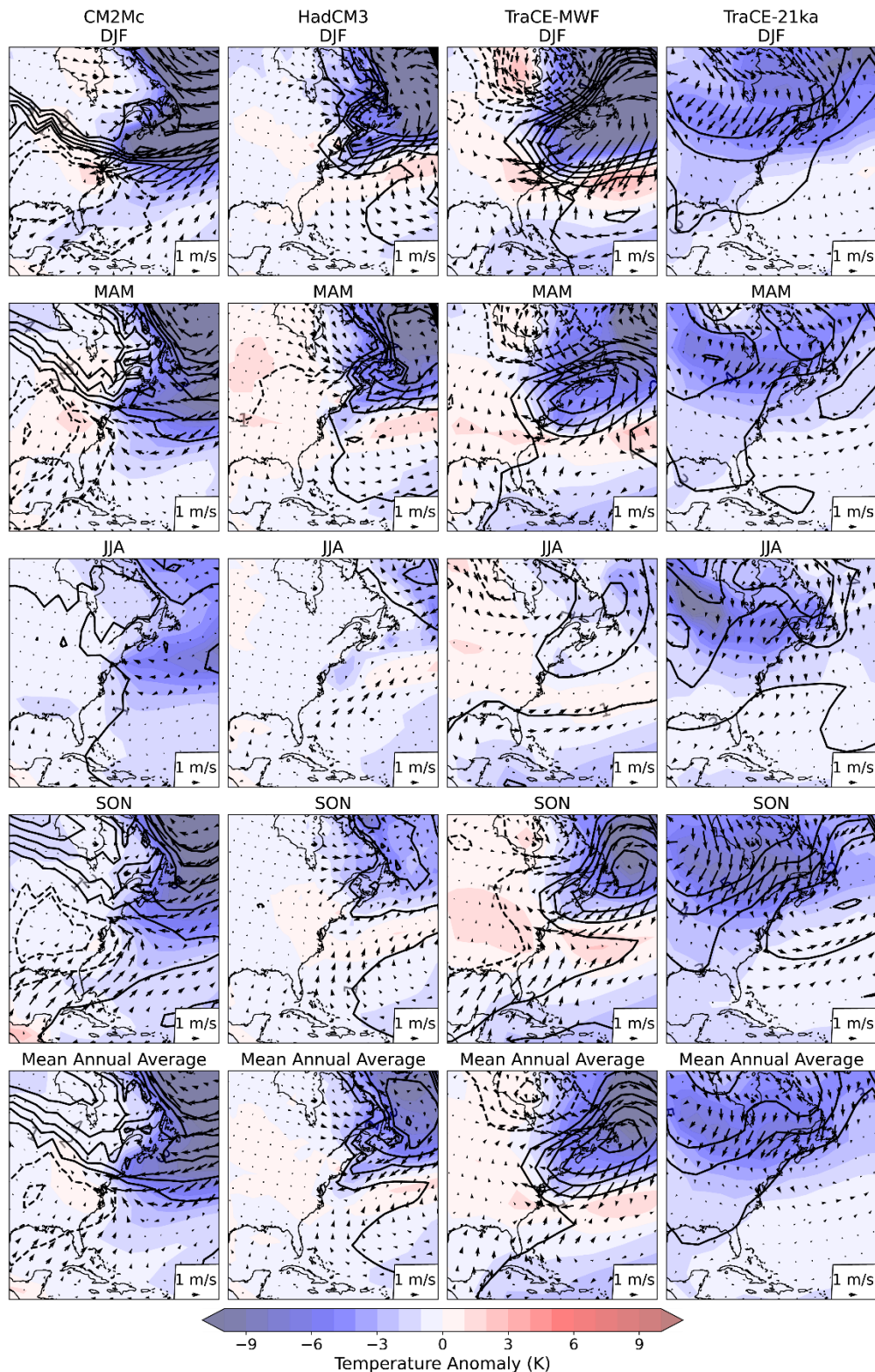
Figure 3.5

As in Figure 3.4, for precipitation anomaly reconstructions.

Figure 3.6

Mean seasonal surface temperature, near-surface wind, and mean sea level pressure response to freshwater hosing (hosed - unhosed). Mean sea level pressure contours interval is 1 mb, with solid contours indicating positive anomalies and dashed contours indicating negative anomalies. Zero contours are omitted. Map projection follows Figure 3.1.
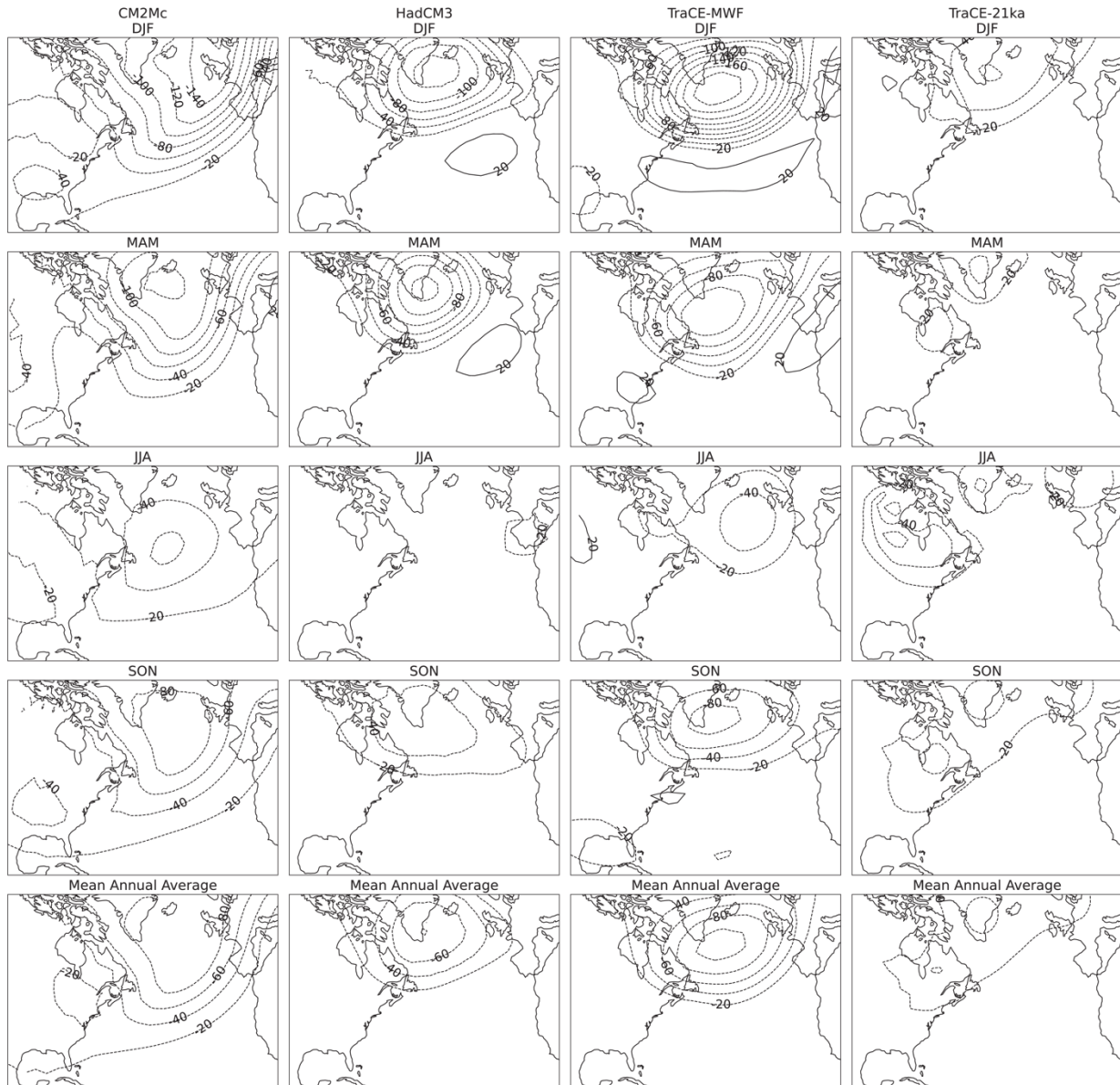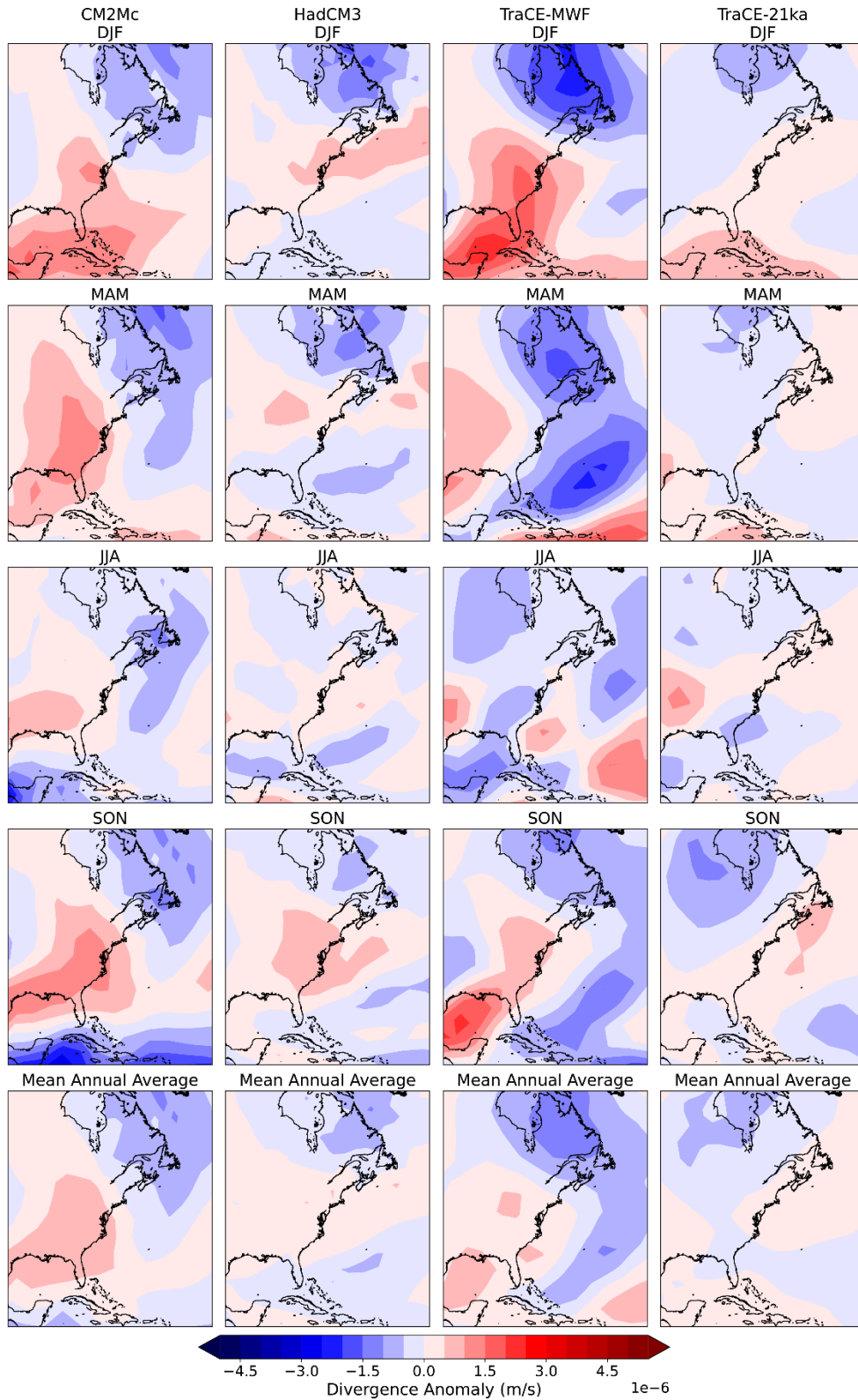
Figure 3.7

Mean seasonal 500 mb geopotential height response to freshwater hosing (hosed - unhosed).

Geopotential height contours interval is 20 mb, with solid contours indicating positive anomalies

and dashed contours indicating negative anomalies. Zero contours are omitted. Map projection

follows Figure 3.1.

Figure 3.8

Mean seasonal upper-level wind (200 mb) divergence response to freshwater hosing (hosed -

unhosed). Positive values indicate increased divergence with hosing and negative values indicate

increased convergence. All values are scaled by 10^6. Map projection follows follows Figure 3.1.

DOI	10.1023/a:1007971226750
Reference	(Schwalb and Dean 1998)
Interpretation Basis	" We speculate that the cold and dry phase may correspond to the Younger Dryas event [relative to the Bolling]." " The sediments from Pickerel Lake suggest that climate before 12 ka [^{14}C years]" and " Increases in both 13C and 18O in marl between 10.3 and 9.5 ka [14 C], as well as the presence of L. herricki and C. rawsoni in the ostracode assemblages, indicate that evaporation increased and that Pickerel Lake became more saline, probably reaching the highest salinity in the history of the lake."
Mid-Younger Dryas (12.3 ka) - early-Holocene (11.1 ka)	Wet
Longitude (°)	-97.27
Latitude (°)	45.51
Age Type	Radiocarbon (uncalibrated)
Archive Type	Lacustrine sediment
Site Name	Pickerel Lake

New Long Pond	Rocky Pond
Lacustrine sediment	Lacustrine sediment
Radiocarbon (calibrated)	Radiocarbon (calibrated)
41.85	41.89
-70.71	-70.69
Dry	Dry
• " The YD-related increase in percent coarse fraction at New Long Pond (Unit III) peaks around 12.6 ka, after the abrupt onset of cold conditions across the circum North Atlantic (Ruddiman and McIntyre, 1981; Rind et al., 1986; Rasmussen et al., 2007)." "	• " We infer these low stands accompanied the cold YD before ca 12.2 ka at Rocky Pond, after which, water levels were high until 11.6 ka, based on the relatively low values for coarse fraction (Fig. 12)."
(Newby et al. 2009)	(Newby et al. 2009)
10.1016/j.quascirev.2009.02.020	10.1016/j.quascirev.2009.02.020

Mohonk Lake	Lake Minnewaska
Lacustrine sediment	Lacustrine sediment
Radiocarbon (calibrated)	Radiocarbon (calibrated)
41.77	41.73
-74.16	-74.24
Wet	Wet
• See Table 2	• see Figure 9
• "In Mohonk Lake, the Younger Dryas was marked by a cessation of bryophyte growth (Fig. 6). The onset of silt deposition at 132 cm suggests a possible cause, which is an increase in turbidity that diminished photosynthetically active radiation levels at the lake floor. The silt further suggests increased inflow to Mohonk Lake from the ephemeral streams along its southern shore and therefore wetter conditions and/or typical increase in clastic sedimentation associated with colder conditions."	
(Menking et al. 2012)	(Menking et al. 2012)
10.1016/j.palaeo.2012.06.033	10.1016/j.palaeo.2012.06.033

| Dos Anas Cave (Stalagmite Cuba Pequeno) | Speleothem | U/Th | 22.38 | -83.97 | Dry | • "Furthermore, the chronology at the boundary to the lower section, which shows evidence for recrystallization, is poorly constrained and we cannot unambiguously infer climate conditions in the Caribbean for this important climate phase. However, around 12 ka, the δ¹⁸O signal of CP shows up to 1% higher values than during the Preboreal (Fig. 4a). This may indicate drier climate in the northern Caribbean during the YD." | (Fensterer et al. 2013) | 10.1016/j.epsl.2012.11.019 |
| Savannah River, SC | Eolian dunes | OSL | 32.48457 | -81.20333 | Dry | • "These three ages are approximately coincident with the Younger Dryas (YD), which is dated by Alley et al. (1993) at 12,800 to 11,500 cal yr BP. One of these three samples (GAW11) is from a relatively isolated sand ridge on the west side of the main dune field, and the other two samples (GAW12, GAW13) are from relatively isolated dunes to the south of the main dune field. These younger OSL ages attest to a minor episode of eolian sand mobilization, but the paucity of similar ages from the main dune field indicates that conditions during this time were not sufficient to remobilize the main dune field." | (Swezey et al. 2013) | 10.1016/j.yqres.2013.06.007 |

Location	Type	Method	Latitude	Longitude	Climate	Notes	Reference	DOI
Savannah River, SC	Eolian dunes	OSL	32.42373	-81.1573	Dry	• Same as above	(Swezey et al. 2013)	10.1016/j.yqres.2013.06.007
Savannah River, SC	Eolian dunes	OSL	32.4374	-81.14857	Dry	• Same as above	(Swezey et al. 2013)	10.1016/j.yqres.2013.06.007
AB-DC-09	Speleothem	U/Th	26.14	-77.1	Dry	• "The Mg/Ca ratios and $\delta^{13}C_c$ values for AB-DC-09 and AB-DC-12, did not show statistically significant correlations (Fig. 4a), although AB-DC-09 and AB-DC-12 exhibit increased $\delta^{13}C_c$ values across Heinrich stadials 1-6. We therefore tentatively propose the increased $\delta^{13}C_c$ values across Heinrich stadials 1-6 were potentially driven by increased aridity resulting in increased water/rock interactions and a lower biogenic CO_2 component of the DIC (Genty et al., 2003) in the Bahamas stalagmites."	(Arienzo et al. 2015, 2017)	10.1016/j.epsl.2015.08.035 10.1016/j.quascirev.2017.02.004

Singletary Lake	Jones Lake
Lacustrine sediment	Lacustrine sediment
Radiocarbon (calibrated)	Radiocarbon (calibrated)
34.588	34.685
-78.456	-78.602
Dry	Dry
• "Conversely, shifts to more positive $\delta^2H_{MAP\_reconstructed}$ values ($\Delta^2H = \sim20‰$) in the Jones Lake record coincident with the Younger Dryas event are indicative of decreased moisture availability and increased evapotranspiration (Fig. 6). The same general pattern in the $\delta^2H_{MAP\_reconstructed}$ values exists in the Singletary Lake record, but appears to lag the Jones Lake record by approximately 500 years."	• "Conversely, shifts to more positive $\delta^2H_{MAP\_reconstructed}$ values ($\Delta^2H = \sim20‰$) in the Jones Lake record coincident with the Younger Dryas event are indicative of decreased moisture availability and increased evapotranspiration (Fig. 6). The same general pattern in the $\delta^2H_{MAP\_reconstructed}$ values exists in the Singletary Lake record, but appears to lag the Jones Lake record by approximately 500 years."
(Lane et al. 2018)	(Lane et al. 2018)
10.1016/j.quascirev.2017.12.022	10.1016/j.quascirev.2017.12.022

Lake Tulane	Buckeye Creek Cave (BCC-010)
Lacustrine sediment	Speleothem
Radiocarbon (calibrated)	U/Th
27.585	37.97
-81.504	-80.4
Wet	Dry
• "Increased Δ_{leaf} values during North Atlantic cold spells indicate lower water-use-efficiency among angiosperms around Lake Tulane. Combined δD values from terrestrial and aquatic lipids, confirm that aridity decreased during cold, stadial periods (Heinrich Events), and increased during warm, interstadials."	• "The sharpest δ¹³C increase during this event starts at ~47 ka, consistent with the beginning of Heinrich event 5 [*Hemming*, 2004], when the LIS disgorged a flotilla of icebergs into the North Atlantic, profoundly disrupting climate patterns."
(Arnold et al. 2018)	(Springer et al. 2014)
10.1016/j.quascirev.2018.06.012	10.1002/2014gl059884

Big Eddy	Stalagmite Cuba Medio
Terrace sediment sequence (paleosol)	Speleothem
Radiocarbon (calibrated)	U/Th
37.5	22.52
-93.9	-83.85
Dry	Dry
• "Between ca. 13,200 and 11,900 yr ago, the abundance of C4 grasses increased by upwards of 50% of the total biomass, indicating expansion of grassland most likely driven by increased aridity during this period."	• "These excursions are interpreted as dry events, and their majority coincide with prominent events of reduced AMOC (Heinrich stadials) and/or cooler temperatures in the North Atlantic during stadials. Some of these cold/dry events, such as e.g., during Heinrich stadials 1, 2, 3, 5a, 6, and 7b, but also around 35 and 65 ka BP, are also characterized by high P/Ca ratios in stalagmite CM (Fig. 8), which further indicates a decrease in soil activity and/or a shift to more abundant C4 vegetation similar to the LGM (section 4.2.2). These findings are further supported by several growth stops in CM during the Younger Dryas (YD, 12.8-11.7 ka), HS 1 (17-15 ka), H7 a/b (~73 and ~76 ka), and HS 8/9 (between 93 and 84 ka), and comparably slow speleothem growth rates associated with HS 2 (22-24 ka), HS 3 (~30 ka), HS 4 (~38 ka), and HS 6 (~63 ka)"
(Dorale et al. 2010)	(Warken et al. 2019)
10.1130/g30781.1	10.1016/j.quascirev.2019.06.019

Site	Archive	Proxy	Latitude	Longitude	Hydroclimate	Quote	Reference	DOI
Onondaga Caverns (ON-3)	Speleothem	U/Th	38.05	-91.216	Wet	"The interval associated with the Allerød-YD transition was characterized by a shift toward a cooler climate and increased C3 vegetation in southern Missouri, central USA."	(Denniston et al. 2001)	10.1016/s0031-0182(01)00334-0
Lake Tulane	Lacustrine sediment	Radiocarbon (calibrated)	27.585	-81.504	Wet	"During the last glacial period, C_4 plant abundance decreased dramatically during the pine phases when precipitation increased, indicating that increasing precipitation overrode the impact of low atmospheric pCO_2, leading to expansions of C_3 plants."	(Huang et al. 2006)	10.1016/j.palaeo.2005.12.014
Brooksville Ridge Cave (BRC03-03)	Speleothem	U/Th	28.682	-82.444	Wet	"The H2 event in the speleothem occurs at ~24 kyr BP which is temporally similar to its timing in other paleoclimate reconstructions. However, the oxygen and carbon isotope values indicate the climate in Florida was relatively warm and wet for a glacial period rather than extremely cool and dry, as seen in other regions."	(van Beynen et al. 2017)	10.1016/j.quaint.2017.05.008

AB-DC-12	AB-DC-01
Speleothem	Speleothem
U/Th	U/Th
26.14	26.14
-77.1	-77.1
Dry	Dry
• " The Mg/Ca ratios and $\delta^{13}C_c$ values for AB-DC-09 and AB-DC-12, did not show statistically significant correlations (Fig. 4a), although AB-DC-09 and AB-DC-12 exhibit increased d13Cc values across Heinrich stadials 1-6. We therefore tentatively propose the increased $\delta^{13}C_c$ values across Heinrich stadials 1-6 were potentially driven by increased aridity resulting in increased water/rock interactions and a lower biogenic CO_2 component of the DIC (Genty et al., 2003) in the Bahamas stalagmites."	• " The periods of elevated Mg/Ca ratios and $\delta^{13}C_c$ values for both stalagmites AB-DC-01 and AB-DC-03 are coincident with Heinrich stadials 1 and 2 suggesting that Heinrich stadials 1 and 2 in the Bahamas were potentially characterized by increased aridity as well as decreased temperature."
(Arienzo et al. 2017)	(Arienzo et al. 2017)
10.1016/j.quascirev.2017.02.004	10.1016/j.quascirev.2017.02.004

AB-DC-03	Makepeace Cedar Swamp
Speleothem	Lacustrine sediment
U/Th	Radiocarbon (calibrated)
26.14	41.94
-77.1	-70.76
Dry	Wet
• "The periods of elevated Mg/Ca ratios and $\delta^{13}C_c$ values for both stalagmites AB-DC-01 and AB-DC-03 are coincident with Heinrich stadials 1 and 2 suggesting that Heinrich stadials 1 and 2 in the Bahamas were potentially characterized by increased aridity as well as decreased temperature."	• "By correlating intervals in cores A and D, we estimated that the minimum water depth at the onset of the Younger Dryas interval (13,000 cal yr B.P.) and at ~11,500 cal yr B.P. was ~2.5 m. This estimated depth fits well with our inference of shallow conditions at ~11,200 cal yr B.P., based on the presence of the aquatic plants and indicators in core A" • "We infer increasingly dry conditions after 11,200 cal yr B.P., as the area of open water diminished, peat formed, and accumulation slowed or became nonconstant first near core D by 10,680 cal yr B.P., and then near core A by 9720 cal yr B.P."
(Arienzo et al. 2017)	(Newby et al. 2000)
10.1016/j.quascirev.2017.02.004	10.1006/qres.1999.2120

Site	Proxy material	Dating method	Latitude	Longitude	Precipitation response	Notes	Citation	DOI
Blanding Lake	Lacustrine sediment	Radiocarbon (calibrated)	41.79	-75.68	Wet	• See Figure 3D	(Shuman and Burrell 2017)	10.1017/qua.2017.62
Crooked Pond	Lacustrine sediment	Radiocarbon (calibrated)	41.89	-70.65	Wet	• See Figure 7 and Table 3	(Shuman et al. 2001)	10.1006/qres.2001.2273
N/A	Sub-fossil wood	Radiocarbon (calibrated)	Midwestern United States	Midwestern United States	Wet	• *Not included in Figure 1 of this paper given relative humidity reconstruction methods did not sample from a single site* • "Midcontinental RH [relative humidity] was similar to modern conditions during the Last Glacial Maximum, progressively increased during the Bølling-Allerød, peaked during the Younger-Dryas, and declined sharply during the early Holocene"	(Voelker et al. 2015)	10.1016/j.yqres.2015.01.001

Table 3.1
Existing proxy records used for precipitation responses to an Atlantic meridional overturning circulation weakening.

Chapter 4 Detecting legacies of millennial scale climate oscillations on modern biodiversity: lessons from a proxy-model comparison

Note: This chapter is currently in preparation for submission to the *Global Ecology and Biogeography* with coauthors David P. Helmers, Volker C. Radeloff, Benjamin Zuckerberg, and John W. Williams.

Citation: Fastovich, D., D. P. Helmers, V. C. Radeloff, B. Zuckerberg, and J. W. Williams, *in prep*: Detecting legacies of millennial scale climate oscillations on modern biodiversity: lessons from a proxy-model comparison. *Glob. Ecol. Biogeogr.*

4.1 Abstract

Aim: Recent papers have suggested that contemporary distributions and hotspots of biodiversity are shaped, in part, by climate stability during the late Quaternary. For example, the stable temperatures of the lower latitudes acted as refuges for biodiversity while higher temperature variability in the high latitudes contributed to lower biodiversity. These analyses have not explicitly assessed the effect of abrupt millennial-scale variability forced by meltwater pulses into the North Atlantic. Additionally, the effect of uncertainties resulting from choice of climate model simulation remains under-explored. We aim to assess the legacies of millennial-scale climate changes within the contemporary distribution of amphibians, birds, mammals, reptiles, and trees in eastern North America, using meltwater forcing experiments from climate models and the Younger Dryas as the focal time period.

Location: Eastern North America (east of 90°W)

Time period: 12,900 years before present to 1964-2019 AD

Major taxa studied: Amphibians, birds, mammals, reptiles, and trees

Methods: We use a suite of 12 climate simulations driven by meltwater forcing into the North Atlantic and proxy-based climate reconstructions of temperature and precipitation changes associated with the Younger Dryas climate event in eastern North America. We then build

generalized linear models that predict contemporary species richness as a function of these simulated and reconstructed paleoclimate anomalies, modern climate variables, and spatial predictors.

Results: There is weak to no signal of past meltwater forcing and millennial-scale variability on contemporary patterns of biodiversity in eastern North America. Alternative simulations of millennial-scale climate event yield opposing predicted effects of paleotemperature and paleoprecipitation changes on contemporary species richness. The percent deviance explained by paleoclimatic predictors ranges from 0.01% to 16.12% and are roughly a third of those for modern climate predictors. The strength and form of paleoclimate-biodiversity relationships are sensitive to choice of spatial modeling terms.

Main conclusions: Several hypotheses may explain the weak predicted relationships between past millennial-scale uncertainty and contemporary biodiversity. The spatial fingerprints of climate anomalies associated with past hosing remains uncertain and variable among models and proxy-based reconstructions. The effects of meltwater forcing may be weaker in eastern North America, given its westerly position relative to the North Atlantic. Rates of species responses to past climate changes may have been fast enough to remove any legacy effects associated with millennial-scale variability, e.g. with fewer dispersal barriers in eastern North America than in other regions such as Europe where there is clearer evidence that spatial variations in late-Quaternary climate stability left imprints on contemporary biodiversity.

4.2 Introduction

Multiple studies have reported detectable legacies of past climate changes in the contemporary distribution of flora and fauna, both globally and in well-studied regions such as western Europe (Brown et al. 2020; Petit et al. 2002; Sandel et al. 2011; Svenning et al. 2008;

Svenning and Skov 2004, 2007; Jansson 2003). All assessments of the effects of past climate

changes on modern biodiversity and endemism rely upon climate simulations from Earth System

Models (ESM, Brown et al. 2020; Rangel et al. 2018; Sandel et al. 2011; Weigelt et al. 2016)

because they offer complete spatial coverage and a full array of climate variables. However, past

climate simulations have several well-known limitations. First, climate simulations always differ

from the true past state of the climate system to some degree, with the directionality and

magnitude of biases varying among models; a major effort in paleoclimatology is to build proxy

networks that can test and refine model simulations (COHMAP Project Members 1988; Bartlein

et al. 2011; Lora and Ibarra 2019; Hargreaves et al. 2013; Delworth and Mann 2000; Wanner et

al. 2008; Tierney et al. 2020; Osman et al. 2021). The potential issue of data-model discrepancies

is particularly acute for simulations of millennial-scale climate variability that may have been

forced by pulses of meltwater into the North Atlantic (Broecker et al. 1985; Clark et al. 2002;

Ganopolski and Rahmstorf 2001; Rahmstorf 2002), because models continue to show substantial

differences in the predicted spatial fingerprints at regional to sub-hemispheric scales. Globally,

the redistribution of heat and subsequent interhemispheric temperature changes and the position

and strength of the Intertropical Convergence Zone remain variable across climate models[1]

(Kageyama et al. 2013). In eastern North America, a recent multi-model and data-model

comparison by Fastovich et al. (in revision) documented large data-model discrepancies in

simulated precipitation changes following abrupt climate changes forced by pulses of meltwater

into the North Atlantic in three atmosphere-ocean general circulation models.

Model biases are also present in state-of-the-science simulations for the 20th- and early

21st-century from the Coupled Model Intercomparison Project Phase 6 (Eyring et al. 2016) which

---

[1]We use the general term 'climate model' to refer to climate simulations from models of varying complexity, from Earth System Models to general circulation models.

over- and underestimate precipitation changes since the pre-Industrial in the United States (Srivastava et al. 2020) and continue to struggle to accurately simulate the Intertropical Convergence Zone (Tian and Dong 2020). Data-model comparisons for the past also demonstrate disparities between model simulations and proxy-based reconstructions (Lora and Ibarra 2019; Hargreaves et al. 2013; Fastovich et al. in revision). The Holocene Conundrum is a notable disagreement between geologic evidence and models wherein geologic evidence suggests that temperatures have cooled since the mid-Holocene (ca. 9,000 years before present, Marcott et al. 2013) while models indicate temperatures increased (Liu et al. 2014). Recent research has demonstrated that this discrepancy may be caused by seasonal biases in proxy-based climate reconstructions (Bova et al. 2021). While alternate analyses based on proxy reconstructions from terrestrial environments suggest that regional biases in prior global syntheses may be the cause of the Holocene Conundrum (Marsicek et al. 2018). Similar discrepancies exist in hydroclimate proxy reconstruction-climate simulation comparisons of the most recent deglaciation in North America. Lora and Ibarra (2019) compare the TraCE-21ka climate simulations to a multi-proxy network and identify that proxy reconstruction-climate simulation agreement is limited to the coastal southwestern and northwestern United States. In the northcentral and northeastern United States, proxy reconstructions and climate simulations produce opposing trends. Proxies suggest a drier deglaciation while simulations indicate wetter conditions when compared to the pre-Industrial (Lora and Ibarra 2019).

Inaccuracies in ESMs are a well-known challenge in global change ecology and biodiversity modeling, where it is viewed as one of the top uncertainties in predicting future species distributions, particularly at finer spatial scales. For example, Thuiller et al. (2019) analyzed the impact that climate simulation uncertainties can have on future projected climate

suitability for amphibians, birds, and mammals and demonstrated that climate simulation selection was among the largest sources of variability in projections of species loss and beta diversity in the North Africa, Western Asia, and West Africa Intergovernmental Science-Policy Platform on Biodiversity and Ecosystem Services subregions, second only to climate simulation boundary conditions. However, despite the known issue of inaccuracies in ESM simulations, biodiversity modeling research interested in the legacy effects of past climate change often employ just one or two paleoclimatic simulations and do not consider the potential effects of climate model inaccuracy or discrepancies among climate simulations (Brown et al. 2020; Araújo et al. 2008). Most early efforts relied upon paleoclimate simulations from the Paleoclimate Model Intercomparison Project Phase II (PMIP2, Braconnot et al. 2007) that were post-processed to extract bioclimatic variables and statistically downscaled for WorldClim v1.4 (Hijmans et al. 2005). However, only three of the seven Last Glacial Maximum simulations from PMIP2 are available in WorldClim v1.4 (Hijmans et al. 2005) and numerous studies use two of the paleoclimate simulations, often averaging the alternate simulations for analysis (Sandom et al. 2014; Waltari et al. 2007; Leite et al. 2016; Weigelt et al. 2016; Jakob et al. 2009; Gugger et al. 2013) but infrequently discussing the role of intermodel uncertainty on ecological interpretations (Thomé et al. 2010; Peterson and Nyári 2008). Other groups have selected several the climate simulations from PMIP, but the climate simulation selection process is not well documented (Sandel et al. 2011; Werneck et al. 2012; Carnaval and Moritz 2008; Werneck et al. 2011). This is problematic because the climate sensitivity from PMIP2 varies widely among ESMs, resulting in Last Glacial Maximum climate simulations that are too warm or too cold relative to observations (Hargreaves et al. 2012; Annan et al. 2022). For example, the Last Glacial Maximum simulation from MIROC-ESM have seen extensive use because of availability

in WorldClim v1.4 (Hijmans et al. 2005), but this simulation only shows moderate skill at simulating proxy reconstructions of the Last Glacial Maximum climate (Hargreaves et al. 2013). These issues are compounded in biogeographic studies that examine the effects of climate changes across the most recent deglaciation, because most studies rely on only one transient climate simulation, the TraCE-21ka experiments (He 2011; Liu et al. 2009). The TraCE-21 ka experiments are able to reproduce many key features of deglacial climate evolution (Liu et al. 2009), but these simulations also have well-documented inaccuracies, such as poor skill at simulating deglacial hydroclimate changes (Lora and Ibarra 2019).

As our understanding of past climate variability has advanced, biodiversity modelers have become increasingly interested in understanding the effects of late-Quaternary variability on past and present species distributions and diversity. Much of the work on the relationship between past climate changes and contemporary biodiversity has focused on interpreting the effects of past glacial-to-interglacial climate changes, with emphasis on the Last Glacial Maximum, to explain regional and global gradients in species endemism and richness (Brown et al. 2020; Rangel et al. 2018; Sandel et al. 2011; Weigelt et al. 2016). The legacies of past glacial and interglacial climate changes in contemporary biodiversity have been largely attributed to dispersal limitations and speciation rates. In Europe, poorly dispersing amphibians inhabit regions that were warmer during the Last Glacial Maximum, like the Balkan, Iberian, and Italian peninsulas, while being absent from habitats that are climatically suitable today but experienced greater glacial cooling, likely because the range shifts for these species lagged climate changes since the end of the Last Glacial Maximum (Araújo et al. 2008). Legacies of the last glacial period are also expressed in the distribution of trees in Europe (Svenning and Skov 2004, 2007; Fløjgaard et al. 2011, 2009) which are among the slowest dispersing organisms and have yet to

infill all climatically suitable environments. More vagile organisms such as birds and mammals with large ranges appear to have been more capable of keeping pace with climate velocity since the end of the Last Glacial Maximum, occupy nearly all of their contemporary climatically suitable environments, and weakly exhibit legacies of past glacial climate changes (Sandel et al. 2011). Climate stability and instability is also invoked in hypotheses that seek to explain global species richness gradients through speciation rates. High climate variability in the high latitudes may have played a dual role at lowering species richness by imparting adaptations that inhibit speciation. Indeed, organisms in the high latitudes tend to be larger with broader niches more capable of surviving climate variability than the smaller, more specialized organisms of the low latitudes (Dynesius and Jansson 2000; Stevens 1989). Far-ranging organisms are also less likely to become isolated, limiting the likelihood of allopatric speciation (Dynesius and Jansson 2000). Higher diversity in the low latitudes contrasts the hypothesized role of high climate variability in the high latitudes. More stable temperatures through glacial cycles would have allowed organisms to specialize, opening niche space, thereby enabling rapid radiation (Dynesius and Jansson 2000).

The next frontier is to better understand the effects of past millennial-scale variability on contemporary biodiversity (Hof et al. 2011; Huntley et al. 2013). These abrupt climate changes, prominent over the last 250,000 years, onset within decades and last millennia (Dansgaard et al. 1982, 1993; Grootes et al. 1993; North Greenland Ice Core Project Members 2004) and can have global impacts on temperature and precipitation (Blunier and Brook 2001; Cheng et al. 2020; Markle et al. 2017; Sachs and Lehman 1999; WAIS Divide Project Members 2015). Such abrupt climate changes are attributed to changes in ocean circulation through the input of freshwater into the North Atlantic, thereby altering global heat budgets and climate (Broecker et al. 1985;

Carlson et al. 2007). Rates of climate change for millennial-scale climate oscillations exceed those of the most recent deglaciation at regional scales (Williams et al. 2021). The Younger Dryas, the most recent millennial-scale climate oscillation, is associated with hemispheric climate changes of 2 to 5°C in ~100 years and regional climate changes of as much as 3°C in as little as 50 years (Overpeck et al. 2003; Williams and Burke 2019). Millennial scale climate variability can manifest differently from glacial-interglacial variability: millennial-scale climate oscillations can have antiphased climate changes at regional and hemispheric scales while glacial-interglacial cycles tend to produce temperature changes of the same direction globally (i.e., global warming or cooling) because of the strong greenhouse gas forcing. At hemispheric scales, millennial-scale climate oscillations lead to colder conditions in the Northern Hemisphere and warmer conditions in the Southern Hemisphere (WAIS Divide Project Members 2015; Shakun and Carlson 2010). At regional scales, shifts in the Intertropical Convergence Zone produce wet/dry dipoles across Amazonia (Chiang and Bitz 2005; Peterson et al. 2000; Zhang et al. 2017). Similarly, summer temperatures decreased across the coast of western Europe while increasing in central Europe (Schenk et al. 2018). Recent studies suggest deglacial climate stability is an important predictor of modern biodiversity, but have not disentangled the unique contributions of glacial and millennial climate variability. Brown et al. (2020) looked at both temperature and precipitation variability effects across the most recent deglaciation and demonstrated that deglacial temperature stability and precipitation instability were predictors of greater contemporary richness in amphibians, mammals, and birds, relying on the TraCE-21ka simulations.

Here we test the hypothesis that temperature and precipitation stability in the southeastern United States enabled organisms to persist and flourish through millennial-scale climate

oscillations and may explain the modern configuration of species richness in eastern North America. Eastern North America is well suited to assess the effects of millennial-scale climate oscillations, proxy-model disagreement, and intermodel differences upon contemporary biodiversity. Climate models have demonstrated high divergence among simulated temperature and precipitation changes for millennial-scale climate events in eastern North America (Kageyama et al. 2013; Fastovich et al. in revision). Eastern North America also contains a spatially dense network of proxy records that can serve as a benchmark to compare against modern biodiversity-paleoclimate relationships derived from climate models. These proxies provide histories of temperature (Fastovich et al. 2020a) and precipitation (Fastovich et al. in revision) and demonstrate that eastern North America experienced complex spatial fingerprints of climate changes during the Younger Dryas. Temperature changes during the Younger Dryas climate event followed a dipole pattern, with cooling north of 35°N and warming south of this latitude. A dipole in temperature changes is contrasted by precipitation changes which exhibited a tripole pattern (Fastovich et al. in revision, 2020a). Warming and wetting in the southeastern United States (Fastovich et al. in revision; Grimm et al. 2006) during the Younger Dryas is particularly notable and has been hypothesized to be a mechanism by which the southeastern United States was a refuge from millennial-scale climate variability (Fastovich et al. 2020a).

The southeastern United States is today a biodiversity hotspot with high amphibian, avian, and arboreal species richness (Jenkins et al. 2015) that has been interpreted as a refuge from glacial and interglacial climate changes (Soltis et al. 2006; Deevey 1949). One explanation is that past environmental filtering and slow response times left a legacy on the modern biodiversity. Alternatively, muted millennial-scale climate variability in the southeastern United States may have preserved biodiversity, while greater millennial-scale climate variability north

of 35 °N may have acted as a strong environmental filter on species distributions during the end Pleistocene (Fastovich et al. 2020a). Analyses of fossil pollen data suggest that the mismatch between late-glacial plant assemblages and climate increased during the late-glacial period (Knight et al. 2020), which may be explainable by no-analog climate changes (Veloz et al. 2012), or lagged vegetation responses to rapid climate change. However, other analyses of fossil-pollen records in the northeastern United States (Williams et al. 2002; Shuman et al. 2004) indicate that past vegetation assemblages tracked abrupt changes of the most recent deglaciation, suggesting that plant distributions should contain few legacies of millennial-scale climate oscillations. Moreover, recent phylogenetic analysis demonstrates little influence of glacial cycles on the contemporary genetic diversity of fourteen woody tree taxa (Lumibao et al. 2017), perhaps because glacial cooling was pronounced across most of eastern North America (Osman et al. 2021; Tierney et al. 2020). Undetected 'cryptic' refugia may explain the lack of glacial signatures in the genetic diversity of tree taxa across eastern North America (Soltis et al. 2006; McLachlan et al. 2005). The lack of large migration barriers in eastern North America would have allowed organisms to track their climate preferences across successive millennial-scale climate events, unlike Europe where the Alps are critical to understanding the contemporary distribution of trees and amphibians by acting as a barrier for postglacial migration (Svenning and Skov 2007, 2004; Hewitt 1999).

Here, we assess whether imprints of past millennial-scale climate changes are present in the modern distribution of amphibians, birds, mammals, reptiles, and trees in eastern North America by testing whether estimates of past climate change from proxies and climate models are significant predictors of contemporary biodiversity. Our proxy reconstructions focus on the Younger Dryas (ca. 12,900 to 11,700 ka), the most recent millennial-scale climate event

commonly attributed to an input of freshwater into the North Atlantic Ocean (Broecker et al. 1985; Carlson et al. 2007) or the Arctic Ocean (Keigwin et al. 2018). We build relationships between contemporary species richness, paleotemperature, paleoprecipitation, modern temperature, and modern precipitation using generalized linear models. Within these generalized linear models, we assess the role of spatial autocorrelation by fitting two sets of statistical models that vary how spatial autocorrelation is modeled. Lastly, we determine the effects of climate model bias and uncertainty on the statistical paleoclimate-biodiversity relationships by using a suite of 12 climate simulations forced with freshwater that mimics the onset of a millennial-scale climate event within our statistical modeling approach. Our analyses highlight that differences between alternate paleoclimate estimates are a key source of uncertainty in paleoclimate-biodiversity relationships and alter resulting ecological interpretations.

4.3 Climate Variations at Orbital and Millennial Timescales: Processes, Patterns, and Implications for Contemporary Biodiversity

The repeated transitions from cold, glacial climate states to warm, interglacial climate states are well documented over the last 5 million years and are associated with global changes in ice volume (Lisiecki and Raymo 2005). These changes in ice volume and climate are paced by variations in insolation, altering Earth's energy budget and causing global cooling or warming, thereby initiating glaciation or deglaciation, respectively (Berger 1978). The eccentricity of Earth's orbit around the Sun, the precession of the vernal equinox within this orbit, and the obliquity of Earth's axial tilt alter insolation and control the pacing of glacial cycles and are termed Milankovitch cycles (Berger 1978; Milankovitch 1941). Insolation changes forced by precession are antiphased between the two hemispheres (i.e. an insolation maximum in the Northern Hemisphere is matched by an insolation minimum in the Southern Hemisphere), so

global changes in greenhouse gas concentrations are invoked to explain globally synchronous glaciation and deglaciation (Broecker 1982). Greenhouse gas concentrations from Antarctic ice cores spanning the last 850,000 years confirm the close association between CO_2 concentrations and global climates (Petit et al. 1999; Lüthi et al. 2008; Siegenthaler et al. 2005), with recent evidence suggesting uptake and release of dissolved CO_2 in global oceans is essential to making glaciation and deglaciation globally synchronous despite antiphased insolation changes (Kobayashi et al. 2021; Sigman et al. 2010).

Transitions between glacial and interglacial climate states can be modeled within Earth System Models and general circulation models because orbital geometries are deterministic over the last 50 million years (Berger 1989; Berger and Loutre 1991; Laskar et al. 2004). Values for eccentricity, obliquity, and precession are prescribed for a climate model experiment and then the climate model simulates the resulting climate state. Orbital parameters can be unchanged in 'snapshot' simulations where the climate model is run until a statistical equilibrium in climatology is reached, as in most of the Paleoclimate Modelling Intercomparison Project experiments (e.g. Kageyama et al. 2017), or the values can be updated transiently, following the gradual changes in orbital parameters through time, as in the TraCE-21ka experiments (He 2011; Liu et al. 2009). Climate simulations have broad success in simulating the climates of the Last Glacial Maximum and last deglaciation in response to changes in orbital parameters (Hargreaves et al. 2013), owing to smooth forcings and quasi-linear responses of the climate system to precession and obliquity (Imbrie et al. 1992). Even though the 100,000 year glacial cycles of the late-Pleistocene are attributed to nonlinearities in the atmosphere-ocean system (Clark et al. 2006; Hays et al. 1976; Imbrie et al. 1993; Pisias and Moore 1981), climate models still accurately simulate glaciation in response to eccentricity changes (Abe-Ouchi et al. 2013).

The ecological effects of climate changes across glacial cycles has become integral to understanding global contemporary biodiversity. Escape from glacial climate variability is a longstanding hypothesis to explain high species richness and endemism in the tropics and low biodiversity at high latitudes and has been applied to explain amphibian, avian, mammalian, floral, and arboreal diversity globally (Araújo et al. 2008; Dynesius and Jansson 2000; Fjeldsaå and Lovett 1997a,b; Haffer 1969; Harrison and Noss 2017; Hewitt 2000; Jansson 2003; Wallace 1878). Climate models forced by changes to orbital parameters have enabled a direct assessment of these hypotheses and have broadly supported the importance of temperature stability (Araújo et al. 2008; Jansson 2003; Sandel et al. 2011) and, to a lesser extent, precipitation instability (Brown et al. 2020). The earliest uses of paleoclimate simulations from climate models to explain contemporary patterns of global endemism supported the role of climate stability and the orbitally forced range dynamics hypothesis (Dynesius and Jansson 2000; Jansson and Dynesius 2002). This hypothesis proposed that speciation rates were lower in the high latitudes from climate-induced local extirpations of isolated populations necessary for allopatric speciation (Dynesius and Jansson 2000). Sandel et al. (2011) demonstrated that temperature velocity following the most recent deglaciation is a key predictor of contemporary endemism globally, with the strongest relationship for poorly dispersing amphibians. This finding highlighted the possibility that contemporary species distributions may not be in equilibrium with contemporary climate (Svenning and Skov 2004, 2007). Beyond the most recent deglaciation, Rangel et al. (2018) modeled the history of life for mammals and birds by including evolutionary and ecological processes over successive glacial and interglacial cycles throughout South America with a striking similarity to modern distributions of birds and mammals.

Climate varies at a continuum of timescales from the annual to orbital periodicity (Huybers and Curry 2006), so focusing too much on modes of climate variation at glacial to interglacial timescales risks excluding the possible influences of other modes of climate variability. In particular, climate of the last 250,000 years was marked by rapid, global climate changes at millennial time scales that were first recognized in the Greenland ice cores (Dansgaard et al. 1982, 1993; Grootes et al. 1993; North Greenland Ice Core Project Members 2004). Unlike the regular orbital pacing of glacial cycles, millennial-scale climate oscillations occur episodically with a quasi-periodicity of ~1,470 years (Schulz 2002). Two classes of millennial-scale climate oscillations are recognized with hypothesized links between them. Dansgaard-Oeschger events were first identified in the Greenland Ice Cores (Dansgaard et al. 1982) as climatic warming (termed interstadial) that initiated abruptly followed by a comparatively gradual cooling to a colder climate (termed stadial), of which 26 have been identified (North Greenland Ice Core Project Members 2004). The causes of Dansgaard-Oeschger events remain highly debated between forced and unforced mechanisms (Bond et al. 1999; Broecker et al. 1985; Clark et al. 2002; Ganopolski and Rahmstorf 2001; Li and Born 2019; Shaffer et al. 2004; Wunsch 2006), but a change in deep ocean circulation and global heat redistribution is a commonly invoked mechanism (Broecker et al. 1985; Clark et al. 2002; Ganopolski and Rahmstorf 2001; Rahmstorf 2002). The quasi-periodicity of millennial-scale climate oscillations has caused some to hypothesize that millennial-scale climate changes are caused by stochastic resonance, whereby noise amplifies deterministic processes and enables abrupt changes in deep ocean circulation and global climate (Alley et al. 2001; Claussen et al. 2003; Ganopolski and Rahmstorf 2002). Heinrich events (Heinrich 1988) occurred following a destabilization of ice sheets in the Northern Hemisphere during the coldest conditions of a

Dansgaard-Oeschger event (Bond et al. 1993), and are identified as coarse sediments in North

Atlantic ocean cores, likely rafted by icebergs (Bond et al. 1992; Hemming 2004). Surface ocean

waters subduct in the North Atlantic which drives the Atlantic meridional overturning circulation

(AMOC), a circulation cell that transports warm, equatorial waters to the North Atlantic making

it a key component of global heat budgets (Ganachaud and Wunsch 2000). This outflow of ice

into the North Atlantic Ocean during a Heinrich event is hypothesized to prevent the subduction

of surface ocean waters, weakening the AMOC, and may be responsible for a key feature of

millennial-scale climate events: the 'bipolar seesaw'. The hallmark feature of the bipolar seesaw

is Northern Hemispheric cooling and Southern Hemispheric warming (Broecker 1998). Although

this conceptualization oversimplifies the regionally variable climate changes within each

hemisphere, it captures the broad reorganization of heat distribution between the two

hemispheres and resulting global climate change. Beyond temperature changes, there is a close

connection between millennial-scale climate oscillations and shifts in the Intertropical

Convergence Zone (Chiang and Bitz 2005; Peterson et al. 2000), changes in the strength of the

Asian monsoon (Wang et al. 2001), shifts in the austral westerlies (Markle et al. 2017; Whittaker

et al. 2011), among many other climate changes. The magnitude of climate changes, rate of

climate changes, the abundance of millennial-scale climate events within the last 250,000 years,

and the rarity of species extinction amidst this variability suggest that organisms coped with

these abrupt climate change through range shifts, phenotypic plasticity, or still unrecognized

ways (Hof et al. 2011). Vegetation communities in eastern North America (Williams et al. 2002;

Shuman et al. 2002) responded to past millennial-scale climate oscillations by migrating while

megafaunal turnover during abrupt warming events in the late Quaternary (Cooper et al. 2015)

suggest that contemporary biodiversity may contain legacies of millennial-scale climate changes.

Simulating millennial-scale climate events within climate models contains challenges that complicate climatic and biogeographic interpretations. The imposed addition of freshwater to the North Atlantic Ocean is a prescribed forcing in 'hosing' climate model experiments meant to mimic the natural input of freshwater through the destabilization of ice sheets and ice rafting. First, climate models are simulated to a state of statistical equilibrium (i.e. control simulation). Then, a freshwater forcing is applied that prevents the subduction of surface ocean water, reducing the strength of the AMOC, and the climate model is allowed to reach equilibrium under these new conditions. Freshwater hosing produces abrupt climate changes, similar to Dansgaard-Oeschger events, within climate models because the AMOC is bistable, and because abrupt changes between strong and weak circulation states of the ocean propagate to rapidly change global climate (Rahmstorf 1995; Stocker and Wright 1991; Stommel 1961). Bistability of the AMOC, and consequently of global climate, is a key feature of millennial-scale climate events but also challenges accurate simulations. Climate models vary in their sensitivity to this tipping element, and the application of the same freshwater forcing can produce climate changes that differ in magnitude and spatial fingerprint among climate models (Kageyama et al. 2013, 2010; Otto-Bliesner and Brady 2010). Uncertainties in the location and amount of freshwater forcing is an additional complication, with the North Atlantic Ocean as a common region of freshwater forcing (Kageyama et al. 2010), and meltwater forcing hosing in the Pacific (Maier et al. 2018), Arctic (Tarasov and Peltier 2005), and Southern Oceans (Ivanovic et al. 2018b) also potential drivers of millennial-scale climate variations. Within these regions, a greater freshwater forcing results in larger changes to the AMOC and global climates (Kageyama et al. 2010, 2013) but many climate model experiments tend to overprescribe freshwater relative to glaciological evidence (Ivanovic et al. 2018a) in order to produce climate signals commensurate with

paleoclimatic proxies. Despite these challenges, climate models run with hosing experiments can accurately simulate the broad reorganization of global heat and demonstrate widespread cooling throughout the Northern Hemisphere and warming in the Southern Hemisphere (Kageyama et al. 2013). At regional scales, climate models forced with meltwater also demonstrate accurate changes in temperature seasonality in Europe (Schenk et al. 2018), monsoon changes in Asia (He et al. 2021; Pausata et al. 2011; Sun et al. 2012), and precipitation changes in the western United States (McGee et al. 2018b).

4.4 1 Methods

4.4.1 Climate model experiments

We combine 10 climate models of varying resolution and complexity that employ a hosing experimental design with the transient TraCE-21ka experiments (He 2011; Liu et al. 2009) and the statistically downscaled variant of the TraCE-21ka experiments by Lorenz et al. (2016) for a total of 12 climate simulation products. The climate models are sourced from compilations by Kageyama et al. (2013) and Fastovich et al. (in revision). There are two classes of experimental designs within our compilation. The first class is 'hosing-only' experiments where only freshwater input is altered and all other climate forcings are held constant at Last Glacial Maximum conditions. The second class of experiments uses boundary conditions that represent the most recent deglaciation with transient changes in ice sheets, greenhouse gases, freshwater input, and orbital parameters (He 2011; Liu et al. 2009). For both sets of models, we analyze the differences between the control, or 'unhosed' state, and the experimental, or 'hosed' state. For the transient simulations (TraCE-21ka, TraCE-21ka Downscaled), we mirrored the proxy climate anomalies by taking the difference of a 100-year average centered on 11,100 years before present (representing the early Holocene, with minimal meltwater forcing) from a 100-

year average centered on 12,300 years before present (representing the Younger Dryas, with high meltwater forcing).

4.4.2 Proxy paleoclimate estimates

We use paleotemperature and paleoprecipitation reconstructions for the Younger Dryas from Fastovich et al. (in revision) and Fastovich et al. (2020a) that were developed using fossil-pollen and branched glycerol dialkyl glycerol tetraethers (brGDGTs) from lacustrine sediments at 42 sites. All proxy-based reconstructed climate changes used here are calculated as anomalies centered around the Younger Dryas climate event with the mid-Younger Dryas (12,300 years before present) analogous to the 'hosed' state of the climate simulations and the early-Holocene (11,100 years before present) as the 'unhosed' state. Site selection in Fastovich et al. (in revision) and Fastovich et al. (2020a) balanced chronological control quality and spatial coverage. Mean annual temperature and total annual precipitation changes were reconstructed from fossil-pollen using three types of transfer functions (modern analog technique, weighted averaging, weighted averaging-partial least squares, Overpeck et al. 1985; Ter Braak et al. 1993; Ter Braak and Looman 1986). Although transfer-function-based reconstructions of micropaleontological data have known drawbacks, their use has been instrumental in constraining past climatic changes throughout the late Quaternary (Bartlein et al. 2011; Marsicek et al. 2018). Precipitation reconstructions have greater inherent uncertainty than temperature reconstructions (Salonen et al. 2019), but comparisons between our fossil-pollen precipitation reconstructions and precipitation-sensitive proxies from throughout eastern North America demonstrate high agreement (Fastovich et al. in revision).

brGDGTs are organic compounds produced by microorganisms ubiquitous in soils and lake sediments (Schouten et al. 2002; Weijers et al. 2007). Quantitative temperature estimates are

produced through modern calibrations of brGDGT abundances in soils (De Jonge et al. 2014; Weijers et al. 2007; Peterse et al. 2012) and lakes (Martinez-Sosa et al. 2021; Russell et al. 2018). These calibrations are then used on abundances of brGDGTs in lacustrine environments to produce quantitative paleotemperature estimates.

4.4.3 Climate model skill

As in Fastovich et al. (in revision), we use the climate model skill score (Hargreaves et al. 2013) to quantitatively compare our climate model compilation to our proxy network and assess the accuracy of climate model simulations. The climate model skill score is defined as

$$S = 1 - \sqrt{\frac{\Sigma(m_i - o_i)^2 - \Sigma(e_i)^2}{\Sigma(n_i - o_i)^2 - \Sigma(e_i)^2}}$$

where m_i is a simulated climate variable from a climate model, o_i is the proxy reconstructions, e_i is the 1-σ error of the proxy reconstructions, and n_i is a reference result, or null. This metric can assess proxy-model disagreement while accounting for proxy reconstruction uncertainty and is relative to a reference result. We use two reference results that assess whether the climate models can accurately simulate the magnitude and sign of climate change in the proxy record ($n_i = 0$) or the spatial patterns of climate change (Hargreaves et al. 2013)($n_i = $ mean of proxy record). We apply this metric by bilinearly interpolating the climate model simulations (m_i) to the nearest proxy estimate (o_i). During climate model skill calculation, we also perform a spatial debiasing procedure, because our proxy network has a higher density of sites in New England than the Great Lakes region and the southeastern United States. We minimize this spatial bias by resampling proxy sites at a grid cell level. For example, if four proxy sites share a climate model grid cell, one will be randomly selected and used to calculate the climate model skill score. This

procedure is repeated 10,000 times from which we retain the median skill score and 95% confidence interval.

4.4.4 Contemporary species richness

We estimate species richness from the International Union for the Conservation of Nature (IUCN) Red List of Threatened species range maps (IUCN 2017) and tree species range maps from a digitized version of the Atlas of United States Trees (United States Geological Survey 1999) following the methods of Radeloff et al. (2019). Unlike occupancy maps, these range maps outline species ranges that we use to estimate species richness by rasterizing the IUCN Red List and the digitized Atlas of United States Trees polygons to an equal-area 50-km grid and summing overlapping ranges. During rasterizing, we assume species presence in all grid cells that overlap with the species range (Hurlbert and Jetz 2007) and do not employ a threshold of grid cell coverage for a species to be considered present within the grid cell. We follow this procedure to produce estimates of species richness for birds, terrestrial mammals, amphibians, reptiles, and trees. Despite these estimates of species richness being based on range maps instead of occupancy data, at coarse scales, these range maps produce reasonable estimates of species richness with broad use in biogeographic research (Brown et al. 2020; Jenkins et al. 2015; Mittermeier et al. 2003; Sandel et al. 2011).

All analyses were performed on a common 50-km grid using the North America Albers Equal Area projection. All climate model simulations were bilinearly interpolated to this grid. Because the proxy reconstructions are point estimates, we use universal kriging to interpolate the point estimates from the proxy data to the common 50-km grid. We use PyKrige (Murphy et al. 2021) for all kriging routines and use semivariogram range estimates based on mean annual average temperature from 1951-1980 and mean annual precipitation from 1951-1980 from the

National Centers for Environmental Prediction/National Center (NCEP) for Atmospheric

Research Reanalysis (Kalnay et al. 1996) and the Global Precipitation Climatology Centre data

products (Schneider et al. 2017), respectively (Figure S3.13). We perform sensitivity analyses to

assess the role of resolution upon our conclusions by replicating our methods on a 100km grid,

as recommended by Hurlbert and Jetz (2007). We find that grid cell size had little effect on final

results and minimal effect on our conclusions (Figure S3.14-Figure S3.18). Larger grid cells

made the effect of paleotemperature less significant (Figure S3.15, Figure S3.17), likely because

of fewer grid cells, while the effect of paleoprecipitation is largely insensitive to grid cell size

(Figure S3.16, Figure S3.18).

4.4.5 Generalized linear modeling

We built statistical relationships between past millennial-scale temperature and

precipitation changes and contemporary biodiversity using generalized linear models (GLM) that

assume species richness along environmental gradients follows a Gaussian distribution. We opt

for this modeling approach because of a lack of overdispersion in the data when fitted by the

GLMs, few zero values in the species richness estimates, and interpretability of GLMs fit with a

Gaussian distribution. We also tested generalized linear models where species richness follows a

Poisson and negative binomial distributions with a log-link that can be appropriate for species

richness estimates and found minimal improvement in model diagnostics. Using these GLMs, we

separately predict contemporary species richness for amphibians, mammals, resident birds,

reptiles, and trees as a response to past temperature and precipitation changes from the 11

climate models, the kriged proxy reconstructions, and statistically downscaled TraCE-21ka

simulations from Lorenz et al. (2016). Each GLM also includes contemporary annual

temperature and total annual precipitation based on climate means for 1970-2000 from

WorldClim2 (Fick and Hijmans 2017) as additional predictors. We also perform a variant on these analyses in which the error term in the GLM is assumed to follow a Matérn correlation function to account for spatial autocorrelation in the residuals (Dormann et al. 2007).

4.5 Results

4.5.1 Spatial patterns of contemporary species richness and paleoclimate estimates

Species richness for the five classes of organisms and climate simulations demonstrate spatially coherent patterns in eastern North America (east of 92 °W). Species richness is particularly high for amphibians, trees, and reptiles in the southeastern United States (south of 35°N), while mammals demonstrate heightened species richness in the Appalachian Mountains and birds have greater richness along coastlines (Figure 4.1). Greater amphibian, reptilian, and arboreal diversity in Florida and the adjacent region is a well-documented phenomenon and is captured in our richness estimates (Dobson et al. 1997; Jenkins et al. 2015; Mishler et al. 2020; Noss et al. 2015). Our kriged proxy reconstructions and eight of the climate simulations demonstrate that temperatures increased in the southeastern United States while greater magnitude temperature change to colder conditions is a common feature across all but two of the paleoclimate estimates (Figure 4.1, Figure S3.1). With the exception of the TraCE-21ka paleoprecipitation estimates, all paleoprecipitation estimates indicate a precipitation increase in the southeastern United States (Figure S3.2). The alignment between paleotemperature and paleoprecipitation increase in the southeastern United States and heightened biodiversity in the southeastern United States from our estimates of species richness suggests a possible relationship between contemporary richness and millennial-scale climate changes.

The climate models analyzed reproduce the broad spatial characteristics of a millennial-scale climate oscillation. Large regions of the North Atlantic cool in response to freshwater

forcing (Figure 4.2A), a hallmark of millennial-scale climate events (Stocker 1998). The 11

climate models generally agree on the sign of climate change across the Northern and Southern

Hemispheres, but the magnitude of climate change varies (Figure 4.2). However, many regions

exhibit substantial differences among climate simulations, both in eastern North America and

globally (Figure 4.2C, D), that can have impacts on inferred richness-paleoclimate relationships.

The North Atlantic and areas marginal to the Laurentide Ice Sheet exhibit particularly high

model disagreement, likely a result of differential model sensitivity to a weakening in AMOC

resulting from meltwater forcing (Figure 4.2C). Some models demonstrate high sensitivity to the

AMOC and larger climate changes, while other models suggest very low climate sensitivity to

AMOC (Kageyama et al. 2013). For instance, COSMOS-S and COSMOS-W have the greatest

reduction in the AMOC but a moderate change in temperature, indicating lower sensitivity

(Figure S3-1, Kageyama et al. 2013). The greatest temperature changes are reported for models

forced by intermediate reductions in the strength of the AMOC (Figure S3.1, Kageyama et al.

2013). Globally and regionally, precipitation changes are also spatially coherent across the

climate simulations with wetter conditions simulated in eastern North America and much of the

Southern Hemisphere and drier conditions in much of the Northern Hemisphere (Figure 4.2).

Lower temperatures and a shifted Intertropical Convergence Zone likely caused reductions in

precipitation in the North Atlantic and northern Amazonia, respectively (Figure 4.2B). As with

temperature changes, climate models generally agree on the sign of precipitation change but

disagree on the magnitude of precipitation change, with high variability in the North Atlantic and

throughout the northern and southern extent of the Intertropical Convergence Zone (Figure 4.2D,

Figure S3.1). The Indo-Pacific portion of the Intertropical Convergence Zone stands out as a

region of climate model disagreement that is identifiable through small mean change, but high

standard deviation (Figure 4.2D). Climate model disagreement is unsurprising in this region, because accurately modeling the Intertropical Convergence Zone continues to be a challenge (Tian and Dong 2020). Hence, a broad point is that uncertainty in both hosing strength and climate model sensitivity to hosing translates to uncertainty in simulations of past temperature and precipitation. In the next section we explore the effects of this uncertainty on biogeographic modeling of the impacts of millennial-scale variability on present species distributions and diversity.

All climate models simulate little to no cooling across eastern North America south of 35 °N (Figure 4.2A, Figure S3.1). The ability of climate models to accurately simulate mean temperature changes in the proxy record is reflected in positive, albeit low, skill scores for seven climate models (Figure 4.3A). However, the models generally fail to capture the spatial fingerprint reconstructed from the proxy temperature reconstructions which indicate monotonic warming south of 35 °N and a thermal maximum in Florida (Figure 4.2A), resulting in mostly negative skill scores when spatial pattern-matching is tested (Figure 4.3B). Simulated millennial-scale precipitation changes are less spatially variable across all climate models than temperature changes in eastern North America but also are spatially misaligned with proxy reconstructions. All ten climate models simulate wetter conditions under a freshwater forcing in eastern North America that is concentrated on the coast near 38 °N, with variable magnitude and extent (Figure 4.2B, Figure S3.2). Additionally, drying is simulated in maritime Canada and Florida (Figure 4.2B), indicating a spatial tripole of changes in precipitation from the Younger Dryas to early Holocene. Proxy precipitation reconstructions also suggest a tripole pattern but one that is spatially antiphased to the climate models (Figure 4.2B). Multiple proxy records suggest that precipitation increased in Florida during millennial-scale climate oscillations (Arnold et al. 2018;

Fastovich et al. in revision; Huang et al. 2006; Grimm et al. 2006; van Beynen et al. 2017) and

New England during the Younger Dryas (Figure 4.2B)(Menking et al. 2012; Shuman et al.

2001). Antiphased precipitation patterns between the climate models and our multi-proxy

network are reflected in negative climate model skill scores for both the mean and the spatial

configuration skill of precipitation changes (Figure 4.3).

The difference between the ten 'hosing-only' climate model experiments (Figure 4.2A,

B) and the TraCE-21ka experiments (Figure 4.2E, F) helps show the effect of other boundary

conditions on patterns of temperature and precipitation change during the Younger Dryas. Key

features of the TraCE-21ka paleoclimate anomalies (Younger Dryas – early-Holocene) include

the broad-scale temperature decrease across the domain of the Laurentide Ice Sheet (Figure

4.2E). Greenhouse gas concentrations were lower 12,300 years before present than 11,100 years

before present, hence the dominant temperature anomaly is negative (Figure 4.2D). This global

temperature increase associated with increasing greenhouse gas concentrations masks the

canonical 'bipolar-seesaw' pattern commonly associated with a millennial-scale climate event

caused by meltwater forcing (Fig. 4.2E, inset). However, even with other boundary conditions

included, the effects of meltwater forcing can be seen in the equatorial and subtropical Atlantic

(Figure 4.2F, inset), where the southward displacement of the Intertropical Convergence Zone

has been identified as a response to freshwater forcing in the North Atlantic in TraCE-21ka

(McGee et al. 2018a). Thus, for the Younger Dryas, climate signals associated with meltwater

forcing are superimposed upon other climate changes driven by other boundary conditions.

4.5.2 Comparing contemporary biodiversity and paleoclimate estimates

The paleoclimate anomalies for the Younger Dryas to Early Holocene do not emerge as

an important predictor of the contemporary distribution of flora and fauna in eastern North

America (Figure 4.4, Figure 4.5, Table 4.1). Moreover, the effects of paleotemperature and paleoprecipitation vary depending on the paleoclimate estimate analyzed (Figure 4.2, Figure S3.1, Figure S3.2), which indicates high sensitivity to choice of paleoclimatic model. High intermodel variability makes it difficult to determine the directionality of the relationship between contemporary biodiversity and millennial-scale climate change and leads to the risk of false inference when relying on a single model. Additionally, the inclusion of modern environmental predictors substantially changes the predicted relationship between the magnitude of paleoclimate change and species richness in sign and magnitude (e.g. Figure 4.4A vs Figure 4.4B). For instance, when considering GLMs where modern climate correlates are included, the deviance explained by our paleoclimate estimates range from 0.48% to 15.15% and averaging 7.77% (Table 4.1). In contrast, modern climate correlates explain 15.08% of the deviance when averaged across all classes of organisms and paleoclimate estimates (Table 4.1).

Moreover, when spatial covariates are included in, the GLMs, nearly all contemporary climate- and paleoclimate-species richness relationships become insignificant because of high spatial autocorrelation in the species richness estimates (Figure S3.3, Figure S3.4, Figure S3.5, Figure S3.6, Table 4.1). The high sensitivity of paleotemperature and paleoprecipitation GLM coefficients to change in magnitude and sign across varying paleoclimate estimates is likely a result of little covariance between contemporary species richness and millennial-scale climate change, suggesting that any imprints of millennial-scale climate events on contemporary biodiversity are not detectible.

Varying relationships between paleoclimate estimates and contemporary climate richness yield diverging ecological interpretations and highlight the pitfalls of relying on a single source of paleoclimatic information. Our proxy reconstructions suggest that increased millennial-scale

temperature change for trees, mammals, amphibians, and birds is predictive of greater

contemporary richness (Figure 4.4A), cohering with hypotheses that suggest environmental

disturbance is necessary for greater biodiversity (Connell 1978; Brown et al. 2020). Reptilian

richness has an opposing pattern where smaller millennial-scale temperature change is predictive

of greater richness, as expected if the organisms lagged millennial-scale temperature change

(Araújo et al. 2008). Comparing the effects of paleoclimate on contemporary richness estimates

using proxy-based paleoclimate estimates to those from climate simulations, three classes of

effects emerge: 1) effects that agree with GLMs based on proxy reconstructions, 2) effects that

are opposite to the proxy records, and 3) no effect of paleoclimate estimates. Climate models that

agree with the paleotemperature-biodiversity relationship based on the proxy network share a

similar directionality in the Younger Dryas temperature dipole across eastern North America and

similar spatial structure, reflected in high temperature anomaly skill scores (Figure 4.3)

(Fastovich et al., 2020). The temperature dipole separating positive and negative temperature

anomalies in the kriged proxy climate reconstructions runs west-northwest to east-southeast,

matched by CM2Mc and TraCE-MWF in the southeastern United States (Figure S3.1). Indeed,

both of these climate models produce temperature effects similar to the proxy record for reptiles,

birds, and trees (Figure S3.1, Figure S3.9). Climate models with a temperature dipole that is

opposite to the kriged proxy reconstructions, running from west-southwest to east-northeast, like

IPSL produce opposing effects for paleotemperature, with greater climate stability predictive of

higher contemporary biodiversity (Figure 4.4, Figure S3.1, Figure S3.9), cohering with

temperature stability hypotheses (Dynesius and Jansson 2000; Jansson 2003).

4.6 Discussion

4.6.1 Does millennial-scale climate change shape contemporary biodiversity?

These findings indicate that, so far, there is no detectable effect of past abrupt changes to AMOC on contemporary biodiversity in eastern North America. Our GLMs suggest that the statistically modeled effect of millennial-scale temperature oscillations is highly sensitive to the choice of taxonomic group and the paleoclimate estimate analyzed (Figure 4.4, Figure 4.5), suggesting no detectible imprints of millennial-scale climate change. This finding contrasts with prior research supporting the role of past climate stability (Sandel et al. 2011; Araújo et al. 2008; Jansson and Dynesius 2002; Dynesius and Jansson 2000; Jansson 2003) and variability (Brown et al. 2020) for preserving biodiversity.

Several hypotheses can explain why this study detects no effect of millennial-scale climate variability (as represented by climate model hosing experiments and proxy data for the Younger Dryas) on contemporary biodiversity. First, there may be a true effect of the Younger Dryas on contemporary biodiversity, but the uncertainty in climate model simulations is too large to be able to detect it. GLMs vary in their ability to predict contemporary biodiversity and this variability is linked to the magnitude of simulated climate changes and the spatial fingerprints of those changes. Climate variability at the millennial timescale is controlled by nonlinear processes that can be difficult to simulate accurately within a climate model (Rahmstorf 1995; Stocker and Wright 1991). Here, sensitivity among climate model responses to freshwater forcing yields opposing ecological interpretations regarding the role of past climate changes as alternate climate simulations suggest that temperatures may have warmed or cooled and precipitation increased or decreased in eastern North America during a millennial-scale climate event (Figure 4.4, Figure 4.5, Figure S3.1, Figure S3.2).

Attempts to reconcile contemporary biodiversity using past estimates of climate velocity (Sandel et al. 2011) and temperature and precipitation change since the Last Glacial Maximum (Brown et al. 2020) have lacked these issues because spatial patterns of temperature changes are similar across many climate models simulating the Last Glacial Maximum at the global scale (i.e. global cooling focused on ice sheet location, Kageyama et al. 2021). Therefore, prior comparisons of glacial climate and contemporary richness based on individual climate models are likely robust in the direction of these relationships (Brown et al. 2020; Sandel et al. 2011; Araújo et al. 2008). However, Last Glacial Maximum climate simulations can vary substantially at regional scales (Hargreaves et al. 2013) suggesting that finer scale analyses likely under-report uncertainties. Climate models under Last Glacial Maximum conditions also vary in the magnitude of cooling caused by differences in climate model sensitivity to greenhouse gases and ice sheets (Hargreaves et al. 2012; Kageyama et al. 2021). Some models suggest that the global climate was 6 °C cooler during the Last Glacial Maximum, while others simulate a lower climate sensitivity and total temperature change of 3.5 °C when compared to the pre-Industrial (Hargreaves et al. 2012; Kageyama et al. 2021). Thus, estimates of ecoclimate sensitivity (e.g. Nolan et al. 2018) based on individual Last Glacial Maximum climate simulations may be more uncertain in magnitude but robust in sign.

Second, there may be a true effect of the Younger Dryas on contemporary biodiversity, but this signal is removed by our handling of spatial autocorrelation. All analyses performed here were replicated using GLMs that were fit assuming error in the model followed a Matérn covariance function (Figure S3.3, Figure S3.4, Figure S3.5, Figure S3.6). In all analyses and interpretations we did not include the effects of spatial autocorrelation in the GLMs due to concerns of model overfitting. While the assumption of spatial autocorrelation in the residuals of

the GLMs improved model fit and entirely removed all residual spatial autocorrelation, pseudo-R^2 values for these models averaged ~.99 and all environmental correlates were insignificant despite overwhelming autecological evidence for the role of contemporary climate at controlling contemporary patterns of species richness (Willig et al. 2003). In light of this, future work should incorporate simultaneous autoregressive models (SAR) or conditional autoregressive models (CAR) that also allow for spatial structure in the response variable (Dormann et al. 2007). Unlike GLMs fit assuming spatial autocorrelation in the residuals, SAR and CAR models include spatial autocorrelation through the addition of a coefficient and adjacency matrix that properly account for spatial autocorrelation in the model coefficients and residuals. The adjacency matrix removes spatial autocorrelation for a grid cell and its neighbors, while retaining global spatial structure, unlike using a function that models spatial autocorrelation in the residuals. SAR and CAR models have seen broad use in biogeographic applications (e.g. Sandel et al. 2011; Tittensor et al. 2010; Araújo et al. 2008) and offer a promising avenue to better account for spatial autocorrelation

Third, the magnitude of millennial-scale climate changes in eastern North America may not have been sufficiently large or long-lasting to leave imprints in the contemporary biodiversity of eastern North America. Proxy based climate reconstructions of temperature and precipitation in eastern North America suggest that regional temperatures varied by 2 °C, at most, (Fastovich et al. 2020a) while precipitation changes were ~0.7 mm/day when averaged across all of eastern North America (Fastovich et al. in revision). Additionally, millennial-scale climate events were short lived; peak cooling commonly lasted 500 to 1,000 years (North Greenland Ice Core Project Members 2004), which is less than 2 to 4 generations for most arboreal taxa. In contrast, climate change since the end of the Last Glacial Maximum averages 5

°C to 10 °C across eastern North America (Bartlein et al. 2011; Tierney et al. 2020) and persisted

for thousands of years. Within the climate simulations assessed here, temperature changes of this

magnitude for a millennial-scale climate event are present in northern Europe (Figure 4.2) and

agreement between modeled and reconstructed vegetation communities in Europe for the Last

Glacial Maximum was only possible when millennial-scale climate oscillations were included in

the dynamic global vegetation model (Huntley et al. 2013). Collectively, this suggest that

legacies of millennial-scale climate oscillations may be more strongly expressed in the

contemporary European biodiversity and may offer a contrasting perspective to eastern North

America. Lastly, regional scale analyses may not be appropriate to detect millennial-scale

climate legacies. A prior analysis that demonstrated legacies of millennial-scale climate

oscillations on contemporary biodiversity, albeit implicitly, was of global extent (Brown et al.

2020) where contemporary species richness gradients and paleoclimate gradients are much

larger.

Fourth, fast ecological responses to climate changes during and after the end of the

Younger Dryas may have removed any detectable signal from contemporary patterns of

biodiversity. Paleoecological archives throughout eastern North America demonstrate that

arboreal taxa responded quickly to Younger Dryas climate changes (Williams et al. 2002) and

were able to keep pace with climate velocities through the most recent deglacial period (Ordonez

and Williams 2013), highlighting that certain taxa may have been in equilibrium with climate

changes since the end of the Last Glacial Maximum (Webb 1986). Few dispersal barriers exist in

eastern North America with mountain ranges and large rivers oriented meridionally and unlikely

to inhibit northward migration. A comparative assessment of the phylogenetic richness of woody

tree taxa in eastern North America and Europe support each of these hypotheses. Phylogenetic

richness demonstrates no coherent spatial pattern in eastern North America (Lumibao et al. 2017), although a latitudinal gradient would be expected if the southeastern United States acted as a refuge from millennial-scale climate change. In contrast, phylogenetic diversity for similar woody tree taxa in Europe demonstrate a latitudinal gradient in phylogenetic richness with greater richness in the south and lower richness in the north (Lumibao et al. 2017), and cohere with the hypothesized importance of southern refugia. Although a synthesis of Younger Dryas temperatures is lacking in Europe, our climate simulation compilation suggests that Europe may have also experience greater millennial-scale climate variability (Figure 4.2A). The difference in phylogeographic patterns between eastern North America and Europe highlight how dispersal barriers shaped contemporary biodiversity. Phylogeographic analysis in Europe have constrained post-glacial expansion for several classes of organisms, with the Alps acting as a dispersal barrier since the end of the Last Glacial Maximum (Hewitt 1999; Petit et al. 2002). Eastern North America lacks similar evidence, where identical phylogeographic analyses are unable to find distinct routes of post-glacial dispersal (Soltis et al. 2006). What's more, phylogeographic evidence even suggests that small populations of mesic tree taxa were able to persist as close as 500-km from the Laurentide Ice Sheet margin (McLachlan et al. 2005). Soltis et al., (2006) hypothesized that topographic differences between Europe and eastern North America are responsible for differences in phylogenetic structure across the regions. Although eastern North America contains the Appalachian Mountains, the Appalachian Mountains are positioned meridionally and would have minimally limited migration of organisms from southern refugia, but have left distinct east/west signatures in the phylogeography of eastern North America (Soltis et al. 2006). Lastly, these alternative explanations may have operated simultaneously, allowing organisms to keep pace with millennial-scale climate change.

4.6.2 Implications for biodiversity modeling

In light of our findings, we urge caution when interpreting ecological relationships from individual climate models, especially at regional scales. Incorporating multiple climate models, like the ensembles provided by the Climate Model Intercomparison Project (Eyring et al. 2016) and the Paleoclimate Modelling Intercomparison Project (Joussaume and Taylor 2000; Kageyama et al. 2017), is common throughout climatological and paleoclimatological analyses (e.g. Dai et al. 2015; Diffenbaugh et al. 2015; Ortega et al. 2015; Oster et al. 2015; Stouffer et al. 2006) and is becoming more common in ecological research (e.g. Fordham et al. 2012; Garcia et al. 2012; Pearson et al. 2014). The paleoclimate simulations downscaled in WorldClim v1.4 (Hijmans et al. 2005) saw broad use in biogeographic applications because of ease-of-use and accessibility. New downscaled paleoclimate estimates based on all Paleoclimate Modelling Intercomparison Project 4 simulations would enable easily incorporating state-of-the-science paleoclimate simulation ensembles within biogeographic models. A preferable alternative would be the creation of open-source workflows that enable end-users to easily access and post-process climate simulation output from the Paleoclimate Modelling Intercomparison Project and the Coupled Model Intercomparison Project, enabling end-users to incorporate continually improving climate simulations within their analyses. In certain circumstances incorporating an ensemble of climate simulations within biogeographic analyses may not be possible. Few transient simulations of the most recent deglacial climate exist with TraCE-21ka (He 2011; Liu et al. 2009) standing as a pillar in paleoclimatic, paleoecological, and contemporary ecological research. The TraCE-21ka simulations have advanced our understanding of ecoclimatic changes since the end of the Last Glacial Maximum (e.g. Nolan et al. 2018; Brown et al. 2020; Veloz et al. 2012; Ordonez and Williams 2013) but have notably deficiencies. For instance, the meltwater

forcing is larger than proxy-constrained estimates (Ivanovic et al. 2018b) and the timing of greenhouse gas forcings for the Bølling-Allerød and Younger Dryas is delayed by ~600 years (Monnin et al. 2001; Marcott et al. 2014) that contribute uncertainty in the climate simulations. Precipitation is notably uncertain as TraCE21-ka demonstrate no skill at simulating mean changes in precipitation during the Younger Dryas across North America and antiphase changes in the spatial configuration of precipitation changes (Fastovich et al. in revision). This pattern holds throughout North America across the most recent deglaciation where TraCE-21ka frequently simulates the wrong sign when compared to the proxy record (Lora and Ibarra 2019).

4.7 Conclusion

We examine the legacies of past millennial-scale climate change in the contemporary distribution of amphibians, birds, mammals, reptiles, and trees in eastern North America and demonstrate that past variations in the strength of the AMOC did not influence contemporary patterns of species richness. The relationship between past climate changes and contemporary species richness is highly sensitive to the paleoclimatic estimates used and the organisms analyzed. We hypothesize that the biodiversity of eastern North America lacks signatures of millennial-scale climate changes because of minimal barriers to dispersal or climate change too small and brief to leave imprints. Diverging estimates of past climate change from climate models and proxies highlights that caution should be taken when making ecological interpretations for the future or past from a single climate simulation. Proxy evidence suggests that increased millennial-scale climate change is predictive of greater species richness for all organisms, conflicting with climate stability hypotheses (Dynesius and Jansson 2000; Haffer 1969; Jansson 2003; Wallace 1878) and supporting the role of climate instability in driving higher richness (Connell 1978). Climate model simulations exhibit similarly confounding results,

with some suggesting that increased paleotemperature change is predictive of greater

contemporary richness while others agree with ecological interpretations based on the proxy

record. These uncertainties are caused by nonlinearities in the climate system associated with

millennial-scale climate changes, namely the AMOC (Rahmstorf 1995; Stocker and Wright

1991), which climate models have difficulty simulating accurately because of varied

sensitivities. Considering these uncertainties, we urge caution when making ecological

interpretations based on analyses of a single climate model.

4.8 Figures
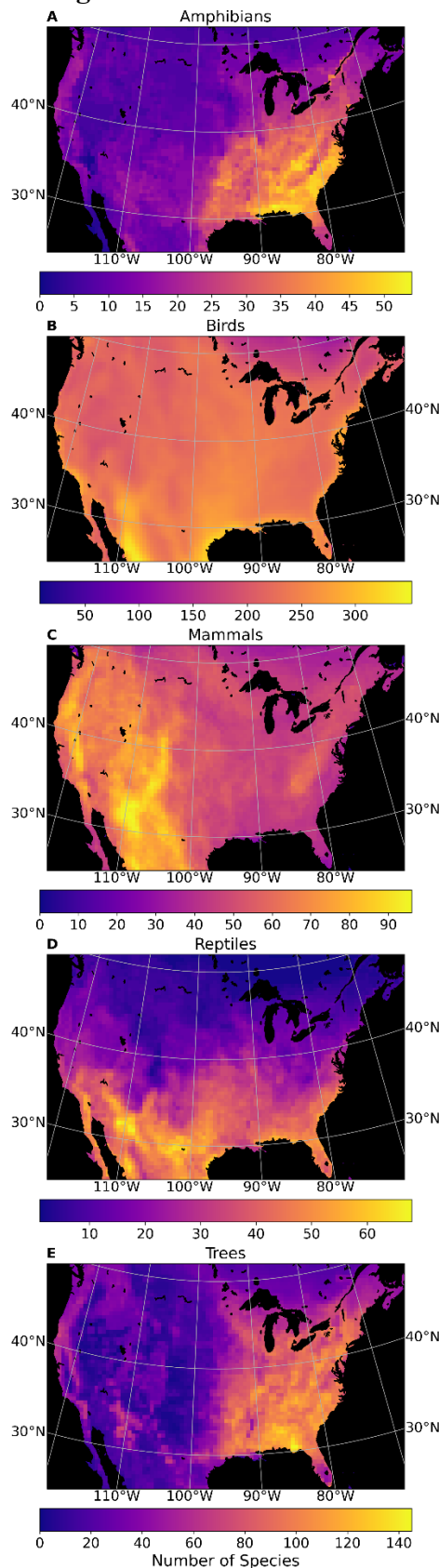
Figure 4.1

(A, B, C, D, E) Species richness estimates for **(A)** amphibians, **(B)** birds, **(C)** mammals, **(D)** reptiles, and **(E)** trees based on range maps from the International Union for the Conservation of Nature (IUCN) Red List of Threatened species (IUCN 2017) and the digitized version of the Atlas of United States Trees (United States Geological Survey 1999).

A Mean Annual Temperature Anomaly

B Mean Annual Precipitation Anomaly

Multi-Model Mean (K)

Multi-Model Mean (mm/day)

C Mean Annual Temperature Anomaly Std. Dev.

D Mean Annual Precipitation Anomaly Std. Dev.

■ Fossil-Pollen
▲ brGDGT

Multi-Model Std. Dev. (K)

Multi-Model Std. Dev. (mm/day)

E TraCE-21Ka Mean Annual Temperature Anomaly

F TraCE-21Ka Mean Annual Precipitation Anomaly

Temperature Anomaly (K)

Precipitation Anomaly (mm/day)
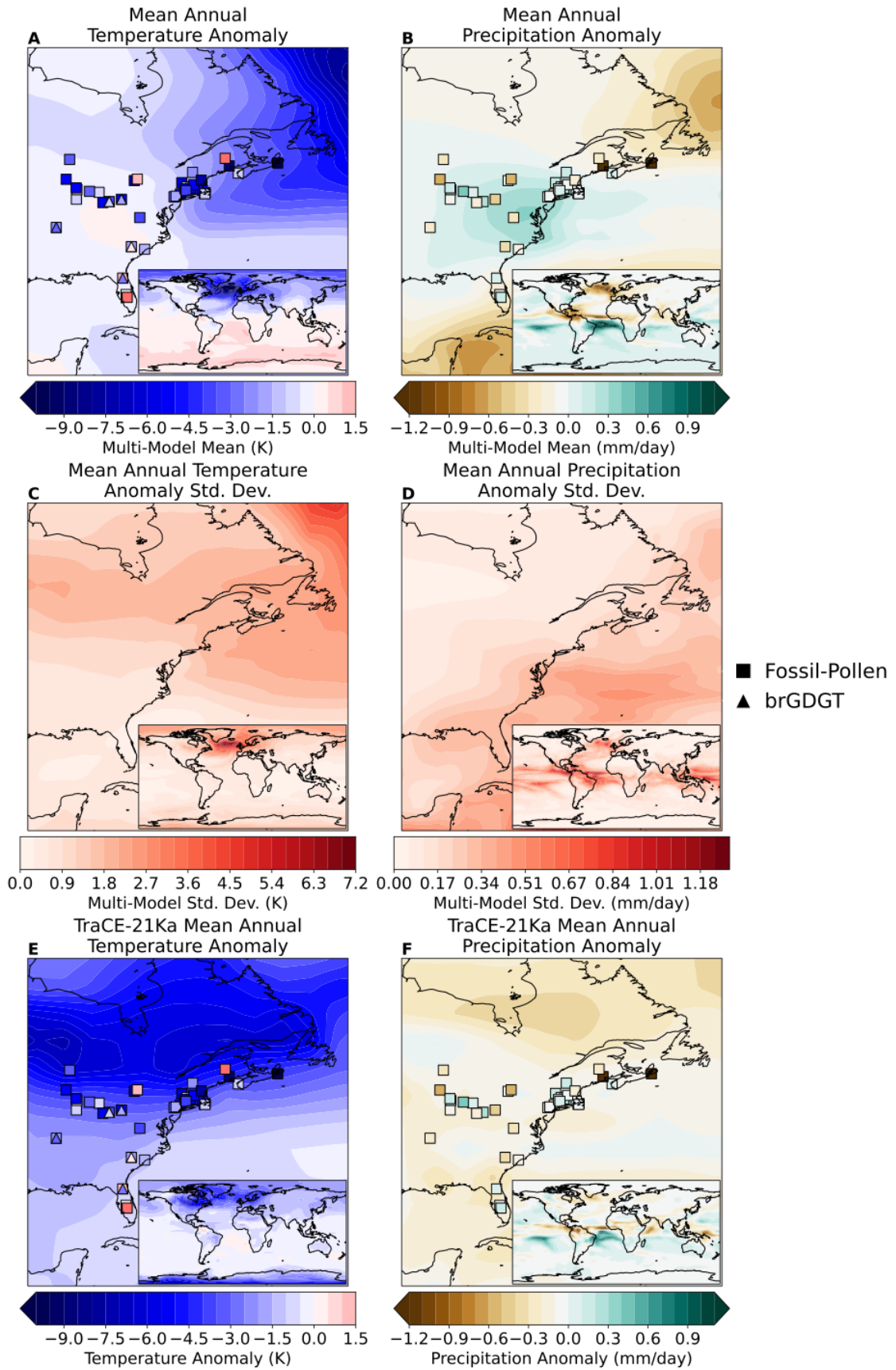
Figure 4.2

Hosed-unhosed climate anomalies from 11 climate simulations of a millennial-scale climate event through the input of freshwater into the North Atlantic Ocean. **(A, B)** The 11 climate models are averaged to produce a multi-model mean of (A) temperature and (B) precipitation anomalies, including TraCE-21ka but excluding the statistically downscaled estimates from Lorenz et al. (2016) for North America. **(C, D)** The standard deviation of (C) temperature and (D) precipitation anomalies for the 11 climate models. **(E, F)** Climate anomalies for the Younger Dryas climate event in the TraCE-21ka experiment only (He 2011; Liu et al. 2009). TraCE-21ka is shown separately to highlight the influence of boundary conditions on resulting climate simulations. (E) Temperature and (F) precipitation anomalies are calculated as the difference between a 100-year mean centered on 11,100 years before present (unhosed state) taken from a 100-year mean centered on 12,300 years before present (hosed state). Each dot represents proxy-based climate reconstruction from fossil-pollen and brGDGTs (Fastovich et al. in revision, 2020a). Negative temperature anomalies indicate that temperatures decreased during the Younger Dryas and positive temperature anomalies indicate that temperatures increased. Positive precipitation anomalies represent a wetter Younger Dryas and negative precipitation anomalies indicate a drier Younger Dryas.
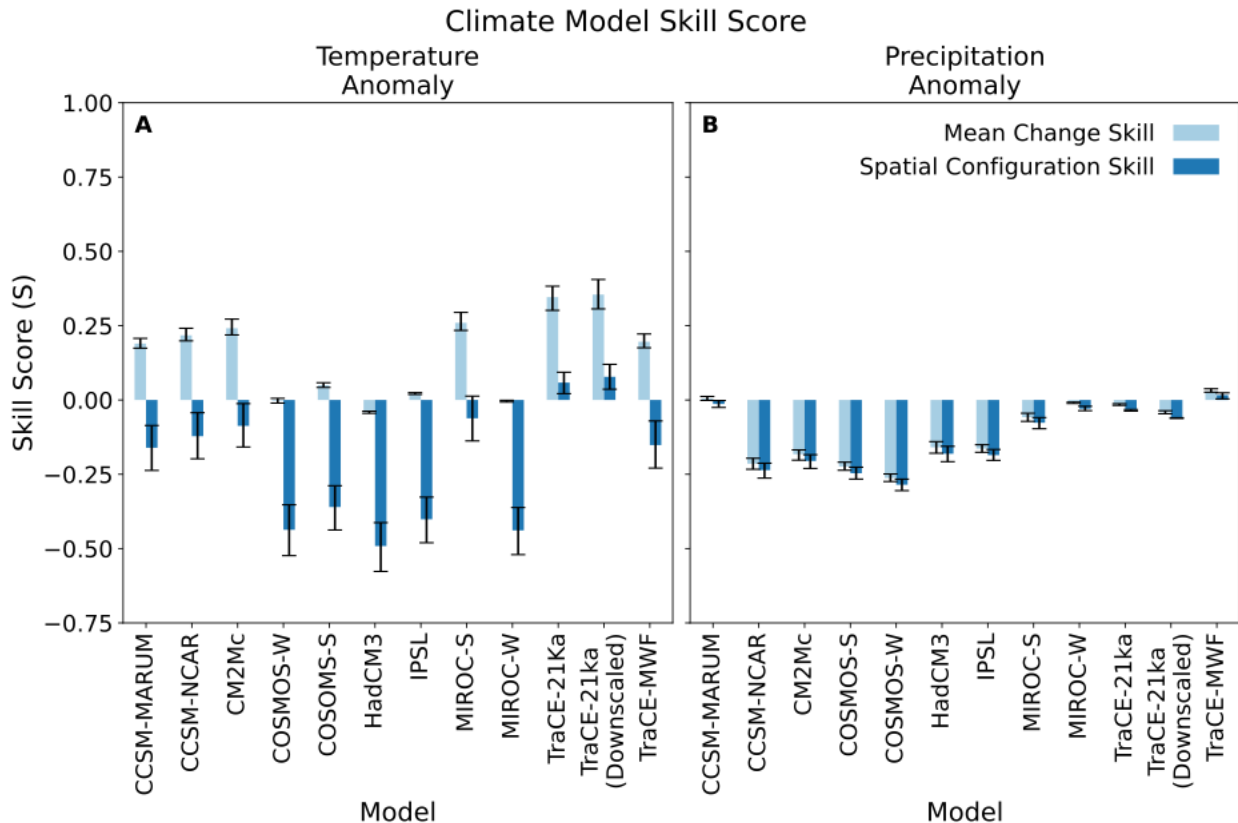
Figure 4.3

(A, B) Climate model skill for (A) temperature and (B) precipitation anomalies determined by comparing simulations from 11 climate simulations and the statistically downscaled TraCE-21ka simulations from Lorenz et al. (2016) to our proxy network. These tests assess a climate model's ability to accurately simulate mean-field changes (dark blue bars) and the spatial configuration of climate changes (light blue bars). A score of 1 indicates perfect climate model performance while a score of 0 indicates no skill. Scores less than 0 suggest model performance that is worse than the null expectation of no climate change for the mean change skill or spatially uniform climate change for the spatial configuration test. Error bars represent the 95% confidence interval.
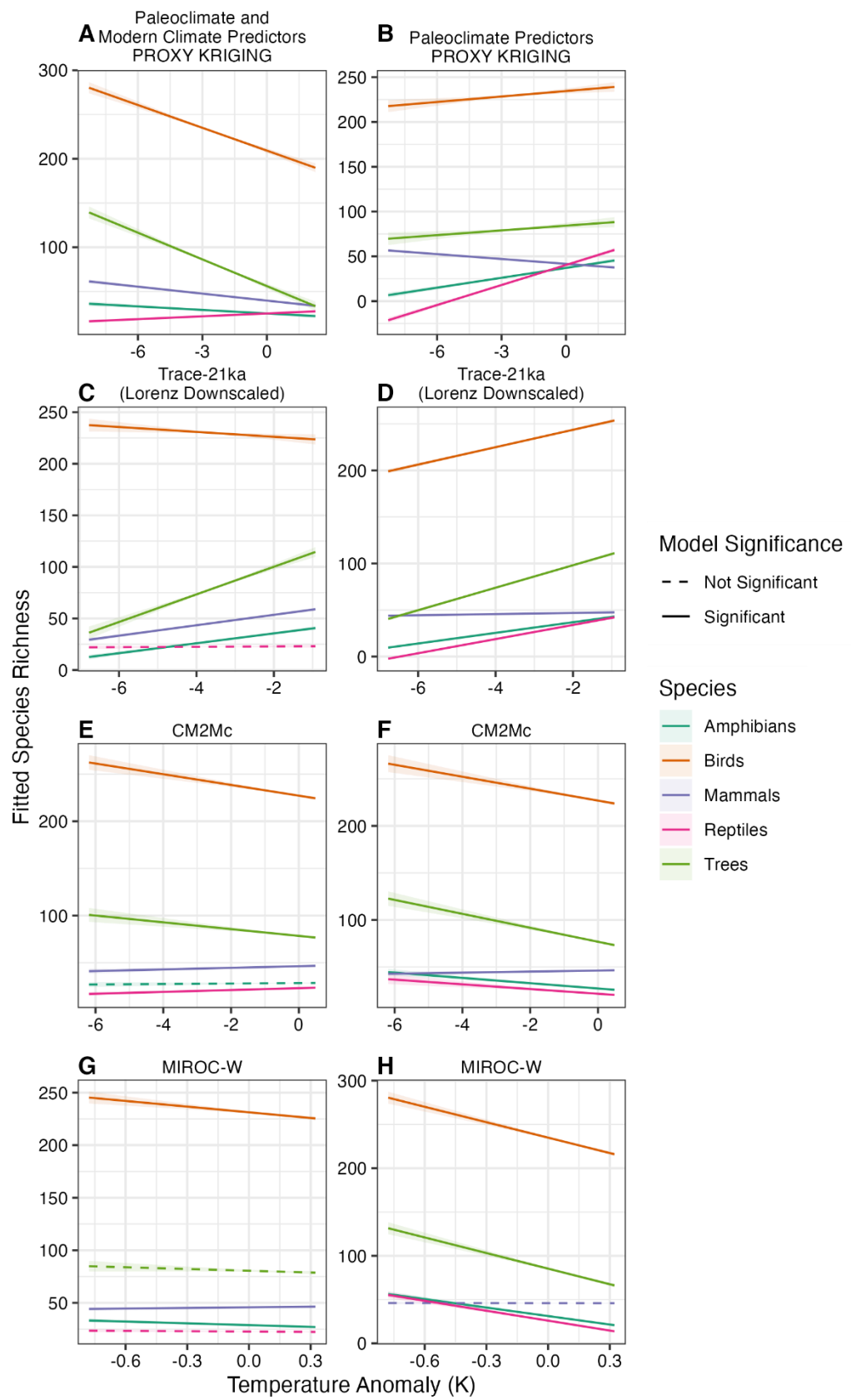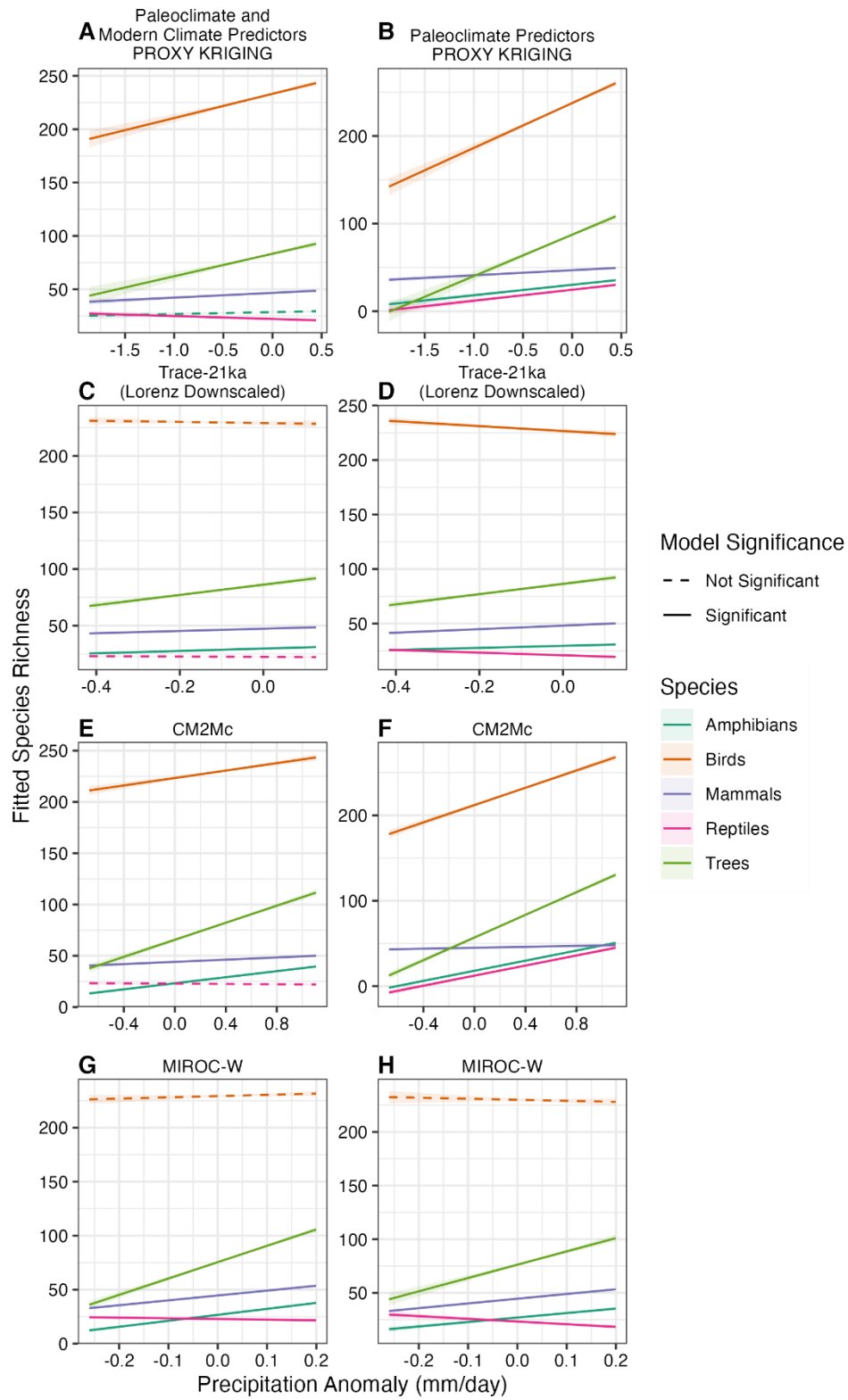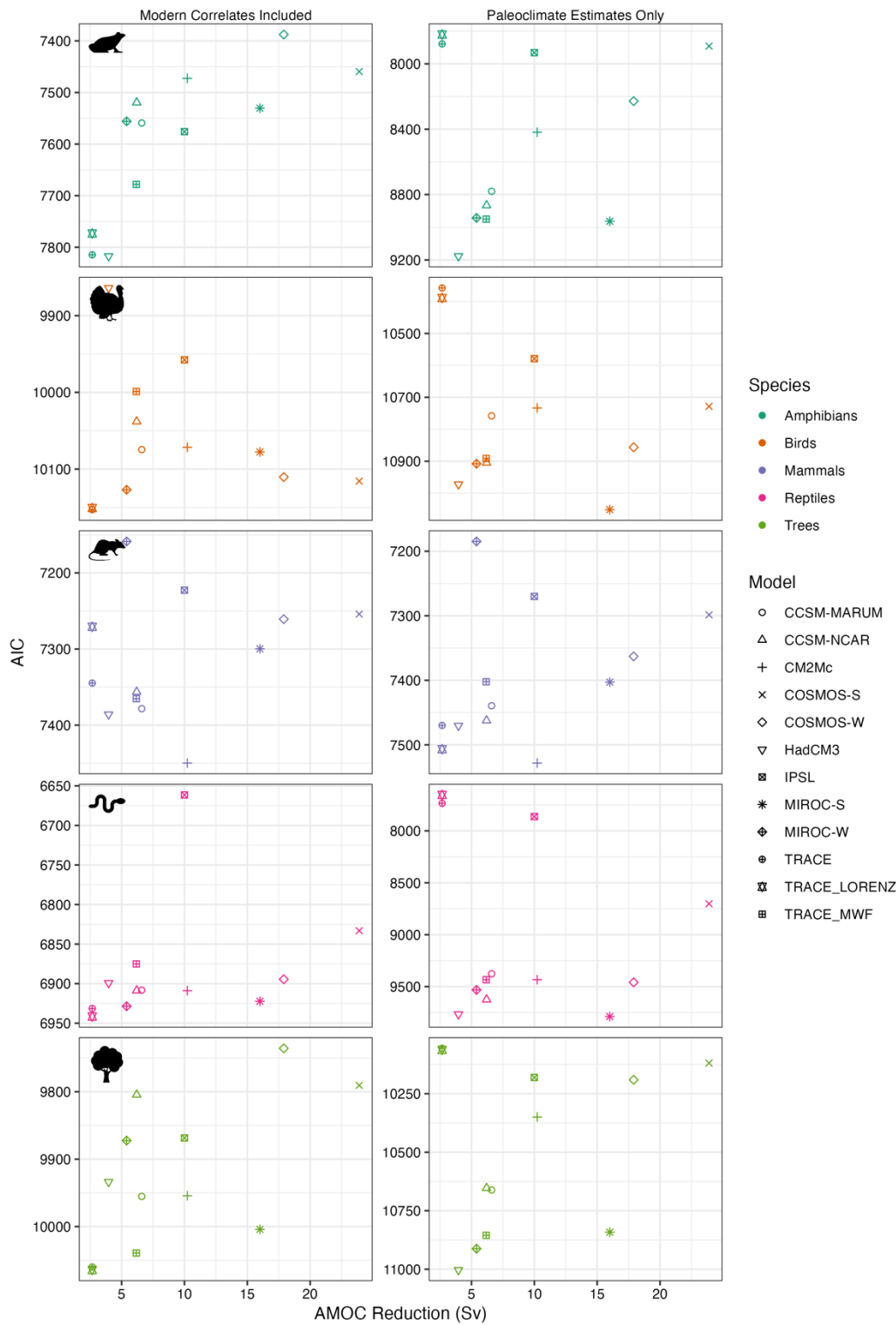
Figure 4.4

(A-H) The effect of temperature anomalies from a millennial-scale climate event on contemporary species richness from GLMs that were fitted either including contemporary temperature and precipitation as predictors **(A, C, E, G)** or excluding these variables **(B, D, F, H)**. GLMs were fitted to paleotemperature and paleoprecipitation estimates from 11 climate simulations, kriged proxy estimates, and the statistically downscaled TraCE-21ka simulations from Lorenz et al. (2016). **(A, B)** The effects of temperature change reconstructed from proxies on species richness serve as the benchmark for climate simulations. To reduce figure complexity, a selected subset of the GLM results is shown, with GLMs selected to show the three typical patterns. The full set of GLMs is available in Supplementary Figure S3.9-Figure S3.12. **(C, D)** TraCE-21ka represents GLMs with paleoclimatic relationships that are significantly predictive of modern biodiversity but produce trends with opposite directionality to the proxy record. **(E, F)** CM2Mc represents GLMs that are also significantly predictive of contemporary biodiversity and agree with the proxy record in directionality. **(G, H)** MIROC-W represents models that are weakly or not predictive of modern biodiversity.

Figure 4.5
As in Figure 4.4, but for the effects of paleoprecipitation anomalies.

Figure 4.6

A comparison between the magnitude of AMOC reduction forced in each climate simulation through the input of freshwater into the North Atlantic and GLM information loss. Information loss is calculated using the Akaike information criterion (AIC, Akaike 1973). Each panel represents a combination of GLM correlates and taxonomic group. Each dot represents a different climate simulation. The AMOC and GLM information loss relationships were significant at the 95% confidence interval for GLMs that modeled tree richness including and excluding modern correlates and the 90% confidence interval for GLMs that modeled amphibian richness when modern correlates were included.
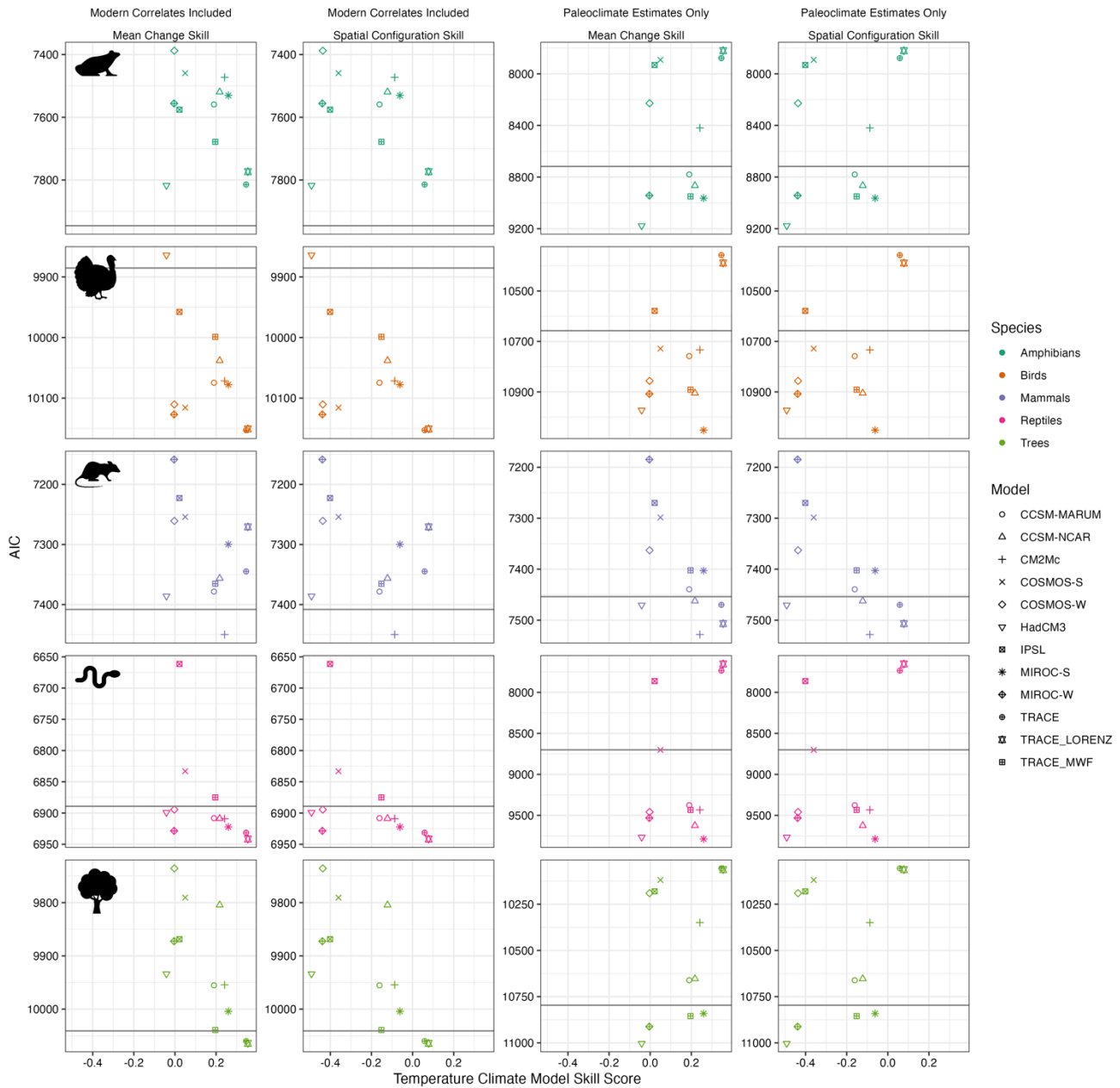
Figure 4.7

A comparison between climate model skill in simulating temperature anomalies (based on

comparison to proxy reconstructions) and information loss for GLMs that assess the effects of

paleoclimatic estimates on contemporary biodiversity. Each panel represents a different

combination of taxonomic group, climate model skill test, and set of predictor variables used in

the GLMs . Each dot represents a paleotemperature estimate from different climate models. The grey horizontal line corresponds to the AIC from GLMs with the paleoclimate estimates from the proxy network as predictors. Temperature model skill and GLM AIC is significant at the 90% confidence interval for all combinations of climate model skill test and predictor variables for mammalian species richness and the 95% confidence interval for tree richness.
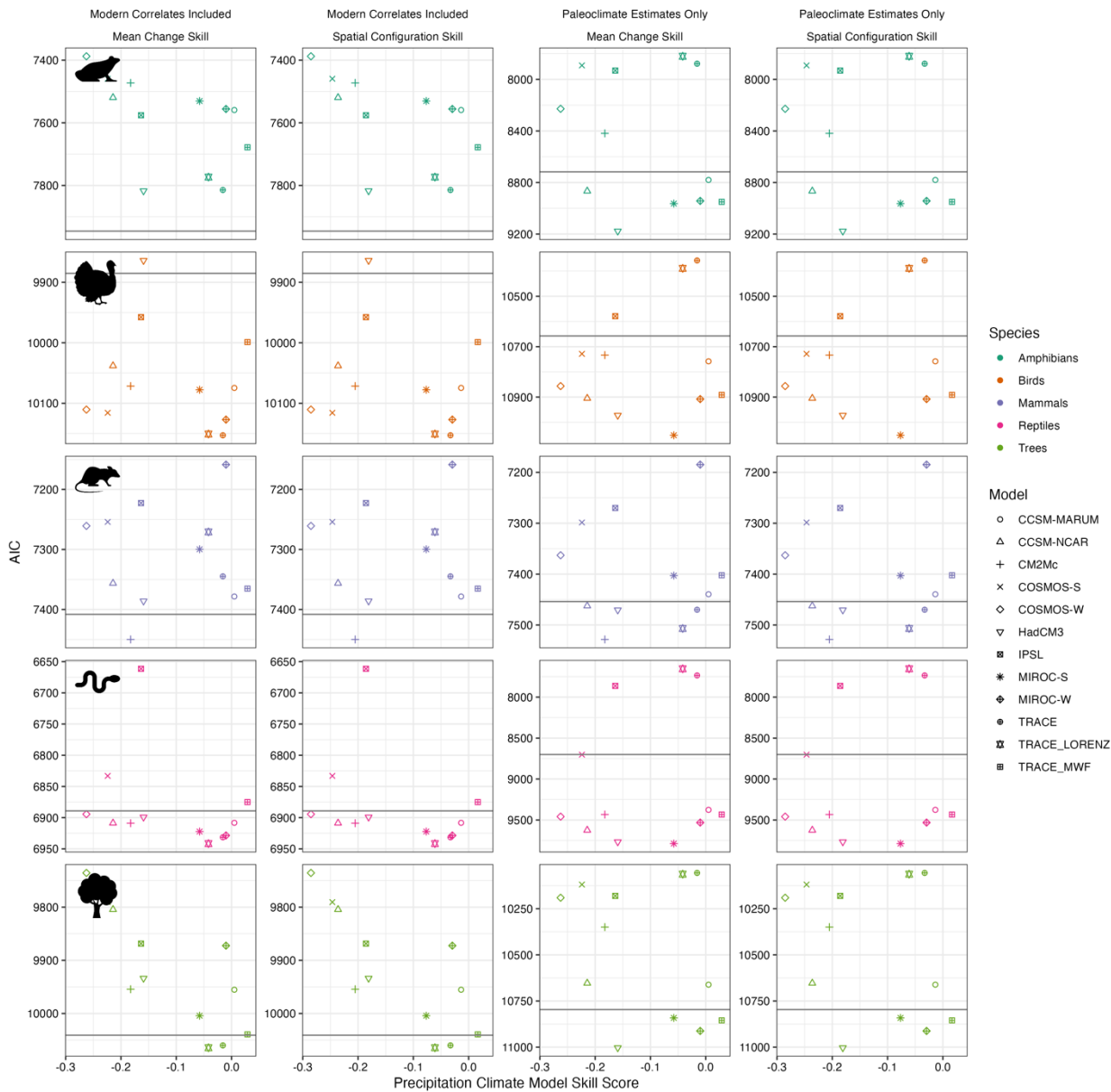
Figure 4.8

As in Figure 4.7, but for paleoprecipitation. The only significant relationships are between GLMs that model reptilian richness, excluding modern climatic predictors and the mean change precipitation skill null at the 90% confidence interval.

	Amphibians	Birds	Mammals	Reptiles	Proxy Trees
Contemporary Mean Annual Temperature	2.67%	1.04%	0.90%	0.02%	0.83%
Contemporary Total Annual Precipitation	13.23%	27.58%	0.82%	20.83%	19.73%
Paleotemperature	0.09%	2.85%	2.05%	0.12%	2.40%
Paleoprecipitation	0.85%	7.56%	13.19%	0.33%	10.10%
Average of all climate models					
Contemporary Mean Annual Temperature	3.31%	1.70%	2.22%	0.09%	1.05%
Contemporary Total Annual Precipitation	6.68%	23.46%	5.50%	23.41%	8.00%
Paleotemperature	5.58%	2.51%	8.79%	0.20%	9.39%
Paleoprecipitation	1.64%	1.44%	6.36%	0.27%	2.68%
TraCE-21ka (Lorenz et al., (2016) Downscaled Variant)					
Contemporary Mean Annual Temperature	6.21%	10.68%	37.66%	6.95%	9.39%
Contemporary Total Annual Precipitation	1.23%	1.78%	0.13%	0.04%	0.00%
Paleotemperature	0.01%	8.64%	16.12%	6.89%	0.07%
Paleoprecipitation	0.59%	0.03%	2.14%	0.01%	2.29%

Table 4.1

Percentage of deviance explained by each GLM term when modern temperature and precipitation are included as correlates in the `GLMs. Note, the average of all climate models is the average deviance explained across all GLMs fitted using the 11 paleoclimate simulations and the statistically downscaled variant of the TraCE-21ka experiments by Lorenz et al. (2016).

References

Abe-Ouchi, A., F. Saito, K. Kawamura, M. E. Raymo, J. Okuno, K. Takahashi, and H. Blatter, 2013: Insolation-driven 100,000-year glacial cycles and hysteresis of ice-sheet volume. *Nature*, **500**, 190–193, https://doi.org/10.1038/nature12374.

Akaike, H., 1973: Information Theory and an Extension of the Maximum Likelihood Principle. *Proceedings of the 2nd International Symposium on Information Theory*, B.N. Petrov and F. Csaki, Eds., Akademiai Kiado, 267–281.

Alley, R. B., S. Anandakrishnan, and P. Jung, 2001: Stochastic resonance in the North Atlantic. *Paleoceanography*, **16**, 190–198, https://doi.org/10.1029/2000PA000518.

Annan, J., J. Hargreaves, and T. Mauritsen, 2022: A new global climate reconstruction for the Last Glacial Maximum. *Clim. Past Discuss.*, 1–20, https://doi.org/10.5194/cp-2022-12.

Araújo, M. B., D. Nogués-Bravo, J. A. F. Diniz-Filho, A. M. Haywood, P. J. Valdes, and C. Rahbek, 2008: Quaternary climate changes explain diversity among reptiles and amphibians. *Ecography*, **31**, 8–15, https://doi.org/10.1111/j.2007.0906-7590.05318.x.

Arienzo, M. M., P. K. Swart, A. Pourmand, K. Broad, A. C. Clement, L. N. Murphy, H. B. Vonhof, and B. Kakuk, 2015: Bahamian speleothem reveals temperature decrease associated with Heinrich stadials. *Earth Planet. Sci. Lett.*, **430**, 377–386, https://doi.org/10.1016/j.epsl.2015.08.035.

——, ——, K. Broad, A. C. Clement, A. Pourmand, and B. Kakuk, 2017: Multi-proxy evidence of millennial climate variability from multiple Bahamian speleothems. *Quat. Sci. Rev.*, **161**, 18–29, https://doi.org/10.1016/j.quascirev.2017.02.004.

Arnold, T. E., A. F. Diefendorf, M. Brenner, K. H. Freeman, and A. A. Baczynski, 2018: Climate response of the Florida Peninsula to Heinrich events in the North Atlantic. *Quat. Sci. Rev.*, **194**, 1–11, https://doi.org/10.1016/j.quascirev.2018.06.012.

Atkinson, T. C., K. R. Briffa, and G. R. Coope, 1987: Seasonal temperatures in Britian during the past 22,000 years, reconstructed using beetle remains. *Nature*, **325**, 587–592, https://doi.org/10.1038/325587a0.

Bakke, J., O. Lie, E. Heegaard, T. Dokken, G. H. Haug, H. H. Birks, P. Dulski, and T. Nilsen, 2009: Rapid oceanic and atmospheric changes during the Younger Dryas cold period. *Nat. Geosci.*, **2**, 202–205, https://doi.org/10.1038/ngeo439.

Baldini, L. M., and Coauthors, 2015: Regional temperature, atmospheric circulation, and sea-ice variability within the Younger Dryas Event constrained using a speleothem from northern Iberia. *Earth Planet. Sci. Lett.*, **419**, 101–110, https://doi.org/10.1016/j.epsl.2015.03.015.

Bard, E., F. Rostek, J. L. Turon, and S. Gendreau, 2000: Hydrological impact of Heinrich events in the subtropical northeast Atlantic. *Science*, **289**, 1321–1324, https://doi.org/DOI 10.1126/science.289.5483.1321.

Bartlein, P. J., I. C. Prentice, and T. Webb, 1986: Climatic Response Surfaces from Pollen Data for Some Eastern North American Taxa. *J. Biogeogr.*, **13**, 35–57, https://doi.org/10.2307/2844848.

Bartlein, P. J., and Coauthors, 2011: Pollen-based continental climate reconstructions at 6 and 21 ka: a global synthesis. *Clim. Dyn.*, **37**, 775–802, https://doi.org/10.1007/s00382-010-0904-1.

Batchelor, C. J., S. A. Marcott, I. J. Orland, and K. Kitajima, 2022: Late Holocene increase of winter precipitation in midcontinental North America from a seasonally resolved speleothem record. *Geology*, https://doi.org/10.1130/G50096.1.

Berger, A., 1989: Pleistocene climatic variability at astronomical frequencies. *Quat. Int.*, **2**, 1–14, https://doi.org/10.1016/1040-6182(89)90016-5.

——, and M. F. Loutre, 1991: Insolation values for the climate of the last 10 million years. *Quat. Sci. Rev.*, **10**, 297–317, https://doi.org/10.1016/0277-3791(91)90033-q.

Berger, A. L., 1978: Long-Term Variations of Caloric Insolation Resulting from the Earth's Orbital Elements1. *Quat. Res.*, **9**, 139–167, https://doi.org/10.1016/0033-5894(78)90064-9.

van Beynen, P., J. S. Polk, Y. Asmerom, and V. Polyak, 2017: Late Pleistocene and mid-Holocene climate change derived from a Florida speleothem. *Quat. Int.*, **449**, 75–82, https://doi.org/10.1016/j.quaint.2017.05.008.

Bishop, D. A., and Coauthors, 2019a: Investigating the causes of increased twentieth-century fall precipitation over the southeastern United States. *J. Clim.*, **32**, 575–590, https://doi.org/10.1175/jcli-d-18-0244.1.

——, A. P. Williams, and R. Seager, 2019b: Increased fall precipitation in the southeastern United States driven by higher-intensity, frontal precipitation. *Geophys. Res. Lett.*, **46**, 8300–8309, https://doi.org/10.1029/2019gl083177.

Bjerknes, J., 1964: Atlantic Air-Sea Interaction. *Advances in Geophysics*, H.E. Landsberg and J. Van Mieghem, Eds., Vol. 10 of, Academic Press, 1–82.

Bjorck, S., O. Bennike, P. Rosen, C. S. Andresen, S. Bohncke, E. Kaas, and D. Conley, 2002: Anomalously mild Younger Dryas summer conditions in southern Greenland. *Geology*, **30**, 427–430, https://doi.org/10.1130/0091-7613(2002)030<0427:Amydsc>2.0.Co;2.

Blaauw, M., and J. A. Christen, 2011: Flexible paleoclimate age-depth models using an autoregressive gamma process. *Bayesian Anal.*, **6**, 457–474.

Blunier, T., and E. J. Brook, 2001: Timing of Millennial-Scale Climate Change in Antarctica and Greenland During the Last Glacial Period. *Science*, **291**, 109–112, https://doi.org/10.1126/science.291.5501.109.

Bond, G., and Coauthors, 1992: Evidence for massive discharges of icebergs into the North-Atlantic Ocean during the last glacial period. *Nature*, **360**, 245–249, https://doi.org/10.1038/360245a0.

——, W. Broecker, S. Johnsen, J. Mcmanus, L. Labeyrie, J. Jouzel, and G. Bonani, 1993: Correlations between Climate Records from North-Atlantic Sediments and Greenland Ice. *Nature*, **365**, 143–147, https://doi.org/DOI 10.1038/365143a0.

Bond, G. C., W. Showers, M. Elliot, M. Evans, R. Lotti, I. Hajdas, G. Bonani, and S. Johnson, 1999: The North Atlantic's 1-2 Kyr Climate Rhythm: Relation to Heinrich Events, Dansgaard/Oeschger Cycles and the Little Ice Age. *Mechanisms of Global Climate Change at Millennial Time Scales*, American Geophysical Union (AGU), 35–58.

Bova, S., Y. Rosenthal, Z. Y. Liu, S. P. Godad, and M. Yan, 2021: Seasonal origin of the thermal maxima at the Holocene and the last interglacial. *Nature*, **589**, 548-+, https://doi.org/10.1038/s41586-020-03155-x.

Boyle, E. A., and L. Keigwin, 1987: North Atlantic thermohaline circulation during the past 20,000 years linked to high-latitude surface temperature. *Nature*, **330**, 35–40, https://doi.org/10.1038/330035a0.

Braconnot, P., and Coauthors, 2007: Results of PMIP2 coupled simulations of the Mid-Holocene and Last Glacial Maximum - Part 1: experiments and large-scale features. *Clim. Past*, **3**, 261–277, https://doi.org/10.5194/cp-3-261-2007.

Brauer, A., G. H. Haug, P. Dulski, D. M. Sigman, and J. F. W. Negendank, 2008: An abrupt wind shift in western Europe at the onset of the Younger Dryas cold period. *Nat. Geosci.*, **1**, 520–523, https://doi.org/10.1038/ngeo263.

Broccoli, A. J., K. A. Dahl, and R. J. Stouffer, 2006: Response of the ITCZ to Northern Hemisphere cooling. *Geophys. Res. Lett.*, **33**, https://doi.org/10.1029/2005gl024546.

Broecker, W. S., 1982: Glacial to interglacial changes in ocean chemistry. *Prog. Oceanogr.*, **11**, 151–197, https://doi.org/10.1016/0079-6611(82)90007-6.

——, 1998: Paleocean circulation during the Last Deglaciation: A bipolar seesaw? *Paleoceanography*, **13**, 119–121, https://doi.org/doi:10.1029/97PA03707.

——, D. M. Peteet, and D. Rind, 1985: Does the ocean–atmosphere system have more than one stable mode of operation? *Nature*, **315**, 21–26, https://doi.org/10.1038/315021a0.

Broecker, W. S., J. P. Kennett, B. P. Flower, J. T. Teller, S. Trumbore, G. Bonani, and W. Wolfli, 1989: Routing of metlwater from the Laurentide Ice Sheet during the Younger Dryas cold episode. *Nature*, **341**, 318–321, https://doi.org/10.1038/341318a0.

Bromwich, D. H., E. R. Toracinta, H. L. Wei, R. J. Oglesby, J. L. Fastook, and T. J. Hughes, 2004: Polar MM5 simulations of the winter climate of the Laurentide Ice Sheet at the

LGM. *J. Clim.*, **17**, 3415–3433, https://doi.org/10.1175/1520-0442(2004)017<3415:Pmsotw>2.0.Co;2.

——, ——, R. J. Oglesby, J. L. Fastook, and T. J. Hughes, 2005: LGM summer climate on the southern margin of the Laurentide Ice Sheet: Wet or dry? *J. Clim.*, **18**, 3317–3338, https://doi.org/10.1175/jcli3480.1.

Brown, N., and E. D. Galbraith, 2016: Hosed vs. unhosed: interruptions of the Atlantic Meridional Overturning Circulation in a global coupled model, with and without freshwater forcing. *Clim. Past*, **12**, 1663.

Brown, S. C., T. M. L. Wigley, B. L. Otto-Bliesner, C. Rahbek, and D. A. Fordham, 2020: Persistent Quaternary climate refugia are hospices for biodiversity in the Anthropocene. *Nat. Clim. Change*, **10**, 244-+, https://doi.org/10.1038/s41558-019-0682-7.

Buizert, C., and Coauthors, 2014: Greenland temperature response to climate forcing during the last deglaciation. *Science*, **345**, 1177–1180, https://doi.org/10.1126/science.1254961.

Burnett, A. W., and H. T. Mullins, 2002: Atmospheric circulation and the oxygen isotopic composition of meteoric precipitaiton over the eastern United States. Vol. 2002 of, AGU Fall Meeting Abstracts, PP52A-0307.

Burns, R. M., and B. H. Honkala, 1990: Silvics of North America: 1. Conifers; 2. Hardwoods Agriculture Handbook 654. *US Dep. Agric. For. Serv. Wash. DC,*.

Carlson, A. E., P. U. Clark, B. A. Haley, G. P. Klinkhammer, K. Simmons, E. J. Brook, and K. J. Meissner, 2007: Geochemical proxies of North American freshwater routing during the Younger Dryas cold event. *Proc. Natl. Acad. Sci.*, **104**, 6556–6561, https://doi.org/10.1073/pnas.0611313104.

Carlson, A. E., D. W. Oppo, R. E. Came, A. N. LeGrande, L. D. Keigwin, and W. B. Curry, 2008: Subtropical Atlantic salinity variability and Atlantic meridional circulation during the last deglaciation. *Geology*, **36**, 991–994, https://doi.org/10.1130/G25080a.1.

Carnaval, A. C., and C. Moritz, 2008: Historical climate modelling predicts patterns of current biodiversity in the Brazilian Atlantic forest. *J. Biogeogr.*, **35**, 1187–1201, https://doi.org/10.1111/j.1365-2699.2007.01870.x.

Chang, P., and Coauthors, 2008: Oceanic link between abrupt changes in the North Atlantic Ocean and the African monsoon. *Nat. Geosci.*, **1**, 444–448, https://doi.org/10.1038/ngeo218.

Cheng, H., and Coauthors, 2020: Timing and structure of the Younger Dryas event and its underlying climate dynamics. *Proc. Natl. Acad. Sci. U. S. A.*, **117**, 23408–23417, https://doi.org/10.1073/pnas.2007869117.

Chevalier, M., and Coauthors, 2020: Pollen-based climate reconstruction techniques for late Quaternary studies. *Earth-Sci. Rev.*, **210**, 33, https://doi.org/10.1016/j.earscirev.2020.103384.

Chiang, J. C. H., and C. M. Bitz, 2005: Influence of high latitude ice cover on the marine Intertropical Convergence Zone. *Clim. Dyn.*, **25**, 477–496, https://doi.org/10.1007/s00382-005-0040-5.

——, W. Cheng, and C. M. Bitz, 2008: Fast teleconnections to the tropical Atlantic sector from Atlantic thermohaline adjustment. *Geophys. Res. Lett.*, **35**, https://doi.org/10.1029/2008gl033292.

Clark, P. U., N. G. Pisias, T. F. Stocker, and A. J. Weaver, 2002: The role of the thermohaline circulation in abrupt climate change. *Nature*, **415**, 863–869, https://doi.org/10.1038/415863a.

——, and Coauthors, 2006: The middle Pleistocene transition: characteristics, mechanisms, and implications for long-term changes in atmospheric pCO2. *Quat. Sci. Rev.*, **25**, 3150–3184, https://doi.org/10.1016/j.quascirev.2006.07.008.

——, and Coauthors, 2012: Global climate evolution during the last deglaciation. *Proc. Natl. Acad. Sci.*, **109**, E1134–E1142, https://doi.org/10.1073/pnas.1116619109.

Claussen, M., A. Ganopolski, V. Brovkin, F.-W. Gerstengarbe, and P. Werner, 2003: Simulated global-scale response of the climate system to Dansgaard/Oeschger and Heinrich events. *Clim. Dyn.*, **21**, 361–370, https://doi.org/10.1007/s00382-003-0336-2.

Clement, A. C., and L. C. Peterson, 2008: Mechanisms of abrupt climate change of the last glacial period. *Rev. Geophys.*, **46**, https://doi.org/10.1029/2006rg000204.

COHMAP Project Members, 1988: Climatic Changes of the Last 18,000 Years - Observations and Model Simulations. *Science*, **241**, 1043–1052.

Connell, J. H., 1978: Diversity in Tropical Rain Forests and Coral Reefs. *Science*, **199**, 1302–1310, https://doi.org/10.1126/science.199.4335.1302.

Cooper, A., C. Turney, K. A. Hughen, B. W. Brook, H. G. McDonald, and C. J. A. Bradshaw, 2015: Abrupt warming events drove late Pleistocene Holarctic megafaunal turnover. *Science*, **349**, 602–606, https://doi.org/10.1126/science.aac4315.

Crampton-Flood, E. D., J. E. Tierney, F. Peterse, F. M. S. A. Kirkels, and J. S. S. Damste, 2020: BayMBT: A Bayesian calibration model for branched glycerol dialkyl glycerol tetraethers in soils and peats. *Geochim. Cosmochim. Acta*, **268**, 142–159, https://doi.org/10.1016/j.gca.2019.09.043.

Dai, A., J. C. Fyfe, S.-P. Xie, and X. Dai, 2015: Decadal modulation of global surface temperature by internal climate variability. *Nat. Clim. Change*, **5**, 555–559, https://doi.org/10.1038/nclimate2605.

Dalton, A. S., and Coauthors, 2020: An updated radiocarbon-based ice margin chronology for the last deglaciation of the North American Ice Sheet Complex. *Quat. Sci. Rev.*, **234**, 27, https://doi.org/10.1016/j.quascirev.2020.106223.

Dansgaard, W., H. B. Clausen, N. Gundestrup, C. U. Hammer, S. F. Johnsen, P. M. Kristinsdottir, and N. Reeh, 1982: A New Greenland Deep Ice Core. *Science*, **218**, 1273–1277, https://doi.org/10.1126/science.218.4579.1273.

——, and Coauthors, 1993: Evidence for general instability of past climate from a 250-kyr ice-core record. *Nature*, **364**, 218–220, https://doi.org/10.1038/364218a0.

De Jonge, C., E. C. Hopmans, C. I. Zell, J.-H. Kim, S. Schouten, and J. S. Sinninghe Damsté, 2014: Occurrence and abundance of 6-methyl branched glycerol dialkyl glycerol tetraethers in soils: Implications for palaeoclimate reconstruction. *Geochim. Cosmochim. Acta*, **141**, 97–112, https://doi.org/10.1016/j.gca.2014.06.013.

De Jonge, C., D. Radujkovic, B. D. Sigurdsson, J. T. Weedon, I. Janssens, and F. Peterse, 2019: Lipid biomarker temperature proxy responds to abrupt shift in the bacterial community composition in geothermally heated soils. *Org. Geochem.*, **137**, 13, https://doi.org/10.1016/j.orggeochem.2019.07.006.

Deevey, E. S., 1949: Biogeography of the Pleistocene: Part I: Europe and North America. *Geol. Soc. Am. Bull.*, **60**, 1315–1416.

Delworth, T. L., and M. E. Mann, 2000: Observed and simulated multidecadal variability in the Northern Hemisphere. *Clim. Dyn.*, **16**, 661–676, https://doi.org/10.1007/s003820000075.

Denniston, R. F., L. A. Gonzalez, Y. Asmerom, V. Polyak, M. K. Ragan, and M. R. Saltzman, 2001: A high-resolution speleothem record of climatic variability at the Allerod-Younger Dryas transition in Missouri, central United States. *Palaeogeogr. Palaeoclimatol. Palaeoecol.*, **176**, 147–155, https://doi.org/10.1016/s0031-0182(01)00334-0.

Denton, G. H., R. B. Alley, G. C. Comer, and W. S. Broecker, 2005: The role of seasonality in abrupt climate change. *Quat. Sci. Rev.*, **24**, 1159–1182, https://doi.org/10.1016/j.quascirev.2004.12.002.

Deser, C., and M. L. Blackmon, 1993: Surface climate variations over the North Atlantic during the witner: 1900-1989. *J. Clim.*, **6**, 1743–1753, https://doi.org/10.1175/1520-0442(1993)006<1743:scvotn>2.0.co;2.

Diffenbaugh, N. S., D. L. Swain, and D. Touma, 2015: Anthropogenic warming has increased drought risk in California. *Proc. Natl. Acad. Sci.*, **112**, 3931–3936, https://doi.org/10.1073/pnas.1422385112.

Dobson, A. P., J. P. Rodriguez, W. M. Roberts, and D. S. Wilcove, 1997: Geographic Distribution of Endangered Species in the United States. *Science*, **275**, 550–553, https://doi.org/10.1126/science.275.5299.550.

Donders, T. H., H. J. de Boer, W. Finsinger, E. C. Grimm, S. C. Dekker, G. J. Reichart, and F. Wagner-Cremer, 2011: Impact of the Atlantic Warm Pool on precipitation and temperature in Florida during North Atlantic cold spells. *Clim. Dyn.*, **36**, 109–118, https://doi.org/10.1007/s00382-009-0702-9.

Dorale, J. A., L. A. Wozniak, E. A. Bettis, S. J. Carpenter, R. D. Mandel, E. R. Hajic, H. Lopinot, and J. H. Ray, 2010: Isotopic evidence for Younger Dryas aridity in the North American midcontinent. *Geology*, **38**, 519–522, https://doi.org/10.1130/g30781.1.

Dormann, C. F., and Coauthors, 2007: Methods to account for spatial autocorrelation in the analysis of species distributional data: a review. *Ecography*, **30**, 609–628, https://doi.org/10.1111/j.2007.0906-7590.05171.x.

Durkee, J. D., J. D. Frye, C. M. Fuhrmanny, M. C. Lacke, H. G. Jeong, and T. L. Mote, 2008: Effects of the North Atlantic Oscillation on precipitation-type frequency and distribution in the eastern United States. *Theor. Appl. Climatol.*, **94**, 51–65, https://doi.org/10.1007/s00704-007-0345-x.

Dyke, A. S., A. Moore, and L. Robertson, 2003: *Deglaciation of North America*.

Dynesius, M., and R. Jansson, 2000: Evolutionary consequences of changes in species' geographical distributions driven by Milankovitch climate oscillations. *Proc. Natl. Acad. Sci.*, **97**, 9115–9120, https://doi.org/10.1073/pnas.97.16.9115.

Ellis, K. G., H. T. Mullins, and W. P. Patterson, 2004: Deglacial to middle Holocene (16,600 to 6000 calendar years BP) climate change in the northeastern United States inferred from multi-proxy stable isotope data, Seneca Lake, New York. *J. Paleolimnol.*, **31**, 343–361, https://doi.org/10.1023/b:jopl.0000021853.03476.95.

Elsner, J. B., and B. Kocher, 2000: Global tropical cyclone activity: A link to the North Atlantic Oscillation. *Geophys. Res. Lett.*, **27**, 129–132, https://doi.org/10.1029/1999gl010893.

Enfield, D. B., A. M. Mestas-Nunez, and P. J. Trimble, 2001: The Atlantic multidecadal oscillation and its relation to rainfall and river flows in the continental US. *Geophys. Res. Lett.*, **28**, 2077–2080, https://doi.org/10.1029/2000gl012745.

Eyring, V., S. Bony, G. A. Meehl, C. A. Senior, B. Stevens, R. J. Stouffer, and K. E. Taylor, 2016: Overview of the Coupled Model Intercomparison Project Phase 6 (CMIP6) experimental design and organization. *Geosci. Model Dev.*, **9**, 1937–1958, https://doi.org/10.5194/gmd-9-1937-2016.

Fastovich, D., J. M. Russell, S. T. Jackson, T. R. Krause, S. A. Marcott, and J. W. Williams, 2020a: Spatial fingerprint of Younger Dryas cooling and warming in eastern North America. *Geophys. Res. Lett.*, **47**, e2020GL090031, https://doi.org/10.1029/2020GL090031.

——, J. M. Russell, S. T. Jackson, and J. W. Williams, 2020b: Deglacial temperature controls on no-analog community establishment in the Great Lakes Region. *Quat. Sci. Rev.*, **234**, 106245, https://doi.org/10.1016/j.quascirev.2020.106245.

——, ——, S. A. Marcott, and J. W. Williams, in revision: Spatial fingerprints and mechanisms of temperature and precipitation changes during the Younger Dryas in Eastern North America. *Quat. Sci. Rev.*,.

Feakins, S. J., M. E. Kirby, M. I. Cheetham, Y. Ibarra, and S. R. H. Zimmerman, 2014: Fluctuation in leaf wax D/H ratio from a southern California lake records significant variability in isotopes in precipitation during the late Holocene. *Org. Geochem.*, **66**, 48–59, https://doi.org/10.1016/j.orggeochem.2013.10.015.

Fensterer, C., D. Scholz, D. L. Hoffmann, C. Spotl, A. Schroder-Ritzrau, C. Horn, J. M. Pajon, and A. Mangini, 2013: Millennial-scale climate variability during the last 12.5 ka recorded in a Caribbean speleothem. *Earth Planet. Sci. Lett.*, **361**, 143–151, https://doi.org/10.1016/j.epsl.2012.11.019.

Fick, S. E., and R. J. Hijmans, 2017: WorldClim 2: new 1-km spatial resolution climate surfaces for global land areas. *Int. J. Climatol.*, **37**, 4302–4315, https://doi.org/10.1002/joc.5086.

Fjeldsaå, J., and J. C. Lovett, 1997a: Geographical patterns of old and young species in African forest biota: the significance of specifc montane areas as evolutionary centres. *Biodivers. Conserv.*, **6**, 325–346.

——, and J. C. Lovett, 1997b: Biodiversity and environmental stability. *Biodivers. Conserv.*, **6**, 315–323, https://doi.org/10.1023/A:1018304522320.

Fløjgaard, C., S. Normand, F. Skov, and J.-C. Svenning, 2009: Ice age distributions of European small mammals: insights from species distribution modelling. *J. Biogeogr.*, **36**, 1152–1163, https://doi.org/10.1111/j.1365-2699.2009.02089.x.

——, ——, ——, and ——, 2011: Deconstructing the mammal species richness pattern in Europe – towards an understanding of the relative importance of climate, biogeographic history, habitat heterogeneity and humans. *Glob. Ecol. Biogeogr.*, **20**, 218–230, https://doi.org/10.1111/j.1466-8238.2010.00604.x.

Fordham, D. A., and Coauthors, 2012: Plant extinction risk under climate change: are forecast range shifts alone a good indicator of species vulnerability to global warming? *Glob. Change Biol.*, **18**, 1357–1371, https://doi.org/10.1111/j.1365-2486.2011.02614.x.

Galbraith, E. D., and Coauthors, 2011: Climate Variability and Radiocarbon in the CM2Mc Earth System Model. *J. Clim.*, **24**, 4230–4254, https://doi.org/10.1175/2011jcli3919.1.

Ganachaud, A., and C. Wunsch, 2000: Improved estimates of global ocean circulation, heat transport and mixing from hydrographic data. *Nature*, **408**, 453–457, https://doi.org/10.1038/35044048.

Ganopolski, A., and S. Rahmstorf, 2001: Rapid changes of glacial climate simulated in a coupled climate model. *Nature*, **409**, 153, https://doi.org/10.1038/35051500.

——, and ——, 2002: Abrupt Glacial Climate Changes due to Stochastic Resonance. *Phys. Rev. Lett.*, **88**, 038501, https://doi.org/10.1103/PhysRevLett.88.038501.

Garcia, R. A., N. D. Burgess, M. Cabeza, C. Rahbek, and M. B. Araújo, 2012: Exploring consensus in 21st century projections of climatically suitable areas for African vertebrates. *Glob. Change Biol.*, **18**, 1253–1269, https://doi.org/10.1111/j.1365-2486.2011.02605.x.

Gates, D. M., 1968: Transpiration and leaf temperature. *Annu. Rev. Plant Physiol.*, **19**, 211–238, https://doi.org/10.1146/annurev.pp.19.060168.001235.

Gildor, H., and E. Tziperman, 2001: A sea ice climate switch mechanism for the 100-kyr glacial cycles. *J. Geophys. Res.-Oceans*, **106**, 9117–9133, https://doi.org/10.1029/1999jc000120.

Gill, J. L., J. W. Williams, S. T. Jackson, K. B. Lininger, and G. S. Robinson, 2009: Pleistocene megafaunal collapse, novel plant communities, and enhanced fire regimes in North America. *Science*, **326**, 1100–1103, https://doi.org/10.1126/science.1179504.

Gill, J. L., J. W. Williams, S. T. Jackson, J. P. Donnelly, and G. C. Schellinger, 2012: Climatic and megaherbivory controls on late-glacial vegetation dynamics: a new, high-resolution, multi-proxy record from Silver Lake, Ohio. *Quat. Sci. Rev.*, **34**, 66–80.

Gilliam, R. C., and J. E. Pleim, 2010: Performance Assessment of New Land Surface and Planetary Boundary Layer Physics in the WRF-ARW. *J. Appl. Meteorol. Climatol.*, **49**, 760–774, https://doi.org/10.1175/2009jamc2126.1.

Gonzales, L. M., and E. C. Grimm, 2009: Synchronization of late-glacial vegetation changes at Crystal Lake, Illinois, USA with the North Atlantic Event Stratigraphy. *Quat. Res.*, **72**, 234–245, https://doi.org/10.1016/j.yqres.2009.05.001.

Gonzales, L. M., J. W. Williams, and E. C. Grimm, 2009: Expanded response-surfaces: a new method to reconstruct paleoclimates from fossil pollen assemblages that lack modern analogues. *Quat. Sci. Rev.*, **28**, 3315–3332, https://doi.org/10.1016/j.quascirev.2009.09.005.

Goring, S., A. Dawson, G. Simpson, K. Ram, R. Graham, E. Grimm, and J. Williams, 2015: Neotoma: A programmatic interface to the Neotoma Paleoecological Database. *Open Quat.*, **1**, 1–17.

Gregoire, L. J., A. J. Payne, and P. J. Valdes, 2012: Deglacial rapid sea level rises caused by ice-sheet saddle collapses. *Nature*, **487**, 219-U1506, https://doi.org/10.1038/nature11257.

——, P. J. Valdes, and A. J. Payne, 2015: The relative contribution of orbital forcing and greenhouse gases to the North American deglaciation. *Geophys. Res. Lett.*, **42**, 9970–9979, https://doi.org/10.1002/2015gl066005.

Grimm, E. C., G. L. Jacobson, W. A. Watts, B. C. S. Hansen, and K. A. Maasch, 1993: A 50,000-year record of climate oscillations from Florida and its temporal correlation with the Heinrich Events. *Science*, **261**, 198–200, https://doi.org/DOI 10.1126/science.261.5118.198.

——, W. A. Watts, G. L. Jacobson, B. C. S. Hansen, H. R. Almquist, and A. C. Dieffenbacher-Krall, 2006: Evidence for warm wet Heinrich events in Florida. *Quat. Sci. Rev.*, **25**, 2197–2211, https://doi.org/10.1016/j.quascirev.2006.04.008.

Grimm, E. C., L. J. Maher, and D. M. Nelson, 2009: The magnitude of error in conventional bulk-sediment radiocarbon dates from central North America. *Quat. Res.*, **72**, 301–308, https://doi.org/10.1016/j.yqres.2009.05.006.

Grootes, P. M., M. Stuiver, J. W. C. White, S. Johnsen, and J. Jouzel, 1993: Comparison of oxygen isotope records from the GISP2 and GRIP Greenland ice cores. *Nature*, **366**, 552–554, https://doi.org/10.1038/366552a0.

Gugger, P. F., M. Ikegami, and V. L. Sork, 2013: Influence of late Quaternary climate change on present patterns of genetic variation in valley oak, Quercus lobata Née. *Mol. Ecol.*, **22**, 3598–3612, https://doi.org/10.1111/mec.12317.

Haffer, J., 1969: Speciation in Amazonian Forest Birds: Most species probably originated in forest refuges during dry climatic periods. *Science*, **165**, 131–137, https://doi.org/10.1126/science.165.3889.131.

Hall, R., R. Erdélyi, E. Hanna, J. M. Jones, and A. A. Scaife, 2015: Drivers of North Atlantic Polar Front jet stream variability. *Int. J. Climatol.*, **35**, 1697–1720, https://doi.org/10.1002/joc.4121.

Hargreaves, J. C., J. D. Annan, M. Yoshimori, and A. Abe-Ouchi, 2012: Can the Last Glacial Maximum constrain climate sensitivity? *Geophys. Res. Lett.*, **39**, https://doi.org/10.1029/2012GL053872.

——, ——, R. Ohgaito, A. Paul, and A. Abe-Ouchi, 2013: Skill and reliability of climate model ensembles at the Last Glacial Maximum and mid-Holocene. *Clim. Past*, **9**, 811–823, https://doi.org/10.5194/cp-9-811-2013.

Harrison, S., and R. Noss, 2017: Endemism hotspots are linked to stable climatic refugia. *Ann. Bot.*, **119**, 207–214, https://doi.org/10.1093/aob/mcw248.

Hays, J. D., J. Imbrie, and N. J. Shackleton, 1976: Variations in the Earth's Orbit: Pacemaker of the Ice Ages. *Science*, **194**, 1121–1132, https://doi.org/10.1126/science.194.4270.1121.

He, C., and Coauthors, 2021: Hydroclimate footprint of pan-Asian monsoon water isotope during the last deglaciation. *Sci. Adv.*, **7**, 11, https://doi.org/10.1126/sciadv.abe2611.

He, F., 2011: *Simulating transient climate evolution of the last deglaciation with CCSM 3*.

He, F., J. D. Shakun, P. U. Clark, A. E. Carlson, Z. Y. Liu, B. L. Otto-Bliesner, and J. E. Kutzbach, 2013: Northern Hemisphere forcing of Southern Hemisphere climate during the last deglaciation. *Nature*, **494**, 81–85, https://doi.org/10.1038/nature11822.

Heinrich, H., 1988: Origin and consequences of cyclic ice rafting in the Northeast Atlantic Ocean during the past 130,000 years. *Quat. Res.*, **29**, 142–152, http://dx.doi.org/10.1016/0033-5894(88)90057-9.

Hemming, S. R., 2004: Heinrich events: Massive late Pleistocene detritus layers of the North Atlantic and their global climate imprint. *Rev. Geophys.*, **42**, https://doi.org/10.1029/2003RG000128.

Henderson, K. G., and A. J. Vega, 1996: Regional precipitation variability in the southern United States. *Phys. Geogr.*, **17**, 93–112, https://doi.org/10.1080/02723646.1996.10642576.

Hewitt, G., 2000: The genetic legacy of the Quaternary ice ages. *Nature*, **405**, 907–913, https://doi.org/10.1038/35016000.

Hewitt, G. M., 1999: Post-glacial re-colonization of European biota. *Biol. J. Linn. Soc.*, **68**, 87–112, https://doi.org/10.1111/j.1095-8312.1999.tb01160.x.

Hijmans, R. J., S. E. Cameron, J. L. Parra, P. G. Jones, and A. Jarvis, 2005: Very high resolution interpolated climate surfaces for global land areas. *Int. J. Climatol.*, **25**, 1965–1978, https://doi.org/10.1002/joc.1276.

Hof, C., I. Levinsky, M. B. Araujo, and C. Rahbek, 2011: Rethinking species' ability to cope with rapid climate change. *Glob. Change Biol.*, **17**, 2987–2990, https://doi.org/10.1111/j.1365-2486.2011.02418.x.

Hopmans, E. C., S. Schouten, and J. S. Sinninghe Damsté, 2016: The effect of improved chromatography on GDGT-based palaeoproxies. *Org. Geochem.*, **93**, 1–6, https://doi.org/10.1016/j.orggeochem.2015.12.006.

Hostetler, S. W., P. J. Bartlein, P. U. Clark, E. E. Small, and A. M. Solomon, 2000: Simulated influences of Lake Agassiz on the climate of central North America 11,000 years ago. *Nature*, **405**, 334–337, https://doi.org/10.1038/35012581.

Huang, Y. S., B. Shuman, Y. Wang, T. Webb III, E. C. Grimm, and G. L. Jacobson, 2006: Climatic and environmental controls on the variation of C_3 and C_4 plant abundances in central Florida for the past 62,000 years. *Palaeogeogr. Palaeoclimatol. Palaeoecol.*, **237**, 428–435, https://doi.org/10.1016/j.palaeo.2005.12.014.

Huntley, B., and Coauthors, 2013: Millennial climatic fluctuations are key to the structure of last glacial ecosystems. *PloS One*, **8**, https://doi.org/10.1371/journal.pone.0061963.

Hurlbert, A. H., and W. Jetz, 2007: Species richness, hotspots, and the scale dependence of range maps in ecology and conservation. *Proc. Natl. Acad. Sci.*, **104**, 13384–13389, https://doi.org/10.1073/pnas.0704469104.

Hurrell, J. W., 1995: Decadal trends in the North Atlantic Oscillation: regional temperatures and precipitation. *Science*, **269**, 676–679, https://doi.org/10.1126/science.269.5224.676.

Hurrell, J. W., Y. Kushnir, G. Ottersen, and M. Visbeck, 2003: An overview of the North Atlantic oscillation. *Geophys. Monogr.-Am. Geophys. Union*, **134**, 1–36.

Hussey, T. C., 1993: A 20,000-year history of vegetation and climate at Clear Pond, northeastern South Carolina. University of Maine, .

Huybers, P., and W. Curry, 2006: Links between annual, Milankovitch and continuum temperature variability. *Nature*, **441**, 329–332, https://doi.org/10.1038/nature04745.

Imbrie, J., and Coauthors, 1992: On the Structure and Origin of Major Glaciation Cycles 1. Linear Responses to Milankovitch Forcing. *Paleoceanography*, **7**, 701–738, https://doi.org/10.1029/92PA02253.

——, and Coauthors, 1993: On the structure and origin of major glaciation cycles 2. The 100,000-year cycle. *Paleoceanography*, **8**, 699–735, https://doi.org/10.1029/93PA02751.

Isarin, R. F. B., and S. J. P. Bohncke, 1999: Mean July temperatures during the Younger Dryas in northwestern and central Europe as inferred from climate indicator plant species. *Quat. Res.*, **51**, 158–173, https://doi.org/10.1006/qres.1998.2023.

IUCN, 2017: *The IUCN Red List of Threatened Species. Version 2017-1.*

Ivanovic, R. F., L. J. Gregoire, A. D. Wickert, P. J. Valdes, and A. Burke, 2017: Collapse of the North American ice saddle 14,500years ago caused widespread cooling and reduced ocean overturning circulation. *Geophys. Res. Lett.*, **44**, 383–392, https://doi.org/10.1002/2016gl071849.

——, and Coauthors, 2018a: Acceleration of Northern Ice Sheet Melt Induces AMOC Slowdown and Northern Cooling in Simulations of the Early Last Deglaciation. *Paleoceanogr. Paleoclimatology*, **33**, 807–824, https://doi.org/10.1029/2017pa003308.

——, L. J. Gregoire, A. D. Wickert, and A. Burke, 2018b: Climatic Effect of Antarctic Meltwater Overwhelmed by Concurrent Northern Hemispheric Melt. *Geophys. Res. Lett.*, **45**, 5681–5689, https://doi.org/10.1029/2018gl077623.

Jackson, D. A., 1993: Stopping rules in pricipal components analysis: A comparison of heuristical and statistical approaches. *Ecology*, **74**, 2204–2214, https://doi.org/10.2307/1939574.

Jackson, S. T., J. T. Overpeck, T. Webb III, S. E. Keattch, and K. H. Anderson, 1997: Mapped plant-macrofossil and pollen records of late Quaternary vegetation change in eastern North America. *Quat. Sci. Rev.*, **16**, 1–70.

——, R. S. Webb, K. H. Anderson, J. T. Overpeck, T. Webb III, J. W. Williams, and B. C. S. Hansen, 2000: Vegetation and environment in eastern North America during the Last

Glacial Maximum. *Quat. Sci. Rev.*, **19**, 489–508, https://doi.org/10.1016/S0277-3791(99)00093-1.

Jakob, S. S., E. Martinez-Meyer, and F. R. Blattner, 2009: Phylogeographic Analyses and Paleodistribution Modeling Indicate Pleistocene In Situ Survival of Hordeum Species (Poaceae) in Southern Patagonia without Genetic or Spatial Restriction. *Mol. Biol. Evol.*, **26**, 907–923, https://doi.org/10.1093/molbev/msp012.

Jansson, R., 2003: Global patterns in endemism explained by past climatic change. *Proc. R. Soc. Lond. B Biol. Sci.*, **270**, 583–590, https://doi.org/10.1098/rspb.2002.2283.

Jansson, R., and M. Dynesius, 2002: The fate of clades in a world of recurrent climatic change: Milankovitch oscillations and evolution. *Annu. Rev. Ecol. Syst.*, **33**, 741–777, https://doi.org/10.1146/annurev.ecolsys.33.010802.150520.

Jenkins, C. N., K. S. Van Houtan, S. L. Pimm, and J. O. Sexton, 2015: US protected lands mismatch biodiversity priorities. *Proc. Natl. Acad. Sci. U. S. A.*, **112**, 5081–5086, https://doi.org/10.1073/pnas.1418034112.

Jensen, A. M., and Coauthors, 2021: More than one way to kill a spruce forest: The role of fire and climate in the late-glacial termination of spruce woodlands across the southern Great Lakes. *J. Ecol.*, **109**, 459–477, https://doi.org/10.1111/1365-2745.13517.

Jones, R. A., J. W. Williams, and S. T. Jackson, 2017: Vegetation history since the last glacial maximum in the Ozark highlands (USA): A new record from Cupola Pond, Missouri. *Quat. Sci. Rev.*, **170**, 174–187, https://doi.org/10.1016/j.quascirev.2017.06.024.

Joussaume, S., and K. E. Taylor, 2000: The paleoclimate modeling intercomparison project. *World Meteorol. Organ.-Publ.-WMO TD*, 9–24.

Juggins, S., 2013: Quantitative reconstructions in palaeolimnology: new paradigm or sick science? *Quat. Sci. Rev.*, **64**, 20–32, https://doi.org/10.1016/j.quascirev.2012.12.014.

Juggins, S., 2015: rioja: Analysis of Quaternary science data. *R Package Version 09-5 Compr. R Arch. Netw.*,.

Kageyama, M., A. Paul, D. M. Roche, and C. J. Van Meerbeeck, 2010: Modelling glacial climatic millennial-scale variability related to changes in the Atlantic meridional overturning circulation: a review. *Quat. Sci. Rev.*, **29**, 2931–2956, https://doi.org/10.1016/j.quascirev.2010.05.029.

——, and Coauthors, 2013: Climatic impacts of fresh water hosing under Last Glacial Maximum conditions: a multi-model study. *Clim. Past*, **9**, 935–953.

——, and Coauthors, 2017: The PMIP4 contribution to CMIP6-Part 4: Scientific objectives and experimental design of the PMIP4-CMIP6 Last Glacial Maximum experiments and PMIP4 sensitivity experiments. *Geosci. Model Dev.*, **10**, 4035–4055, https://doi.org/10.5194/gmd-10-4035-2017.

——, and Coauthors, 2021: The PMIP4 Last Glacial Maximum experiments: preliminary results and comparison with the PMIP3 simulations. *Clim. Past*, **17**, 1065–1089, https://doi.org/10.5194/cp-17-1065-2021.

Kalnay, E., and Coauthors, 1996: The NCEP/NCAR 40-year reanalysis project. *Bull. Am. Meteorol. Soc.*, **77**, 437–471, https://doi.org/10.1175/1520-0477(1996)077<0437:tnyrp>2.0.co;2.

Kaufman, D., and Coauthors, 2020a: A global database of Holocene paleotemperature records. *Sci. Data*, **7**, 34, https://doi.org/10.1038/s41597-020-0445-3.

——, N. McKay, C. Routson, M. Erb, C. Datwyler, P. S. Sommer, O. Heiri, and B. Davis, 2020b: Holocene global mean surface temperature, a multi-method reconstruction approach. *Sci. Data*, **7**, 13, https://doi.org/10.1038/s41597-020-0530-7.

Keigwin, L. D., and S. J. Lehman, 1994: Deep circulation change linked to Heinrich Event 1 and Younger Dryas in a middepth North Atlantic Core. *Paleoceanography*, **9**, 185–194, https://doi.org/10.1029/94PA00032.

Keigwin, L. D., G. A. Jones, S. J. Lehman, and E. A. Boyle, 1991: Deglacial meltwater discharge, North Atlantic deep circulation, and abrupt climate change. *J. Geophys. Res.-Oceans*, **96**, 16811–16826, https://doi.org/10.1029/91jc01624.

——, S. Klotsko, N. Zhao, B. Reilly, L. Giosan, and N. W. Driscoll, 2018: Deglacial floods in the Beaufort Sea preceded Younger Dryas cooling. *Nat. Geosci.*, **11**, 599-+, https://doi.org/10.1038/s41561-018-0169-6.

Kirby, M. E., H. T. Mullins, W. P. Patterson, and A. W. Burnett, 2002a: Late glacial-Holocene atmospheric circulation and precipitation in the northeast United States inferred from modern calibrated stable oxygen and carbon isotopes. *Geol. Soc. Am. Bull.*, **114**, 1326–1340, https://doi.org/10.1130/0016-7606(2002)114<1326:Lghaca>2.0.Co;2.

——, W. P. Patterson, H. T. Mullins, and A. W. Burnett, 2002b: Post-Younger Dryas climate interval linked to circumpolar vortex variability: isotopic evidence from Fayetteville Green Lake, New York. *Clim. Dyn.*, **19**, 321–330, https://doi.org/10.1007/s00382-002-0227-y.

Klinger, B. A., and J. Marotzke, 2000: Meridional heat transport by the subtropical cell. *J. Phys. Oceanogr.*, **30**, 696–705, https://doi.org/Doi 10.1175/1520-0485(2000)030<0696:Mhtbts>2.0.Co;2.

Kneller, M., and D. Peteet, 1993: Late-Quaternary climate in the Ridge and Valley of Virginia, U.S.A.: Changes in vegetation and depositional environment: A contribution to the 'North Atlantic seaboard programme' of IGCP-253, 'Termination of the Pleistocene.' *Quat. Sci. Rev.*, **12**, 613–628, https://doi.org/10.1016/0277-3791(93)90003-5.

Kneller, M., and D. Peteet, 1999: Late-glacial to early Holocene climate changes from a central Appalachian pollen and macrofossil record. *Quat. Res.*, **51**, 133–147, https://doi.org/DOI 10.1006/qres.1998.2026.

Knight, C. A., J. L. Blois, B. Blonder, M. Macias-Fauria, A. Ordonez, and J.-C. Svenning, 2020: Community Assembly and Climate Mismatch in Late Quaternary Eastern North American Pollen Assemblages. *Am. Nat.*, **195**, 166–180, https://doi.org/10.1086/706340.

Kobayashi, H., A. Oka, A. Yamamoto, and A. Abe-Ouchi, 2021: Glacial carbon cycle changes by Southern Ocean processes with sedimentary amplification. *Sci. Adv.*, **7**, eabg7723, https://doi.org/10.1126/sciadv.abg7723.

Krause, T. R., J. M. Russell, R. Zhang, J. W. Williams, and S. T. Jackson, 2018: Late Quaternary vegetation, climate, and fire history of the Southeast Atlantic Coastal Plain based on a 30,000-yr multi-proxy record from White Pond, South Carolina, USA. *Quat. Res.*, 1–20, https://doi.org/10.1017/qua.2018.95.

Kumar, S., J. Kinter, P. A. Dirmeyer, Z. T. Pan, and J. Adams, 2013: Multidecadal Climate Variability and the "Warming Hole" in North America: Results from CMIP5 Twentieth- and Twenty-First-Century Climate Simulations. *J. Clim.*, **26**, 3511–3527, https://doi.org/10.1175/jcli-d-12-00535.1.

Lane, C. S., A. Brauer, S. P. E. Blockley, and P. Dulski, 2013: Volcanic ash reveals time-transgressive abrupt climate change during the Younger Dryas. *Geology*, **41**, 1251–1254, https://doi.org/10.1130/g34867.1.

——, A. K. Taylor, J. Spencer, and K. B. Jones, 2018: Compound-specific isotope records of late-quaternary environmental change in southeastern North Carolina. *Quat. Sci. Rev.*, **182**, 48–64, https://doi.org/10.1016/j.quascirev.2017.12.022.

Laskar, J., P. Robutel, F. Joutel, M. Gastineau, A. C. M. Correia, and B. Levrard, 2004: A long-term numerical solution for the insolation quantities of the Earth. *Astron. Astrophys.*, **428**, 261–285, https://doi.org/10.1051/0004-6361:20041335.

Latham, R. E., and R. E. Ricklefs, 1993: Continental comparisons of temperate-zone tree species diversity. *Species diversity in ecological communities: historical and geographical perspectives*, R.E. Ricklefs and D. Schluter, Eds., University of Chicago Press, 294–314.

Leite, Y. L. R., and Coauthors, 2016: Neotropical forest expansion during the last glacial period challenges refuge hypothesis. *Proc. Natl. Acad. Sci.*, **113**, 1008–1013, https://doi.org/10.1073/pnas.1513062113.

Levesque, A. J., L. C. Cwynar, and I. R. Walker, 1997: Exceptionally steep north–south gradients in lake temperatures during the last deglaciation. *Nature*, **385**, 423.

Li, C., and A. Born, 2019: Coupled atmosphere-ice-ocean dynamics in Dansgaard-Oeschger events. *Quat. Sci. Rev.*, **203**, 1–20, https://doi.org/10.1016/j.quascirev.2018.10.031.

Li, L. F., W. H. Li, and Y. Kushnir, 2012: Variation of the North Atlantic subtropical high western ridge and its implication to Southeastern US summer precipitation. *Clim. Dyn.*, **39**, 1401–1412, https://doi.org/10.1007/s00382-011-1214-y.

Lim, Y. K., and S. D. Schubert, 2011: The impact of ENSO and the Arctic Oscillation on winter temperature extremes in the southeast United States. *Geophys. Res. Lett.*, **38**, 5, https://doi.org/10.1029/2011gl048283.

Lisiecki, L. E., and M. E. Raymo, 2005: A Pliocene-Pleistocene stack of 57 globally distributed benthic delta O-18 records. *Paleoceanography*, **20**, https://doi.org/Artn Pa1003 10.1029/2004pa001071.

Liu, Z., and Coauthors, 2009: Transient Simulation of Last Deglaciation with a New Mechanism for Bølling-Allerød Warming. *Science*, **325**, 310–314, https://doi.org/10.1126/science.1171041.

Liu, Z. Y., and Coauthors, 2014: The Holocene temperature conundrum. *Proc. Natl. Acad. Sci. U. S. A.*, **111**, E3501–E3505, https://doi.org/10.1073/pnas.1407229111.

Loomis, S. E., J. M. Russell, B. Ladd, F. A. Street-Perrott, and J. S. Sinninghe Damsté, 2012: Calibration and application of the branched GDGT temperature proxy on East African lake sediments. *Earth Planet. Sci. Lett.*, **357–358**, 277–288, https://doi.org/10.1016/j.epsl.2012.09.031.

van Loon, H., and J. C. Rogers, 1978: The Seesaw in Winter Temperatures between Greenland and Northern Europe. Part I: General Description. *Mon. Weather Rev.*, **106**, 296–310, https://doi.org/10.1175/1520-0493(1978)106<0296:TSIWTB>2.0.CO;2.

Lora, J. M., 2018: Components and Mechanisms of Hydrologic Cycle Changes over North America at the Last Glacial Maximum. *J. Clim.*, **31**, 7035–7051, https://doi.org/10.1175/jcli-d-17-0544.1.

——, and D. E. Ibarra, 2019: The North American hydrologic cycle through the last deglaciation. *Quat. Sci. Rev.*, **226**, 25, https://doi.org/10.1016/j.quascirev.2019.105991.

——, J. L. Mitchell, and A. E. Tripati, 2016: Abrupt reorganization of North Pacific and western North American climate during the last deglaciation. *Geophys. Res. Lett.*, **43**, 11796–11804, https://doi.org/10.1002/2016gl071244.

Lorenz, D. J., D. Nieto-Lugilde, J. L. Blois, M. C. Fitzpatrick, and J. W. Williams, 2016: Downscaled and debiased climate simulations for North America from 21,000 years ago to 2100AD. *Sci. Data*, **3**, 160048, https://doi.org/10.1038/sdata.2016.48.

Lumibao, C. Y., S. M. Hoban, and J. McLachlan, 2017: Ice ages leave genetic diversity "hotspots" in Europe but not in Eastern North America. *Ecol Lett*, **20**, 1459–1468, https://doi.org/10.1111/ele.12853.

Lüthi, D., and Coauthors, 2008: High-resolution carbon dioxide concentration record 650,000–800,000 years before present. *Nature*, **453**, 379–382, https://doi.org/10.1038/nature06949.

Maier, E., and Coauthors, 2018: North Pacific freshwater events linked to changes in glacial ocean circulation. *Nature*, **559**, 241–245, https://doi.org/10.1038/s41586-018-0276-y.

Mandl, M. B., B. N. Shuman, J. Marsicek, and L. Grigg, 2016: Estimating the regional climate signal in a late Pleistocene and early Holocene lake-sediment delta O-18 record from Vermont, USA. *Quat. Res.*, **86**, 67–78, https://doi.org/10.1016/j.yqres.2016.02.009.

Marchal, O., R. François, T. F. Stocker, and F. Joos, 2000: Ocean thermohaline circulation and sedimentary 231Pa/230Th ratio. *Paleoceanography*, **15**, 625–641, https://doi.org/10.1029/2000PA000496.

Marcott, S. A., J. D. Shakun, P. U. Clark, and A. C. Mix, 2013: A Reconstruction of Regional and Global Temperature for the Past 11,300 Years. *Science*, **339**, 1198–1201, https://doi.org/10.1126/science.1228026.

Marcott, S. A., and Coauthors, 2014: Centennial-scale changes in the global carbon cycle during the last deglaciation. *Nature*, **514**, 616, https://doi.org/10.1038/nature13799 https://www.nature.com/articles/nature13799#supplementary-information.

Markle, B. R., and Coauthors, 2017: Global atmospheric teleconnections during Dansgaard–Oeschger events. *Nat. Geosci.*, **10**, 36–40, https://doi.org/10.1038/ngeo2848.

Marsicek, J., B. N. Shuman, P. J. Bartlein, S. L. Shafer, and S. Brewer, 2018: Reconciling divergent trends and millennial variations in Holocene temperatures. *Nature*, **554**, 92, https://doi.org/10.1038/nature25464.

Martinez-Sosa, P., J. E. Tierney, I. C. Stefanescu, E. D. Crampton-Flood, B. N. Shuman, and C. Routson, 2021: A global Bayesian temperature calibration for lacustrine brGDGTs. *Geochim. Cosmochim. Acta*, **305**, 87–105, https://doi.org/10.1016/j.gca.2021.04.038.

Masson-Delmotte, V., and Coauthors, 2006: Past and future polar amplification of climate change: climate model intercomparisons and ice-core constraints. *Clim. Dyn.*, **26**, 513–529, https://doi.org/10.1007/s00382-005-0081-9.

McCreary, J. P., and P. Lu, 1994: Interaction between the subtropical and equatorial ocean circulations - the subtropical cell. *J. Phys. Oceanogr.*, **24**, 466–497.

McGee, D., E. Moreno-Chamarro, B. Green, J. Marshall, E. Galbraith, and L. Bradtmiller, 2018a: Hemispherically asymmetric trade wind changes as signatures of past ITCZ shifts. *Quat. Sci. Rev.*, **180**, 214–228, https://doi.org/10.1016/j.quascirev.2017.11.020.

——, ——, J. Marshall, and E. D. Galbraith, 2018b: Western U.S. lake expansions during Heinrich stadials linked to Pacific Hadley circulation. *Sci. Adv.*, **4**, eaav0118, https://doi.org/10.1126/sciadv.aav0118.

McLachlan, J. S., J. S. Clark, and P. S. Manos, 2005: Molecular indicators of tree migration capacity under rapid climate change. *Ecology*, **86**, 2088–2098, https://doi.org/Doi 10.1890/04-1036.

McManus, J. F., R. Francois, J. M. Gherardi, L. D. Keigwin, and S. Brown-Leger, 2004: Collapse and rapid resumption of Atlantic meridional circulation linked to deglacial climate changes. *Nature*, **428**, 834–837, https://doi.org/10.1038/nature02494.

Meehl, G. A., J. M. Arblaster, and G. Branstator, 2012: Mechanisms Contributing to the Warming Hole and the Consequent US East-West Differential of Heat Extremes. *J. Clim.*, **25**, 6394–6408, https://doi.org/10.1175/jcli-d-11-00655.1.

Menking, K. M., D. M. Peteet, and R. Y. Anderson, 2012: Late-glacial and Holocene vegetation and climate variability, including major droughts, in the Sky Lakes region of southeastern New York State. *Palaeogeogr. Palaeoclimatol. Palaeoecol.*, **353**, 45–59, https://doi.org/10.1016/j.palaeo.2012.06.033.

Milankovitch, M. K., 1941: Kanon der Erdbestrahlung und seine Anwendung auf das Eiszeitenproblem. *R. Serbian Acad. Spec. Publ.*, **133**, 1–633.

Mishler, B. D., R. Guralnick, P. S. Soltis, S. A. Smith, D. E. Soltis, N. Barve, J. M. Allen, and S. W. Laffan, 2020: Spatial phylogenetics of the North American flora. *J. Syst. Evol.*, **58**, 393–405, https://doi.org/10.1111/jse.12590.

Mittermeier, R. A., C. G. Mittermeier, T. M. Brooks, J. D. Pilgrim, W. R. Konstant, G. A. B. da Fonseca, and C. Kormos, 2003: Wilderness and biodiversity conservation. *Proc. Natl. Acad. Sci.*, **100**, 10309–10313, https://doi.org/10.1073/pnas.1732458100.

Mix, A. C., W. F. Ruddiman, and A. McIntyre, 1986a: Late Quaternary paleoceanography of the tropical Atlantic, 1: Spatial variability of annual mean sea-surface temperatures, 0-20,000 years BP. *Paleoceanography*, **1**, 43–66, https://doi.org/10.1029/PA001i001p00043.

——, ——, and ——, 1986b: Late Quaternary paleoceanography of the tropical Atlantic, 2: Spatial variability of annual mean sea-surface temperatures, 0-20,000 years BP. *Paleoceanography*, **1**, 339–353, https://doi.org/10.1029/PA001i003p00339.

Mo, K. C., 2010: Interdecadal modulation of the impact of ENSO on precipitation and temperature over the United States. *J. Clim.*, **23**, 3639–3656, https://doi.org/10.1175/2010jcli3553.1.

Monnin, E., A. Indermühle, A. Dällenbach, J. Flückiger, B. Stauffer, T. F. Stocker, D. Raynaud, and J.-M. Barnola, 2001: Atmospheric CO2 Concentrations over the Last Glacial Termination. *Science*, **291**, 112–114, https://doi.org/10.1126/science.291.5501.112.

Mottl, O., and Coauthors, 2021: Global acceleration in rates of vegetation change over the past 18,000 years. *Science*, **372**, 860–864, https://doi.org/10.1126/science.abg1685.

Murphy, B., S. Müller, and R. Yurchak, 2021: *GeoStat-Framework/PyKrige: v1.6.1*. Zenodo,.

Newby, P. E., P. Killoran, M. R. Waldorf, B. N. Shuman, R. S. Webb, and T. Webb, 2000: 14,000 years of sediment, vegetation, and water-level changes at the Makepeace Cedar Swamp, southeastern Massachusetts. *Quat. Res.*, **53**, 352–368, https://doi.org/10.1006/qres.1999.2120.

——, J. P. Donnelly, B. N. Shuman, and D. MacDonald, 2009: Evidence of centennial-scale drought from southeastern Massachusetts during the Pleistocene/Holocene transition. *Quat. Sci. Rev.*, **28**, 1675–1692, https://doi.org/10.1016/j.quascirev.2009.02.020.

Nolan, C., and Coauthors, 2018: Past and future global transformation of terrestrial ecosystems under climate change. *Science*, **361**, 920–923, https://doi.org/10.1126/science.aan5360.

North, G. R., 1984: The small ice cap instability in diffusive climate models. *J. Atmospheric Sci.*, **41**, 3390–3395, https://doi.org/10.1175/1520-0469(1984)041<3390:tsicii>2.0.co;2.

——, T. L. Bell, R. F. Cahalan, and F. J. Moeng, 1982: Sampling errors in the estimate of empirical orthogonal functions. *Mon. Weather Rev.*, **110**, 699–706, https://doi.org/10.1175/1520-0493(1982)110<0699:seiteo>2.0.co;2.

North Greenland Ice Core Project Members, 2004: High-resolution record of Northern Hemisphere climate extending into the last interglacial period. *Nature*, **431**, 147–151, https://doi.org/10.1038/nature02805.

Noss, R. F., W. J. Platt, B. A. Sorrie, A. S. Weakley, D. B. Means, J. Costanza, and R. K. Peet, 2015: How global biodiversity hotspots may go unrecognized: lessons from the North American Coastal Plain. *Divers. Distrib.*, **21**, 236–244, https://doi.org/10.1111/ddi.12278.

Okumura, Y. M., C. Deser, A. Hu, A. Timmermann, and S. P. Xie, 2009: North Pacific climate response to freshwater forcing in the subarctic North Atlantic: oceanic and atmospheric pathways. *J. Clim.*, **22**, 1424–1445, https://doi.org/10.1175/2008jcli2511.1.

Ordonez, A., and J. W. Williams, 2013: Climatic and biotic velocities for woody taxa distributions over the last 16 000 years in eastern North America. *Ecol. Lett.*, **16**, 773–781.

Ortega, P., F. Lehner, D. Swingedouw, V. Masson-Delmotte, C. C. Raible, M. Casado, and P. Yiou, 2015: A model-tested North Atlantic Oscillation reconstruction for the past millennium. *Nature*, **523**, 71–74, https://doi.org/10.1038/nature14518.

Osman, M. B., J. E. Tierney, J. Zhu, R. Tardif, G. J. Hakim, J. King, and C. J. Poulsen, 2021: Globally resolved surface temperatures since the Last Glacial Maximum. *Nature*, **599**, 239–244, https://doi.org/10.1038/s41586-021-03984-4.

Oster, J. L., D. E. Ibarra, M. J. Winnick, and K. Maher, 2015: Steering of westerly storms over western North America at the Last Glacial Maximum. *Nat. Geosci.*, **8**, 201–205, https://doi.org/10.1038/ngeo2365.

Otto-Bliesner, B. L., and E. C. Brady, 2010: The sensitivity of the climate response to the magnitude and location of freshwater forcing: last glacial maximum experiments. *Quat. Sci. Rev.*, **29**, 56–73, https://doi.org/10.1016/j.quascirev.2009.07.004.

Overpeck, J., C. Whitlock, and B. Huntley, 2003: Terrestrial Biosphere Dynamics in the Climate System: Past and Future. *Paleoclimate, Global Change and the Future*, K.D. Alverson, T.F. Pedersen, and R.S. Bradley, Eds., *Global Change — The IGBP Series*, Springer, 81–103.

Overpeck, J. T., T. Webb, and I. C. Prentice, 1985: Quantitative interpretation of fossil pollen spectra - dissimilarity coefficients and the method of modern analogs. *Quat. Res.*, **23**, 87–108, https://doi.org/10.1016/0033-5894(85)90074-2.

Pausata, F. S. R., D. S. Battisti, K. H. Nisancioglu, and C. M. Bitz, 2011: Chinese stalagmite δ18O controlled by changes in the Indian monsoon during a simulated Heinrich event. *Nat. Geosci.*, **4**, 474–480, https://doi.org/10.1038/ngeo1169.

Pearson, R. G., and Coauthors, 2014: Life history and spatial traits predict extinction risk due to climate change. *Nat. Clim. Change*, **4**, 217–221, https://doi.org/10.1038/nclimate2113.

Pedro, J. B., T. D. van Ommen, S. O. Rasmussen, V. I. Morgan, J. Chappellaz, A. D. Moy, V. Masson-Delmotte, and M. Delmotte, 2011: The last deglaciation: timing the bipolar seesaw. *Clim. Past*, **7**, 671–683, https://doi.org/10.5194/cp-7-671-2011.

Pedro, J. B., M. Jochum, C. Buizert, F. He, S. Barker, and S. O. Rasmussen, 2018: Beyond the bipolar seesaw: Toward a process understanding of interhemispheric coupling. *Quat. Sci. Rev.*, **192**, 27–46, https://doi.org/10.1016/j.quascirev.2018.05.005.

Peltier, W. R., 2004: Global glacial isostasy and the surface of the ice-age Earth: the ICE-5G (VM2) model and GRACE. *Annu. Rev. Earth Planet. Sci.*, **32**, 111–149, https://doi.org/10.1146/annurev.earth.32.082503.144359.

——, D. F. Argus, and R. Drummond, 2015: Space geodesy constrains ice age terminal deglaciation: The global ICE-6G_C (VM5a) model. *J. Geophys. Res.-Solid Earth*, **120**, 450–487, https://doi.org/10.1002/2014jb011176.

Peterse, F., J. van der Meer, S. Schouten, J. W. H. Weijers, N. Fierer, R. B. Jackson, J.-H. Kim, and J. S. Sinninghe Damsté, 2012: Revised calibration of the MBT–CBT paleotemperature proxy based on branched tetraether membrane lipids in surface soils. *Geochim. Cosmochim. Acta*, **96**, 215–229, http://dx.doi.org/10.1016/j.gca.2012.08.011.

Peterson, A. T., and Á. S. Nyári, 2008: Ecological Niche Conservatism and Pleistocene Refugia in the Thrush-Like Mourner, Schiffornis Sp., in the Neotropics. *Evolution*, **62**, 173–183, https://doi.org/10.1111/j.1558-5646.2007.00258.x.

Peterson, L. C., G. H. Haug, K. A. Hughen, and U. Röhl, 2000: Rapid Changes in the Hydrologic Cycle of the Tropical Atlantic During the Last Glacial. *Science*, **290**, 1947–1951, https://doi.org/10.1126/science.290.5498.1947.

Petit, J. R., and Coauthors, 1999: Climate and atmospheric history of the past 420,000 years from the Vostok ice core, Antarctica. *Nature*, **399**, 429–436, https://doi.org/10.1038/20859.

Petit, R. J., and Coauthors, 2002: Identification of refugia and post-glacial colonisation routes of European white oaks based on chloroplast DNA and fossil pollen evidence. *For. Ecol. Manag.*, **156**, 49–74, https://doi.org/Pii S0378-1127(01)00634-X Doi 10.1016/S0378-1127(01)00634-X.

Pisias, N. G., and T. C. Moore, 1981: The evolution of Pleistocene climate: A time series approach. *Earth Planet. Sci. Lett.*, **52**, 450–458, https://doi.org/10.1016/0012-821X(81)90197-7.

Prentice, I. C., P. J. Bartlein, and T. Webb, 1991: Vegetation and Climate Change in Eastern North America Since the Last Glacial Maximum. *Ecology*, **72**, 2038–2056, https://doi.org/10.2307/1941558.

Raberg, J. H., and Coauthors, 2021: Revised fractional abundances and warm-season temperatures substantially improve brGDGT calibrations in lake sediments. *Biogeosciences*, **18**, 3579–3603, https://doi.org/10.5194/bg-18-3579-2021.

Radeloff, V. C., and Coauthors, 2019: The Dynamic Habitat Indices (DHIs) from MODIS and global biodiversity. *Remote Sens. Environ.*, **222**, 204–214, https://doi.org/10.1016/j.rse.2018.12.009.

Rahmstorf, S., 1995: Bifurcations of the Atlantic thermohaline circulation in response to changes in the hydrological cycle. *Nature*, **378**, 145–149, https://doi.org/10.1038/378145a0.

——, 2002: Ocean circulation and climate during the past 120,000 years. *Nature*, **419**, 207–214, https://doi.org/10.1038/nature01090.

Rangel, T. F., and Coauthors, 2018: Modeling the ecology and evolution of biodiversity: Biogeographical cradles, museums, and graves. *Science*, https://doi.org/10.1126/science.aar5452.

Rasmussen, S. O., and Coauthors, 2006: A new Greenland ice core chronology for the last glacial termination. *J. Geophys. Res.-Atmospheres*, **111**, 16, https://doi.org/10.1029/2005jd006079.

Rea, B. R., and Coauthors, 2020: Atmospheric circulation over Europe during the Younger Dryas. *Sci. Adv.*, **6**, 13, https://doi.org/10.1126/sciadv.aba4844.

Reimer, P. J., and Coauthors, 2013: IntCal13 and Marine13 radiocarbon age calibration curves 0-50,000 years cal BP.

Renssen, H., M. Lautenschlager, and C. J. E. Schuurmans, 1996: The atmospheric winter circulation during the Younger Dryas stadial in the Atlantic/European sector. *Clim. Dyn.*, **12**, 813–824, https://doi.org/10.1007/s003820050145.

——, H. Goosse, D. M. Roche, and H. Seppa, 2018: The global hydroclimate response during the Younger Dryas event. *Quat. Sci. Rev.*, **193**, 84–97, https://doi.org/10.1016/j.quascirev.2018.05.033.

Rey, F., and Coauthors, 2017: Vegetational and agricultural dynamics at Burgaschisee (Swiss Plateau) recorded for 18,700 years by multi-proxy evidence from partly varved sediments. *Veg. Hist. Archaeobotany*, **26**, 571–586, https://doi.org/10.1007/s00334-017-0635-x.

Rodwell, M. J., D. P. Rowell, and C. K. Folland, 1999: Oceanic forcing of the wintertime North Atlantic Oscillation and European climate. *Nature*, **398**, 320–323, https://doi.org/10.1038/18648.

Rogers, J. C., 1990: Patterns of low frequency monthly sea level pressure variability (1899-1986) and associated wave cyclone frequencies. *J. Clim.*, **3**, 1364–1379, https://doi.org/10.1175/1520-0442(1990)003<1364:polfms>2.0.co;2.

Ruhlemann, C., S. Mulitza, P. J. Muller, G. Wefer, and R. Zahn, 1999: Warming of the tropical Atlantic Ocean and slowdown of thermohaline circulation during the last deglaciation. *Nature*, **402**, 511–514, https://doi.org/Doi 10.1038/990069.

Russell, J. M., E. C. Hopmans, S. E. Loomis, J. Liang, and J. S. Sinninghe Damsté, 2018: Distributions of 5- and 6-methyl branched glycerol dialkyl glycerol tetraethers (brGDGTs) in East African lake sediment: Effects of temperature, pH, and new lacustrine paleotemperature calibrations. *Org. Geochem.*, **117**, 56–69, https://doi.org/10.1016/j.orggeochem.2017.12.003.

Sachs, J. P., and S. J. Lehman, 1999: Subtropical North Atlantic Temperatures 60,000 to 30,000 Years Ago. *Science*, **286**, 756–759, https://doi.org/10.1126/science.286.5440.756.

Sakai, A., and C. J. Weiser, 1973: Freezing resistance of trees in North America with reference to tree regions. *Ecology*, **54**, 118–126, https://doi.org/10.2307/1934380.

Salonen, J. S., M. Korpela, J. W. Williams, and M. Luoto, 2019: Machine-learning based reconstructions of primary and secondary climate variables from North American and European fossil pollen data. *Sci Rep*, **9**, 13, https://doi.org/10.1038/s41598-019-52293-4.

Sandel, B., L. Arge, B. Dalsgaard, R. G. Davies, K. J. Gaston, W. J. Sutherland, and J. C. Svenning, 2011: The influence of late Quaternary climate-change velocity on species endemism. *Science*, **334**, 660–664, https://doi.org/10.1126/science.1210173.

Sandom, C., S. Faurby, B. Sandel, and J.-C. Svenning, 2014: Global late Quaternary megafauna extinctions linked to humans, not climate change. *Proc. R. Soc. B Biol. Sci.*, **281**, 20133254, https://doi.org/10.1098/rspb.2013.3254.

Schartman, A. K., A. F. Diefendorf, T. V. Lowell, E. J. Freimuth, A. K. Stewart, J. D. Landis, and B. R. Bates, 2020: Stable source of Holocene spring precipitation recorded in leaf

wax hydrogen-isotope ratios from two New York lakes. *Quat. Sci. Rev.*, **240**, 17, https://doi.org/10.1016/j.quascirev.2020.106357.

Schenk, F., and Coauthors, 2018: Warm summers during the Younger Dryas cold reversal. *Nat. Commun.*, **9**, 13, https://doi.org/10.1038/s41467-018-04071-5.

Schneider, U., A. Becker, P. Finger, A. Meyer-Christoffer, B. Rudolf, and M. Ziese, 2011: GPCC full data reanalysis version 6.0 at 0.5: Monthly land-surface precipitation from rain-gauges built on GTS-based and historic data. *GPCC Data Repos.*, **10**.

——, P. Finger, A. Meyer-Christoffer, E. Rustemeier, M. Ziese, and A. Becker, 2017: Evaluating the Hydrological Cycle over Land Using the Newly-Corrected Precipitation Climatology from the Global Precipitation Climatology Centre (GPCC). *Atmosphere*, **8**, 52, https://doi.org/10.3390/atmos8030052.

Schouten, S., E. C. Hopmans, E. Schefuß, and J. S. Sinninghe Damsté, 2002: Distributional variations in marine crenarchaeotal membrane lipids: a new tool for reconstructing ancient sea water temperatures? *Earth Planet. Sci. Lett.*, **204**, 265–274, https://doi.org/10.1016/S0012-821X(02)00979-2.

Schulz, M., 2002: On the 1470-year pacing of Dansgaard-Oeschger warm events. *Paleoceanography*, **17**, 4-1-4–9, https://doi.org/10.1029/2000PA000571.

Schwalb, A., and W. E. Dean, 1998: Stable isotopes and sediments from pickerel lake, South Dakota, USA: a 12ky record of environmental changes. *J. Paleolimnol.*, **20**, 15–30, https://doi.org/10.1023/a:1007971226750.

Severinghaus, J. P., T. Sowers, E. J. Brook, R. B. Alley, and M. L. Bender, 1998: Timing of abrupt climate change at the end of the Younger Dryas interval from thermally fractionated gases in polar ice. *Nature*, **391**, 141, https://doi.org/10.1038/34346.

Shaffer, G., S. M. Olsen, and C. J. Bjerrum, 2004: Ocean subsurface warming as a mechanism for coupling Dansgaard-Oeschger climate cycles and ice-rafting events. *Geophys. Res. Lett.*, **31**, https://doi.org/10.1029/2004GL020968.

Shakun, J. D., and A. E. Carlson, 2010: A global perspective on Last Glacial Maximum to Holocene climate change. *Quat. Sci. Rev.*, **29**, 1801–1816, https://doi.org/10.1016/j.quascirev.2010.03.016.

Shane, L. C. K., and K. H. Anderson, 1993: Intensity, gradients and reversals in late glacial environmental change in east-central north America. *Quat. Sci. Rev.*, **12**, 307–320, http://dx.doi.org/10.1016/0277-3791(93)90039-O.

Shuman, B., J. Bravo, J. Kaye, J. A. Lynch, P. Newby, and T. Webb, 2001: Late Quaternary water-level variations and vegetation history at Crooked Pond, southeastern Massachusetts. *Quat. Res.*, **56**, 401–410, https://doi.org/10.1006/qres.2001.2273.

——, T. Webb III, P. Bartlein, and J. W. Williams, 2002: The anatomy of a climatic oscillation: vegetation change in eastern North America during the Younger Dryas chronozone. *Quat. Sci. Rev.*, **21**, 1777–1791, https://doi.org/Pii S0277-3791(02)00030-6 Doi 10.1016/S0277-3791(02)00030-6.

——, P. Newby, Y. S. Huang, and T. Webb, 2004: Evidence for the close climatic control of New England vegetation history. *Ecology*, **85**, 1297–1310, https://doi.org/10.1890/02-0286.

——, Y. S. Huang, P. Newby, and Y. Wang, 2006: Compound-specific isotopic analyses track changes in seasonal precipitation regimes in the Northeastern United States at ca 8200cal yrBP. *Quat. Sci. Rev.*, **25**, 2992–3002, https://doi.org/10.1016/j.quascirev.2006.02.021.

Shuman, B. N., and S. A. Burrell, 2017: Centennial to millennial hydroclimatic fluctuations in the humid northeast United States during the Holocene. *Quat. Res.*, **88**, 514–524, https://doi.org/10.1017/qua.2017.62.

Siegenthaler, U., and Coauthors, 2005: Stable Carbon Cycle-Climate Relationship During the Late Pleistocene. **310**, 6.

Sigman, D. M., M. P. Hain, and G. H. Haug, 2010: The polar ocean and glacial cycles in atmospheric CO2 concentration. *Nature*, **466**, 47–55, https://doi.org/10.1038/nature09149.

Singarayer, J. S., and P. J. Valdes, 2010: High-latitude climate sensitivity to ice-sheet forcing over the last 120 kyr. *Quat. Sci. Rev.*, **29**, 43–55, https://doi.org/10.1016/j.quascirev.2009.10.011.

Sinninghe Damsté, J. S., and Coauthors, 2018: An overview of the occurrence of ether- and ester-linked iso-diabolic acid membrane lipids in microbial cultures of the Acidobacteria: Implications for brGDGT paleoproxies for temperature and pH. *Org. Geochem.*, **124**, 63–76, https://doi.org/10.1016/j.orggeochem.2018.07.006.

Sjostrom, D. J., and J. M. Welker, 2009: The influence of air mass source on the seasonal isotopic composition of precipitation, eastern USA. *J. Geochem. Explor.*, **102**, 103–112, https://doi.org/10.1016/j.gexplo.2009.03.001.

Solomon, A. M., and T. Webb, 1985: Computer-aided reconstruction of late-Quaternary landscape dynamics. *Annu. Rev. Ecol. Syst.*, **16**, 63–84.

Soltis, D. E., A. B. Morris, J. S. McLachlan, P. S. Manos, and P. S. Soltis, 2006: Comparative phylogeography of unglaciated eastern North America. *Mol. Ecol.*, **15**, 4261–4293, https://doi.org/10.1111/j.1365-294X.2006.03061.x.

Springer, G. S., H. D. Rowe, B. Hardt, H. Cheng, and R. L. Edwards, 2014: East central North America climates during marine isotope stages 3-5. *Geophys. Res. Lett.*, **41**, 3233–3237, https://doi.org/10.1002/2014gl059884.

Srivastava, A., R. Grotjahn, and P. A. Ullrich, 2020: Evaluation of historical CMIP6 model simulations of extreme precipitation over contiguous US regions. *Weather Clim. Extrem.*, **29**, 25, https://doi.org/10.1016/j.wace.2020.100268.

Stevens, G. C., 1989: The Latitudinal Gradient in Geographical Range: How so Many Species Coexist in the Tropics. *Am. Nat.*, **133**, 240–256, https://doi.org/10.1086/284913.

Stocker, T. F., 1998: Climate change - The seesaw effect. *Science*, **282**, 61–62, https://doi.org/DOI 10.1126/science.282.5386.61.

Stocker, T. F., and D. G. Wright, 1991: Rapid transitions of the ocean's deep circulation induced by changes in surface water fluxes. *Nature*, **351**, 729–732, https://doi.org/10.1038/351729a0.

Stocker, T. F., D. G. Wright, and L. A. Mysak, 1992: A zonally averaged, coupled ocean-atmosphere model for paleoclimate studies. *J. Clim.*, **5**, 773–797, https://doi.org/10.1175/1520-0442(1992)005<0773:azacoa>2.0.co;2.

Stommel, H., 1961: Thermohaline Convection with Two Stable Regimes of Flow. *Tellus*, **13**, 224–230, https://doi.org/10.1111/j.2153-3490.1961.tb00079.x.

Stouffer, R. J., and Coauthors, 2006: Investigating the Causes of the Response of the Thermohaline Circulation to Past and Future Climate Changes. *J. Clim.*, **19**, 1365–1387, https://doi.org/10.1175/JCLI3689.1.

Sun, Y., S. C. Clemens, C. Morrill, X. Lin, X. Wang, and Z. An, 2012: Influence of Atlantic meridional overturning circulation on the East Asian winter monsoon. *Nat. Geosci.*, **5**, 46–49, https://doi.org/10.1038/ngeo1326.

Svenning, J. C., and F. Skov, 2004: Limited filling of the potential range in European tree species. *Ecol Lett*, **7**, 565–573, https://doi.org/10.1111/j.1461-0248.2004.00614.x.

——, and ——, 2007: Could the tree diversity pattern in Europe be generated by postglacial dispersal limitation? *Ecol Lett*, **10**, 453–460, https://doi.org/10.1111/j.1461-0248.2007.01038.x.

——, S. Normand, and M. Kageyama, 2008: Glacial refugia of temperate trees in Europe: insights from species distribution modelling. *J. Ecol.*, **96**, 1117–1127, https://doi.org/10.1111/j.1365-2745.2008.01422.x.

Swezey, C. S., A. P. Schultz, W. A. Gonzalez, C. E. Bernhardt, W. R. Doar, C. P. Garrity, S. A. Mahan, and J. P. McGeehin, 2013: Quaternary eolian dunes in the Savannah River valley, Jasper County, South Carolina, USA. *Quat. Res.*, **80**, 250–264, https://doi.org/10.1016/j.yqres.2013.06.007.

Talbot, M. R., M. L. Filippi, N. B. Jensen, and J. J. Tiercelin, 2007: An abrupt change in the African monsoon at the end of the Younger Dryas. *Geochem. Geophys. Geosystems*, **8**, https://doi.org/10.1029/2006gc001465.

Tarasov, L., and W. R. Peltier, 2005: Arctic freshwater forcing of the Younger Dryas cold reversal. *Nature*, **435**, 662, https://doi.org/10.1038/nature03617 https://www.nature.com/articles/nature03617#supplementary-information.

Ter Braak, C. J., 1987: Unimodal models to relate species to environment. Wageningen University, .

——, and I. C. Prentice, 1988: A theory of gradient analysis. *Advances in Ecological Research*, Vol. 18 of, Academic Press, 271–317.

Ter Braak, C. J. F., and C. W. N. Looman, 1986: Weighted averaging, logistic regression and the Gaussian response model. *Vegetatio*, **65**, 3–11.

Ter Braak, C. J. F., and S. Juggins, 1993: Weighted averaging partial least squares regression (WA-PLS): an improved method for reconstructing environmental variables from species assemblages. *Twelfth International Diatom Symposium: Proceedings of the Twelfth International Diatom Symposium, Renesse, The Netherlands, 30 August – 5 September 1992*, H. Van Dam, Ed., Springer Netherlands, 485–502.

Ter Braak, C. J. F., S. Juggins, H. J. B. Birks, and H. Vandervoet, 1993: Weighted Averaging Partial Least-Squares regression (WA-PLS): definition and comparison with other methods for species-environment calibration. *Multivar. Environ. Stat.*, **6**, 525–560.

Thomé, M. T. C., K. R. Zamudio, J. G. R. Giovanelli, C. F. B. Haddad, F. A. Baldissera, and J. Alexandrino, 2010: Phylogeography of endemic toads and post-Pliocene persistence of the Brazilian Atlantic Forest. *Mol. Phylogenet. Evol.*, **55**, 1018–1031, https://doi.org/10.1016/j.ympev.2010.02.003.

Thompson, D. W. J., and J. M. Wallace, 1998: The Arctic Oscillation signature in the wintertime geopotential height and temperature fields. *Geophys. Res. Lett.*, **25**, 1297–1300, https://doi.org/10.1029/98gl00950.

——, and ——, 2000: Annular modes in the extratropical circulation. Part I: Month-to-month variability. *J. Clim.*, **13**, 1000–1016, https://doi.org/10.1175/1520-0442(2000)013<1000:Amitec>2.0.Co;2.

Thompson, R. S., K. H. Anderson, and P. J. Bartlein, 1999a: Atlas of relations between climatic parameters and distributions of important trees and shrubs in North America-Introduction and Conifers. U.S. Department of the Interior, U.S. Geological Survey, p. 269.

——, ——, and ——, 1999b: Atlas of relations between climatic parameters and distributions of important trees and shrubs in North America-Hardwoods. U.S. Department of the Interior, U.S. Geological Survey, p. 423.

Thuiller, W., M. Guéguen, J. Renaud, D. N. Karger, and N. E. Zimmermann, 2019: Uncertainty in ensembles of global biodiversity scenarios. *Nat. Commun.*, **10**, 1446, https://doi.org/10.1038/s41467-019-09519-w.

Tian, B. J., and X. Y. Dong, 2020: The Double-ITCZ Bias in CMIP3, CMIP5, and CMIP6 Models Based on Annual Mean Precipitation. *Geophys. Res. Lett.*, **47**, 11, https://doi.org/10.1029/2020gl087232.

Tierney, J. E., J. M. Russell, Y. S. Huang, J. S. S. Damste, E. C. Hopmans, and A. S. Cohen, 2008: Northern hemisphere controls on tropical southeast African climate during the past 60,000 years. *Science*, **322**, 252–255, https://doi.org/10.1126/science.1160485.

——, J. Zhu, J. King, S. B. Malevich, G. J. Hakim, and C. J. Poulsen, 2020: Glacial cooling and climate sensitivity revisited. *Nature*, **584**, 569-+, https://doi.org/10.1038/s41586-020-2617-x.

Tittensor, D. P., C. Mora, W. Jetz, H. K. Lotze, D. Ricard, E. V. Berghe, and B. Worm, 2010: Global patterns and predictors of marine biodiversity across taxa. *Nature*, **466**, 1098–1101, https://doi.org/10.1038/nature09329.

Toomey, M. R., R. L. Korty, J. P. Donnelly, P. J. van Hengstum, and W. B. Curry, 2017: Increased hurricane frequency near Florida during Younger Dryas Atlantic Meridional Overturning Circulation slowdown. *Geology*, **45**, 1047–1050, https://doi.org/10.1130/G39270.1.

United States Geological Survey, 1999: *Digital representation of "Atlas of United States Trees" by Elbert L. Little, Jr*.

Veloz, S. D., J. W. Williams, J. L. Blois, F. He, B. Otto-Bliesner, and Z. Liu, 2012: No-analog climates and shifting realized niches during the late quaternary: implications for 21st-century predictions by species distribution models. *Glob. Change Biol.*, **18**, 1698–1713, https://doi.org/10.1111/j.1365-2486.2011.02635.x.

Visbeck, M. H., J. W. Hurrell, L. Polvani, and H. M. Cullen, 2001: The North Atlantic Oscillation: Past, present, and future. *Proc. Natl. Acad. Sci. U. S. A.*, **98**, 12876–12877, https://doi.org/10.1073/pnas.231391598.

Voelker, S. L., and Coauthors, 2015: Deglacial hydroclimate of midcontinental North America. *Quat. Res.*, **83**, 336–344, https://doi.org/10.1016/j.yqres.2015.01.001.

WAIS Divide Project Members, 2015: Precise interpolar phasing of abrupt climate change during the last ice age. *Nature*, **520**, 661, https://doi.org/10.1038/nature14401 https://www.nature.com/articles/nature14401#supplementary-information.

Walker, G. T., and E. W. Bliss, 1932: World Weather V. *Memoirs of the Royal Meteorological Society*, Vol. 4 of, Stanford, 53–84.

Wallace, A. R., 1878: *Tropical Nature, and other Essays*. Macmillan and Company,.

Wallace, J. M., and D. S. Gutzler, 1981: Teleconnections in the geopotential height field during the Northern Hemisphere winter. *Mon. Weather Rev.*, **109**, 784–812, https://doi.org/10.1175/1520-0493(1981)109<0784:titghf>2.0.co;2.

Wallace, J. M., and P. V. Hobbs, 2006: *Atmospheric Science: An Introductory Survey*. Elsevier, 505 pp.

Waltari, E., R. J. Hijmans, A. T. Peterson, Á. S. Nyári, S. L. Perkins, and R. P. Guralnick, 2007: Locating Pleistocene Refugia: Comparing Phylogeographic and Ecological Niche Model Predictions. *PLOS ONE*, **2**, e563, https://doi.org/10.1371/journal.pone.0000563.

Wang, C. Z., 2002: Atlantic climate variability and its associated atmospheric circulation cells. *J. Clim.*, **15**, 1516–1536, https://doi.org/10.1175/1520-0442(2002)015<1516:acvaia>2.0.co;2.

Wang, Y., S. J. Goring, and J. L. McGuire, 2019: Bayesian ages for pollen records since the last glaciation in North America. *Sci. Data*, **6**, 8, https://doi.org/10.1038/s41597-019-0182-7.

Wang, Y. J., H. Cheng, R. L. Edwards, Z. S. An, J. Y. Wu, C. C. Shen, and J. A. Dorale, 2001: A high-resolution absolute-dated Late Pleistocene monsoon record from Hulu Cave, China. *Science*, **294**, 2345–2348, https://doi.org/DOI 10.1126/science.1064618.

Wanner, H., and Coauthors, 2008: Mid- to Late Holocene climate change: an overview. *Quat. Sci. Rev.*, **27**, 1791–1828, https://doi.org/10.1016/j.quascirev.2008.06.013.

Warken, S. F., D. Scholz, C. Spotl, K. P. Jochum, J. M. Pajon, A. Bahr, and A. Mangini, 2019: Caribbean hydroclimate and vegetation history across the last glacial period. *Quat. Sci. Rev.*, **218**, 75–90, https://doi.org/10.1016/j.quascirev.2019.06.019.

Watson, B. I., J. W. Williams, J. M. Russell, S. T. Jackson, L. Shane, and T. V. Lowell, 2018: Temperature variations in the southern Great Lakes during the last deglaciation: Comparison between pollen and GDGT proxies. *Quat. Sci. Rev.*, **182**, 78–92, https://doi.org/10.1016/j.quascirev.2017.12.011.

Watts, W. A., 1975: A late Quaternary record of vegetation from Lake Annie, south-central Florida. *Geology*, **3**, 344–346.

Watts, W. A., 1980a: The late Quaternary vegetation history of the southeastern United States. *Annu. Rev. Ecol. Syst.*, **11**, 387–409, https://doi.org/10.1146/annurev.es.11.110180.002131.

——, 1980b: Late-Quaternary vegetation history at White Pond on the inner coastal-plain of South Carolina. *Quat. Res.*, **13**, 187–199, https://doi.org/Doi 10.1016/0033-5894(80)90028-9.

Webb, T., 1986: Is vegetation in equilibrium with climate? How to interpret late-Quaternary pollen data. *Plant Ecol.*, **67**, 75–91.

——, B. Shuman, and J. W. Williams, 2003: Climatically forced vegetation dynamics in eastern North America during the late Quaternary Period. *Dev. Quat. Sci.*, **1**, 459–478.

Weigelt, P., M. J. Steinbauer, J. S. Cabral, and H. Kreft, 2016: Late Quaternary climate change shapes island biodiversity. *Nature*, **532**, 99–102, https://doi.org/10.1038/nature17443.

Weijers, J. W. H., S. Schouten, J. C. van den Donker, E. C. Hopmans, and J. S. Sinninghe Damsté, 2007: Environmental controls on bacterial tetraether membrane lipid distribution in soils. *Geochim. Cosmochim. Acta*, **71**, 703–713, http://dx.doi.org/10.1016/j.gca.2006.10.003.

Werneck, F. P., G. C. Costa, G. R. Colli, D. E. Prado, and J. W. Sites Jr, 2011: Revisiting the historical distribution of Seasonally Dry Tropical Forests: new insights based on palaeodistribution modelling and palynological evidencegeb. *Glob. Ecol. Biogeogr.*, **20**, 272–288, https://doi.org/10.1111/j.1466-8238.2010.00596.x.

——, C. Nogueira, G. R. Colli, J. W. Sites Jr, and G. C. Costa, 2012: Climatic stability in the Brazilian Cerrado: implications for biogeographical connections of South American savannas, species richness and conservation in a biodiversity hotspot. *J. Biogeogr.*, **39**, 1695–1706, https://doi.org/10.1111/j.1365-2699.2012.02715.x.

Whitmore, J., and Coauthors, 2005: Modern pollen data from North America and Greenland for multi-scale paleoenvironmental applications. *Quat. Sci. Rev.*, **24**, 1828–1848, https://doi.org/10.1016/j.quascirev.2005.03.005.

Whittaker, T. E., C. H. Hendy, and J. C. Hellstrom, 2011: Abrupt millennial-scale changes in intensity of Southern Hemisphere westerly winds during marine isotope stages 2–4. *Geology*, **39**, 455–458, https://doi.org/10.1130/G31827.1.

Williams, J. W., 2006: *An atlas of pollen-vegetation-climate relationships for the United States and Canada*. American Association of Stratigraphic Palynologists Foundation,.

Williams, J. W., and B. Shuman, 2008: Obtaining accurate and precise environmental reconstructions from the modern analog technique and North American surface pollen dataset. *Quat. Sci. Rev.*, **27**, 669–687.

Williams, J. W., and K. D. Burke, 2019: Past abrupt changes in climate and terrestrial ecosystems. *Climate Change and Biodiversity: Transforming the Biosphere*, Lovejoy T and Hannah L, Eds., Yale University Press, 128–141.

——, B. N. Shuman, and T. Webb, 2001: Dissimilarity analyses of late-Quaternary vegetation and climate in eastern North America. *Ecology*, **82**, 3346–3362.

Williams, J. W., D. M. Post, L. C. Cwynar, A. F. Lotter, and A. J. Levesque, 2002: Rapid and widespread vegetation responses to past climate change in the North Atlantic region. *Geology*, **30**, 971–974, https://doi.org/10.1130/0091-7613(2002)030<0971:rawvrt>2.0.co;2.

Williams, J. W., and Coauthors, 2018: The Neotoma Paleoecology Database, a multiproxy, international, community-curated data resource. *Quat. Res.*, **89**, 156–177, https://doi.org/10.1017/qua.2017.105.

——, A. Ordonez, and J.-C. Svenning, 2021: A unifying framework for studying and managing climate-driven rates of ecological change. *Nat. Ecol. Evol.*, **5**, 17–26, https://doi.org/10.1038/s41559-020-01344-5.

Willig, M. R., D. M. Kaufman, and R. D. Stevens, 2003: Latitudinal Gradients of Biodiversity: Pattern, Process, Scale, and Synthesis. *Annu. Rev. Ecol. Evol. Syst.*, **34**, 273–309, https://doi.org/10.1146/annurev.ecolsys.34.012103.144032.

Woodward, F. I., 1987: *Climate and Plant Distribution*. Cambridge University Press,.

Wunsch, C., 2006: Abrupt climate change: An alternative view. *Quat. Res.*, **65**, 191–203, https://doi.org/10.1016/j.yqres.2005.10.006.

Yin, Z. Y., 1994: Moisture conditions in the south-eastern USA and teleconnection patterns. *Int. J. Climatol.*, **14**, 947–967, https://doi.org/10.1002/joc.3370140902.

Yu, E.-F., R. Francois, and M. P. Bacon, 1996: Similar rates of modern and last-glacial ocean thermohaline circulation inferred from radiochemical data. *Nature*, **379**, 689–694, https://doi.org/10.1038/379689a0.

Yu, Z. C., J. H. McAndrews, and U. Eicher, 1997: Middle Holocene dry climate caused by change in atmospheric circulation patterns: Evidence from lake levels and stable isotopes. *Geology*, **25**, 251–254, https://doi.org/10.1130/0091-7613(1997)025<0251:Mhdccb>2.3.Co;2.

Zhang, Y., and Coauthors, 2017: Different precipitation patterns across tropical South America during Heinrich and Dansgaard-Oeschger stadials. *Quat. Sci. Rev.*, **177**, 1–9, https://doi.org/10.1016/j.quascirev.2017.10.012.

Ziegler, M., D. Nurnberg, C. Karas, R. Tiedemann, and L. J. Lourens, 2008: Persistent summer expansion of the Atlantic Warm Pool during glacial abrupt cold events. *Nat. Geosci.*, **1**, 601–605, https://doi.org/10.1038/ngeo277.

Supplementary Information for Chapter 2
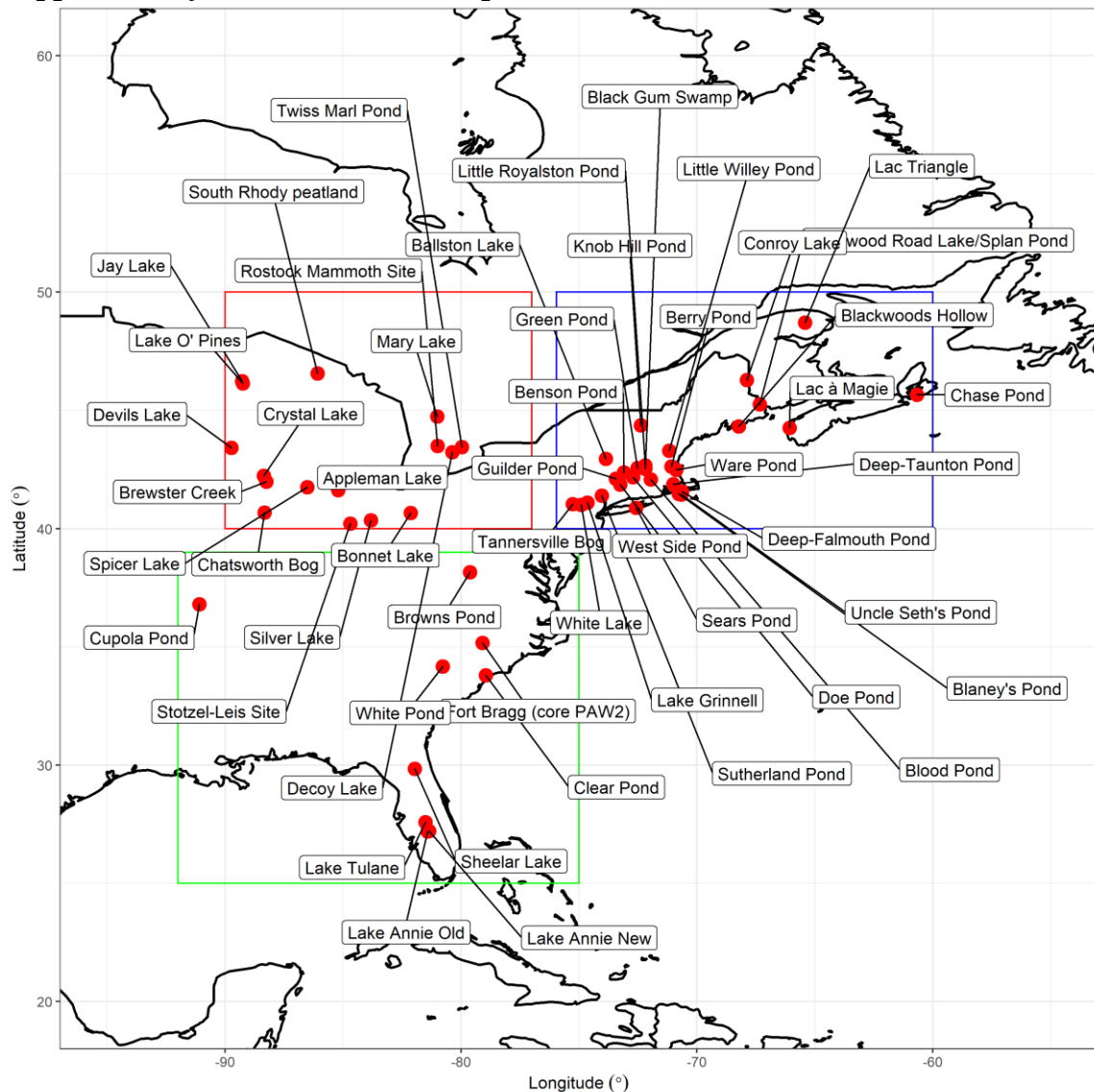
Figure S1.1

Site map of pollen sites and regions used for aggregating sites into the northeastern US, north-central US, and southeastern US.
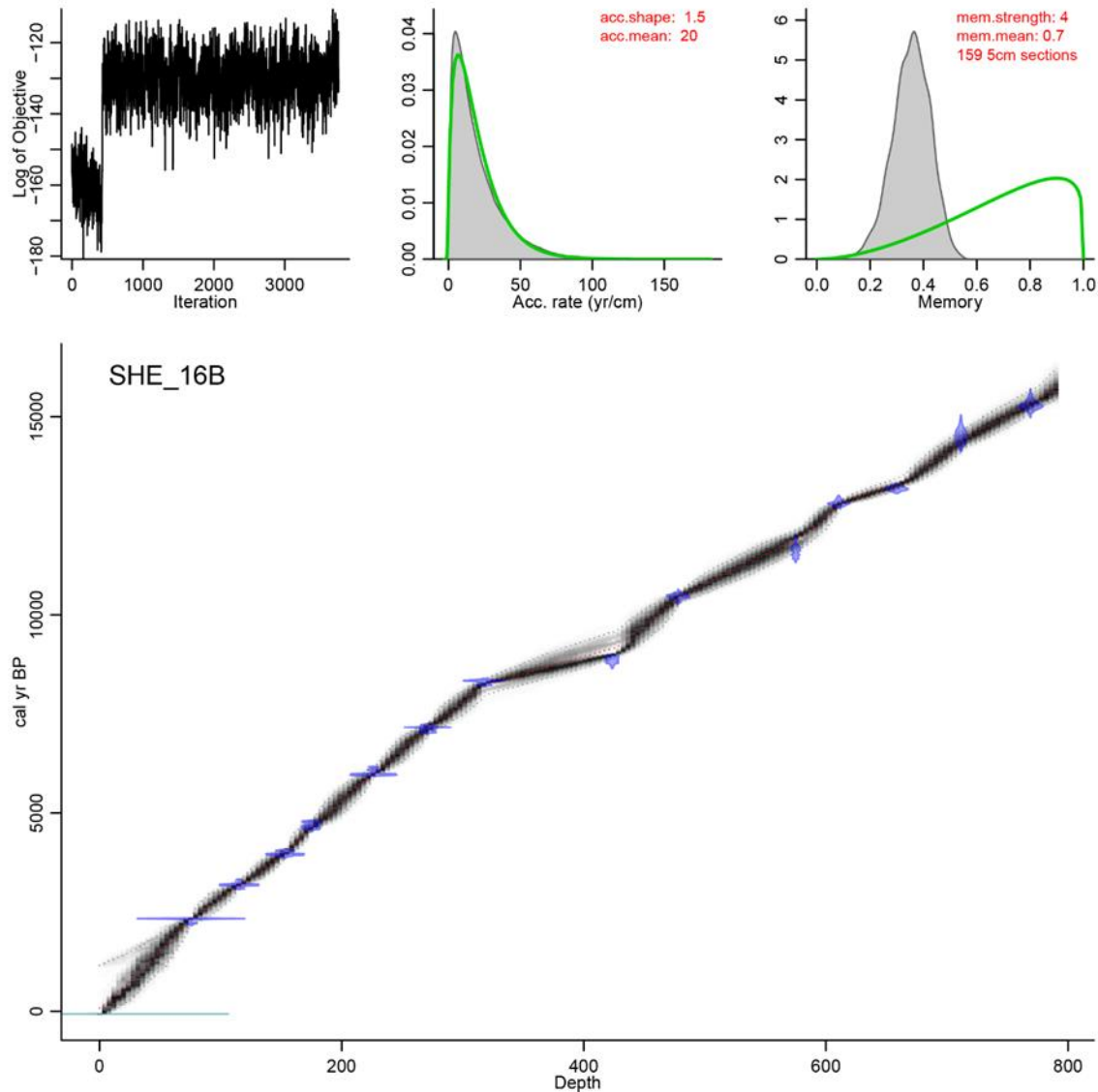
Figure S1.2

Bacon age-depth model for Sheelar Lake, FL core B using the Northern Hemispheric IntCal13

calibration curve (Reimer et al. 2013). The top-left plot represents Markov chain Monte Carlo

iterations and indicates model convergence because of stationarity after iteration 500. The upper-

middle and upper-right plots show prior and posterior distributions for model parameters in

green and gray, respectively. Model priors include sediment accumulation rate in yr/cm (upper-

middle) and sediment memory (autocorrelation) (upper-right). The red text in the upper-middle

and upper-right plots correspond to the parameter values. Model section size is indicated by the

"section" parameter. The bottom panel demonstrates the age-depth model, with the red-line indicating the model mean, and gray envelope as the 95% credible interval for modeled ages. Blue violin plots correspond to the density of calibrated ages from Table 3.
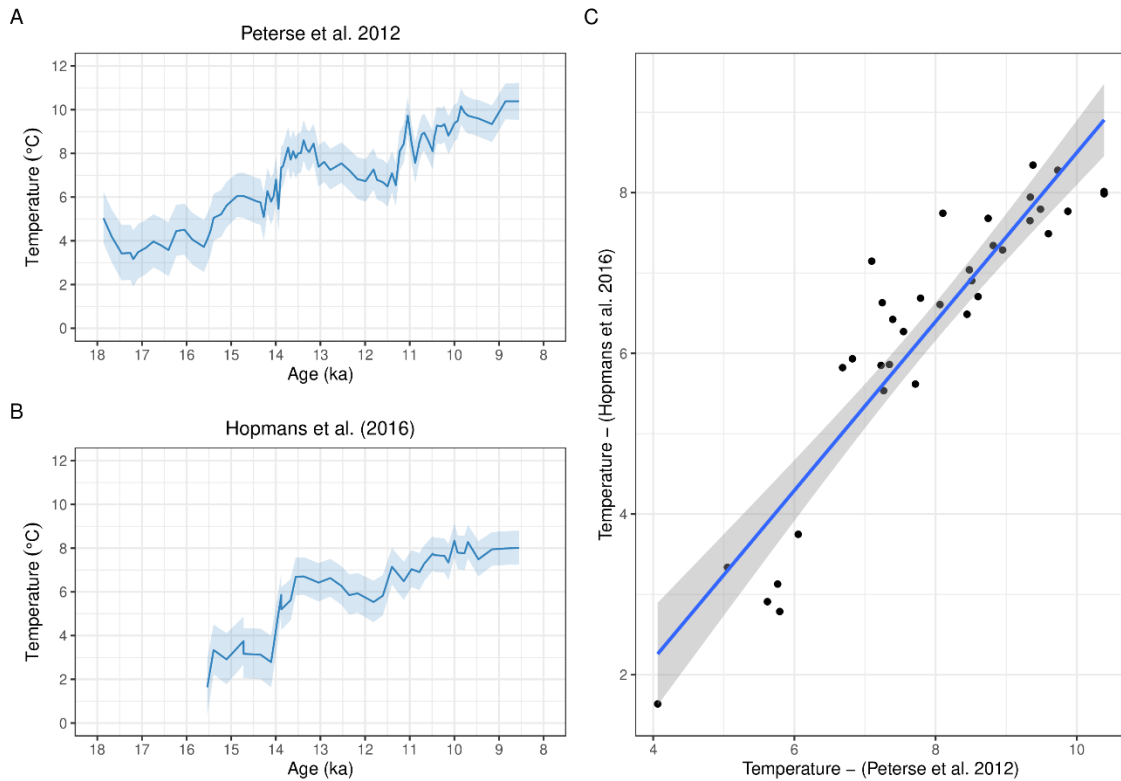
Figure S1.3

a) Silver Lake, OH brGDGT records calibrated using the Peterse et al., (2012) calibration on samples analyzed using earlier liquid chromatography-mass spectrometry methods that do not split 5- and 6- methyl brGDGT isomers. b) brGDGT temperature reconstructions for 37 reanalyzed samples from Silver Lake, Ohio using liquid chromatography-mass spectrometry methods that split 5- and 6- methyl brGDGT isomers and the MAT MBT′$_{5Me}$ calibration c) Ordinary least-squares regression of temperature reconstructions for the 37 samples analyzed using both analytical methods. $y = -2.01047 + 1.05085x$, $R^2 = 0.8541$, $p = 2.39 \times 10^{-15}$.
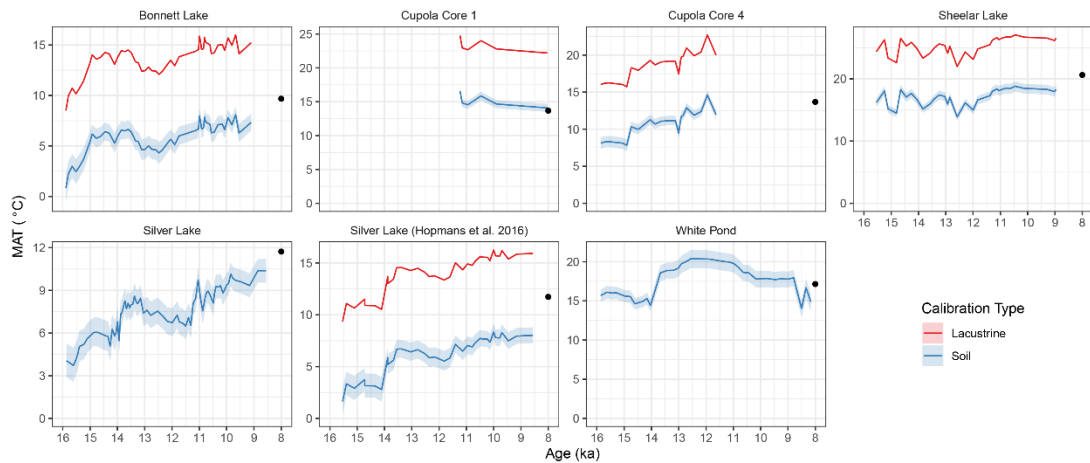
Figure S1.4

Alternative brGDGT temperature reconstructions using the lacustrine calibration from Russell et al., (2018) based on east African lakes, and soil calibrations. The MAT MBT′$_{5Me}$ (De Jonge et al. 2014) soil calibration was used at sites where analytical methods separated the 5- and 6- methyl brGDGT isomers - Bonnet Lake, Cupola Pond, Sheelar Lake, and Silver Lake (reanalyzed samples). The Peterse et al., (2012) soil calibration was used at White Pond and Silver Lake, where earlier analytical methods were used that did not separate 5- and 6- methyl brGDGT isomers. The black point at right corresponds to a 30-year average of mean annual temperature (1981-2010) at each site from PRISM, for comparison. Note, these are median ages, no uncertainty analysis has been performed in this sensitivity analysis. In addition, calibration uncertainty has not been included in the lacustrine temperature estimates but is reported in Russell et al., (2018) as 2.44 °C. The large offsets between early Holocene temperature reconstructions using the Russell et al., (2018) east African lakes calibration and late 20th-century temperatures (average: 6.92 °C), given that hemispheric to global-scale temperature variations during the Holocene were on the order of 1-2 °C (Kaufman et al. 2020b), is interpreted here as evidence of systematic bias in the Russell et al., (2018) calibrations when applied to these ENA lakes.
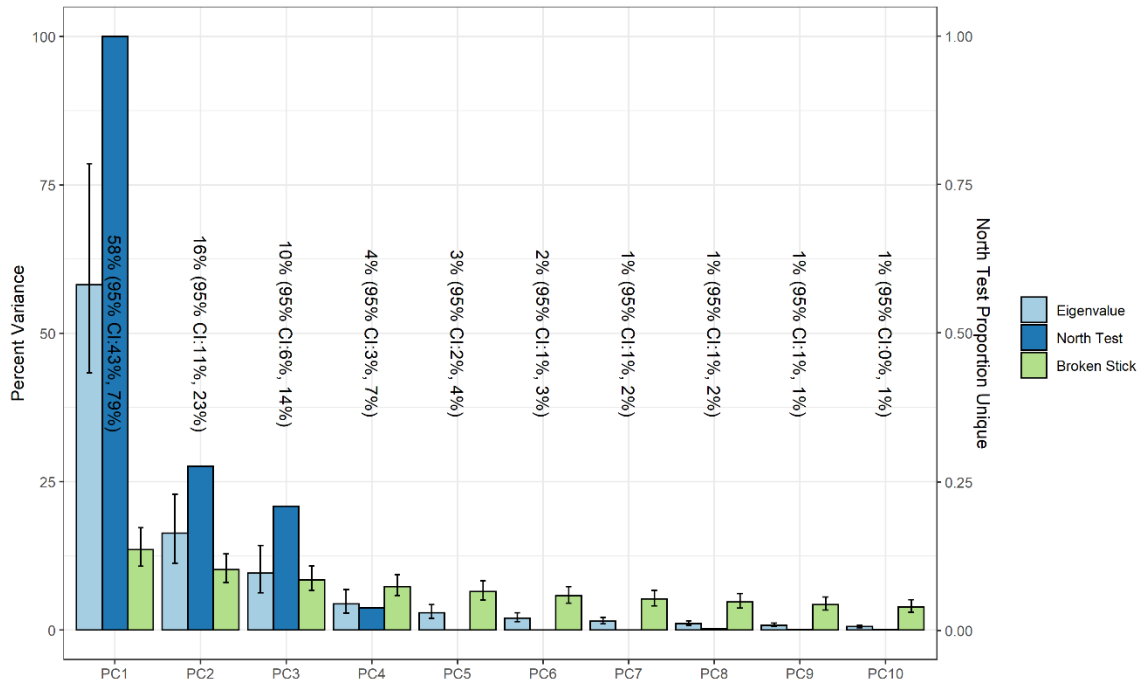
Figure S1.5

Percent variance explained for each principal component and significance testing using the broken-stick null model (Jackson 1993) and the "rule of thumb" from North et al., (1982). Light blue histograms indicate the percent variance explained by the principal component, while light green histograms indicate the percent variance explained of the principal components for a broken-stick null model (left x-axis). The dark blue histograms indicate the proportion of ensemble members where the principal component was unique as defined in North et al., (1982) (right y-axis). Text in the center of the figure corresponds to the proportion of the variance explained by each principal component with the corresponding 95% confidence interval.
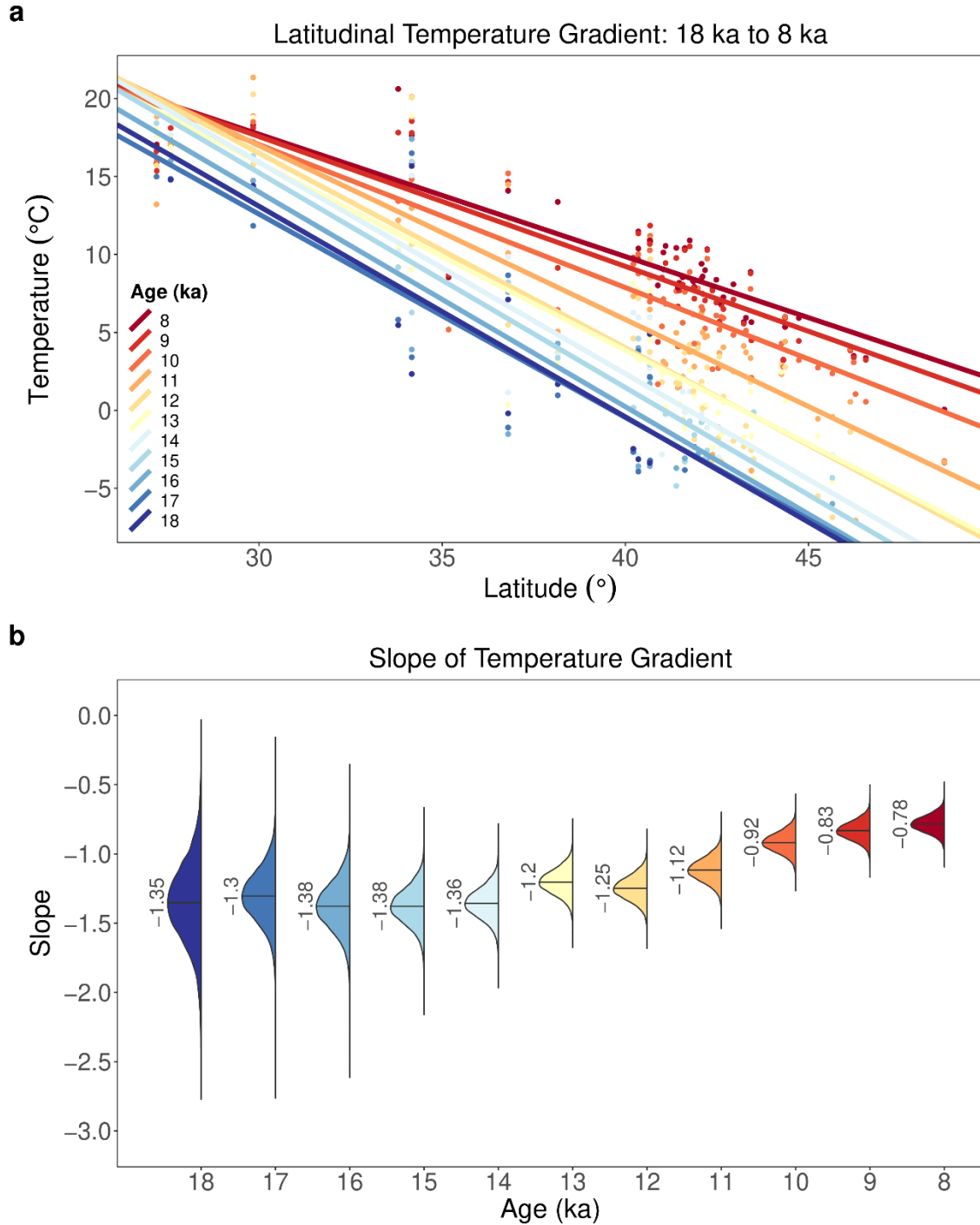
Figure S1.6

a) Bayesian linear regressions of pollen- and brGDGT-inferred mean annual temperatures against latitude, at 1000-year intervals. Sample-level temperature estimates were averaged into 1000-year bins. b) Distribution of the slope parameters for the Bayesian linear regressions.

Criterion (iii) of the site selection (Chapter 1 Methods 2.1) was applied to all analyses of YD

temperature anomalies and their spatial fingerprint (e.g. Fig. 1-1M, 1-2), but was relaxed for the

analysis of temperature latitudinal gradients to better characterize early Holocene gradients.
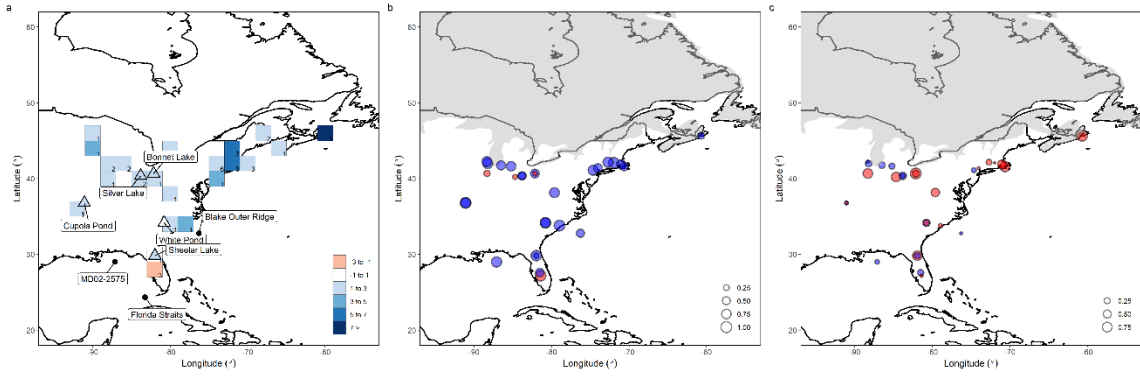
Figure S1.7

A) Temperature anomalies for temperatures reconstructed using the modern analog technique,

comparing 11.1 ka to 12.3 ka. B) PC1 and B) PC2 for pollen-inferred temperatures reconstructed

using the MAT and brGDGT-inferred temperatures for all sites in the study region with

continuous records from 15 ka to 11 ka. Red indicates a negative loading and blue indicates a

positive loading. Figure design follows Figure 1.
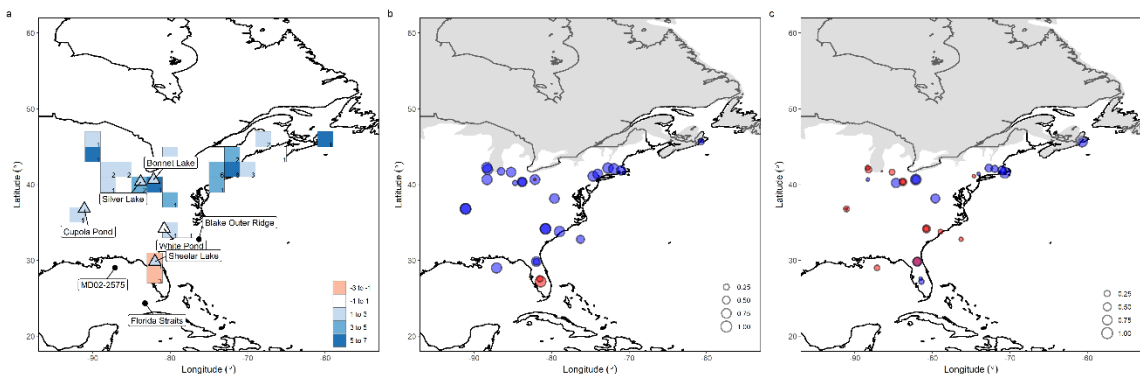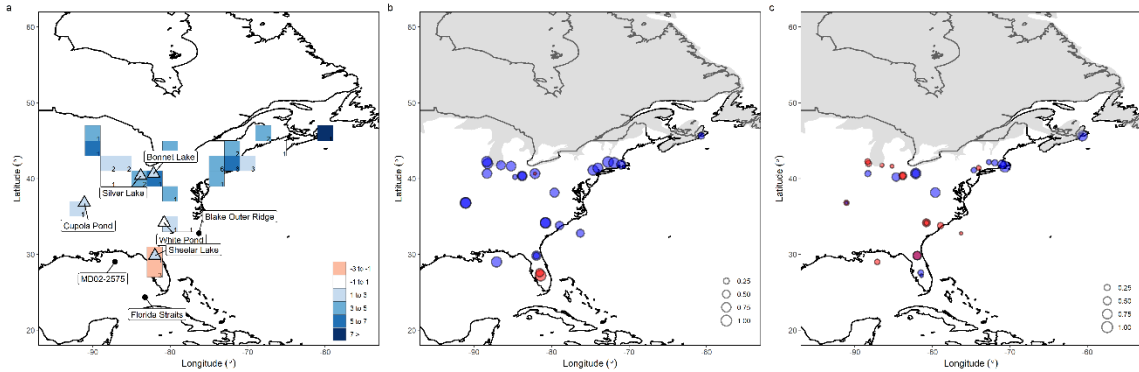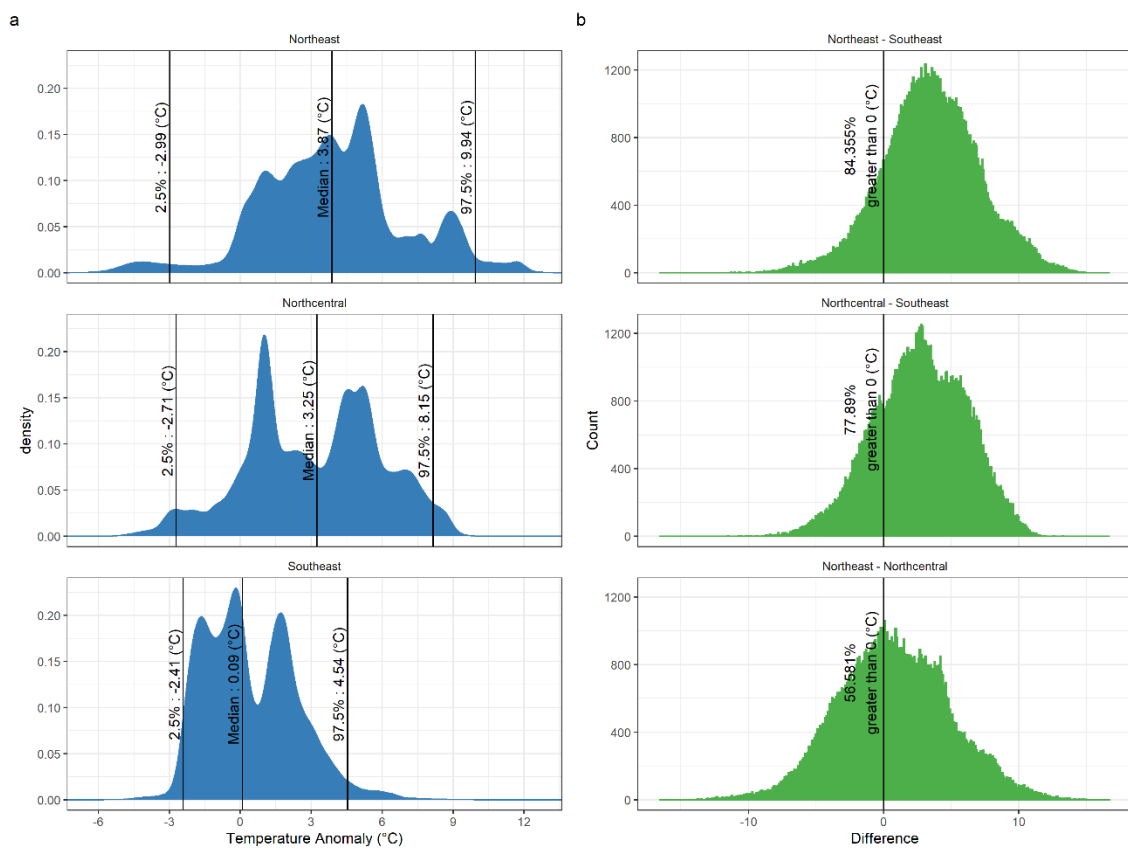
Figure S1.8

As Figure S1.7, for weighted averaging.

Figure S1.9

As Figure S1.7, for weighted averaging-partial least squares.

Figure S1.10

Effect of temporal uncertainty on regional estimates of early-Holocene – YD temperature

anomalies (for the north-central, northeastern, and southeastern US), where temporal uncertainty

was assessed by quantifying the effect of varying age estimates of fossil pollen samples on

interpolated temperatures. Each age model produced an ensemble of posterior age estimates for

each pollen sample at all sites. Each age model ensemble member for a site was then used to interpolate fossil pollen inferred temperatures into 100-year intervals, generating an ensemble of interpolated fossil pollen temperature estimates at each site. This ensemble of interpolated fossil pollen temperature estimates was then used to generate an ensemble of early-Holocene – YD temperature anomalies for each site. a) Density of early-Holocene – YD temperature anomalies for all sites within a region. Positive anomalies indicate warming with the start of Holocene, and a cold YD. Negative anomalies indicate cooling into the Holocene, and a warm YD. Black lines correspond to the 2.5%, 50%, and 97.5% quantiles temperature anomalies, respectively. For the northeast, early Holocene temperatures were on average 3.87 °C warmer (95% CI: -2.99 – 9.94 °C) than YD temperatures. For the north-central region, the Early Holocene – YD difference is 3.25 °C (95% CI: -2.71- 8.15 °C). For the southeast, the Early Holocene – YD difference is 0.09 °C (95% CI: -2.41 – 4.54 °C). b) Frequency of differences of early-Holocene – YD temperature anomalies from (a) between the regions, where a greater proportion of differences greater than 0 °C indicate that two regions are climatically distinct during the YD. 84.355 % of the EH – YD temperature changes among ensemble members were larger in the northeast than in the southeast; 77.89% of the temperature changes were larger in the north-central than in the southeast; and 56.581% were larger in the northeast than north-central region.

Site Name	Neotoma Site ID	Neotoma Dataset ID	Latitude	Longitude	# Dates	# Samples	Normal†	Bulk Sediment*
Lake Annie (new)	1597	unpublished	27.207 31	-81.350875	17	79	1	No
Appleman Lake	10003	14957	41.623 285	-85.212085	14	73	0	No
Ballston Lake	10424	15909	42.949 75	-73.85325	7	59	0	No

Benson Pond	23579	40791	42.377775	-73.09478	11	57	1	No
Berry Pond	23580	40793	42.62006	-71.086805	9	160	1	Yes
Black Gum Swamp	10172	15327	42.5375	-72.1829	3	15	0	No
Blaney's Pond	23582	40797	41.471805	-70.766135	11	71	0	Yes
Blackwoods Hollow	9889	14674	44.313195	-68.22364	9	51	0	No
Blood Pond	23583	40799	42.08019	-71.96105	13	143	1	Yes
Bonnett Lake	26222	45816, 48743 (brGDGT)	40.66737	-82.13957	19	75	0	No
Brewster Creek	9588	14104	41.98044	-88.24441	20	97	0	No
Browns Pond	309	316	38.154722	-79.616389	11	51	1	Yes
Chase Pond	353	361	45.651389	-60.675	7	39	1	No
Chatsworth Bog	364	375	40.675865	-88.324435	8	64	1	Yes
Clear Pond	480	492	33.798895	-78.95336	14	181	0	Yes
Conroy Lake	491	14768	46.283333	-67.883333	5	33	1	No
Crystal Lake	10413	15886	42.234015	-88.357005	38	135	0	No
Cupola Pond	525	47557, 47555, 48745 (brGDGT, Core 1), 48746 (brGDGT Core 4)	36.799197	-91.090036	17	96	0	No
Decoy Lake	656	672	43.233333	-80.366667	7	95	0	No
Deep-Falmouth Pond	23586	40803	41.564035	-70.63573	14	146	1	Yes
Deep-Taunton Pond	23609	40844	41.88215	-71.012	17	46	0	Yes
Devils Lake	666	684	43.4178	-89.73205	13	122	0	Yes
Doe Pond	23614	40854	42.17535	-72.7018	10	91	0	Yes
Green Pond	10433	40861	42.56705	-72.5108	6	22	0	Yes

Lake Grinnell	13583	20515	41.098185	-74.63963	8	89	0	No
Guilder Pond	23625	40875	42.10864	-73.4372	9	55	0	Yes
Jay Lake	10430	15922	46.23435	-89.28155	8	33	0	No
Knob Hill Pond	23647	40914	44.36035	-72.37295	12	138	0	Yes
Lac à Magie	1534	1572	44.263889	-66.079167	4	43	0	No
Lake Annie	1597	1648	27.2	-81.416667	8	73	1	Yes
Mary Lake	13362	19967	44.735655	-81.00256	5	112	1	No
Lake O' Pines	10431	15925	46.140435	-89.2553	7	35	0	No
Fort Bragg (core PAW2)	10103	15191	35.173545	-79.089805	6	21	0	No
Rostock Mammoth Site	2215	2293	43.5	-81	2	32	0	No
Little Royalston Pond	23691	40988	42.67595	-72.19285	7	88	1	Yes
Sears Pond	23698	41001	40.886	-72.5783	10	33	0	Yes
Sheelar Lake	24684	Pollen unpublished, 48748 (brGDGT)	29.839209	-81.958343	23	94	0	No
Silver Lake	2303	17717, 41040 (brGDGT), 48744 (brGDGT, reanalyzed samples)	40.354335	-83.812515	14	83	0	No
Spicer Lake	13350	19937	41.75738	-86.52208	17	145	0	No
Basswood Road Lake/Splan Pond	2959	3775	45.255556	-67.330556	5	38	0	No
South Rhody peatland	13528	20397	46.565795	-86.0752	11	98	0	No
Stotzel-Leis Site	2520	40168	40.216667	-84.689444	8	110	0	No
Sutherland Pond	2527	2617	41.391389	-74.037778	12	183	0	Yes

Tannersville Bog	2536	15866	41.038875	-75.263845	13	67	0	Yes
Lac Triangle	13899	21319	48.710435	-65.41279	9	24	0	No
Lake Tulane	2570	19620	27.58613	-81.503395	52	191	0	Yes
Twiss Marl Pond	10505	16127	43.44083	-79.95551	9	54	0	No
Uncle Seth's Pond	23709	41018	41.43305	-70.66464	7	60	1	Yes
Ware Pond	23713	41025	42.48245	-70.88225	9	59	0	Yes
West Side Pond	23714	41027	41.8545	-73.2566	11	48	1	Yes
White Pond	2839	40111, 48743 (brGDGT)	34.16759	-80.77616	16	92	0	No
Little Willey Pond	23693	40992	43.2917	-71.1781	6	73	0	Yes
White Lake	10415	15892	40.99967	-74.91347	7	44	0	No

Table S1.1

List of sites used in study. 'Normal'† indicates whether a normal distribution was used when generating an age depth model, instead of a Student's t-distribution. *'Bulk sediment' indicates whether any of the radiocarbon dates for a site are measured from bulk sediment. Bulk sediment dates are subject to hardwater effects and can be biased to too-old age estimates (Grimm et al. 2009).

Lab ID	Composite Core Depth (cm)	^{14}C age and 1-σ error	δ^{13}C (‰)	Calibrated median age	95% Calibrated credible interval age range	Dated Material
UCIAMS-202592	75 - 76	2,295 ± 15		2,335	2,221 - 2,346	terrestrial macrofossil (plant/wood)
UCIAMS-182469	115 - 115.5	3,000 ± 15	-27.7	3,186	3,090 - 3,233	leaf

UCIAMS-182470	153.5 - 154	3,650 ± 15	-29.8	3,962	3,908 - 4,066	leaf
UCIAMS-182471	174.5 - 175	4,130 ± 15	-30	4,673	4,578 - 4,805	leaf
UCIAMS-182472	226 - 226.5	5,245 ± 15	-30.5	5,967	5,939 - 6,161	leaf
UCIAMS-202593	270 - 272	6,220 ± 15		7,158	7,027 - 7,232	terrestrial macrofossil (plant/wood)
UCIAMS-202594	317 - 318	7,490 ± 20		8,335	8,217 - 8,371	terrestrial macrofossil (plant/wood)
UCIAMS-202595	423 - 424	7,975 ± 20		8,872	8,729 - 8,981	terrestrial macrofossil (plant/wood)
UCIAMS-202596	477 - 479	9,280 ± 25		10,475	10,336 - 10,559	terrestrial macrofossil (plant/wood)
UCIAMS-202597	574 - 576	10,070 ± 35		11,628	11,408 - 11,899	terrestrial macrofossil (plant/wood)
UCIAMS-194934	610 - 611	10,980 ± 25		12,807	12,727 - 12,947	leaf fragments
UCIAMS-194933	658 - 659	11,340 ± 25		13,180	13,095 - 13,270	leaf fragments
UCIAMS-194932	711 - 712	12,420 ± 30		14,505	14,228 - 14,838	wood
UGAMS-24098	769	12,820 ± 40	-25.5	15,271	15,135 - 15,492	wood

Table S1.2
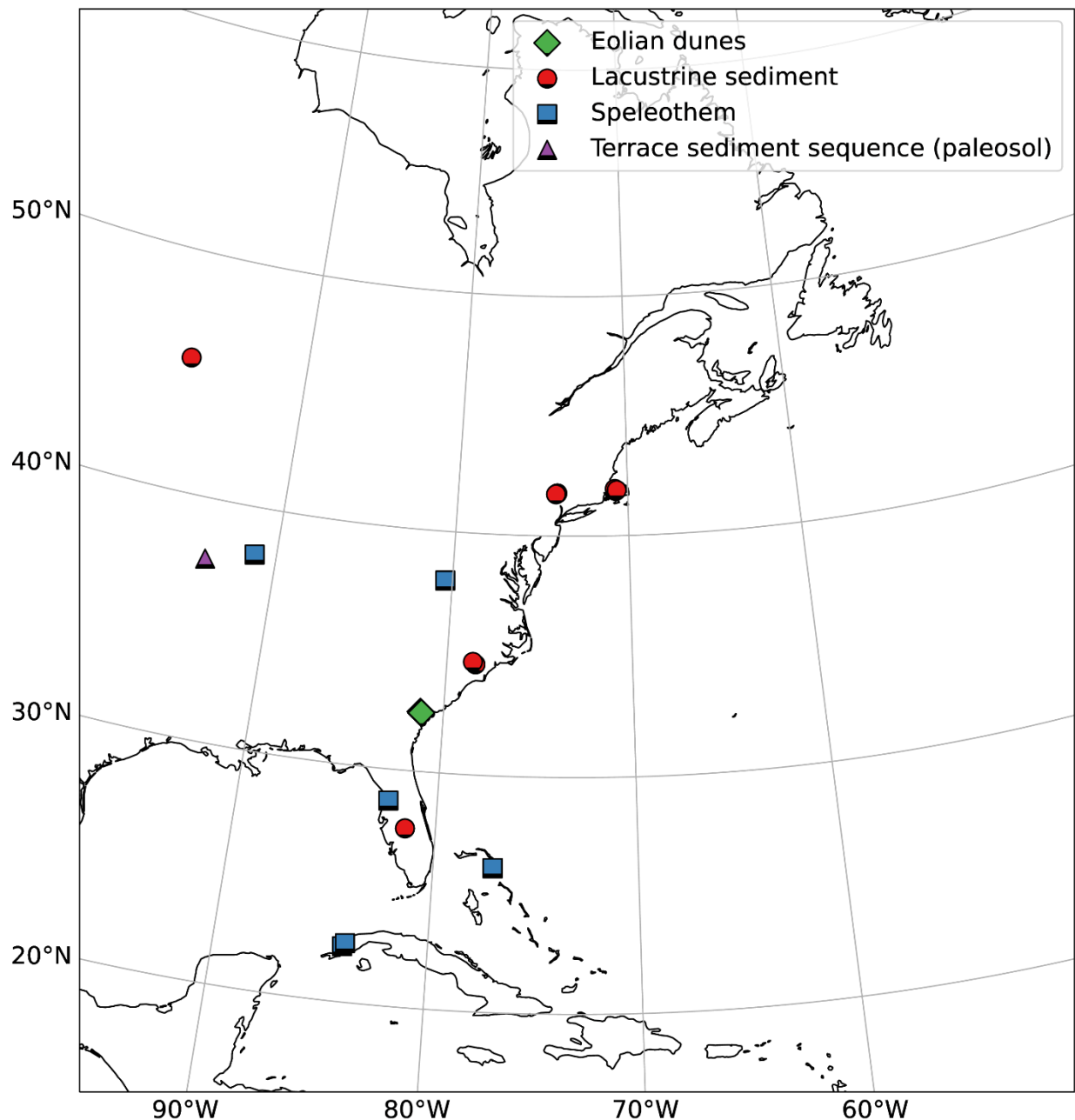
Organic materials used for radiocarbon dating for Sheelar Lake, FL core B calibrated using the

Northern Hemispheric IntCal13 calibration curve (Reimer et al. 2013). Materials were sent to the

University of Georgia Accelerator Mass Spectrometry Laboratory (UGAMS) and the W. M.

Keck Carbon Cycle Accelerator Mass Spectrometry Laboratory at the University of California,

Irvine (UCIAMS). All ages reported as years before radiocarbon present (1950AD). Organic

materials with smaller mass lack $\delta^{13}C$ measurements.
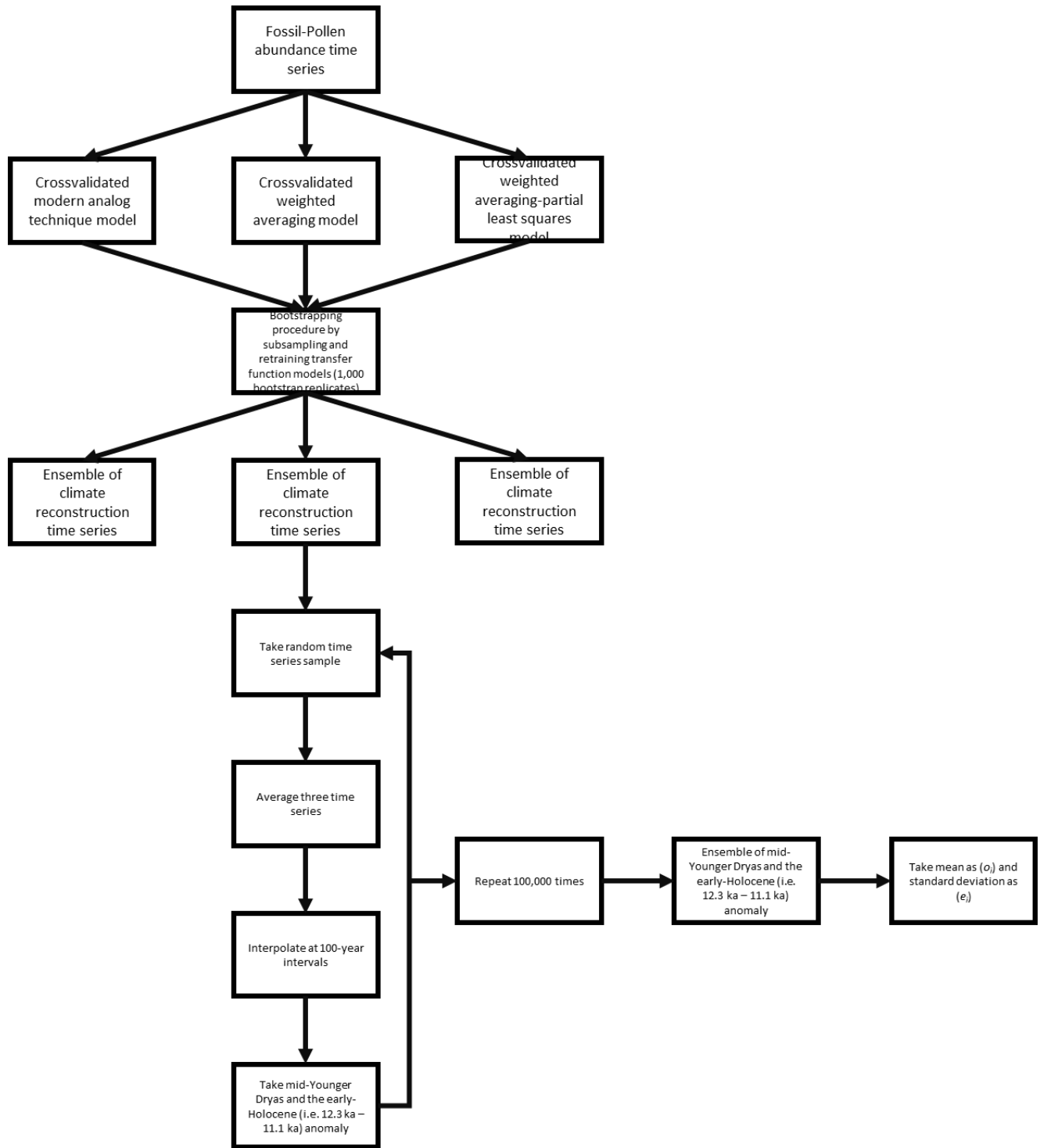
Site	Southern *Pinus* establishment	Reference
Sheelar Lake	Entire Record	Krause et al. (*in prep*)
Lake Annie (new)	Entire Record	Grimm et al. (*in prep*)
Lake Annie (old)	Entire Record	(Watts 1975)
Lake Tulane	Entire Record	(Grimm et al. 2006)
White Pond	11.7 ka	[*Krause et al.*, 2018; *Watts*, 1980a; b] (Krause et al. 2018; Watts 1980a,b)
Clear Pond	13 ka	(Hussey 1993)
Browns Pond	10 ka	(Kneller and Peteet 1993, 1999)
Cupola Pond	10 ka	(Jones et al. 2017)

Table S1.3

Summary of sites and where fossil *Pinus* pollen is assigned to southeastern species.

Supplementary Information for Chapter 3

Figure S2.1

Proxy records used for precipitation responses to an Atlantic meridional overturning circulation weakening used within the literature review. Maps use the Albers Equal Area conic projection (origin: 40°N, 73°W, standard parallels: 20°N, 50°N).

Figure S2.2

Bootstrap procedure used to propagate uncertainties in the ensemble of fossil-pollen

reconstructions to uncertainty estimates in temperature and precipitation anomalies.
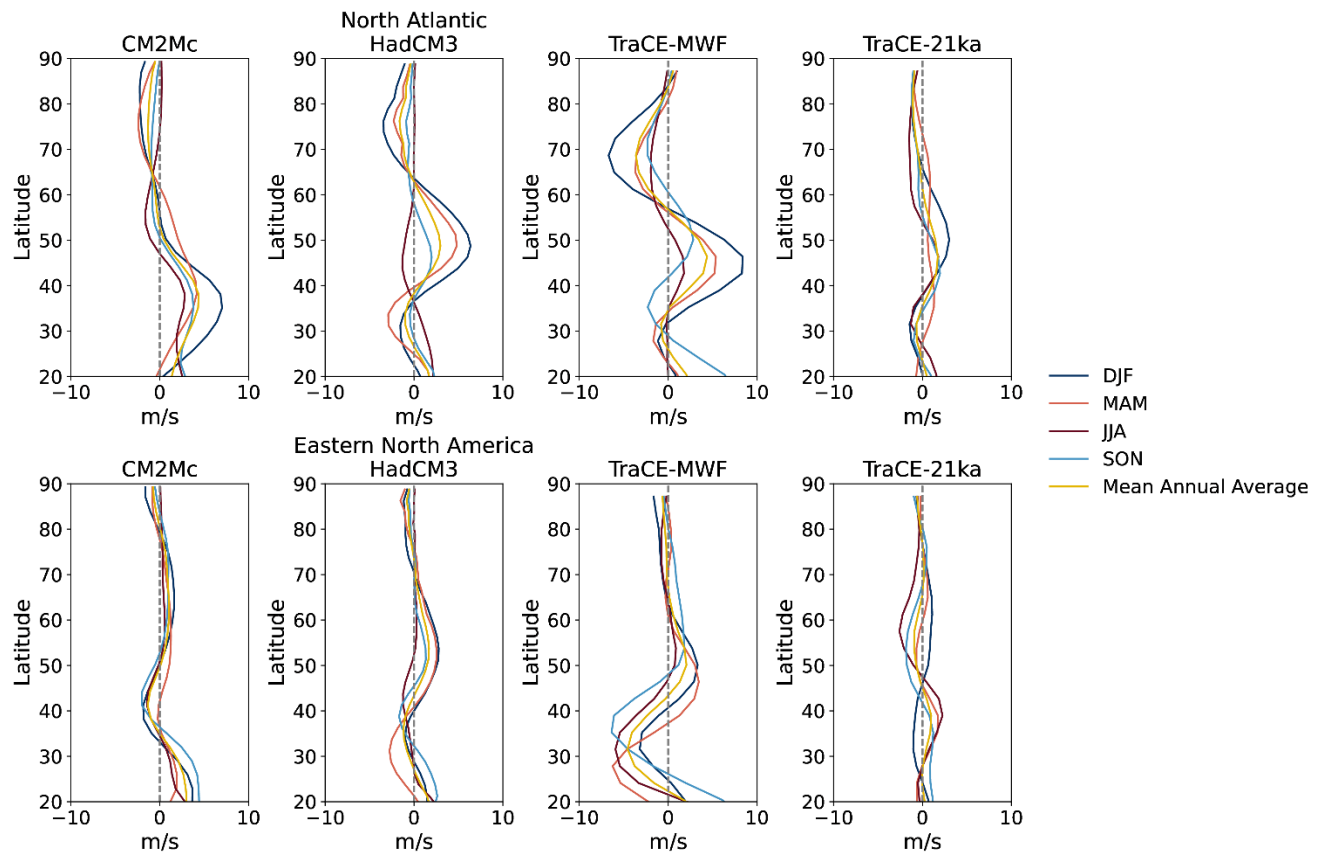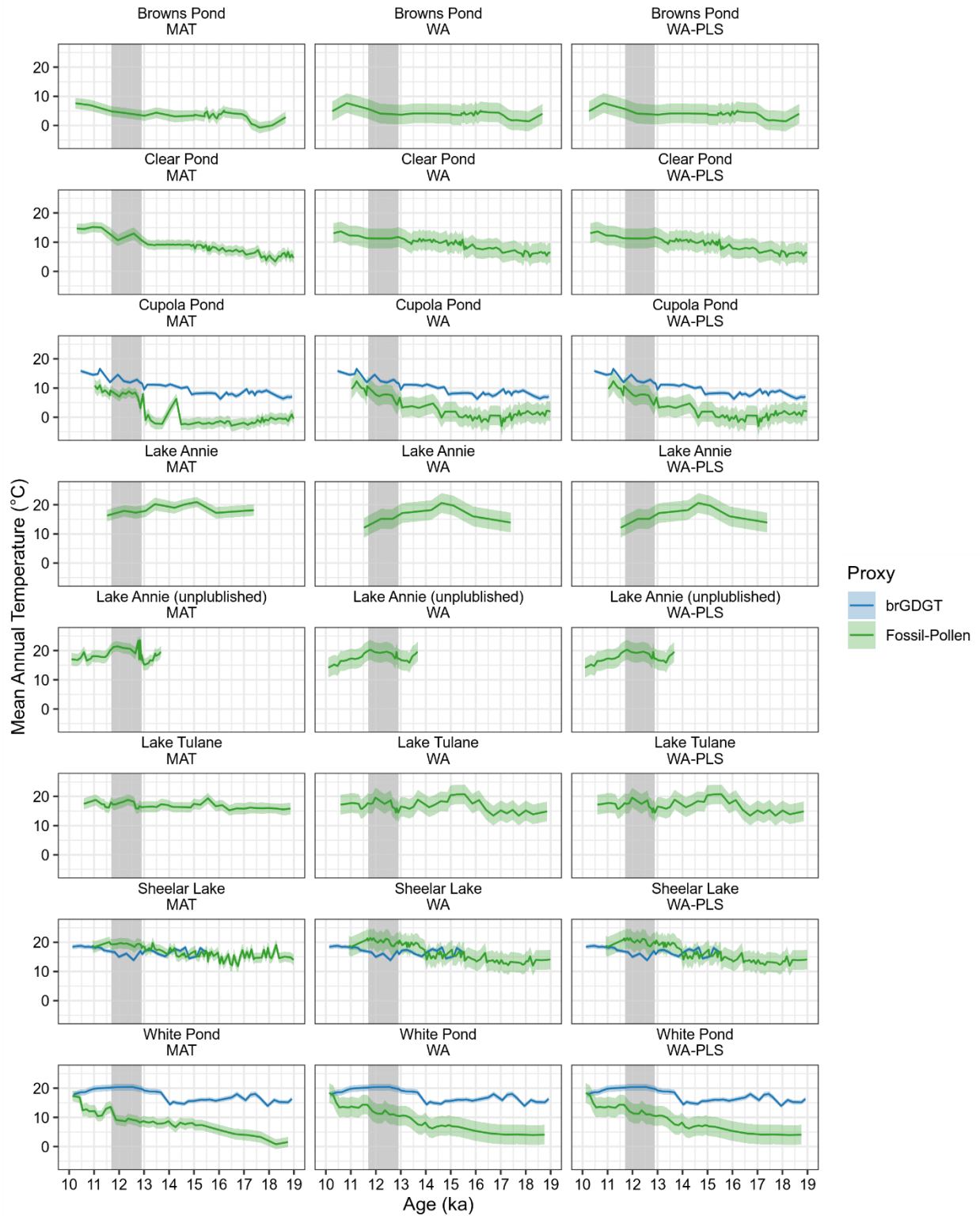
Figure S2.3

Mean seasonal upper-level wind (200 mb) response to freshwater hosing (anomalies: hosed - unhosed) zonally averaged over longitudal ranges representing the North Atlantic (70°W to 0°) and eastern North America (100°W to 70°W). Note the stronger intensification of westerly zonal winds in the North Atlantic compared to eastern North America, suggesting that jet enhancement over the North Atlantic is driving upper-level divergence anomalies in eastern North America.

Figure S2.4

Fossil-pollen (green) and branched glycerol dialkyl glycerol tetraether (brGDGT, blue) temperature reconstructions for all sites in the southeastern United States. Each column corresponds to a different transfer function methodology (MAT, WA, and WA-PLS; results are presented as the average of all three in the main text) while each row corresponds to a different site within the southeastern U.S. Only Cupola Pond, MO, Sheelar Lake, FL, and White Pond, MO have brGDGT records. The brGDGT records are identical across the three columns and are provided for comparison with the different fossil-pollen transfer functions. The Younger Dryas is highlighted in the gray box present in all plots. Note that all southeastern United States temperature reconstructions except for the brGDGT record from Sheelar Lake, FL demonstrate no Younger Dryas cooling with some records (Lake Tulane, FL and Lake Annie, FL) exhibiting warming with the onset of the Younger Dryas.
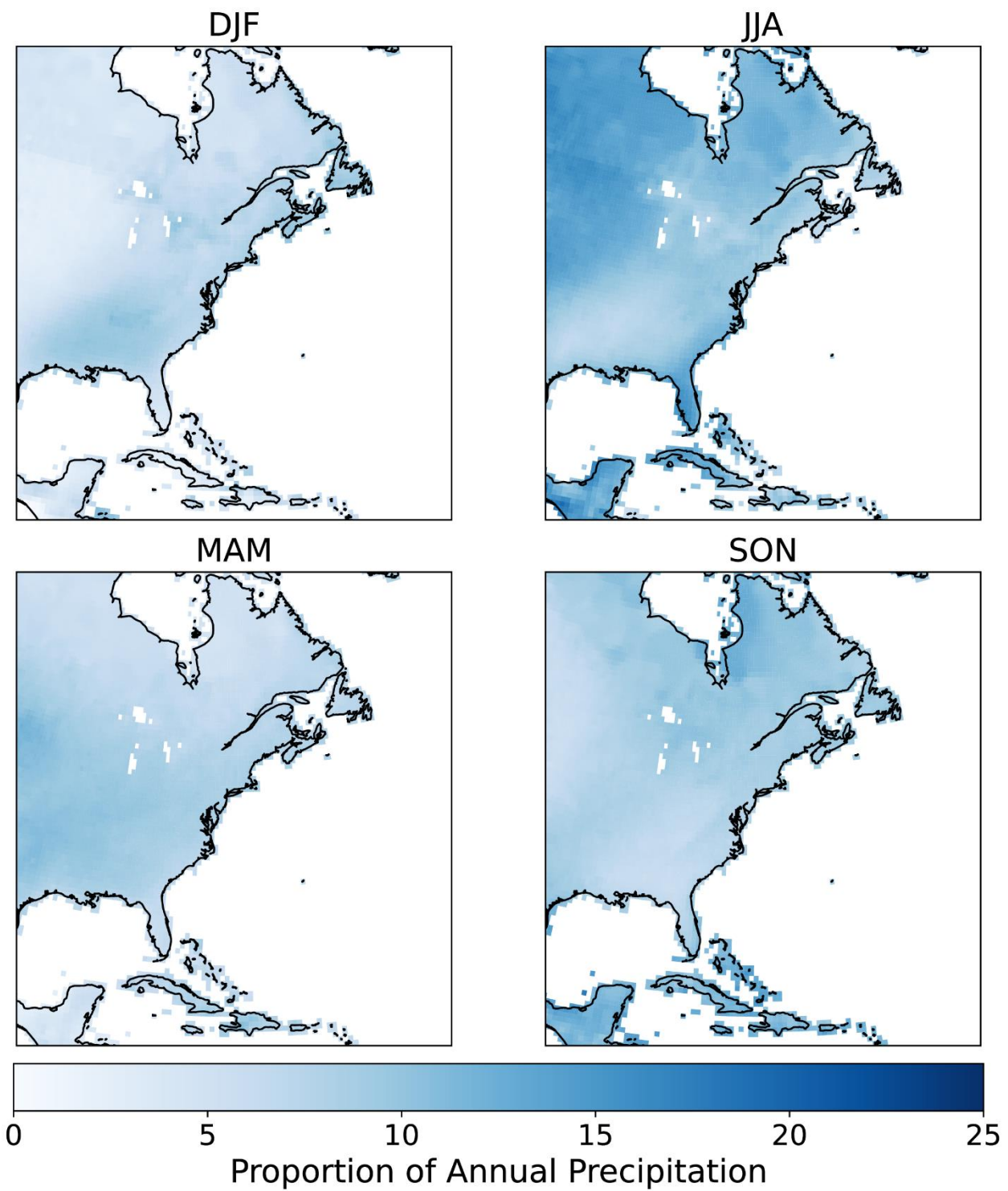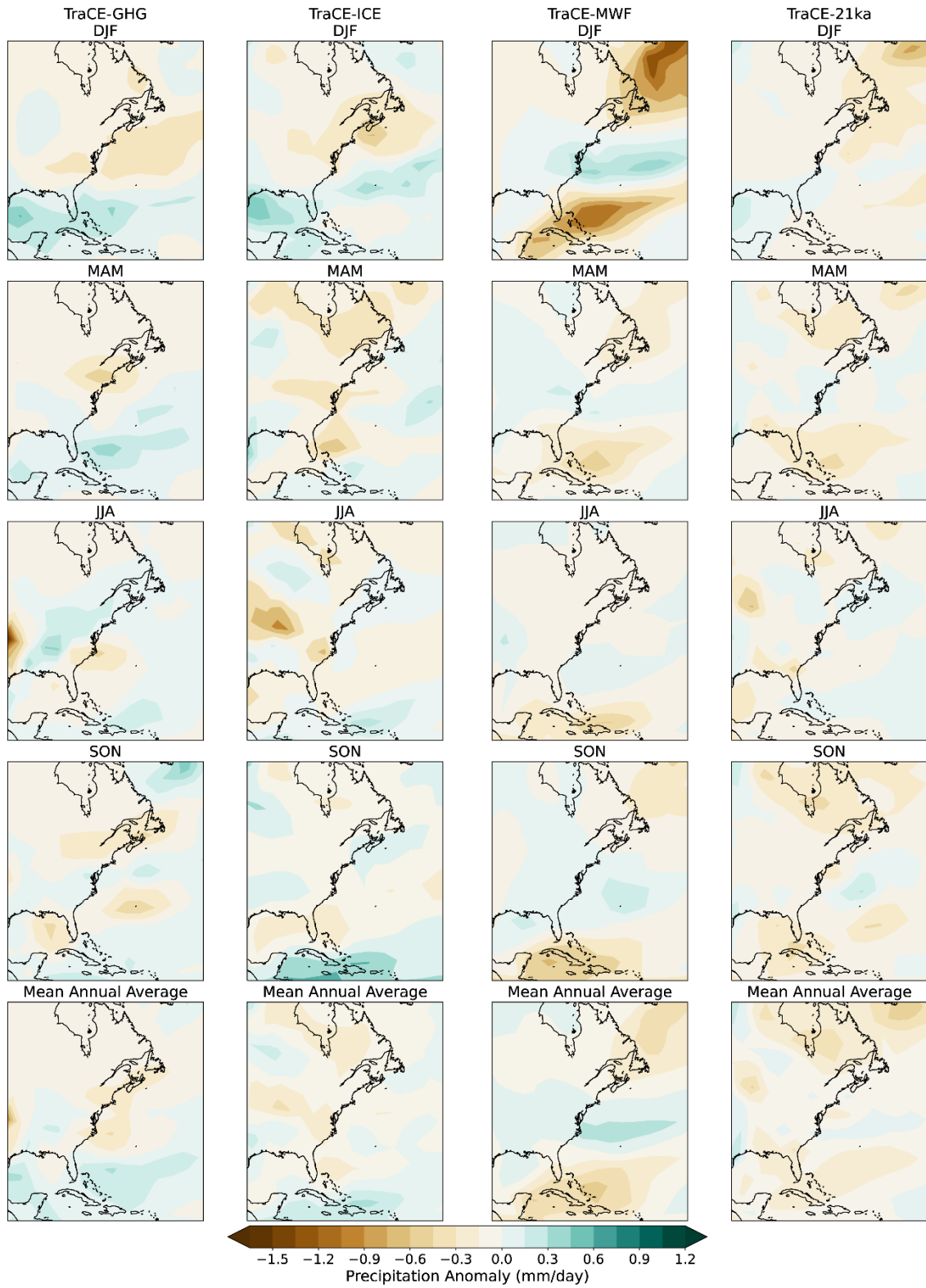
Figure S2.5

Modern proportion of total annual precipitation input for each season in eastern North America based on observational data from Schneider et al. (2011). Data is averaged over the period 1891 to 2016.

Figure S2.6

Mean seasonal precipitation response to freshwater hosing (hosed – unhosed; 12.3 ka – 11.1 ka)

and mean annual anomalies for the TraCE single experiments. Map projection follows Figure S1.
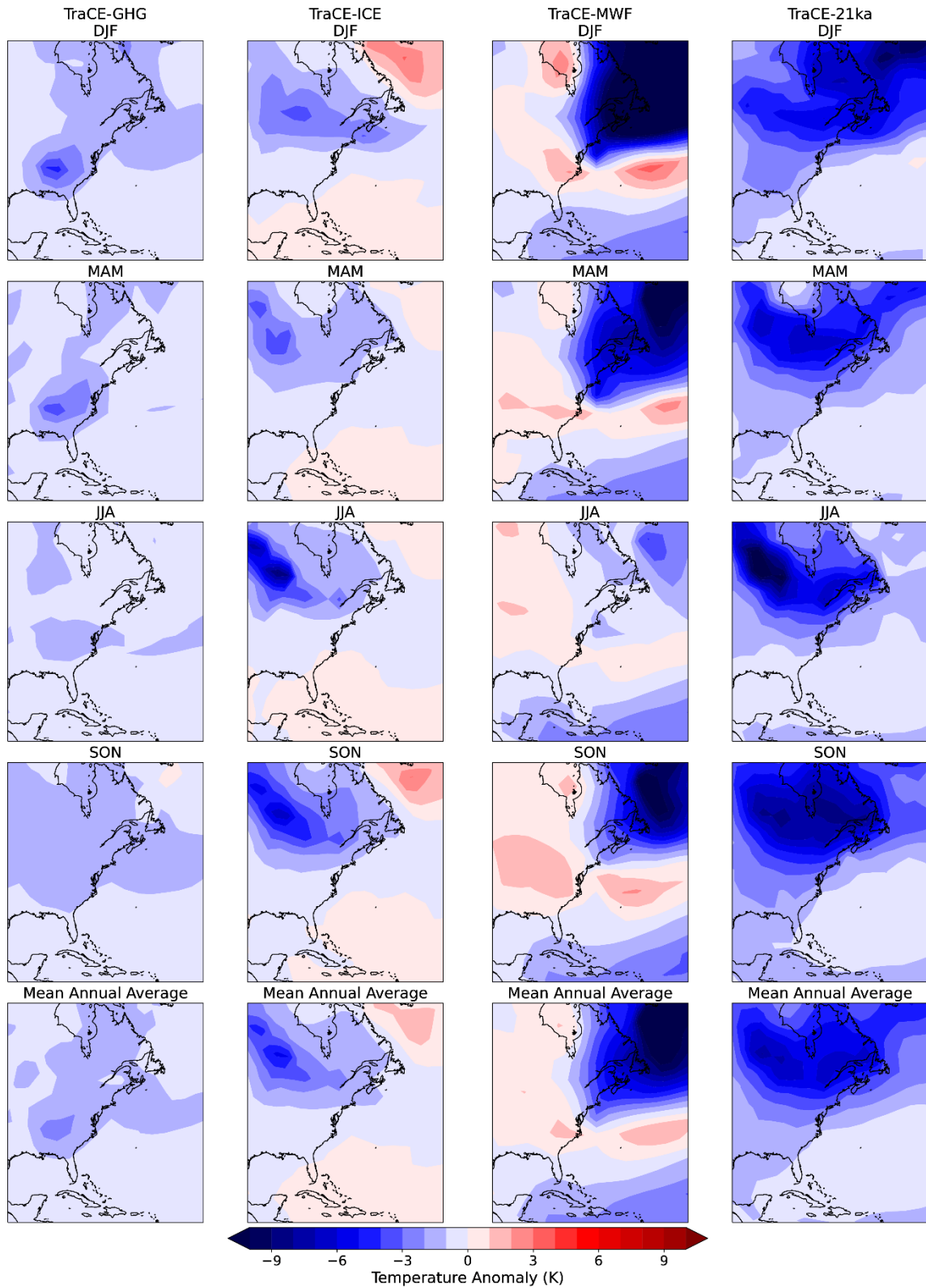
Figure S2.7

Mean seasonal surface air temperature response to freshwater hosing (hosed – unhosed; 12.3 ka – 11.1 ka) and mean annual anomalies for the TraCE single experiments. Map projection follows Figure S1.
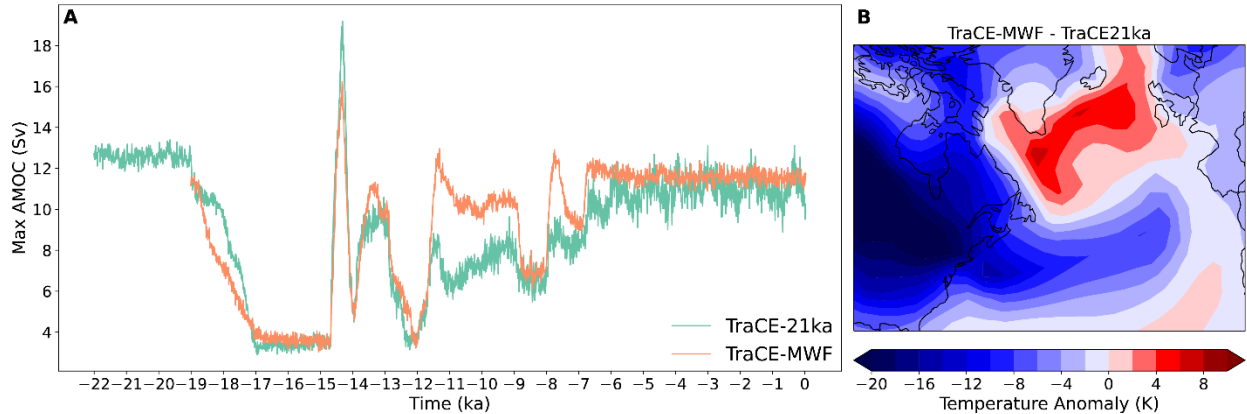
Figure S2.8

A) Maximum strength of the AMOC for TraCE-21ka and TraCE-MWF. Here, AMOC is defined as the streamfunction from 30 °S to 60 °N and below 500 m to ensure flow is non-divergent and surface Ekman transport is excluded. B) Surface temperature differences between TraCE-MWF and TraCE21ka for a 100 year mean centered on 11.1 ka demonstrating that greater AMOC in TraCE-MWF leads to warmer surface temperatures in the North Atlantic Ocean.

Supplementary Information for Chapter 4
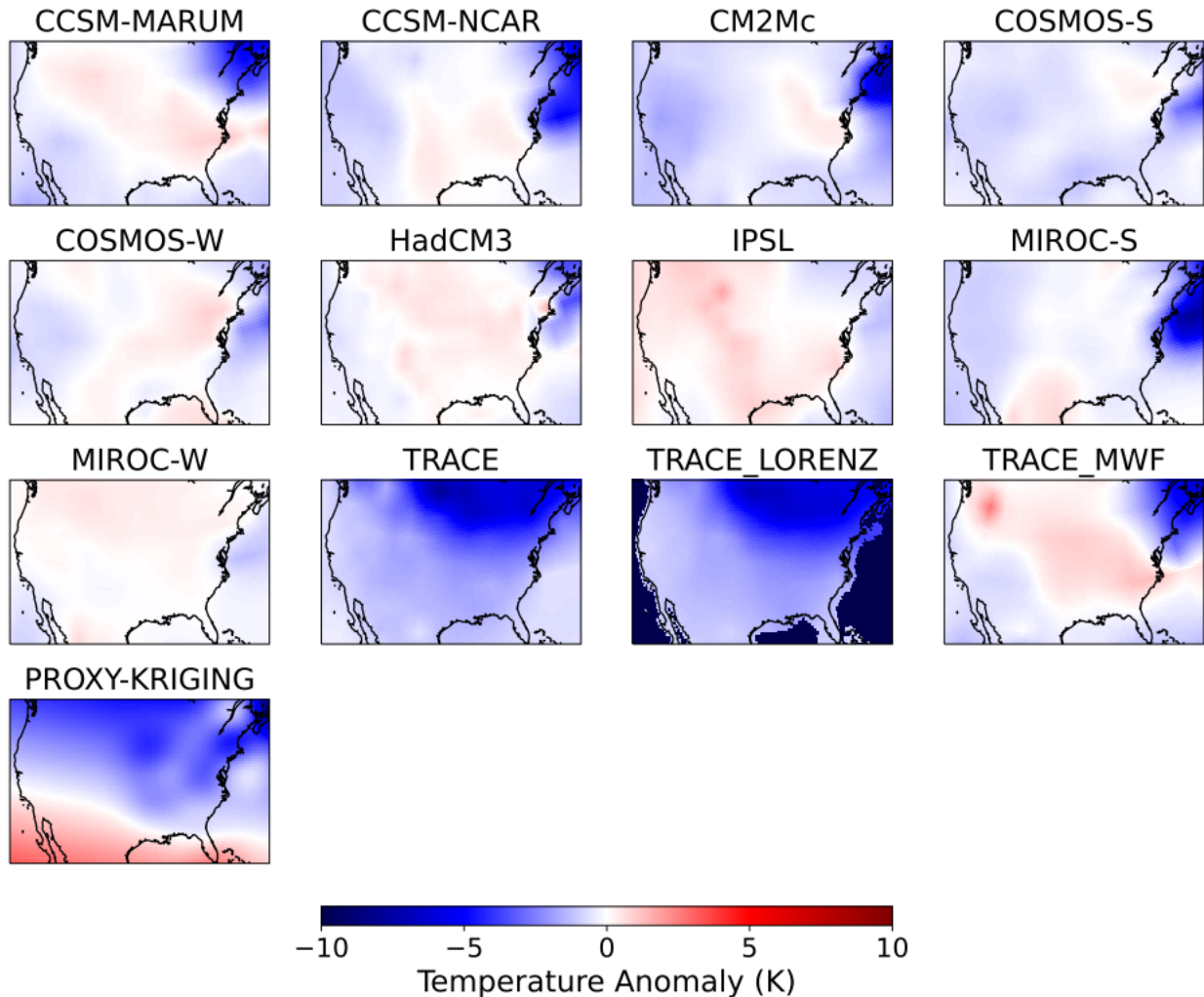
Figure S3.1

Simulated and reconstructed temperature anomalies (hosed-unhosed) from the 11 climate models analyzed and multiproxy reconstructions. TraCE-21ka and TraCE-Lorenz are based on the same set of simulations but the TraCE-Lorenz simulation is statistically downscaled to a 0.5° resolution. The point estimate proxy reconstructions were used to generate full fields of temperature anomalies by universal kriging. Kriging parameters were based on the empirical semivariogram of the NCEP Reanalysis (Kalnay et al. 1996) data product surface temperatures

and the Global Precipitation Climatology Centre precipitation estimates for precipitation

(Schneider et al. 2017).
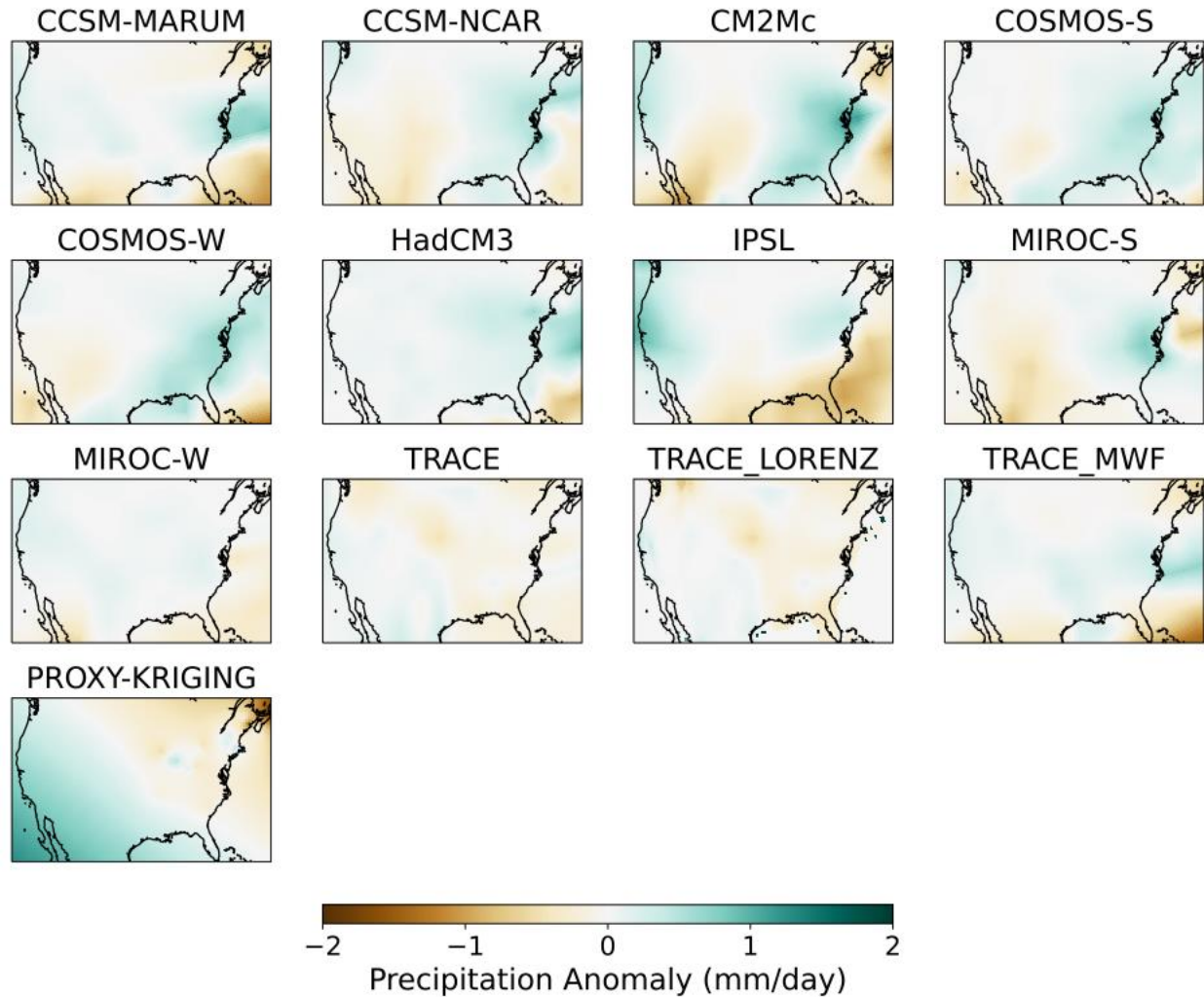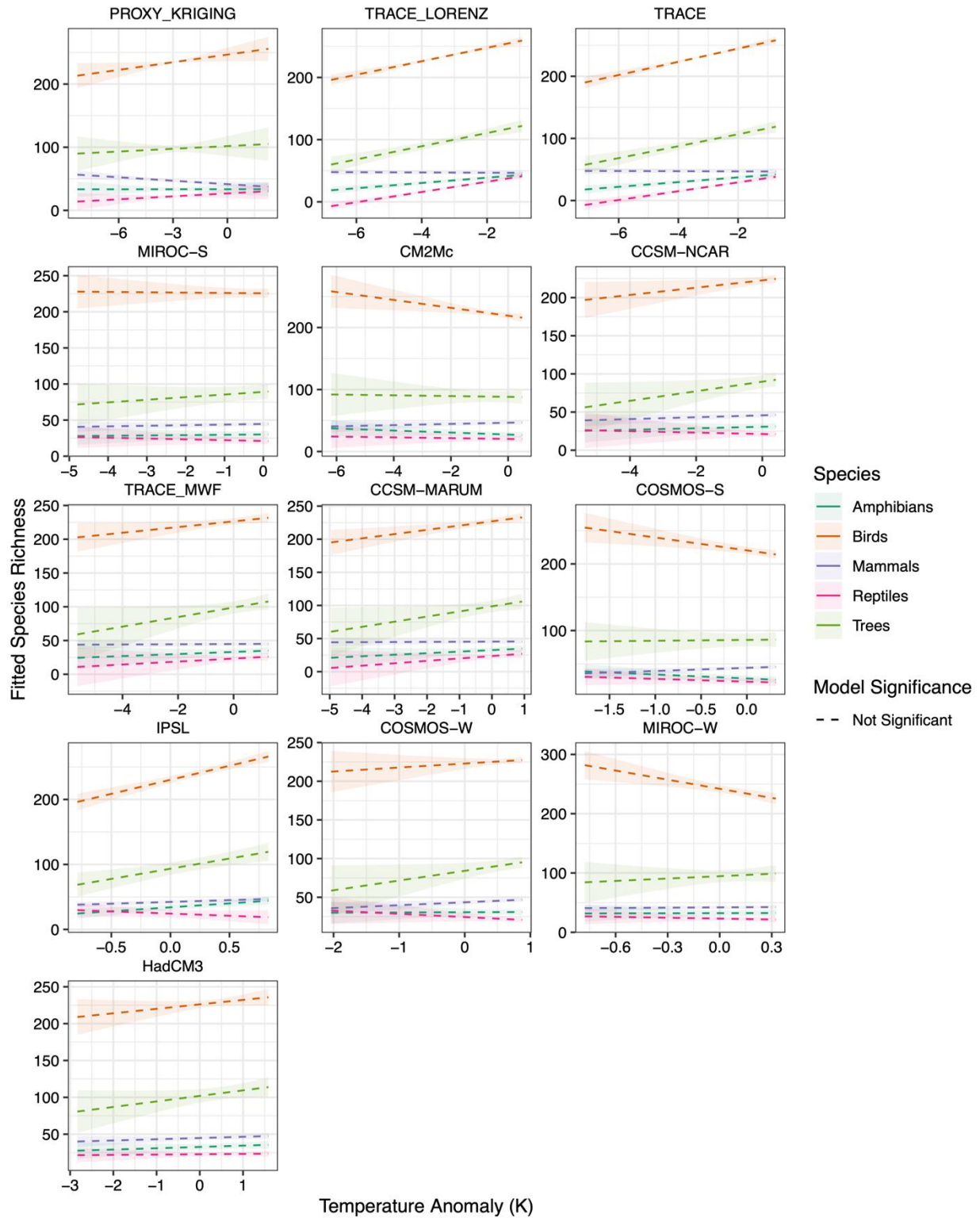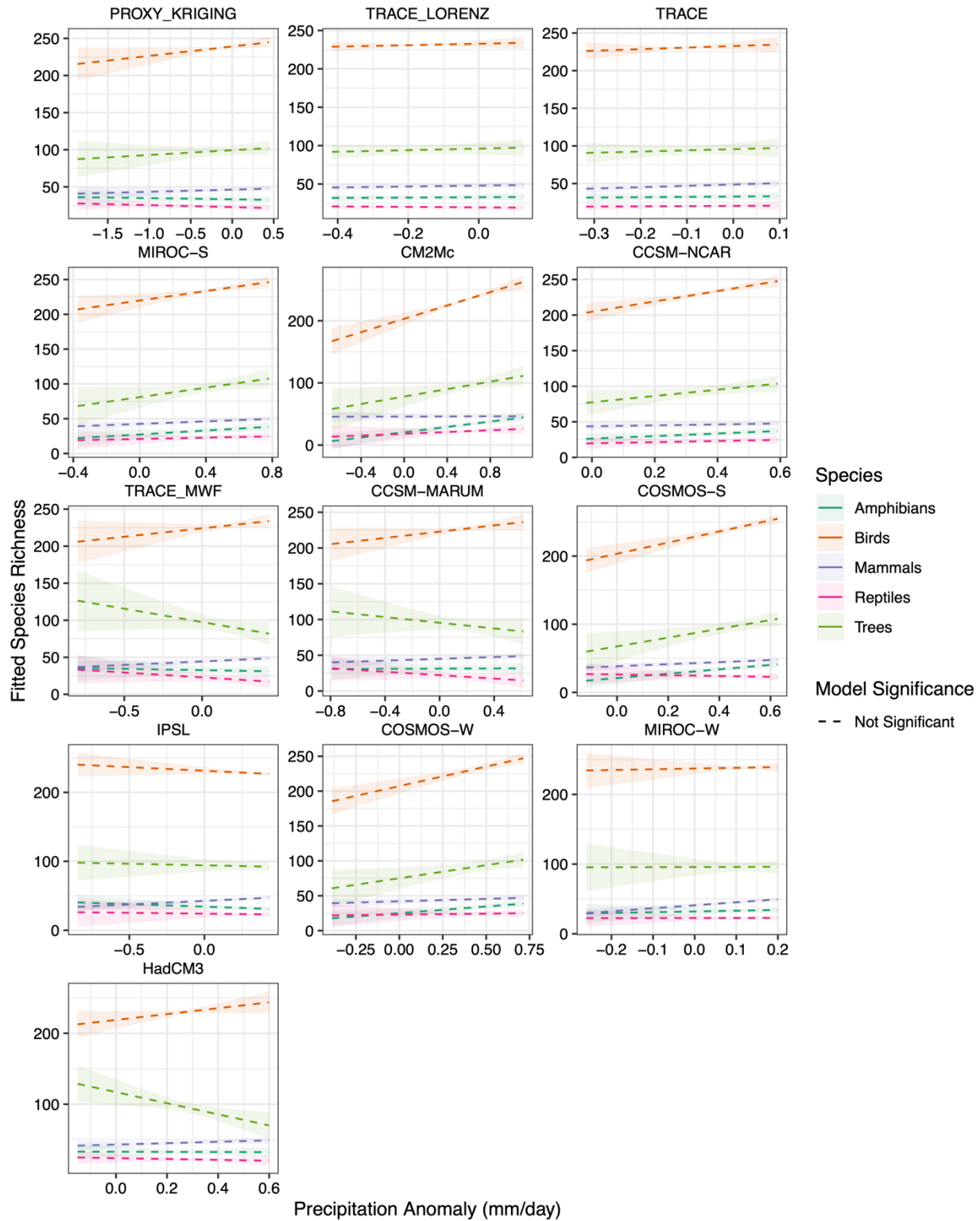
Figure S3.2
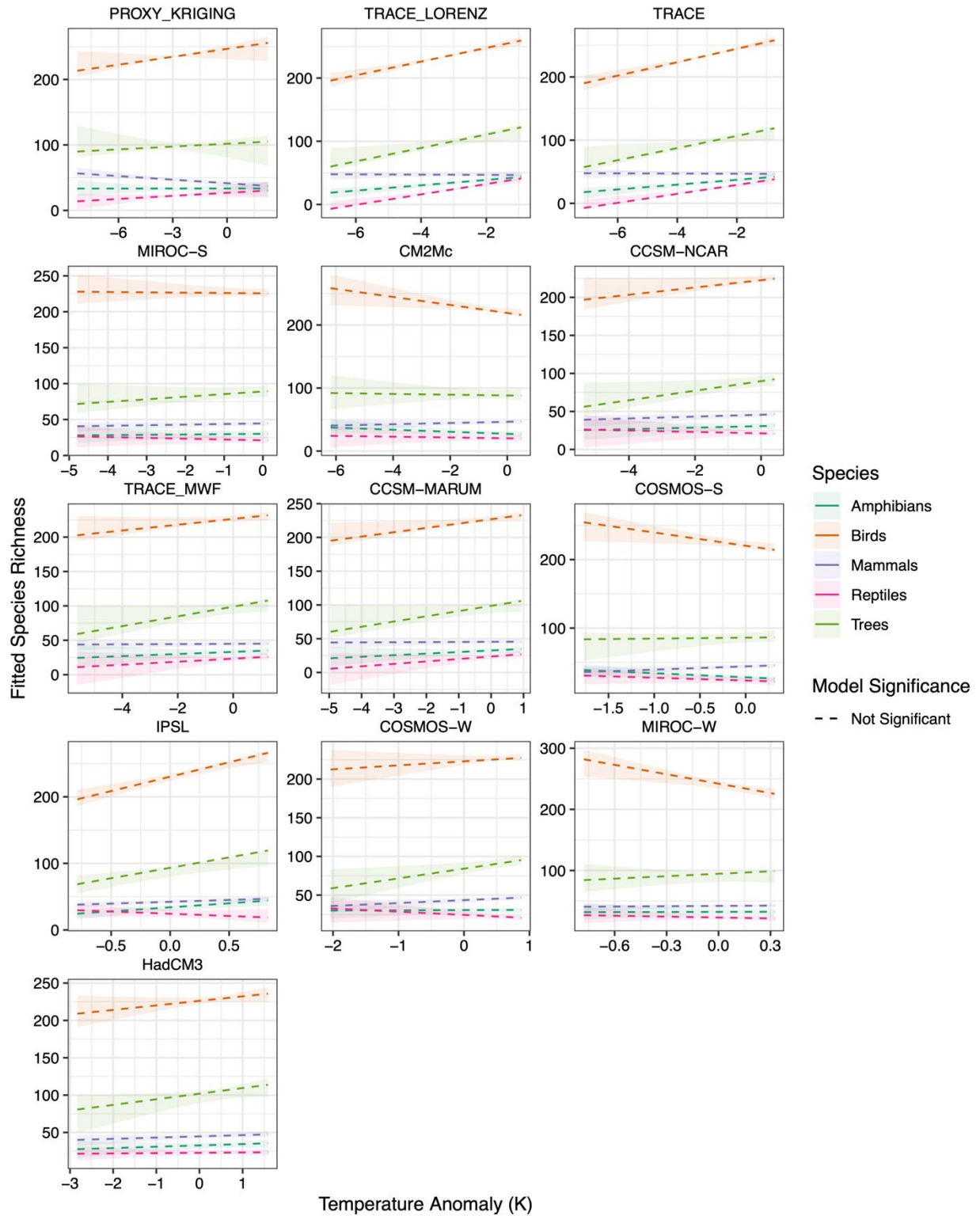
As in Figure S3.1 but for precipitation anomalies.

Figure S3.3

The effects of paleotemperature changes on the contemporary biodiversity of eastern North America from GLMs fit where error is assumed to followed a Matérn covariance function and the only predictors were paleotemperature and paleoprecipitation.

Figure S3.4

As in Figure S3.3 but for paleoprecipitation.

Figure S3.5

The effects of paleotemperature in GLMs that include modern climate correlates, paleoclimate correlates, and model error is assumed to follow a Matérn covariance function.
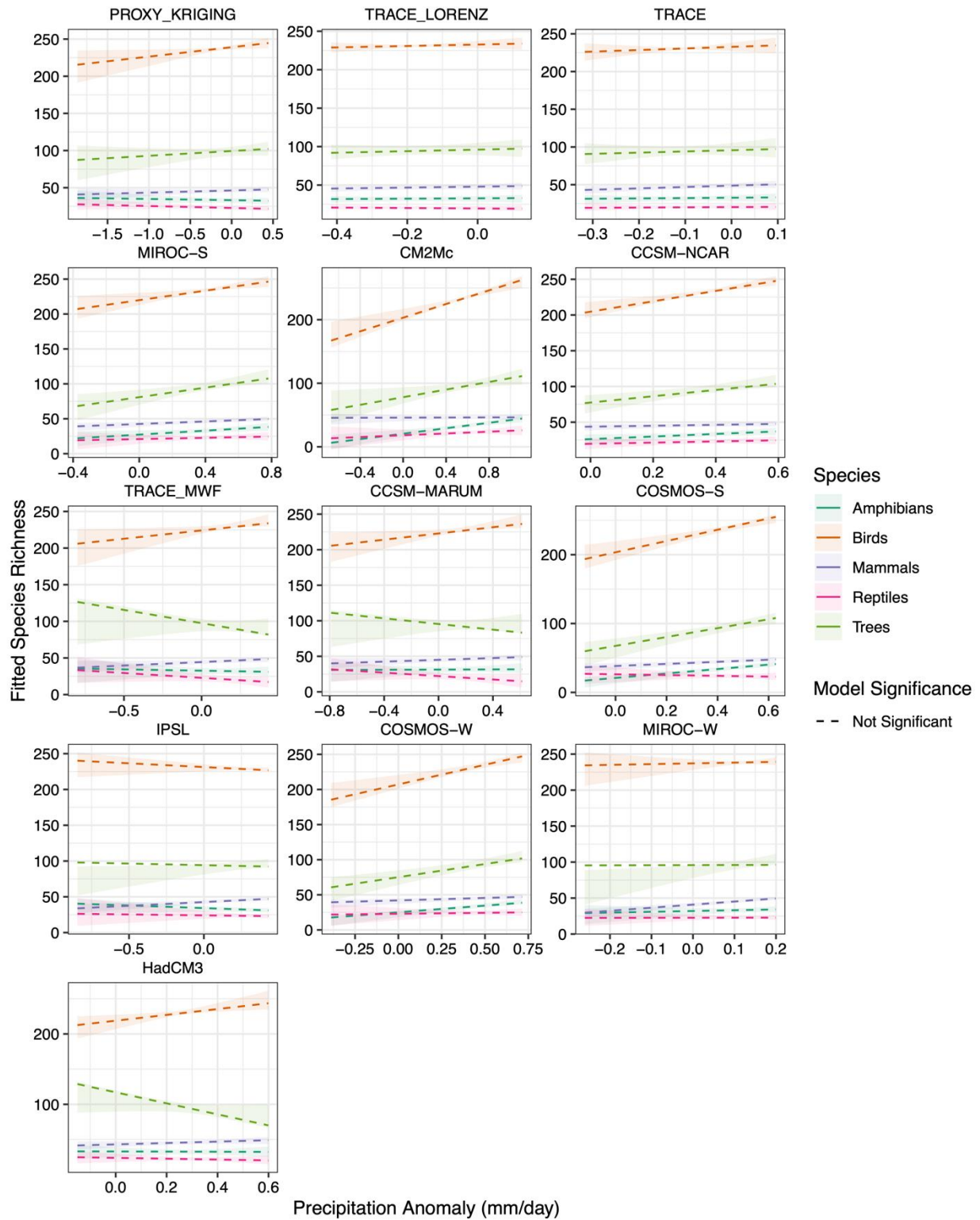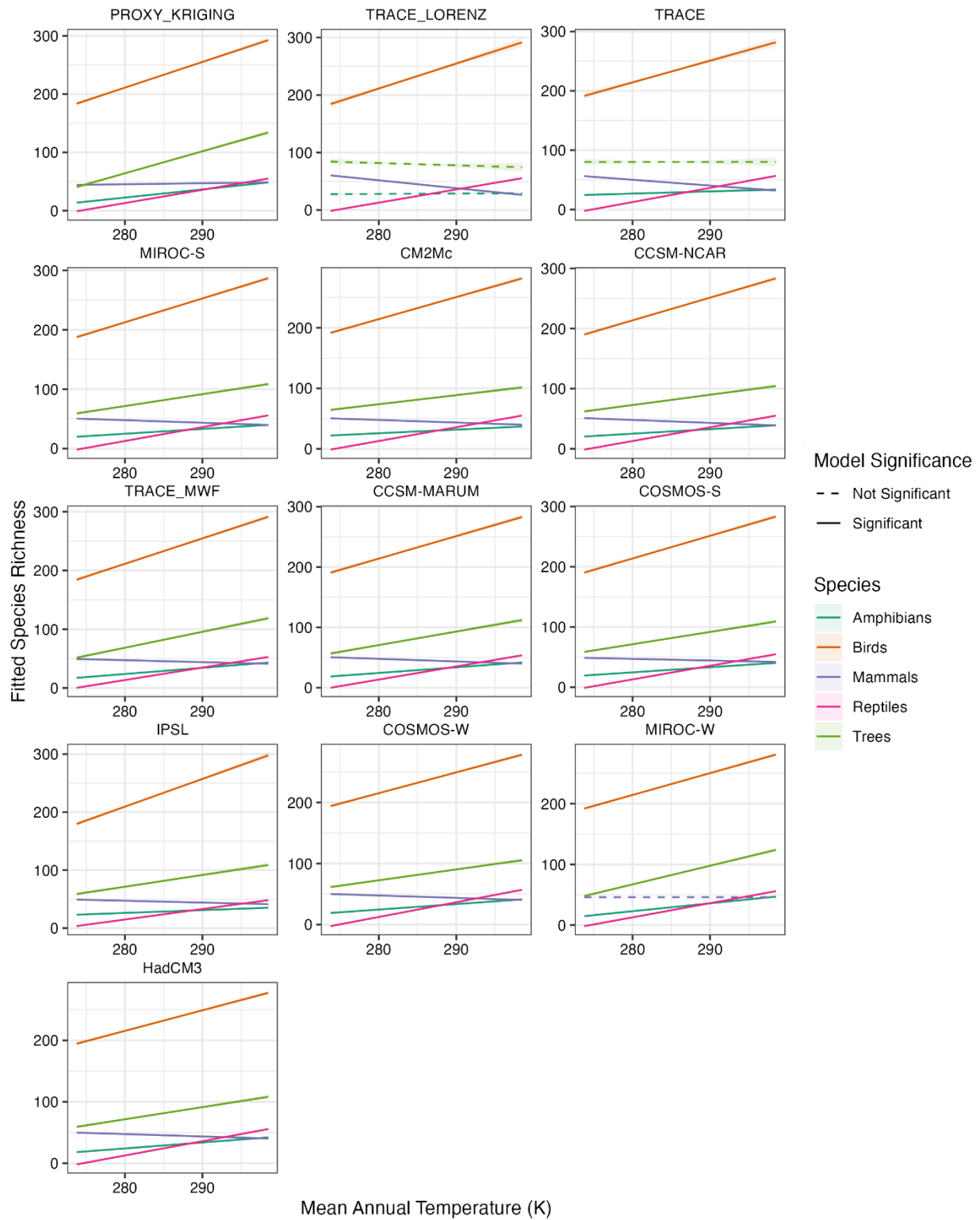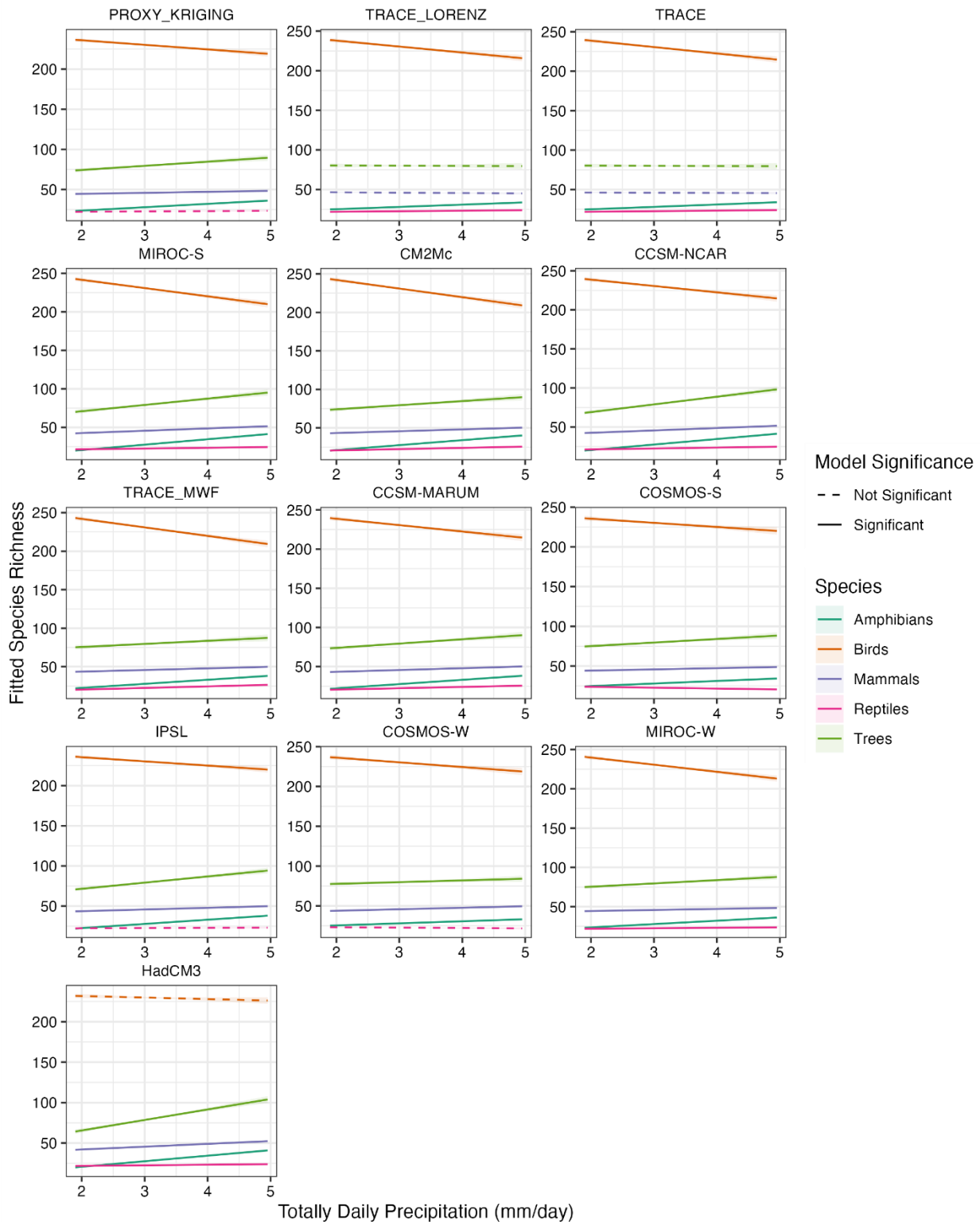
Figure S3.6
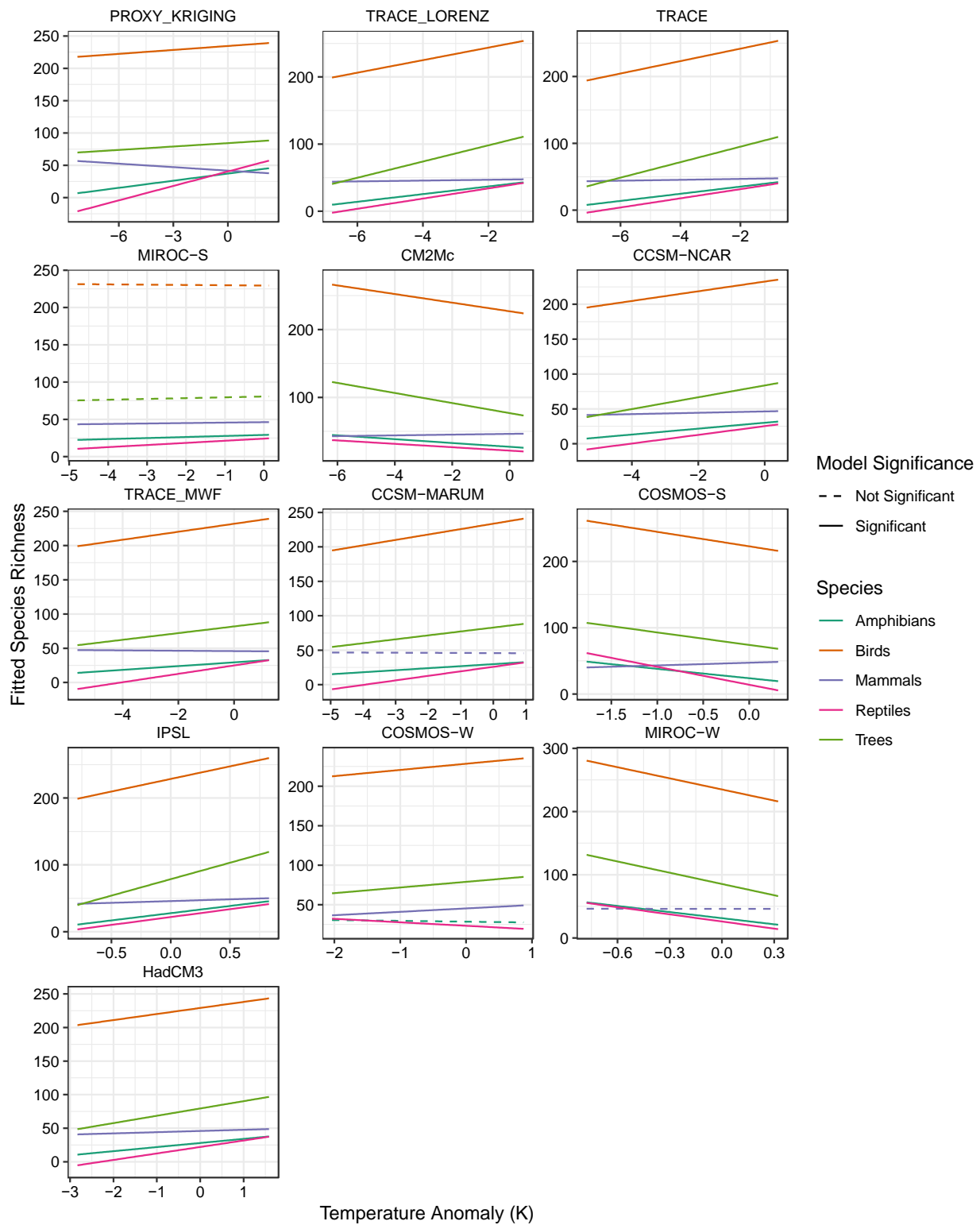
As in Figure S3.5 but for the effects of paleoprecipitation.

Figure S3.7
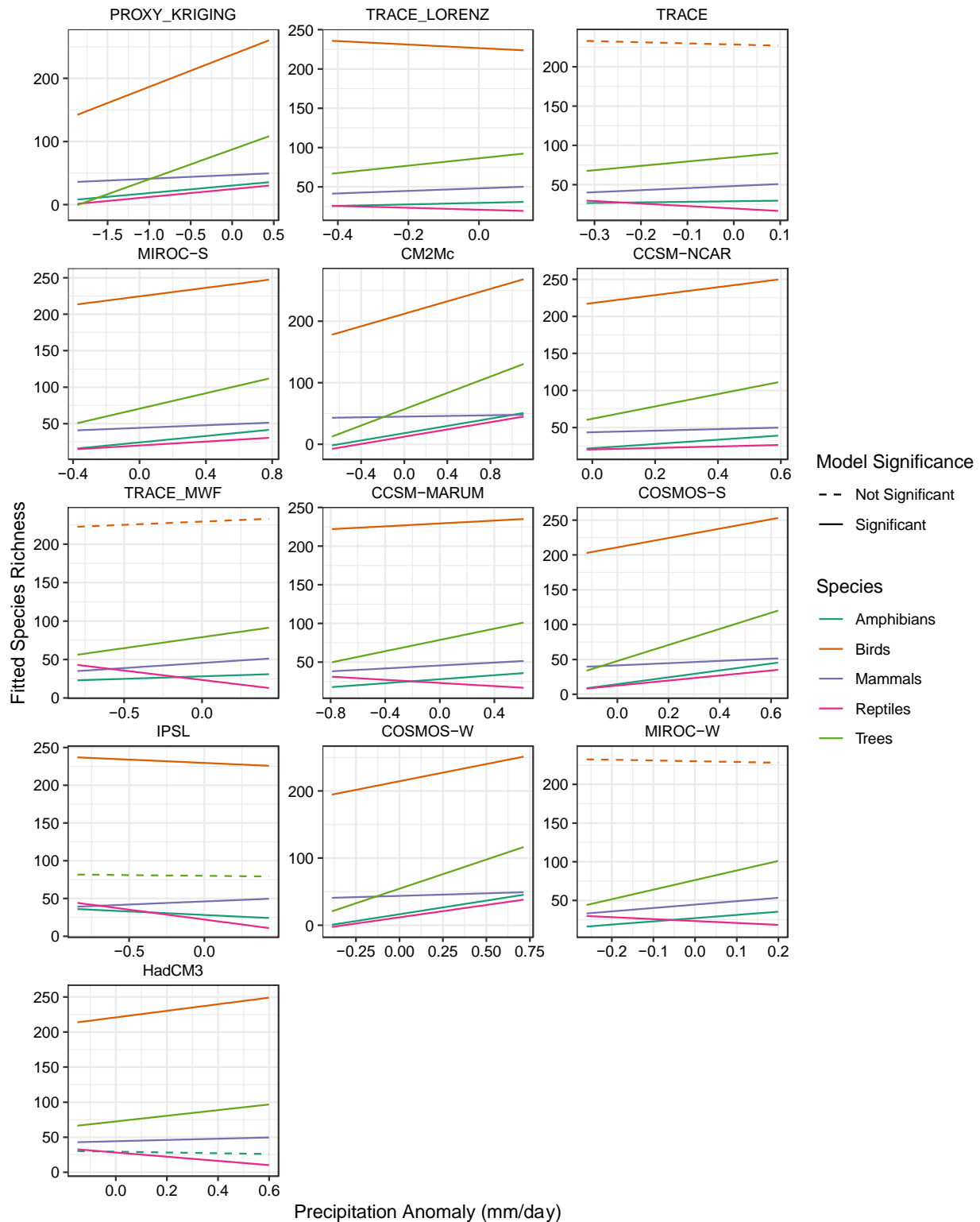
The effect of contemporary mean annual temperature from Fick and Hijmans (2017) on species richness for amphibians, birds, mammals, reptiles and trees. These GLMs also contained paleotemperature, paleoprecipitation, contemporary precipitation, and spatial position as additional correlates.

Figure S3.8
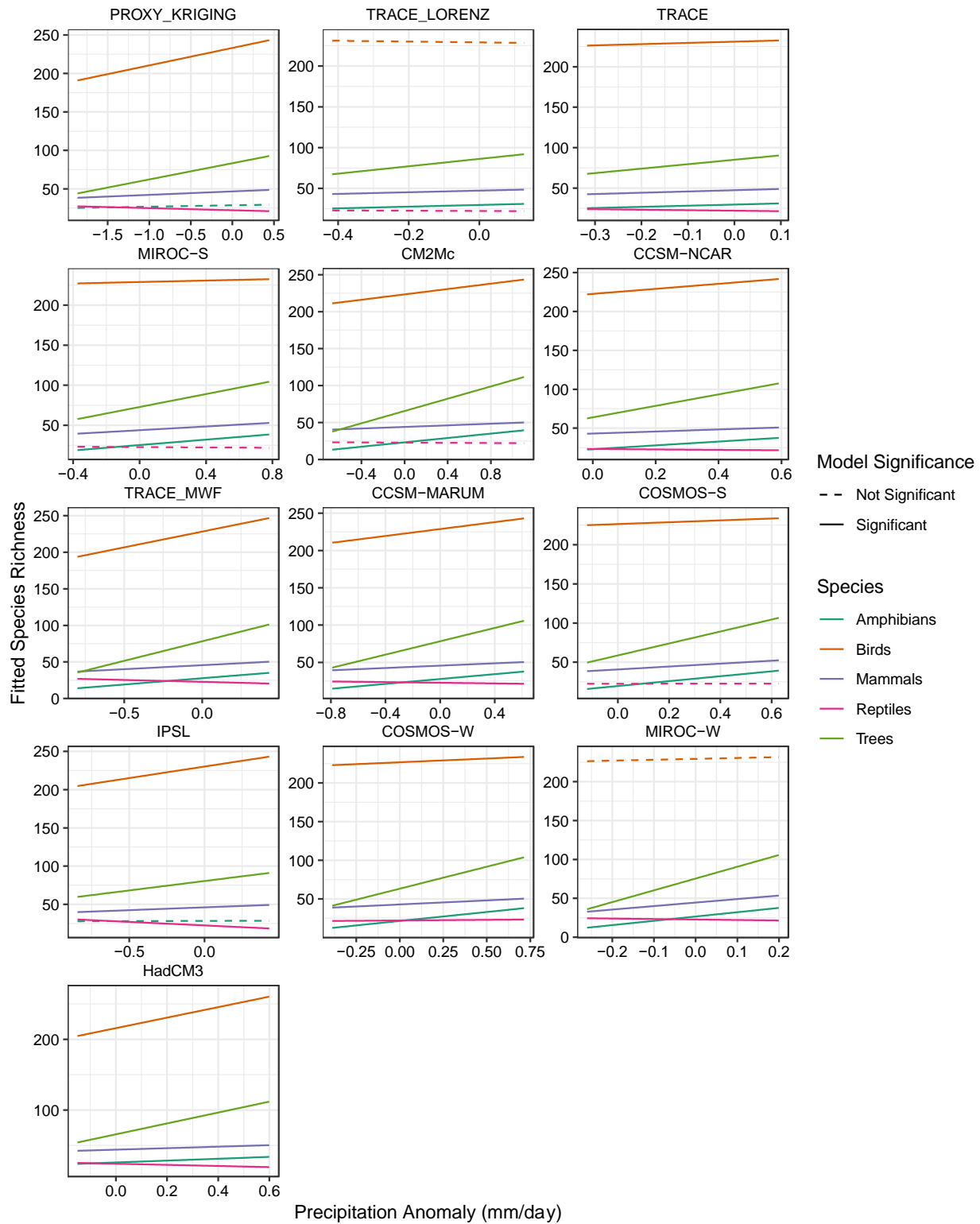
As in Figure S3.7, but for contemporary daily precipitation.

Figure S3.9
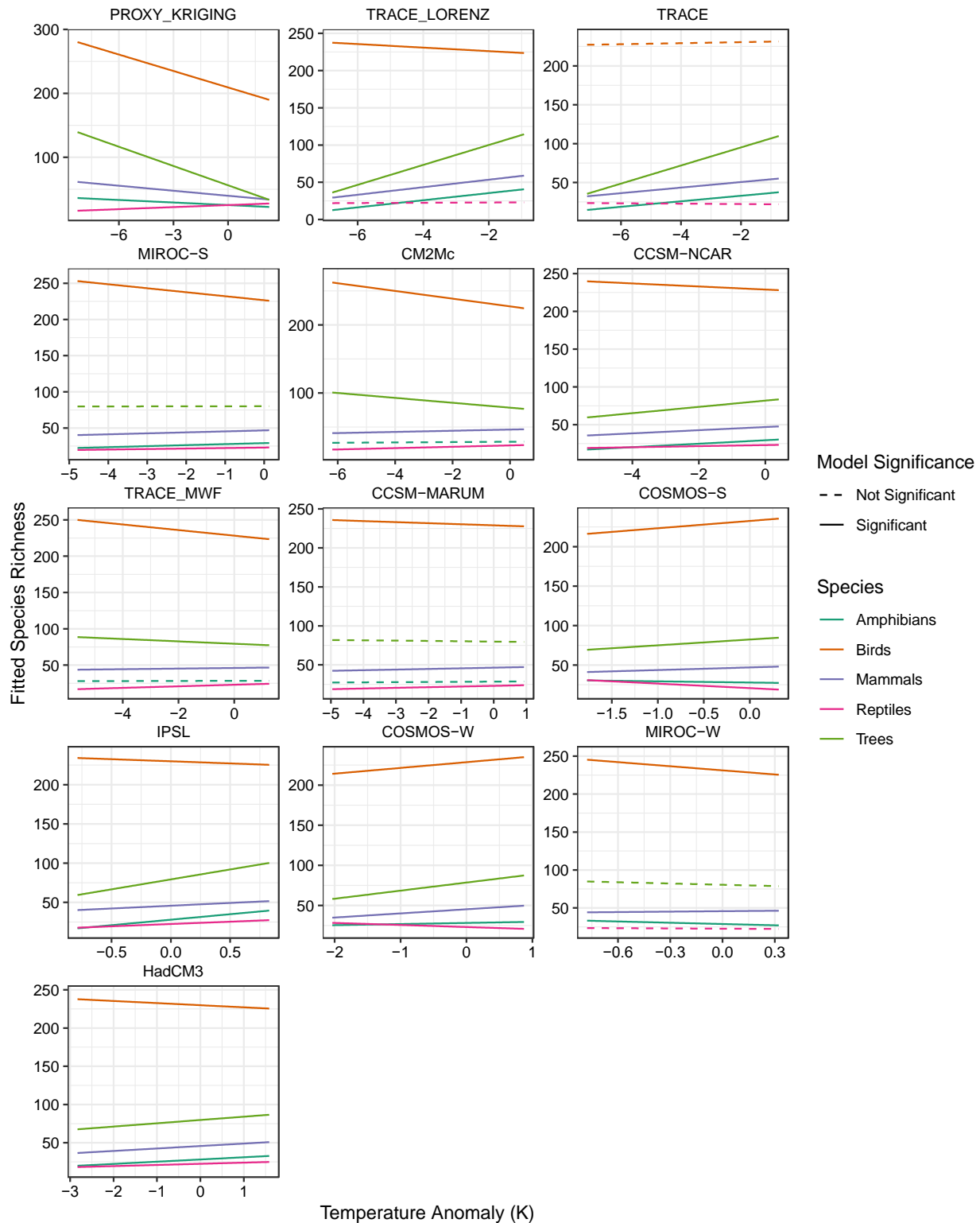
The effect of paleotemperature anomalies from a millennial scale climate event on species richness from GLMs that were fitted excluding modern temperature and precipitation as correlates. GLMs were fitted to paleotemperature estimates from 11 climate models and kriged proxy estimates. All GLMs included paleoprecipitation estimates as correlates.

Figure S3.10

As in Figure S3.9, but for the effect of paleoprecipitation anomalies.

Figure S3.11

The effect of paleoprecipitation anomalies from a millennial scale climate event on species richness from GLMs that were fitted using the following formula: *species richness ~ contemporary mean annual temperature + contemporary total annual precipitation + paleotemperature anomalies + paleoprecipitation anomalies*. Note, that these GLMs include contemporary climate correlates unlike those from Figure S3.9.

Figure S3.12

As in Figure S3.11, for the effects of paleotemperature.
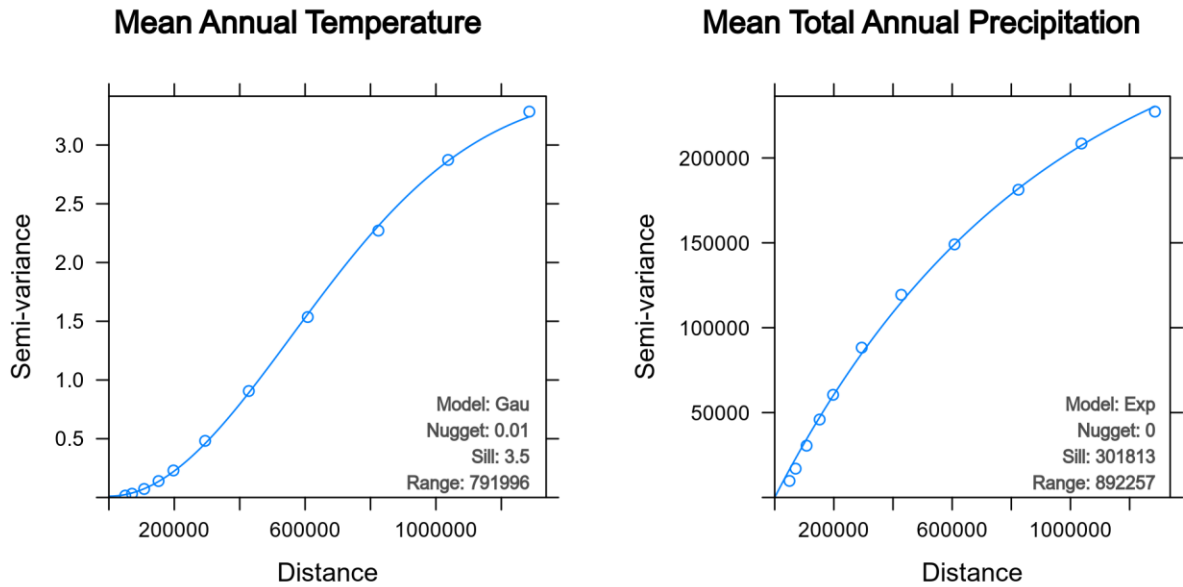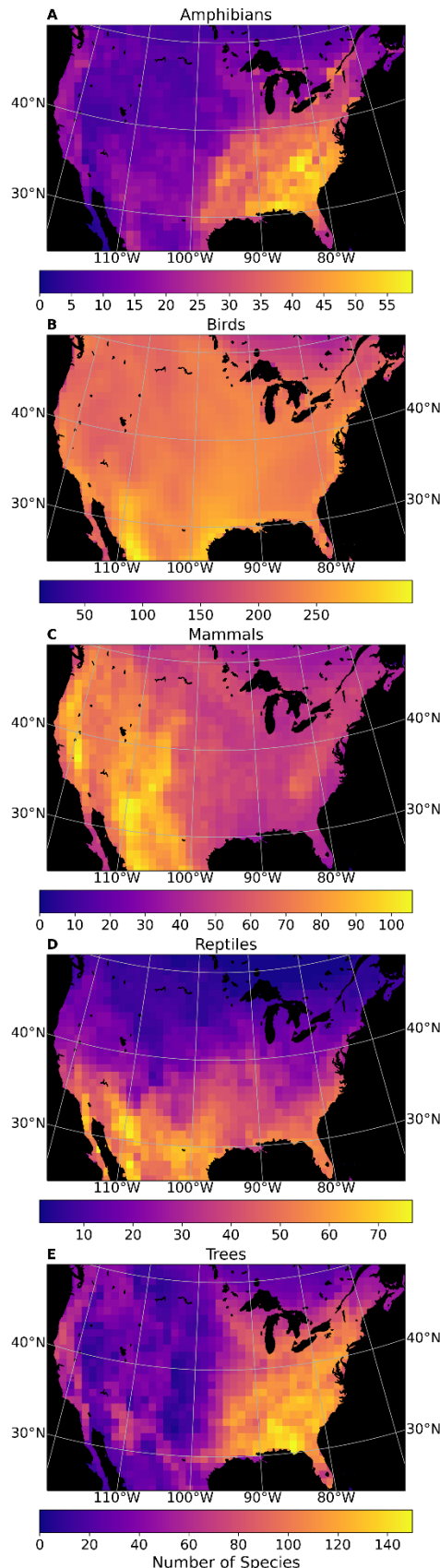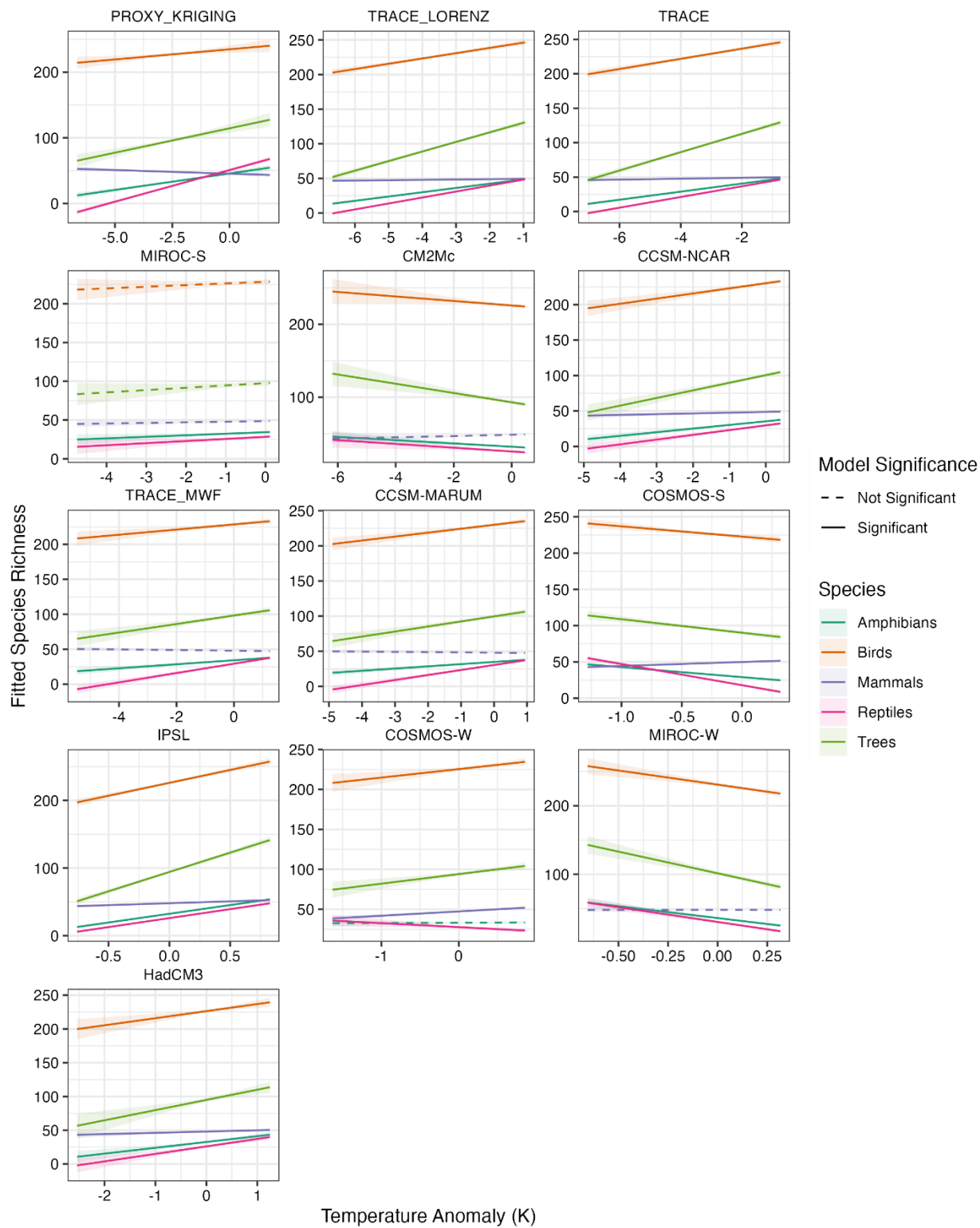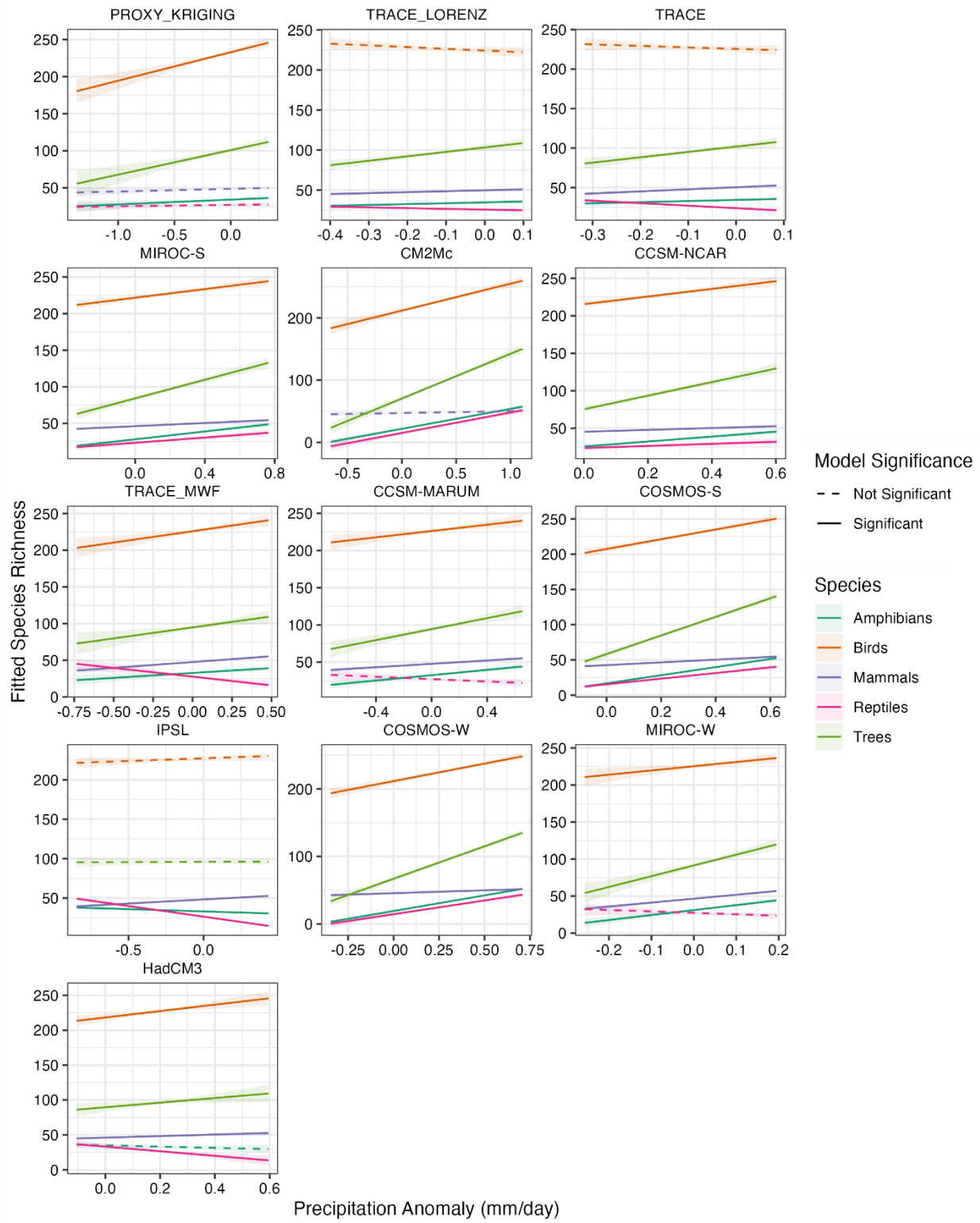
Figure S3.13

Fitted semivariograms for mean annual average temperature from 1951-1980 and mean annual total precipitation from 1951-1980 from the National Centers for Environmental Prediction/National Center (NCEP) for Atmospheric Research Reanalysis (Kalnay et al. 1996) and the Global Precipitation Climatology Centre data products (Schneider et al. 2017), respectively. Range values from these fitted semivariograms are used in the kriging procedure outlined in Section 4.4.4.
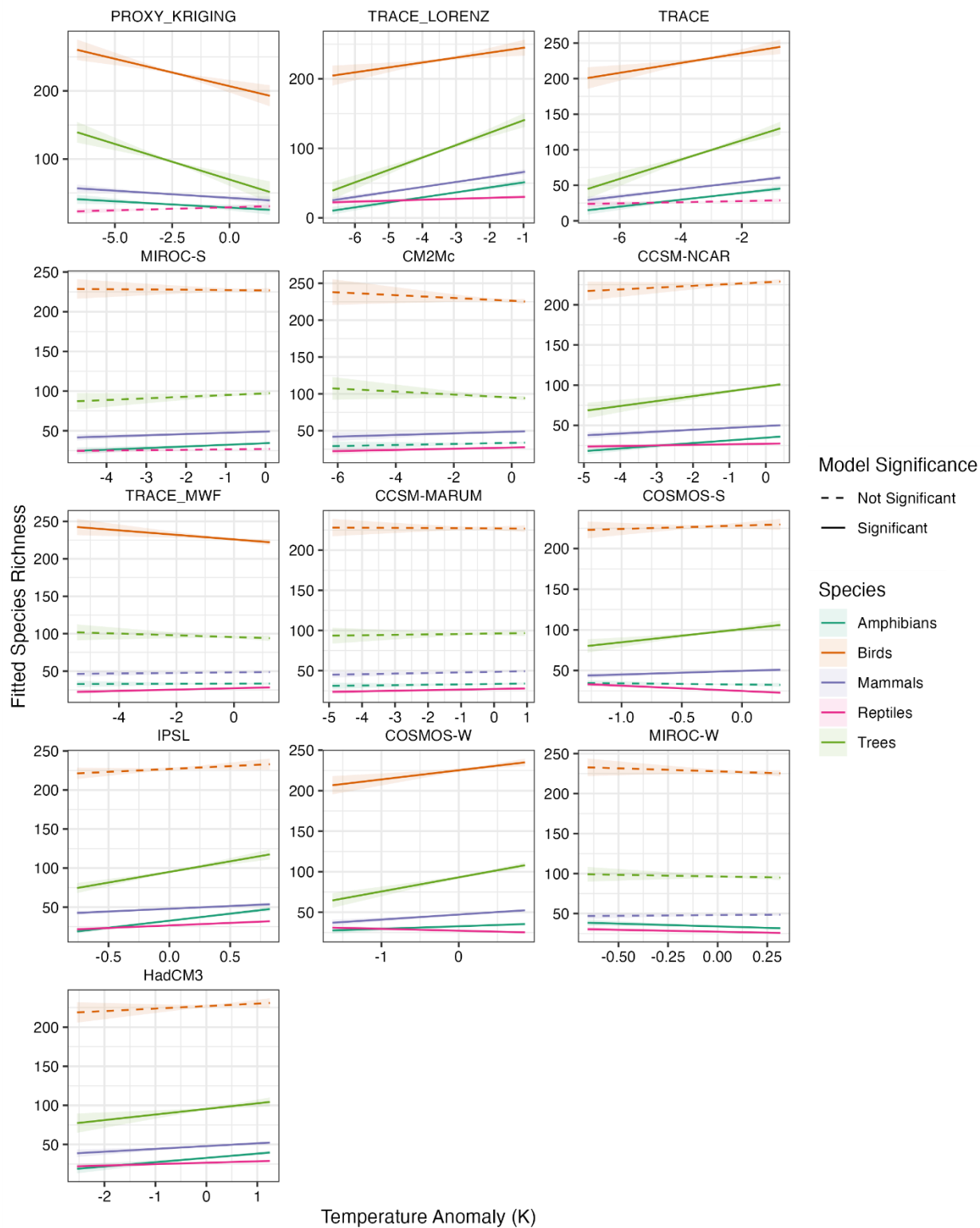
Figure S3.14

Species richness estimates for (A) amphibians, (B) birds, (C) mammals, (D) reptiles, and (E) trees as in Figure 4.1 but at a 100km equal-area grid following the same coordinate reference system.
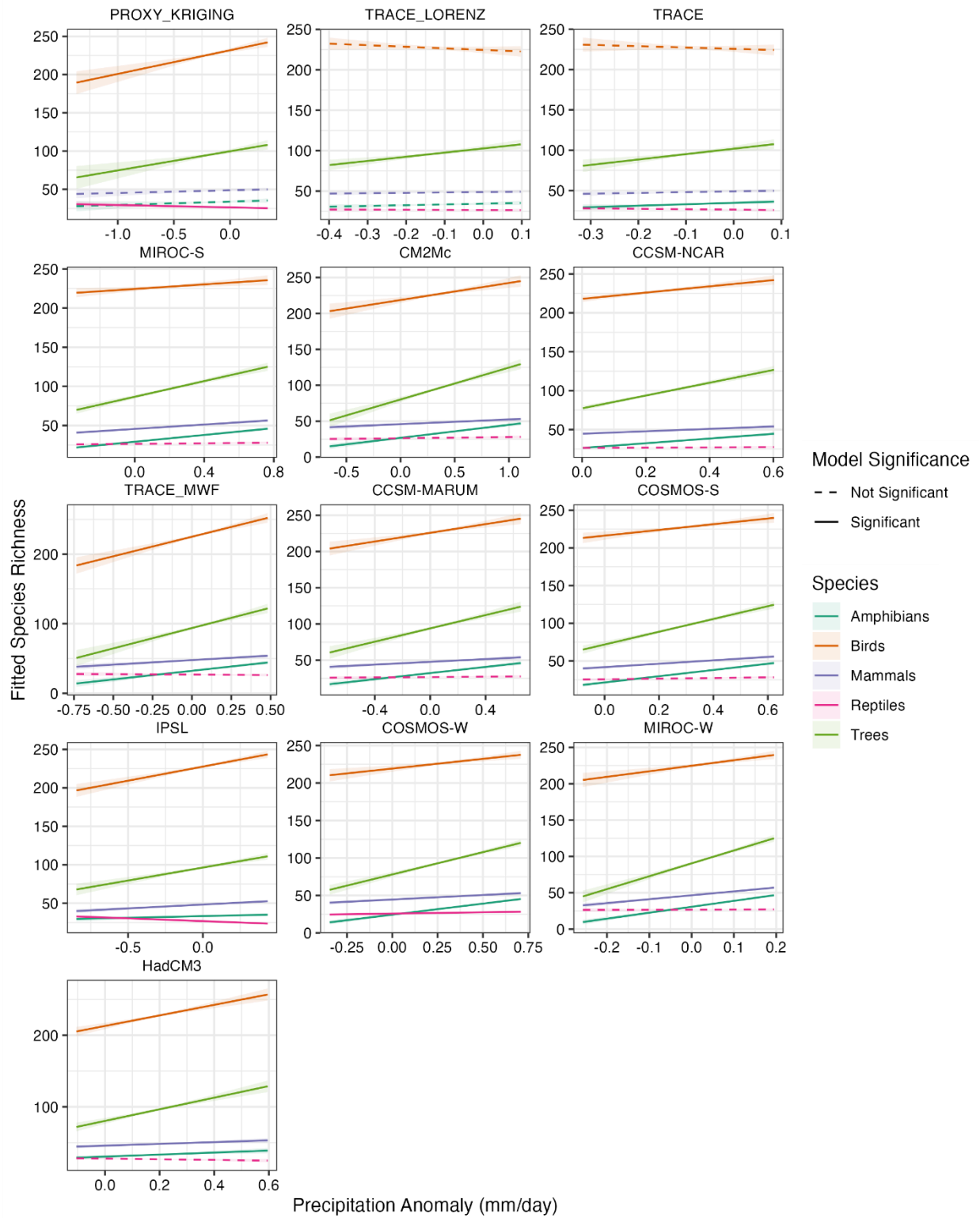
Figure S3.15

Sensitivity analysis of the effect of grid cell size on the effect of paleotemperature anomalies on species richness. The GLM structure is identical to Figure S3.9 but with all paleoclimate fields, modern climate fields, and species richness estimates on a 100km equal area grid with the same coordinate reference system used for analysis in Figure S3.9. The effect of changing spatial resolution on the paleotemperature effects is minimal. Some relationships lose statistical significance because of fewer grid cells but the direction of all relationships is unchanged.

Figure S3.16

As in Figure S3.15, but for the effect of paleoprecipitation anomalies. Similar to resolution sensitivity analyses on the smoothed functional effects of paleotemperature anomalies, the effects of increasing grid cell size to 100km is minimal on the effects of paleoprecipitation anomalies. Some paleoprecipitation effects lose statistical significance but the magnitude and direction of these relationships is largely unchanged.

Figure S3.17

As in Figure S3.15, but for GLMs that include modern temperature and modern precipitation correlates.

Figure S3.18

As in Figure S3.16 but for GLMs that include modern temperature and modern precipitation correlates.